DRAG REDUCTION IN TURBULENT SHEAR FLOW DUE TO INJECTED POLYMER SOLUTIONS

LOTFY HASSAN RABIE

Thesis submitted for the Degree of

Doctor of Philosophy

University of Edinburgh

June 1978

DECLARATION

I declare:

a) that this thesis has been composed by myself,

and

b) that the work described is my own.

Lotfy H. Rabie

Department of Mechanical Engineering

University of Edinburgh

June 1978

CONTENTS

CHAPTER PAGE

ACKNOWLEDGEMENTS

I would like, above all, to express my sincere thanks to my supervisor Dr. W.D. McComb for his invaluable assistance, supervision and constant encouragement, without which this work would not have reached this level.

My thanks to all members of staff of Mechanical Engineering Department and all friends whose help and moral support helped towards the completion of this thesis. I am grateful to the Technical staff of the Mechanical Engineering Department under the guidance of Mr. G. Smith for their help in making the experimental set-up. I am also grateful to Mrs. Isabel Duncan for typing the manuscript in a good presentable form

I would like also to express my sincere thanks to Professor J.L. King for the use of the facilities of the Mechanical Engineering Department.

The financial support of the University of Edinburgh in granting me a studentship during the course of study is acknowledged with sincere thanks.

Finally, I would like to express my sincere thanks and gratitude to my parents and to my wife 'Noussa' for her prolonged forbearance and constant encouragement.

ABSTRACT

The drag reduction, due to injected drag-reducing polymer solutions into the centreline and the wall region of a turbulent water pipe flow, was investigated. The diffusion of these injected solutions into the flow was also studied. The results showed a large reduction in the turbulent diffusivity which was attributed to the viscoelasticity of these solutions and their tendency to form agglomerations.

The drag reduction results were found to exhibit much higher values than those of homogeneous solutions. The difference was pronounced at low values of Reynolds number and polymer concentration. The results showed that flows with polymer injection exhibit very low values of drag reduction onset to which the high drag reduction efficiency is attributed. The polymer agglomerations which were found to characterize such flows is believed to play an important role in these differences.

The results showed that the drag reduction is related to the polymer additives in the near wall region and completely independent of the additives outside this region.

In order to investigate the changes in the flow and turbulence structure with the polymer additives, mean velocity and turbulent intensity profiles, auto-correlations, turbulent energy spectra and bursting times were measured. The measurements were carried out in the flow with and without polymer injection using the laser-doppler anemometer technique. The results showed that when the additives were confined to the core region, the flow and the turbulence structure exhibited no changes from those of water flow indicating that polymer additives interaction with the flow structure in the core region produces neither drag reduction nor changes in the flow and the turbulence

structure even locally. When the additives reached the near-wall region and the drag reduction was established, the flow and turbulent structure exhibited changes across the whole cross section. The results of the bursting time exhibited much higher values than that of water flow even at the reduced wall shear stress supporting the hypothesis that the main influence of the polymer additives is to reduce the production of the turbulence through the suppression of the streak formation and the eruption of bursts.

CHAPTER I

INTRODUCTION

Drag reduction is the phenomenon whereby a few parts per million of dissolved long chain, high molecular weight polymers reduce the skin friction in a turbulent shear flow below that of the solvent alone. The phenomenon of drag reduction has been subjected to extensive studies both theoretically and experimentally in order to understand the mechanism responsible for the effect and to provide the necessary information for engineering applications.

In this work, we present our investigation of the drag reduction by injecting a concentrated drag reducing polymer solution into both the centreline and the wall of a turbulent pipe flow of water.

In this chapter we intend to introduce the drag reduction phenomenon through reviewing most of its aspects. A historical review of the phenomenon is given at the beginning of this chapter. This is followed by a general review of the drag reduction by polymer additives. Finally a scope of the present work reviewing the relevant work conducted previously by injecting polymer solutions into water flow will be presented. Then, the general arrangement of the thesis will be provided.

1.1 HISTORY

The phenomenon was first reported by Toms (1948) (with whose name it is commonly associated) together with Oldroyd (1948). Toms observed that the addition of a few parts per million of polymethylmethacrylate to a turbulent pipe flow of monochlorobenzene reduced the pressure drop substantially below that of the solvent alone at the same flow rate. But the earliest recorded use of additives in the flow systems dates back to 1945. Mysels (1971), during the II world war, led a team at Edgewood Arsenal in studying the flow characteristics of gasoline thickened with aluminum soaps in a small pipe line. They found that, when soap was added, the pressure drop per unit length of the pipe was much less than that of the pure gasoline only when the flow was turbulent. The phenomenon was ignored until it was observed again by workers in the oil industry. Ousterhout et al (1960), Dever et al (1962) and Savins (1964) noticed that when certain gums were used to suspend sand in high pressure sand water mixtures employed in oil-well techniques, the friction was greatly reduced. This attracted the interest of the U.S. Navy to explore the friction reducing effects for possible military applications (Fabula (1963) and Hoyt (1963, 1964).

Since that time the phenomenon has been subjected to an extensive experimental and theoretical investigations, not only because of the promising technical applications it offers, but also in the hope of achieving a deeper understanding of the nature of turbulence, through the unravelling of the mechanism underlying the phenomenon of drag reduction. Drag reduction has been studied by various techniques. As a result of these studies, over the last 20 years, it is now well known that drag reduction occurs with many other polymer-solvent combinations, and the addition of only a very few parts per million of a polymer such as polyox (polyethylene oxide) can readily reduce the

frictional drag in turbulent pipe flows to less than half of the value observed for the solvent alone. In addition to affecting the momentum transport in turbulent flows, as demonstrated by the drag reduction, polymeric additives can also influence the heat and mass transfer processes. Marrucci and Astrita (1967), Wells (1968) and Smith et al (1969) reported that the addition of drag reducing polymers significantly reduces the heat transfer coefficient in turbulent flow. Sidahmed and Griskey (1972) reported that the mass transfer was reduced in turbulent flow of drag reducing solution but not in laminar flow.

Other phenomena associated with drag reducing additives in non-turbulent shear flow fields have also received some attention. McComb (1974) investigated the effect of drag reducing additives on the total number of oscillations of a liquid column. His results showed that the addition of a few parts per million of polyox WSR-301 to a water column more than doubled the number of oscillations relative to the water case. The effect of polymer solutions was found to suppress the inception of cavitation Ellis, et al (1970) and Hoyt (1971) reported that small amounts of polyox added to the flow can suppress the flow generated cavitations by as much as 60%. McComb and Ayyash (1976) investigated the effect of polymer solutions on gas bubble pulsation. They found that polyox reduces the damping constant of the bubble pulsation while the separan was found to be more complex.

1.2 TURBULENT DRAG REDUCTION BY POLYMER ADDITIVES

During the last two decades, the effects of drag-reducing polymers on turbulent shear flow have been investigated. However, despite the combined efforts of specialists from many different fields, no satisfactory explanation of the phenomenon has yet been found. Several reviews of the subject have been published which covered several aspects

of the drag reduction phenomenon. Hoyt (1972) provides a most comprehensive review of the literature at the time. He followed this by two other reviews on the latest progress in polymer drag reduction (Hoyt (1975, 1977). Lumley (1969, 1973) gave some physical insight to the molecular configuration in drag reducing systems looking for a possible mechanism for drag reduction. Landahl (1973) paid much attention to the changes in turbulent structure brought about by the additives. Virk (1975) reviewed the available experimental data in drag reduction. Virk provided his review with correlations between the experimental results and the molecular parameters of the drag reducing polymers, and discussed the proposed physical mechanisms of the phenomenon. In the following section, some aspects of the drag reduction in turbulent shear flow will be discussed with an emphasis on the effects of polymeric additives on the turbulence structure.

1.2.1 Characteristics of Drag Reducing Polymers

It is well known that different polymers exhibit drag reduction when dissolved in good solvents. For example, polymethylmethacrylate in ~~turbulence~~ toluene, polyisobutylene in crude oil, kerosene and benzene, flax meal in sea water and carboxymethyl cullulose, guar gum, polyacrylamide, polyacrylic acid and polyethylene oxide in water. The common properties of these polymers are their high molecular weights (of order 10^6), long chain and linear or random coiled flexible molecules.

The effectiveness of the polymer depends on its molecular weight and its molecular structure. It is said that a polymer is more effective than another when the concentration required to achieve the same percentage of drag reduction under the same conditions is lower than the concentration of the other. In general, polymers of high molecular weights are more effective as drag reducers than low molecular weight polymers. Those of linear structure with few or no side chains

and of simple form are more effective than branched side chain polymers (Hoyt & Fabula (1964)). The effectiveness of the polymer increases as the elasticity of its molecular structure increases. Polymers when dissolved in good solvents were found to be more effective than when dissolved in poor solvents (Hoyt (1972)). The solvent effect arises from the fact that polymer molecules in poor solvent solution are less extended than in good solvent solution. Consequently, low polymer solvent interaction is achieved and low drag reduction results.

1.2.2 Flow Characteristic Effects on Drag Reduction

Systematic studies of pipe flow (e.g. Seyer & Metzner (1967)), Goren & Norbury (1967) and Virk et al (1967, 1970, 1975) have indicated several drag reduction characteristics common to all drag reducing polymeric solutions. At low flow rates, the dilute polymer solutions obey the laminar friction law (Poiseuille's law). At higher flow rates, the flow passes through a transition region to turbulence very similar to the Newtonian fluid flows. In the turbulent flow region, drag reduction onsets at a well defined flow rate corrosponding to a well defined value of wall shear stress, which is known as the onset wall shear stress τ^*_w. Before the onset and in the turbulent region, the dilute polymer solution behaves as a Newtonian fluid and obeys Prandtl. Karman (or Blasius) law described by the equation

$$f^{-\frac{1}{2}} = 4.0 \log_{10} (Re\ f^{\frac{1}{2}}) - 0.4 \qquad (I.1)$$

At a higher flow rate than that of the onset, the friction factor is lower than its Newtonian value. This reduction in the friction factor is what is known as the drag Reduction (D.R.) and is defined as

$$\%DR = \left(\frac{f_s - f_p}{f_s}\right) \times 100 \qquad (I.2)$$

where f_s is the friction factor of the solvent and f_p is the friction factor of the polymer solution. For the same flow rate, equivalently

equation (I.2) can be written as

$$\%DR = \left(\frac{\Delta P_s - \Delta P_p}{\Delta P_s}\right) \times 100 \qquad (I.2)$$

where ΔP_s is the pressure drop of the solvent and ΔP_p is the pressure drop of the polymer solution.

The drag reduction value depend on the polymer properties and the flow parameters. It increases with the increase of the polymer concentration, molecular weight and the flow rate. A maximum drag reduction for any drag reducing polymer and at any Reynolds number can be achieved. Virk et al (1970-9) verified that the maximum drag reduction is described by a unique asymptote which is independent of polymeric parameters.

$$f^{-\frac{1}{2}} = 19.0 \log_{10} (Re\ f^{\frac{1}{2}}) - 32.4 \qquad (I.3)$$

Virk (1971) showed that this relation holds for smooth and rough pipes.

Several attempts have been made to correlate the friction data in the polymeric region below the maximum drag reduction asymptote. Two different approaches have been used, one based on the rheological properties of the solution (Seyer & Metzner (1969)), Astarita et al (1972) and Wang (1972)), and the other is based on the molecular parameters (Virk (1975)). The latter approach is supported by the documented results of a friction reduction of 40% noted in pipe flow with a polymer (polyethylene oxide) concentration of 0.5 part per million (Hoyt (1972)), whereas, at this very low concentration, the rheological properties of the solution are indistinguishable from those of the solvent.

The dependence of drag reduction on wall shear stress, or Reynolds number has been widely investigated. After the onset, the

polymer becomes more effective as the flow rate increases. This effect continues up to a maximum drag reduction value for a given concentration, beyond which the drag reduction decreases due to molecular overstress and consequently mechanical degradation (Hoyt (1972), Garen & Norbury (1967) and Ramu & Tullis (1967)). The effectiveness of the polymer is related to its molecular weight which is a measure of the length of the polymer chain. When the polymer solution is subjected to a high enough shear stress the chain breaks, thus reducing the molecular weight and its drag reduction effectiveness.

1.2.2 Drag Reduction onset

It has been stated that drag reduction sets in at a well defined value for the wall shear stress τ_w, this value is known as the onset wall shear stress. The onset of drag reduction implies that the phenomenon sets in when the turbulence scales reach some value comparable to the polymer molecular scales in the solution. Two hypotheses have been proposed, the length-scale hypothesis (Virk (1966)) and the time-scale hypothesis (Lumley (1973)). Virk (1966) correlated the radius of gyration of the macromolecule in the solution 'R_G' with the dissipative turbulent wave number at the onset k^*_d by the relation

$$R_G \cdot k^*_d = \text{constant} = 0.008 \pm 0.002 \quad \text{(Virk (1975))} \qquad (1.4)$$

where $k^*_d = (\sqrt{\tau_w^*/\rho})/\nu$

However, this small value of the constant suggests that the individual polymer molecules are too small to interact with the turbulence structure, which has a characteristic size two orders of magnitude greater than the molecule size.

The dependence of the turbulence time scale at onset upon the dimension of the macromolecule in the solution 'R_G' has been suggested by Fabula (1966) and verified recently with the available

experimental data by Virk (1975).

$$R_G^3 \quad \tau_w^* = (10 \pm 5) \times 10^6 \qquad (1.5)$$

The onset relationship based on the time scale shows that the molecular and turbulent time scales are comparable. Lumly (1973) proposed that the polymer molecules would interact with the flow when the turbulent time scale t^*_d ($t^*_d = \nu/\sqrt{\tau^*_w/\rho}$) and the molecular relaxation time θ are related together through the relationship

$$\theta/t^*_d = {}^3/_2 \qquad (1.6)$$

The time scale onset hypothesis is supported by the experimental work of Berman & George (1974) and Berman (1977) which indicated that a time-based correlation between the molecular and the turbulent scales is more acceptable. Berman et al (1973) found a strong correspondence between the onset of the pitot tube errors and that of the drag reduction. Their results showed that the onset time scale values for the pitot tube error ($2\overline{U}/d$) and the pipe flow (u^{*2}/ν) were the same at the same experimental conditions, where d is the pitot tube diameter and $\overline{U}$ the flow velocity.

The differences between the length and the time scale hypothesis can be harmonized together by the assumption proposed by Hoyt (1972) that the polymer acts as aggregates of molecules to give the physical size comparable with the small turbulence eddies, but they have relaxation times as a function of the individual molecule parameters. The role of the polymer aggregates on drag reduction will be discussed later.

Another hypothesis based on the strain energy stored by the polymer molecules in a fluctuating shear field have received little attention (Walsh (1967) and Kohn (1974). It states that drag reduction sets in when the turbulence strain energy density and the strain energy stored by the molecules are comparable.

The dependence of onset wall shear stress on polymer concentration and molecular weight has been verified experimentally. In general, the onset shear stress decreases with the increase in the molecular weight. Hunsen & Little (1971), Paterson & Abernathy (1970), and Whitistt et al (1969) observed that the onset shear stress decreases with the increase of polymer concentration. Whereas, Virk (1971, 1975) and Goren & Norbury (1967) reported the independence of the onset wall shear stress upon polymer concentration. Experimental evidence showed that pipe diameter and surface roughness have no effect on the onset shear stress (Virk (1971)), Little et al (1975)).

1.2.4 The Role of Polymer agglomerations on Drag Reduction

There seems little doubt that molecular agglomerations commonly occur in drag reducing polymer solutions, even at high polymer dilutions. Furthermore, such aggregates may often be formed by shearing the solutions (Lumley (1969) and Dunlop & Cox (1977)). Most of the anomalous errors associated with the pitot tubes and hot film anemometer measurements in these solutions are attributed to the presence of these aggregates.

Fabula (1966) observed that polymer solutions form agglomerations spontaneously in the size of the turbulent dissipative scales. These agglomerations produced a sharp signal as they passed near the sensitive surface of the hot film or the pitot tube probe. Smith et al (1967) reported anomalous errors in pitot tube and hot film probe measurements polymer solutions. Presumably, such anomalous errors were due to the influence of polymer aggregates. Kalashnikov & Kudin (1973) observed that the anomalously low pitot-tube readings of the hydrostatic pressure in flows of drag reducing polymer solutions were very similar to that of solid particles in Newtonian flow. They concluded that polymer agglomerations in dilute polymer solutions represent visco-elastic drops. They developed a method to determine the size and volume concentration of these aggregated by relating them to the abnormal readings of the pitot-tube.

Cox et al (1974) added polymer powders suspended in isoproranol to the water in order to investigate the dependence of drag reduction of rotating disc on the presence of polymer agglomerations. Their results provided an evidence for the existence of aggregates in polymer solutions and indicated that they are much more effective as drag reducers than individual molecules. The work of Dunlop and Cox (1977) showed that molecules agglomerations are a common feature of polymer solutions.

The hypothesis of polymer agglomerations has been postulated by a number of investigators to explain their unusual results. Laufer et al (1973) explained the periodic shear stress results of polymer solutions using plate - and - cone viscometer by the formation and the collapse of polymer entanglements. Dunlop & Cox (1977) attributed the time dependent drag reduction of their spinning disc to the presence of transient molecular aggregates which were considered more effective drag reducers than the individual molecules. Hoyt (1972), as mentioned before, used the aggregate hypothesis to reconcile both the length and the time scale onset drag reduction hypothesis.

More evidence for the influence of polymer agglomerations on drag reduction could be obtained from the results of Kowalski & Brundrett (1974). Their turbulent energy spectrum results with and without polymer solutions exhibited changes in the dissipative scales of the flow which they envisaged to be due to the presence of much larger molecules than the individual polymer molecules. They related the size of these agglomerations to the size of the dissipative eddies. Ellis (1970) observed that polymer degradation took place much faster in large diameter tube than in smaller one. The possibility of the molecular degradation was unexpected due to the fact that large diameter tubes exhibit lower shear rate than smaller ones. He explained

his observation as a result of the presence of polymer aggregates which disappeared with the time. Berman & George (1974) postulated the presence of entanglements in polymer solutions as a possible explanation for the deviation in the plot of $\frac{1}{\sqrt{f}}$ against $Re\sqrt{f}$ from a straight line.

Gadd (1968) observed that the aging effect of the polymer solutions on drag reduction was more pronounced in less concentrated polymer solutions. He suggested that large molecular agglomerations were initially present, but were broken up by aging. White (1969) explained the loss of the drag reduction effectiveness of aged polymer solutions by attributing the effect to the breaking up of molecular aggregates initially present.

1.2.5 The Influence of the Polymer on the Mean Velocity Profile

Mean velocity profiles of dilute polymer solutions have been measured using different experimental techniques. Bubble tracing (Rollin & Seyer (1972), Seyer & Metzner (1969) and White (1972)), pitot tube probes (Wells et al (1968), Virk et al (1967) and Goren & Norbury (1967)), hot film anemometers (Patterson & Florez (1969), Virk et al (1967) and Johnson & Barchi (1968)), and Laser doppler anemometer (Chung & Graebel 1972), Goldstein et al (1969), Kumor & Sylvester (1973), Logan (1972), Rudd (1972) and Reischman & Tiederman (1975)) techniques have been used in drag reducing polymer solutions. Although, there were some associated errors in hot film anemometer probe and pitot tube probe measurements, and some uncertainty in bubble tracing technique measurements, their results are generally in agreement with each other and with the laser doppler anemometer results. The general feature of the mean velocity profiles in drag reducing polymer solution is the upward shift (in the semi-logarithmic plot of u^+ against y^+) of the mean velicity profile in the turbulent plug region parall to that of the Newtonian flows.

Comprehensive studies have been done to describe the velocity profiles in drag reducing polymer solutions. One of the earliest descriptions is the two layer model (Meyer (1966), Seyer & Metzner (1969) and Rudd (1969, 1971)) which is characterized by an increase in the thickness of the viscous sublayer. The two layers are

1. a thickened viscous sublayer where,

$$u^+ = y^+ \qquad (1.7)$$

2. a logarithmic region where,

$$u^+ = A \ln y^+ + B + \Delta B \qquad (1.8)$$

where $u^+ = \frac{\overline{U}}{u^*}$ and $y^+ = \frac{y\, u^*}{\nu}$

u^+ and y^+ are the dimensionless mean velocity and distance from the wall, $\overline{U}$ the mean velocity, u^* is the friction velocity, y is the distance from the wall and ν is the kinematic viscosity of the fluid.

Both the constants A and B are the same as in the Newtonian flow. Where ΔB is a new term to describe the upward shift of the logarithmic region in drag reducing solutions. It was emperically related to the shear velocity u^* and the polymer characteristics by

$$\Delta B = \sqrt{2}\delta \log_{10} (u^*/u^*_{cr}) \qquad u^* > u^*_{cr} \qquad (1.9)$$

where, δ is a polymer type and concentration dependent parameter, and u^*_{cr} is the wall shear stress at onset.

Seyer & Metzner (1969) related B with the dimensionless relaxation time θ^+ (sometimes known as Deborah number). This relation was approximated by (Spalding (1972))

$$\Delta B = 1.55\, \theta^+ \qquad o < \theta^+ < 17.1 \qquad (1.10.a)$$

$$\Delta B = 26.5 \qquad \theta > 17.1 \qquad (1.10.b)$$

A three layer model has been introduced by Virk (1971-a) to describe the mean velocity profiles in drag reducing solutions which is characterized by the presence of an elastic layer between the viscous sublayer and the logarithmic region. The three layers are

1. a viscous sublayer with the same thickness as in Newtonian flows,
2. a new intermediate elastic sublayer, and
3. the outermost logarithmic region the same as in the two layer model.

The elastic sublayer is characterized by a universal law derived from the maximum drag reduction asymptote

$$u^+ = 11.7 \ln y^+ - 17.0 \qquad y^+_v < y^+ < y^+_e \tag{1.11}$$

The thickness of this elastic sublayer, which extends from the outer edge of the viscous sublayer y^+_v to the inner edge of the outermost turbulent region y^+_e, is dependent on the value of the drag reduction. It increases with the increase in drag reduction. Eventually, at maximum drag reduction it extends to occupy the whole cross section demolishing the outermost turbulent region. Virk also expressed the upward shift of the mean velocity profile ΔB as

$$\Delta B = \sqrt{2}\,\delta \ln (R^+ / R^+_{cr}) \tag{1.12}$$

δ which is termed 'the slope increament factor', is related to the polymer molecular parameters by

$$\delta = K (c/M)^{\frac{1}{2}} N^{3/2} \tag{1.13}$$

where, K is constant $\simeq 70 \times 10^{-6}$, c is the polymer concentration in wppm, M is the molecular weight of the polymer, and N is the number of backbone chain links in the macromolecule.

The concept of a three layer model have also been adopted by Van Driest (1970) to describe the velocity profile in drag reducing flows. He assumed the existence of a third layer between the usual viscous sublayer and the turbulent logarithmic one, in which the eddying motion is damped by the polymer molecules. He assumed a variable Karman constant k ($A = \frac{2.3}{\sqrt{2}}\ \frac{1}{k}$) dependent on the polymer type and concentration instead of the constant value of 0.0855 in the elastic sublayer assumed by Virk.

Some other models have been proposed to predict a smooth velocity distributions (Spalding (1972), Dimant & Porch (1976), McConaghy & Hanratty (1977) and Tiederman & Reischman (1976). All these models are based on modifying the eddy diffusivity expressions to increase the thickness of the wall damped region. For example, an expression for the eddy diffusivity proposed years ago by Cess (1958), which combines the wall region eddy viscosity expression of Van Driest (1956) and Reichardt's (1951) expression for the centre portion of the pipe flow, has been widely used to describe the velocity distribution in Newtonian flows.

$$\frac{E}{\nu} = \tfrac{1}{2}\{1 + \frac{k^2 R^{+2}}{9} (1 - (\frac{r}{R})^2)^2 (1 + 2(\frac{r}{R})^2)^2 (1 - \exp(-y^+/A^+))^2\}^{\frac{1}{2}} - \tfrac{1}{2} \qquad (1.14)$$

By adjusting the damping constant A^+, this expression predicts the measured velocity distribution in drag reducing flows successfully. Unfortunately this expression fails to express the maximum drag reduction velocity profiles without changing the Karman's constant k (Tiederman & Reischman (1976)).

1.2.6 Polymer Effects on Turbulence Structure

Early measurements of turbulence in drag reducing polymer flows using hot film anemometer probes or pitot tubes are contradictory and unreliable. As mentioned before, these results suffered from errors due to the viscoelastic effects of the polymer solutions. These errors were more pronounced in turbulence measurements than in mean velocity. The only reliable data now are those obtained by Laser doppler anemometer, flow visualization methods, and electrochemical techniques which are free from these viscoelastic errors.

Early measurements of turbulent intensities using LDA technique (Rudd (1969, 1972) and Logan (1972) showed an increase in the streamwise component near the wall but hardly any change in the centre.

The increase in the axial turbulent intensity near the wall is more remarkable in Rudd's data. Both Rudd and Logan used a square tube of 1.27 cm. Laser measurements of turbulent intensities carried out by Goldstein et al (1969) near the transition from laminar to turbulent in a pipe flow (only at the center line) showed no changes due to polymer addition. Chung & Graebel (1972) turbulent intensity results in a pipe flow are, in general, consistant with those of both Rudd and Logan. One of the most interesting results in turbulent intensities is that of Reischman & Tiederman (1975) using LDA technique. Their results in a high aspect ratio rectangular channel showed a little increase near the wall and no changes near the centerline. They envisaged that the large difference between their results and that of Rudd were due to the secondary flows associating the flow near the wall in the square pipe used by Rudd. Kumor and Sylvester (1973) measurements in a flat plate confirmed Rudd's data. Migushina & Usui (1977) measurements in turbulent pipe flow using LDA showed a damping of the axial turbulent intensity near the wall and no changes in the centerline region from that of water.

Due to difficulties in measuring the transverse component of the turbulent fluctuating velocity using LDA, no reliable data ~~is~~ are available except those of Logan (1972). His results indicated that polymer additives seems to suppress the transverse velocity fluctuations near the wall, but it is identically the same as in the solvent in the central core region.

Rudd (1971) measured the spanwise turbulent fluctuating component. From his results, it can be seen that very close to the wall the spanwise component suppressed but increased above its value for the solvent at larger distances. Logan also measured the Reynolds stresses in dilute polymer solution. His results showed that the dimensionless

Reynolds stress ($\overline{u'v'} / u_*^2$) is greatly reduced in the wall region, but no changes from that of water is to be seen in the core region. The observed decrease in the wall region during drag reduction suggests that the polymer molecules reduce the turbulent transport by decoupling the axial and radial velocity components rather than suppressing their intensities.

A few reliable measurements of the turbulent structure in drag reducing polymer flow have been reported. Chung and Graebel (1972) results in a pipe flow using LDA show a similar turbulent energy spectrum in the centreline for both polyox solutions and water. But, near the wall, the low wave number range are higher than those for water flow. Dut to the ambiguty noise associated with LDA measurements, Chung & Graeble results were limited to include the turbulent energy dissipation range. McComb et al (1977) introduced a successful application of LDA to measure the turbulent energy spectrum in drag reducing flows. McComb reported that the intensity and the decay rate of the grid turbulence have been reduced. But at typical drag reducing concentrations, the turbulent energy spectra were the same as those for water.

Achia and Thompson (1977) used laser hologram interferometer to study the turbulence structure near the wall in drag reducing polymer solutions. They reported that the drag reducing additives suppress the formation of the streaks and the eruption of the bursts. Their results indicated that both the sublayer period (bursting time) and the streak spacing had increased by a factor of two to three over the Newtonian value at the same wall shear stress. Wall embedded electrochemical probes (Fortuna & Hanratty (1971, 1972), Shulman et al (1974), Butson & Glass (1974) and Hanratty et al (1977)) have been used to study the turbulence structure in the wall region. Fortuna

and Hanratty (1972) found a strong increase in the transverse spanwise correlation scale as well as a much slower decay in the longitudinal streamwise correlations than in the Newtonian case. Their results in velocity gradient spectrum showed an increase in the low frequency part and a decrease in the high frequency part as the drag reduction increased. Hanratty et al (1977) reported that the most dramatic change observed with the addition of drag-reducing polymers is in the special correlation coefficients and turbulent scales. Butson & Glass (1974) also reported an increase in the turbulence macroscales as measured from the autocorrelations, and no significant changes in the spectral density function.

Donohue et al (1972) and Oldaker & Tiederman (1977) used wall-dye injection for flow visualization to study the structural characteristics of the viscous sublayer in drag reducing flows. These studies have shown that the nondimensional spanwise spacing of the low-speed streaks increases with the increase in drag reduction. Donohue et al reported also that the time between bursts, calculated from the measurements of the bursting rate per unit area in drag reducing flow is the same as in water flow at the same wall shear stress.

In general, the experimental results indicate that the turbulent intensities are not suppressed in the wall region but actually enhanced by polymer addition. The most spectacular change in turbulence structure is the increase in the turbulent scales in both transverse and longitudinal direction, which means an increase in the life time of the big eddies in the wall region. This coupled with reported increase in the streak spacing and the time between bursts leads to a conclusion that polymer additives inhibit the formation of low-speed streaks which yields a decrease in the turbulent momentum transport from the wall to the inner region, hence a reduced Reynolds stresses in the wall region.

1.3 PROPOSED MECHANISMS OF DRAG REDUCTION

Several hypotheses have been proposed to explain the drag reduction phenomenon. So far none is capable of revealing the secrets of the phenomenon and to give a better understanding for the drag reduction. May be, this is because the turbulence phenomenon itself is not yet fully understood. But as a result of the extensive studies through the last two decades, a general picture of the mechanisms can be extracted. In this section a brief discussion about some of these hypotheses will be given.

1. The Shear Thinning Mechanism

This hypothesis was suggested by Toms (1949) to explain his drag reduction results he suggested that there is a possibility of a shear-thinning wall layer in polymer solution flows, which is assumed to be of low viscosity to give the recorded friction reduction. Later on, rheological measurements of effective drag reducers (Polyox and Gaur) showed that these dilute solutions are not shear thinning (Hoyt 1972)). Walsh (1967) showed that drag reduction can be obtained in drag reducing solutions which have shear thickening characteristics. This hypothesis is no longer accepted.

2. The Effective Wall Slip Theory

It was suggested by Oldroyd (1969) to explain the drag reduction by postulating that the tube walls might induce a preferred orientation of the polymer molecules close to the wall in such a way that an abnormally mobile laminar sublayer could arise. The existance of such mobile layer has not been demonstrated.

3. Wall Adsorption Mechanism

The possibility of an adsorbed polymer layer as a mechanism for drag reduction had been first postulated by El'perin (1965). This hypothesis is based on the assumption that a thin layer of adsorbed

or adhered polymer molecules on the wall is formed in the drag reducing polymer flows. By some way this layer interacts with the flow creating a slippery effect at the wall, dampening turbulence fluctuations and prevent the vortex initiation of the wall. Davis & Ponter (1966) have reported a persistence of drag reduction for 15 minutes after switching off the polymer additives to the pure solvent flow. Arunachalam & Fulford (1971) measured the polymer concentration at both the centreline and the wall. They reported an increase in the polymer concentration near the wall. Little et al (1975) reported that their early measurements supported the wall adsorption hypothesis. However, when they repeated the experiments in a transparent pipe with dyed polymer solution, they found that the observed persistance in drag reduction was in fact due to the polymer trapped in the pressure tap connections and slowly diffused back into the solvent flow. Little (1971) showed that while the addition of $Mg\ SO_4$ greatly increase the thickness of the adsorbed films, the observed drag reduction decreases. Finally, they concluded that an adsorbed layer is improbable to perform a major role in drag reduction. Hand & Williams (1973) reported the existence of adsorbed entangled layers of polymers at the flow boundaries which exhibited semi-permanent drag reduction in the presence of solvents. Gyr & Mueller (1974) suggest that the adsorbed layer has a very little effect - if any - in drag reduction. Ayyash & McComb (1976) obtained inconsistent results in their attempts to investigate the effect of the adsorbed layer.

4. Molecular Stretching Hypothesis

Molecular stretching as a mechanism for drag reduction was suggested by Tulin (1966) when he visualized the polymer molecules and found that the molecules became greatly extended in the shear direction. The extended molecules provide a stiffening effect which absorbs energy

from the turbulent eddies (the small eddies) and give it to the main flow as a kinetic energy. The elongated polymer molecules are assumed to interact with the flow and give the drag reduction effect. Virk (1975) suggested that polymer macromolecule extension is involved with one of the turbulent bursting process stages. Lumley (1969, 1973) considered the possibility of molecular extension in order to make the length scale hypothesis more reasonable. He concluded that the polymer molecules are improbable to be fully extended in turbulent shear flow. So, he postulates molecular agglomerations to interact with the sublayer eddies. Millward & Lilley (1974) adopted the molecular expansion of some of the polymer molecules to be of comparable size with the turbulent eddies. Gordon (1970) suggested that the high resistance to stretching caused by molecular expansion inhibits the ejection stage of the bursting process. Ting & Hunston (1977) postulates the same concept as a mechanism for drag reduction. Both Peterlin (1970) and Pfenniger (1967) assumed that molecular stretching absorbes the kinetic energy of the hair pin vortices in the boundary layer, allowing them to grow larger and decreasing the dissipated energy of these microvortices, thus reducing the friction. Almost, all the rheological equations describing the polymer solutions behaviour are based on the assumption that polymer molecules are highly stretched. Yet, there is no direct observation for the molecular stretching in turbulent flows. All molecular stretching observations were in laminar flows, where light scattering technique measurements have shown a slight extension of the polymer molecules (Lumley 1977) and Hinch (1977)).

On the other hand, as it has been discussed before in a separate section, experimental evidence has shown that molecular aggregates are a common feature in drag reducing polymer solutions even at very high dilutions. Furthermore, aggregates may often be formed by shearing the flow (Lumley (1969) and Dunlop & Cox (1977)). Consequently it was

assumed that polymer molecules exist in the solution as tangled balls mostly filled with the solvent, and kept in this agglomerative form by some physical bands. Whether, the polymer molecules exist as individuals or agglomerated, the molecular stretching is necessary to interact with the flow.

5. Anisotropic Viscosity Hypothesis

It was porposed that the polymer solutions have a lower viscosity in the direction of the flow and a higher value in the other directions. This dampens the turbulent fluctuations in these directions (Hoyt (1972)). Many attempts had been done to measure the difference between the normal stress components or to predict them using the known rheological models. Gadd (1966) found a substantial difference in stress components in polyox solutions but polyacrylamide and guar solutions did not exhibit such difference. No other reliable data for normal stress difference are available because most of the work is done at highly concentrated solutions by the drag reduction scale (Patterson & Zakin (1968) and Meister & Biggs (1969)). Therefore no obvious correlation between drag reduction and the normal stress difference results from such changes in viscosity. It is worth noting that this mechanism has been suggested by McComb (1973) to explain drag reduction in fibre suspension flows.

6. Vortex Stretching and Decreased Turbulence Production Mechanism

This mechanism is now widely accepted as the most successful one. It was suggested by Gadd (1965) that drag reduction involves a decrease in turbulence generation. He assumed that polymer molecules or aggregates increase the stretching resistance of the vortices in the wall region. The reduced vortex stretching reduce the mixing and dampen the turbulent eddies. This hypothesis is supported by the well experimentally documented increase in the flow resistance to stretching with the addition of drag reducing polymers.

In Newtonian flows it is well known that the extensional viscosity (a property which represents the flow resistance to stretching) is three times the shear viscosity. In drag reducing polymer solutions, the extensional viscosity is reported to be orders of magnitude higher than the dynamic viscosity depending on the stretch rate and the molecular characteristics of the polymer. Oliver & Bragg (1973) measurements showed an increase in the extensional viscosity of polyox and separan AP-30 as high as three orders of magnitude that of shear viscosity. Balakrishnan & Gordon (1975) reported an extensional viscosity of 1500-3000 times the shear viscosity measured for a 20 wppm solution of separan AP-30 at stretch rate 4000 - 11000 sec^{-1}. Metzner & Metzner (1970) measured an extensional viscosity of several thousand times the shear viscosity for a 100 wppm polyacrylamide solutions. The increase in extensional viscosity of drag reducing polymer solutions has been also predicted using rheological models. (Ting & Hunston (1977), and Little et al (1975)).

On the other hand, numerous experiments by various investigators have shown that the dominant feature of the near wall region in a turbulent flow is a streaky structure which is caused by a spanwise variation in the streamwise velocity component, and moving with low speed in the near wall region. Periodically, individual streaks lift away from the wall into the buffer region, where it oscillates and then breaks up to be ejected away violently from the wall region (Kim et al (1971), Klinc et al (1967), Rao et al (1971), and Offen & Kline (1975)). The turbulence production cycle is to be completed with a inrushing or sweeping process in which a sweep of high velocity fluid moves towards the wall just after the low speed streaks has been ejected outwards from the wall (Corino & Brodley (1969), Wallace et al (1972), and Kim et al (1971). In fact these streaks are formed as

a result of the counter rotating spanwise vortex system whose axes are in the streamwise direction. Kline et al (1967) suggest that the stretching and compressing of these vortex elements in the wall region creates local high and low speed zones. The low speed zones is what we actually see as streaks. The bursting process is well known to consist of three stages, low speed streak formation and lift up into the buffer region, rapid growth with oscillation and finally break up with violent ejection. Offine & Kline (1975) suggested that the first two stages of the burst, process are associated with vortex stretching.

As a result, one can suggest that polymer molecules or aggregates inhibit the bursting process which is responsible for the turbulence generation. Kim et al (1971) showed that most of the turbulent energy is generated during the bursting process. A decrease in turbulence production in drag reducing flows has been suggested by many research workers (Walsh (1967), Gordon (1970), Peterlin (1970), Black (1969) and Gyr (1968)). Johnson & Barchi (1968) showed that the polymer decreases the production of small eddies. Fortuna & Hanratty (1972) using an electrochemical technique measured an increase in the low speed streak spacing higher than that for Newtonian flow at the same shear stress. Eckelman et al (1972) reported the same increase in the low speed streak spacing in drag reducing flows. These results indicate that the turbulent energy production per unit area has been reduced with polymer addition. They have reported also a decrease in the decay time of the streamwise correlation in drag reducing flow compared with Newtonian flow. One can conclude that the life time of the big eddies in the wall region increases with the presence of polymers.

Donohue et al (1972) used a dye visualization method to study the wall region behaviour in drag reducing flows. They found that the time between bursts is the same as that for Newtonian flow at the reduced wall shear. However, the streak spacing is significantly increased even at the reduced wall shear. Achia & Thompson (1977) investigated the structure of wall turbulence in drag reducing pipe flow using laser hologram interferometer visualization technique. They showed that drag reducing additives suppress the formation of the streaks and the eruption of bursts. They reported an increase in both the streak spacing and the bursting time over the same values for Newtonian flows at the reduced wall shear stress. Meek & Baer (1970) measured the sublayer growth time in a drag reducing pipe flow using the auto-correlation technique. They found an increase of the bursting time over that for the pure solvent at the same wall shear stress. Mizushina & Usui (1977) used the auto-correlation of LDA signal to measure the bursting time in a drag reducing pipe flow. Their measurements showed that the bursting time is in a good agreement with the above reported results. A recent study by Oldaker & Tiederman (1977) using dye visualization revealed that the length of the low speed streaks in drag reducing flows is much longer than the average streak length in a water flow at equal shear velocity. Conceivably, the enhanced elongational viscosity has a strong influence on the structure of the longitudinal vortices appearing in the wall layer. In particular a strong resistance to vortex stretching would be expected. Consequently an increase in the streak spacing and the time between the bursts occur resulting in a decrease in the turbulent energy production.

1.4 SCOPE OF THE PRESENT WORK

In the previous sections, a general discussion of some aspects of the drag reduction in turbulent shear flow was presented. The main purpose in this section is to present an introduction to our work namely drag reduction in turbulent shear flow due to injected polymer solutions. In this introduction we review the relevant work conducted previously by other authors. Then, a general arrangement of the thesis will be presented to end the present chapter.

1.4.1 Drag reduction by Injection of Drag Reducing Polymers

It has been suggested that polymer molecules (or aggregates) causing turbulent drag reduction exert their main influence in the near-wall region, and the presence of the polymer in this region is essential. Experimental evidence, both direct and indirect, shows that the significant changes in the flow due to the polymer additives occur in the flow very near to the wall. In this region, containing the viscous sublayer and the buffer zone, the polymer-turbulence interaction responsible for drag reduction is supposed to take place.

We have seen in the previous sections, that most of the observed effects due to drag reduction are localized in the near-wall region. Mean velocity profiles, especially at low drag reduction, show that the most effective region is just outside the viscous sublayer while the core is being unaffected and just shifted up. Turbulence intensity and correlation measurements were seen to exhibit the same features. It has been shown by most of the investigators that the most dramatic changes in the flow structure due to drag reducing polymer additives are in the streaky structure, the bursting time, the spatial correlations and the turbulent scales in the boundary layer (Oldaker & Tiederman (1977), Hinch (1977) and Hanratty et al (1977)). Therefore, one can reach the conclusion that their indirect experimental evidence indicates that

polymer should reach the near-wall region in order to reduce the skin friction in turbulent shear flow. But, does this mean that polymer outside the wall region has no influence upon drag reduction? Does polymer-turbulence interaction in the core region produce drag reduction?

In order to give a satisfactory answer a direct experimental evidence should be made available. This evidence would be seen when polymer is locally introduced into or outside the near-wall region. An attempt has been made to obtain this direct evidence by injecting polymer solution into a turbulent water pipe flow (Wells & Spangler (1967)). It was found that the wall shear stress was reduced directly downstream of the injection point when the polymer was introduced in the wall region. Conversely, when the polymer was injected into the turbulent core, no reduction in the skin friction was observed until the fluid diffused into the wall region. This experiment qualitatively has proved the fact that polymer-turbulence interaction responsible for drag reduction is localized in the near-wall region. Since that time some investigations have been conducted by injecting polymer solutions into the near-wall region to study the drag reduction phenomenon. Most of the injection studies were carried out on external flows over a flat plate or a body of revolution. The effects of different parameters upon drag reduction by injecting the polymer in the wall have been investigated.

Love's (1965) was the earlier work to report a drag reduction by injecting polyox solution from wall slots in the both sides near the leading edge of a flat plate. His results showed that increasing the flow rate and the concentration of the injected solution reduce the effect. Johnson & Barchi (1968) injected concentrated polyox into the wall of a flat plate. Their wall shear stress measurements indicated

that polymer is most effective when it is concentrated in the wall region where, a significant damping in the small eddies have been found. Latto and Shen (1970) observed that the angle and the velocity of polymer injection into the wall region have a pronounced effect on the local skin friction reduction. Wu (1969, 1971) made a complementary analysis of his results and Love's results and showed that the optimum ejection rate corrosponds roughly to the discharge within the inner boundary layer. Later Wu & Tulin (1972) results indicated that the optimum ejected polymer concentration is 100-1000 wppm in smooth surface and one order of magnitude larger for rough plates. They investigated the effect of slot opening, ejection angle and ejection flow rate. They found that the most effective drag reduction was obtained with small angle of injection to the flow direction, an opening size compared with the thickness of the viscous sublayer, and flow rate of ejected polymer solution the same as the viscous sublayer flow rate. Experimental evidence showed that drag reduction achieved by injecting polymer solutions is highly dependent on diffusion and mixing rates with the near wall region flow.

Several investigations have been made to study the diffusion process of the injected polymer solution. Wu (1972) measured the concentration of the polymer in the wall region by ejecting a dyed polymer solution from a slot at the leading edge of a flat plate. The results indicated a suppressed turbulent diffusion of the polymer solution. Latto & Shin (1970) reported a decrease in the eddy diffusivity in the near-wall region as a result of polymer solution, at different correlations, into pure water boundary layer over a flat plate. They developed a correlation relating the drag reduction achieved with the concentration of the polymer at the trailing edge resulting from the diffusion process.

On the other hand, polymer injection into the wall region of a turbulent pipe flow have received more attention in order to investigate the optimum use of polymers as drag reducers, and to find out a satisfactory mechanism for drag reduction. Maus & Wilhelm (1970) reported that there are no differences between drag reduction by injecting polymer solution into the wall region and the homogeneous polymer solution flow. An increase in drag was shown just downstream from the injector due to introducing high viscosity polymer solution into the boundary layer. Walters & Wells (1971, 1972) investigated the drag reduction and the turbulent diffusion for uniformly distributed injection of polymer solution through a porous wall adjacent to a fully developed pipe flow. Polymer effectiveness as a drag reducer was found to be highly dependent on polymer diffusion. They measured the polymer concentration using a fluorescers tracer mixed with the injected polymer solutions. Their results showed that the turbulent diffusion has been greatly reduced near the wall region by one to two orders of magnitude less than the Newtonian flow values. Walters & Wells suggested that there was a critical shear region, where the polymer-turbulence interaction is greatly effective in reducing the drag. This region was estimated to extend over $y^+ = 10 - 80$, where the magnitude of the turbulence production and dissipation have been found to be maximum (Laufer (1953) and Lawn (1971)). Ramu & Tullis (1974, 1976) studied the drag reduction obtained with polymer injection into a developing axisymetric boundary layer in the inlet region of a pipe flow. The experiments were conducted in a 12 inch diameter commercial steel pipe. Ramu & Tullis results show that drag reduction increases to a maximum, sometimes in excess of 90%, just downstream the injector, and then levels off to the homogeneous flow drag reduction value. The average drag reduction achieved was found to be dependent

on the amount of polymer injected and totally independent upon the concentration and velocity of the injected solution. Increasing the Reynolds number increased the drag reduction produced until a maximum was reached, then further increase in flow rate decreased the effectiveness of the polymer.

While it is generally agreed that polymer molecules (or aggregates) causing turbulent drag reduction exert their main influence in the neighbourhood of the wall. The evidence for this tends to be rather indirect. The only attempt to obtain the direct evidence made by Wells & Spangler was incomplete as their measurements were limited to 20 diameters downstream the injector. They used a dilute guar gum solution of concentration 1000 wppm, and 100 wppm solution of copolymer of polyacrylamide and polyacrylic acid. But, a later use of injection techniques has produced contradictory results (Vleggaar & Tels (1973-a,b), Stenberg et al (1977)). Vleggaar & Tels (1973-a,b) injected a concentrated Polymer solution (separon AP-30, 5000 wppm) into the core of a water pipe flow. Pressure measurements were taken 60 tube diameters downstream from the injector and over 110 diameters. Results of drag reduction using polymer injection were higher than those achieved in homogeneous polymer solution. The difference is substantially high at low Reynolds numbers and low average polymer concentration. An interesting result achieved by injecting concentrated polymer solutions is the disappearing of the onset shear stress which makes polymer more effective at low flow rates. Their flow visualization showed that the injected polymer had formed a long polymer thread which persist over a distance of more than 200 tube diameters. They concluded that polymer thread would affect the large eddies in the core, thus reducing the turbulent kinetic energy. Stenberg et al (1977-a,b) investigated the effect of premixing on drag reduction. They injected concentrated polymer

solutions (Polyox WSR-301, 1000, 2000 wppm) into a water pipe flow at the inlet of the pipe via a rotating impeller mixer. Drag reduction measurements were taken when the mixer was not in operation and when it was operating at different speeds. Their results with poor mixing showed the same trend as Vlegaar & Tels results, concerning the disappearance of the onset drag reduction. However, with good premixing of the concentrated solution with the flow, the normal behaviour of the homogenous solutions were retained. Dye visualization and schlieren photograph studies revealed the presence of small visible polymer strands which disappear with premixing into smaller polymer agglomerations.

The drag reduction results obtained by injecting concentrated polymer solutions into the core of turbulent pipe flow gave contradictory results with the concepts of the drag reduction. In order to clarify these contradictions and to find out a better understanding for the phenomenon, this work was designed to investigate the drag reduction using the injection technique, into both the core and the wall regions of water pipe flow.

1.4.2 General Arrangement of The Thesis

In the previous sections of this chapter, we have introduced the phenomenon of drag reduction by reviewing most of its tackled aspects. In the following chapters of this thesis we present the results of our investigation of the drag reduction by injecting a relatively concentrated polymer solutions into both the core and the wall of a turbulent pipe flow of water.

The next chapter will include a description of the experimental set-up and techniques. Following this, we present the results of our investigation in the next four chapters; the first one will be for discussing the results of the turbulent diffusion of the injected polymer solutions. This is followed by the second chapter which

contains the results of drag reduction by injecting the polymer solution into the centreline of the water pipe flow. At the end of the chapter the correlation between polymer concentration measurements and the drag reduction data will be discussed. A discussion of the drag reduction results by wall injection compared with the centreline injection results. The fourth chapter of the results will be for mean velocity profile and turbulent structure measurements using LDA technique

In the last two chapters of this thesis a general discussion of the results will be given. Then, the summary of the results and the conclusions drawn from the study will be provided.

CHAPTER II

THE EXPERIMENTAL SET-UP

2.1 INTRODUCTION

The main object of the investigation was to study the drag reduction by, and the turbulent diffusion of, concentrated drag reducing solutions injected into the centre-line and the wall of a turbulent shear flow. One of our aims was to reveal the differences, if any, between the heterogeneous drag reduction by the injection techniques and that of the homogeneous polymer solutions. Another aim of this research is to measure the mean and the turbulent velocity profiles using the laser doppler anemometer (LDA) technique, and to study any associated changes in the turbulent structure due to the injection of concentrated polymer solutions.

In order to satisfy the basic requirements of this project, an experimental set-up was constructed. The experimental installation basically consisted of the water flow rig, the polymer injection system, the polymer concentration measurement system and the laser doppler anemometer set-up.

In this chapter, we will describe two main parts of the experimental set-up, namely the water flow rig and the polymer injection system. This will be followed by presenting the calibration of the instruments and the results of testing of the experimental set-up. The description of the polymer concentration measurement system and the laser doppler anemometer system will be presented in appropriate chapters.

2.2 THE WATER FLOW RIG

The water flow rig is the basic part of the experimental installation. The rig is mainly a long pipe flow system. The working section was constructed long enough in order to avoid the limitations of the Wells and Spangler (1967) measurements as we have discussed in chapter I. It was also provided with large number of pressure taps to carefully monitor the development of the drag reduction in the flow direction. This enabled us to improve on the gross measurements of drag reduction by injecting concentrated polymer solutions into the centreline of a pipe flow carried out by Vleggaar and Tels (1973 - a, b), and present a more detailed picture of the development of the drag reduction. The system also has the facility of measuring the concentration profiles at any section in the flow. The use of the laser doppler anemometer to measure the velocity and the turbulence structure of the flow has been taken into consideration in the design of the flow rig.

A complete elevational view of the water flow rig and the injection pump is shown in figure (2.1). The flow diagram of the system is also provided in figure (2.2). The flow diagram shows that the water is supplied to a constant head overflow tank from the laboratory's mains system. A centrifugal pump is used to pump the water from the supply tank to the test section through a settling chamber and an entrance length to ensure a fully developed flow in the test section. The piping system at the flow outlet is designed in such a way that the flow can be recirculated or disposed of to the laboratory's drain through a small overflow tank.

The Flow system is supplied with four gate valves of one inch size in order to control the flow in the system. The location of these valves in the flow is shown in figures (2.1) and (2.2). One was constructed just downstream of the pump to control the flow rate. In order to control the flow direction allowing the rig to be used as an open flow or a closed flow system, two valves were fixed at the end of the second pass as shown in figures (2.1, 2.2). The fourth valve was fixed to control the mains supply.

The supply tank was a steel box of 95 x 40 x 60 cm. A baffle plate was welded inside the tank to make it a constant level overflow tank of 75 x 40 x 50 cm^3 capacity. The overflowed water in the supply tank was drained using a flexible PVC tube of 3 cm I.D. The supply tank was provided with a level indicator to show the water level inside its two compartments.

The flow was pumped from the supply tank by a EURAMO centrifugal pump model 1220. The pump was fitted with 0.5 hp AC motor operating on a power supply 220/1/50. The maximum head of the pump was 7 m and the maximum flow rate of zero head was 9.0 m^3/hr. In order to isolate the mechanical viberation of the pump from being transmitted to the system, the pump was fixed to a vibration absorption bed. For the same purpose all the connections between the pump and the system was made of flexible PVC tubing (see figure (2.1)).

The purpose of constructing the settling chamber was to dampen the flow rate variations due to the variation of the speed of the pump. The chamber was made of a Perspex tube of 12 cm I.D., which allows an area ratio of 1 : 20, and of 30 cm long. The chamber was built close to the pump outlet and was supplied with vent and drainage valves.

The test section was connected to the settling chamber by an entrance section made of rigid PVC tube. The entrance section tube had an inner diameter of 26 mm and an outside diameter of 32 mm. It was made of three pipe sections of 70, 105 and 105 cm long respectively. The three pipe sections were connected together with two 90° elbows forming a U-shaped pipe section (see figure 2.1). This section provided an entrance length over a hundred pipe diameters which ensures a fully developed flow in the test section.

The working section in this investigation was a two pass pipe flow system (see figures (2.1, 2.2). It was made of Perspex pipes of 26 mm I.D. and 32 mm O.D. Its total length was 10 metres forming a two pass horizontal continuous pipe flow. The first pass was 6.0 m long and the second pass is 4.0 metres long. The two passes are connected together by a U-shaped connection making the two passes parallel and horizontal. The level of the second pass was 10 cm higher than that of the first pass in order to allow for laser doppler anemometer measurements. The first pass was formed by flanging two pipe sections together. The length of each section was 3 metres. This six metre long pipe represented the test section in the first pass. The second pass was composed of two pipe sections, two metres long each, flanged together. The pipe flanges were carefully machined to ensure smooth joints free of disturbances. The polymer injector was flanged to the pipe flow system just upstream of the test section in the first pass. (see figures (2.1) & (2.2)).

The first pass of the working section was supplied with 18 pressure taps. All the taps were carefully machined to avoid disturbances to the flow. The first tap was located 5 cm downstream

from the injector position. Downstream from the first pressure tap, ten taps were located at successive distance of 30 cm each. These taps were followed by 7 taps at successive distance of 40 cm each. This distribution of the pressure taps covered the whole length of the test section in the first pass, which allowed us to investigate with sufficient accuracy the development of the drag reduction over a distance of 220 pipe diameters downstream from the injector. In the second pass, only two pressure taps were fixed in order to monitor the drag reduction at the end of the test section in the second pass. One of the two taps was located 50 cm upstream at the end of the second pass, and the other tap was 100 cm upstream from the first one.

The pressure tap hole was a fine drilled hole of 1.0 mm diameter to minimize the disturbance in the wall surface. A small perspex tube section (3 mm I.D., 5 mm O.D. and 10 mm long) was cemented to the pipe wall such that the tap hole was centralized in the small tube cross section (see figure (2.3-a) which represents a sectional view of the pressure tap). The pressure taps were connected to a group of scanning valves by transparent silicon rubber tubes. The output from the scanning valves was connected to a DISA differential pressure transducer. The scanning valves permitted the measurement of the pressure drop between a reference tap downstream.

The pressure transducer used was DISA low-pressure transducer model 51 D20. The transducer was of the capacitive type. In this type of transducers the deflections of the diaphragm inside the transducer, caused by a pressure acting on it, are converted into capacitive variations. The capacitive variations are converted into analogue voltage output by means of a frequency modulation

process. The set-up of the transducer and its electronic system is shown in a schematic diagram in figure (2.3.6). The pressure under measurement was applied to the diaphragm of the transducer 51 D20, which in turn was connected to a tuning plug : 51 E03. The transducer and the tuning plug together form a resonant circuit which modulate the frequency of the oscillator 51E02 according to the change of the transducer capacitance. The modulated frequency output of the oscillator, which is proportional to the pressure difference applied to the transducer, is fed to the reactance converter 51E01. The reactance converter output is an analogue DC voltage which is proportional to the pressure applied to the transducer. (For more details see DISA Capacitive measuring equipment instruction and service manual (1974)).

The operating pressure range of the transducer depends upon the thickness of its diaphragm. Therefore, the transducer was provided with a set of ten diaphragms for use at different pressure ranges. The transducer covers wide ranges of pressure measurements from such a small range as 3 cm of water to a high range of 196 metres of water head.

The pressure transducer was calibrated in order to determine the constant of proportionality between the applied pressure difference and the corresponding D.C. output voltage. This calibration was carried out using a static pressure head according to the calibration procedure detailed in the DISA capacitive measuring equipment instruction and service manual (1974). This procedure was normally carried out at different intervals to check the calibration of the instrument.

The flow rate of the water in the system was measured using a calibrated orifice meter. The orifice meter was flanged to the pipe system downstream from the pump (see figures (2.1) & (2.2)). A sectional view of the orifice meter is shown in figure (2.4). It was made of steel plate of 15 mm I.D. 65 mm O.D. and 2.5 mm thickness. The plate was fixed between two steel flanges of 26 mm I.D. 65 mm O.D. and 15 mm thickness each. The two flanges were machined such that each had a groove connected to a pressure tap to measure the static pressure just before and after the orifice plate. The two pressure taps were connected to a DISA transducer system to measure the pressure difference across the orifice plate, and consequently measuring the flow rate.

2.3 THE POLYMER INJECTION SYSTEM

The polymer injection system is the second major part of the experimental set-up in this investigation. It consisted of the polymer injection pump and the injectors. Both were designed to satisfy the requirements of this study. In this section we will discuss in detail the design of the system. First let us start with the injection pump.

2.3.1 The polymer injection pump

When polymer solutions subjected to high shear stresses, they lose some of their effectiveness in reducing the turbulent drag. This process is known as shear degradation. In order to avoid such difficulty, researchers in drag reduction resort to pump the polymer solutions using methods which minimize the shear degradation. The most common methods are pressurized tanks or gravity feeding systems. We used the gravity feeding system to inject the polymer solutions in the early stages of this work but it proved to be cumbersome and the results obtained unreliable.

Therefore, an injection pump operating on the principle of positive displacement and capable of handling large quantities of polymer solution was designed, built and used through out the whole work.

A plan view of the pump and the driving mechanism is shown in figures (2.5). The cylinder was made of a Pyrex glass tube of 154 mm inner diameter, 180 mm outer diameter and one metre long. The cylinder head is made of aluminium alloy plate. It was fitted with two, $\frac{1}{2}$ inch size, globe valves to control the polymer inlet and outlet. The cylinder head was also fitted with a safety valve to protect the pump from any unexpected pressure increase inside the cylinder. Figure (2.6) shows a sectional view of the pump and the driving mechanism. The diagram also shows the details of the cylinder head assembly with the cylinder.

The piston head was machined from Aluminium alloy and sealed against the cylinder wall by composite PTFE/rubber rings. This efficient sealing ensured that the injection rate was entirely governed by the rate of the piston travel. This in turn was controlled by the travel of a threaded steel rod. The threaded rod was 25.4 mm diameter and one metre long, and was provided with 8 threads per inch. A Key-way groove was cut along the rod to allow only sliding motion relative to the driving nut. Three guiding rods were fixed to the piston head in order to prevent any rotational motion of the piston and allow only for a sliding motion. Each of these guidance rods was made of steel rod of 10 mm diameter and one metre long. The details of the piston head assembly is shown in figure (2.6).

The driving system of the pump is shown in both figures (2.5) & (2.6). A D.C. motor drives a rotating nut through a chain drive system. The rotating nut drives the threaded rod to move forward or backward. According to the direction of the nut rotation the piston head moves forward injecting the polymer solution or backward sucking the polymer solution to fill the cylinder with the solution. The nut was made of brass and fitted into the sprocket wheel. The brass nut had an outer diameter of 37 mm and 60 mm long.

The chain drive system was composed of 4 sprocket wheels. Two of these wheels had 57 teeth each, one of 17 teeth and one of 13 teeth. The sprocket wheels were interchangeable to give a wide variety of speed changes.

A D.C. geared motor of $^{1}/_{3}$ hp at 4 r.p.m. (Normand Electrical Co. Ltd.) was used to drive the injection pump through the chain system. The maximum input voltage to the motor was 24 D.C. volts and input current was 10.5 amp. maximum. The use of a D.C. motor gave the advantage of reversing the motor direction of rotation by reversing the supply voltage polarity. The motor output speed could also be varied continuously by varying the input voltage. The D.C. motor was supplied from a D.C. power supply. The output voltage of the power supply was controlled by controlling the A.C. input voltage which was governed by an autotransformer (variac).

Throughout the experimental work of this investigation two sprocket wheels only were used. A 57 tooth wheel was fitted to the motor shaft, and the other of 13 teeth fitted to the driving nut. This arrangement gave a polymer flow rate in the range of 1.0 to 18.0 cc/sec. This range of polymer flow rates covered satisfactorily the needs of the experiments. The capacity of the

cylinder pump is 15 litre. Therefore, the shortest time for the injection stroke was about 15 minutes, which means that the pump can operate continuously injecting the polymer solution for a quite enough time to do the experiments and to take the measurements without changing the experimental conditions by stopping the experiment to recharge the pump.

The drive mechanism of the injection pump was supplied with an automatic switching system to control the stroke of the pump and to reverse the direction of motion.

2.3.2 The polymer injectors

In this work two types of the injectors were used. The centreline and the wall injectors. Both types were carefully designed to fulfil the special requirements of the experiments.

In designing the centreline injector, two matters were taken into consideration. The first matter was that the diameter should be as small as possible to act as a point source for polymer turbulent diffusion study. A small injector was also necessary for allowing the drag reduction by the injected polymer solution to develop gradually to its maximum value over a long distance to permit a careful and accurate study of the phenomenon. It was also required in order to minimize the disturbance of the flow due to the injector itself. The second matter was that polymer solutions are shear degraded, therefore the injector diameter should be large enough to obtain low shear stresses. In both cases the injector should be free of sharp edges.

In order to satisfy the above requirements, a centreline injector was designed as shown in figure (2.7). The injector was made of a stainless steel tube which was bent through 90^{o} at the

pipe centreline to deliver the solution in the streamwise direction. The injector tube had a 2.3 mm inner diameter, 3.0 mm outer diameter and 30 mm long in the direction of the flow. A streamlined body of 25 mm long was attached to injector and carefully finished in order to allow a minimum disturbance due to the injector. The injector was fitted into a Perspex hollow flange as shown in the sectional view of the injector in figure (2.7). The flange had 26 mm inner diameter, 65 mm outer diameter and 16 mm thickness. The injector was flanged to the pipe system just upstream of the test section.

It has been mentioned before that one of the main objects of this investigation was to study the effect of injecting the polymer solution into the wall region. It was also one of our aims in this study to show how does the drag reduction by wall injection developing compared with that of the centreline injection.

A slot type wall injector was constructed to deliver polymer solutions into the wall region. It was simply, two Perspex hollow discs machined such as an inward circumferencial gap was formed when they were assembled together. The two discs were separated by a paper gasket for sealing. A constructional drawing for the injector is shown in figure (2.8). The inner diameter of the injector was 26 mm and the outside diameter of 130 mm. The slot was inclined to the flow direction with 8° which allows the solution to be introduced as tangential to the wall as possible. It was also recommended to keep the injection angle small in order to minimize the flow disturbance due to injection. The slot width in the direction of the flow was 4 mm. However, the slot width can be changed by changing the chickness of the paper gaskets. The injector was supplied with two flanges on both sides in order to allow it to be assembled with the pipe system.

2.4 FLOW RATE CALIBRATION

In the previous sections, we have mentioned that the water flow rate in the pipe system was measured using an orifice meter. It is one of the common devices to measure the discharge rate in pipe flows and is characterized by its simplicity. It is also easy to construct and its performance is not sensitive to the pressure tapping position (Gastorek & Carter (1967)). A sectional view of the meter is shown in figure (2.4). The technical construction was discussed before.

The operating principle is based on the fact that the flow rate across the orifice plate is proportional to the static pressure difference between the taps. This can be deduced by applying Bernoulli's equation to a point upstream and another point just downstream the orifice plate (Duncan, Thom and Young (1970)).

$$Q = Cd \frac{\pi}{4} d^2 \sqrt{\frac{2g}{((\frac{D}{d})^4-1)}} \Delta H = K\sqrt{\Delta H} \qquad 2.1$$

where Q = the flow rate in cc/sec.

ΔH = the static pressure head difference across the orifice plate in cm water

K = constant

d = the orifice diameter

D = the pipe diameter

Cd = discharge coefficient

The constant K in equation (2.1) is experimentally determined by calibrating the orifice meter. The calibration was done using two different methods and was checked from time to time. The two methods were.

1. The first method was to allow a certain volume to be discharged from the supply tank. This method was carried out as follows:-

   After the control valves had been adjusted to the required position, the mains supply to the supply tank was shut allowing the water to be discharged from the tank.

   When the water level in the tank reached a certain level, the stop watch was started and the recording of the pressure drop across the orifice plate started. When the water level reached a certain lower level on the level indicator, the stop watch was stopped and the pressure recording stopped. The time required for a certain volume to be discharged was recorded and the flow rate calculated. A number of pressure drop measurements across the orifice were recorded and an average value was calculated.

2. The second method was to weigh the collected water discharged in a certain interval of time

A series of calibration tests at different flow rates was carried out so as to cover the whole range of the flow system. The results were plotted as water flow rate Q in cc/sec against $\sqrt{\Delta H}$, where ΔH is the static pressure head difference across the orifice plate in cm of water. The calibration graph is presented in figure (2.9). From the slope of the straight time in the graph, the value of K is determined. Hence, equation (2.1) becomes:

$$Q = 140.9 \sqrt{\Delta H} \qquad (2.2)$$

2.5 TESTING THE RIG PERFORMANCE

The flow system has been designed to investigate the turbulent diffusion and the drag reduction of relatively concentrated polymer solutions injected into a fully developed turbulent pipe flow. In order to satisfy the basic requirements of the investigation, the flow in the test section should be fully developed and turbulent over a wide range of Reynolds numbers. In this section we will discuss the capability of the system to satisfy these requirements.

2.5.1 Flow Development in the Test Section

The fully developed region in the flow is characterized by the fact that the cross sectional velocity profile is the same for all sections. Consequently, the flow conditions are independent of the section location in the flow. Since the velocity profile is constant, it follows that the pressure gradient has a constant value in the region of fully developed flow. To reach the fully developed region, the flow passes through a certain pipe length which extends from the pipe entrance. This region is usually termed the entrance length, where the velocity profile across the pipe continuously changes with the distance downstream. The length of this entrance region depends on the flow conditions and the pipe entrance conditions. For practical purposes, a value of 40 pipe diameters is recommended by Hinze (1975) as a minimum value. A value of 50 pipe diameters is suggested by Schlichting (1960) as a good value for the entrance length.

In section 2.2 we mentioned that the test section is located about a meter downstream from the entrance to the horizontal pipe section, and a further distance of 1.8 metres down stream from the settling chamber. This distance allows over one hundred pipe

diameters as an entrance length to the test section with an adequate horizontal distance of about 40 pipe diameters before the test section to settle down any secondary flows due to the 90^{o} turn in the flow direction.

In order to check the fully developed flow in the test section, the pressure gradients at different sections in the test section were measured for different flow rates (Hussain & Reynolds (1975) and Laufer (1953)). At each flow rate the pressure drops between a reference pressure tap and the other taps distributed along the whole length of the test section were measured. The reference point was the first tap in the test section which is 5 cm downstream from the beginning of the test section. A sample of the experimental results is shown in figure (2.10). The figure shows the pipe pressure drop as a function of the distance downstream the reference point. The linearity of the pressure drop with the distance suggests that the mean velocity profile was fully developed in the test section. The suggestion is based on the fact that the axial pressure gradient is uniquely related to the slope of the mean velocity profile at the wall.

2.5.2 The System Performance in a turbulent Water Flow

Before any polymer measurements were carried out, the performance of the flow system in water had been tested. Because newtonian flow in pipes is well established, the comparision between the system results and the well known results checks the system performance.

The experiments were carried out covering most of the operating range of the flow rates. For each experiment, the pressure drops from the reference tap were measured for all the taps. The pressure drop as a function of distance was plotted in a graph similar to figure (2.10). The slope of the straight line is the value of the pressure gradient $\frac{dp}{dx}$. The water flow rate Q was measured through measuring the pressure drop across the orifice meter. Then, the wall shear stress τ_w is calculated from $\frac{dp}{dx}$ as:

$$\tau_w = \frac{D}{4} \frac{dp}{dx} \tag{2.3}$$

Hence, the wall shear velocity u^* was calculated from

$$u^* = \sqrt{\frac{\tau_w}{\rho}} \tag{2.4}$$

From the measured flow rate the average velocity was calculated as

$$\overline{U_{av}} = \frac{4Q}{\pi D^2} \tag{2.5}$$

Consequently, the friction factor f and the Reynolds number Re were calculated as

$$f = 2\left(\frac{u^*}{\overline{U_{av}}}\right)^2 \tag{2.6}$$

$$Re = \frac{\overline{U}av\ D}{\nu}$$

where ν is the kinematic viscosity of the flow

The results of the ten experiments were plotted in figure (2.11). It shows good agreement with Prandtl - Karman Law.

$$f^{-\frac{1}{2}} = 4.0\ (Re.f^{\frac{1}{2}}) - 0.4$$

The results are also presented in table 2.1. These results show that the system operates satisfactorily over a wide range of Reynolds numbers. A maximum flow rate of 1.4×10^3 cc/s can be achieved which allows a Reynold number as high as 6×10^4.

2.6 PREPARATION OF DRAG-REDUCING POLYMER SOLUTIONS

Throughout this investigation two polymers of two different groups were used. One was of the Polyacrylamide group manufactured by DOW Chemicals under the trade name Separan AP-30 of molecular weight 3×10^6 as estimated by the manufacturer. This polymer is efficient drag-reducer in turbulent shear flows, and forms an ionic solution. The other was of the polyethyeleneoxide group which is manufactured by Union Carbide under the trade name polyox WSR-301. It has a molecular weight of 5×10^6 as estimated by the supplier and considered as one of the strongest drag-reducing polymers in turbulent shear flows. This group forms non-ionic polymer solutions. Both the polymers are supplied by the manufacturers in powder form.

As will be discussed in the next chapter, the polymer solutions injected into the pipe flow contained a certain percentage of common salt (NaCl). The salt was added to the polymer solution to act as a tracing material in the diffusion studies of these solutions when they were injected into the pipe flow. A few percent of common salt was added (0.20% - 0.25%) to keep its effect, if any on the drag reduction properties as small as possible. (this will be discussed in both chapters III & IV). This percentage of salt was kept constant for all solutions used throughout this investigation whether it was for turbulent diffusion studies, for drag reduction studies or for LDA measurements in order to cancel the salt effect, if any when comparing these results together.

In preparing the polymer solutions, the required percentage of salt was dissolved in tap water in plastic drums of 90 litre capacity. The polymer was sprinkled evenly on the surface of the salted water solution in the drum and then left for some time to

soak. The solution was then stirred up manually using a wooden stick or mechanically using the stirrer used before by Ayyash (1978). Our experimental observations showed that there is no difference between using the mechanical stirrer or the wooded stick. After checking the homogeneity of the solution by eye, it was used within two or three days to avoid any effect for the aging of the solution.

TABLE 2.1.

Test No.	$\frac{dp}{dx_3}$ N/m	Q c.c/s	$\bar{U}_{av}$ m/s	τ_{w_2} N/m	u* m/s	Re	$fx10^{-3}$ test	$fx10^{-3}$ P.K. Equ.
1	102.2	213.0	0.40	0.664	0.0258	7,812	8.260	8.233
2	136.2	250.	0.47	0.885	0.0298	9,052	8.013	8.099
3	186.5	290.	0.55	1.21	0.0348	10,500	8.007	7.804
4	332.0	415.	0.78	2.16	0.0465	15,051	7.108	7.132
5	549.7	560.	1.05	3.57	0.0598	20,310	6.531	6.617
6	963.3	770.0	1.44	6.26	0.079	27,930	6.020	6.110
7	1386.0	945.0	1.77	9.01	0.095	34,275	5.761	5.806
8	1658	1040	1.96	10.8	0.104	38,133	5.639	5.653
9	1994.3	1170	2.203	12.96	0.114	42,428	5.355	5.498
10	2562.0	1330	2.50	16.65	0.129	48,23	5,325	5.330

The Flow temp. = $9^{o}C$

ν (The Kinamatic viscosity) = 0.0135 $cm^2/sec.$

CHAPTER III

THE DIFFUSION OF DRAG-REDUCING SOLUTIONS IN TURBULENT SHEAR FLOW

3.1 INTRODUCTION

As we discussed in chapter I, it is generally agreed among the researchers that polymer molecules (or aggregates) causing drag reduction in turbulent shear flows exert their influence in the near-wall region. But, later results of drag reduction by injecting concentrated polymer solution in the core of a pipe flow (Vleggaar and Tels (1973-a,b)) showed conflicting results. They found a larger drag reduction than that of homogeneous solutions while the polymer was forming a thread which remained intact in the pipe core over 200 pipe diameters downstream from the injector. In order to resolve the conflict, a careful study of the drag reduction by injecting the polymer solution into both the core and the wall of a pipe flow was made.

It has been experimentally confirmed that the drag reduction by injecting concentrated polymer solutions into a Newtonian turbulent shear flow is related to the diffusion process of the drag reducing agent into the boundary layer of the flow. Consequently, it is related to the polymer concentration in a certain region in the boundary layer. Therefore, in order to study the phenomenon of drag reduction by the injection technique, it is necessary to study the diffusion of the injected polymer solution in the flow. Unfortunately all the injecting polymer diffusion studies were carried out on the diffusion of wall injected polymer solutions. The results available are qualitative and suffer from the high dependence on the shape of the injector and the injected polymer concentration, type and flow rate.

Walters & Wells (1971, 1972) measured the polymer concentration profile of a uniform wall injection through porous media walls of a pipe flow. They used a fluorescein tracer mixed with the polymer solution (Polyox WSR-301, of 500, 100 wppm concentration). Their results showed a large reduction in the turbulent diffusion of order one to two near the pipe wall. They also reported some anomalous drag reduction results over the active wall section (the injection section of the pipe). They attributed these results to the viscosity effects in the wall region over the active section. Ramu and Tullis (1976) measured the polymer concentration profile of injected polymer solutions into a developing boundary layer of a 12 inch diameter pipe. They mixed the polymer solution with rhodamine WT dye before they injected it into the flow. They found that the local drag reduction is highly dependent on the polymer concentration. Jin Wu (1972) injected dyed polymer solutions from a slot at the leading edge of a flat plate. His polymer concentration measurements showed a great suppression of the turbulent diffusion in the boundary layer. The same result was obtained by Fruman and Tulin (1976). Their polymer concentration measurement at the wall showed that the drag reduction can be related to the polymer concentration at the trailing edge of the flat plate as a result of the diffusion process.

At this stage it seems convenient to mention that axial dispersion measurements in turbulent flows of polymer solution give a different picture. Tyler & Middleman (1974) introduced a dye solution into the core of polymer solution pipe flow. They found an increase in the dispersion rate compared with that of water pipe flow. The same results were obtained earlier by Bryson et al (1971) when they injected a salt solution (NaCl, 0.5% concentration) as pulses into the core of a pipe flow of homogeneous polymer solutions (Polyox WSR-301). Their results showed that the increase in the axial dispersion increases with the polymer concentration in the solution.

As we see the dispersion measurements are different from those of the diffusion of the injected polymer solution into a pure water flow. The differences arise from the fact that in the dispersion studies a tracer material of the same physical properties as those of the flow is injected into a homogeneous polymer solution flow. Hence it has no effect on the flow structure and is supposed to follow the flow exactly. While in the diffusion studies, the tracing material is the injected polymer solutions themselves. These polymer solutions do affect the flow structure and do not follow the flow exactly due to their non-Newtonian properties. Therefore the diffusion of these solutions into a pure water flow is highly dependent on the polymer type and the concentration.

In this chapter, we will present our diffusion results of relatively concentrated polymer solution injected both in the centre-line and the wall of a water pipe flow. Theoretical analysis of the turbulent diffusion process will be considered first. Then we will discuss the experimental technique and the data processing. This is followed by discussing the experimental results of polymer concentration profiles. The data analysis of the concentration measurements to calculate the diffusion parameters will be discussed in a separate section. Finally, a general discussion of the diffusion results will end this chapter.

3.2 THEORY

When a tracer with physical properties similar to the fluid is injected continuously from a point source at the centre of the pipe into the flow direction, the spread of the foreign matter by the turbulent diffusion can be described by Taylor's statistical theory of turbulent diffusion by continuous movements (Taylor (1921)). This theory is valid for homogenous turbulent flow. Taylor's diffusion

theory has been extensively applied to describe the diffusion in turbulent flows (Flint et al (1960), Baldwin & Walsh (1961), Groenhof (1970), Taylor & Middleman (1974) and Davidson & McComb (1975)).

Taylor's analysis gives the variance of the displacement of a number of fluid particles (or fluid lump) as:

$$\overline{y^2}_2(t) = 2 \int_0^t dt \int_0^t d\tau \, \overline{(v_2(t)\, v_2(t-\tau)} = v^2_2 \int_0^t (t-\tau)\, R_L(\tau)\, d\tau \qquad (3.1)$$

where $y_2(t)$ is the Lagrangian mean squared displacement of the fluid lump

v^2_2 is the Lagrangian mean squared fluctuating velocity

$R_L(\tau)$ is the Lagrangian time correlation coefficient of the fluctuating velocity defined as:

$$R_L(\tau) = \frac{\overline{v_2(t) \cdot v_2(t-\tau)}}{\overline{v^2}_2} \qquad (3.2)$$

As the time approaches zero, the correlation coefficient $R_L(\tau)$ approaches unity and decreases to zero with increasing the time interval τ. Therefore for long times the velocity fluctuations become uncorrelated and it is convenient to define a Lagrangian integral time scale as:

$$T_L = \int_0^\infty R_L(\tau)\, d\tau \qquad (3.3)$$

Therefore, for small diffusion time compared with the Lagrangian integral time scale T_L, equation (3.1) becomes:

$$\overline{y^2_2(t)} = 2\overline{v^2_2}\, t^2 \qquad (3.4.a)$$

and for long diffusion time $t >> T_L$ equation (3.1) reduces to:

$$\overline{y^2_2(t)} = 2\overline{v^2_2}\, T_L t \qquad (3.4.b)$$

By analogy with Einstein's equation for the diffusivity by Brownian movements, Taylor defined the eddy diffusivity of the fluid lumps in homogeneous turbulent flows as:

$$D = \tfrac{1}{2} \frac{d}{dt} \left(\overline{y^2_2(t)}\right) \qquad (3.5)$$

$$= \overline{v^2_2}\, T_L \quad \text{for long diffusion times}$$

The diffusion time may be equated to the downstream distance x from the source and the streamwise velocity of the flow $\overline{U}_o$ as:

$$t = \frac{x}{\overline{U}_o} \qquad (3.6)$$

If we substitute t and D from equations (3.5) and (3.6) into equations (3.4.a & b), the result of plotting $\overline{y^2_2(t)}$ as a function of x will show that $\overline{y^2_2(t)}$ increases first proportionally with x^2 and finally assymptotes to a straight line (Hinze (1975)). Such assymptote has a slope equal to $\frac{2D}{\overline{U}_o}$ and an intersection x^* with the x-axis. Hence, for long diffusion times:

$$y^2_2(t) = \frac{2D}{\overline{U}_o} (x - x^*) \qquad (3.7)$$

Various experimental results of turbulent diffusion in Newtonian flows confirm this relation (Hinze (1975), Flint et al (1960), Baldwin & Walsh (1961) and Sheriff & O'Kane (1971)) and also in homogeneous drag reducing flows (Taylor & Middleman (1974)).

An expression for x^* can be obtained if we know the form of the Lagrangian correlation coefficient $R_L(\tau)$. Different forms have been proposed by a number of investigators (Flint et al (1960), Frenkiel (1943) and Taylor & Middleman (1974)) for $R_L(\tau)$. A simple exponential form for $R_L(\tau)$ was found to be superior to others suggested in fitting the experimental data. Hence, the Lagrangian correlation coefficient may be approximated by (Hinze (1975)).

$$R_L(\tau) = \exp(-t/T_L) \tag{3.8}$$

Substituting in equation 3.1 and integrating we obtain,

$$y^2{}_2(t) = 2v^2{}_2 \, T_L \, \{t - T_L(1 - \exp(-t/T_L))\} \tag{3.9}$$

For long diffusion times $t > T_L$, $\exp(-t/T_L) \longrightarrow o$

Hence,

$$y^2{}_2(t) = 2v^2{}_2 \, T_L \, (t - T_L) \tag{3.10}$$

$$= \frac{2D}{\overline{U}_o} \, (x - x^*)$$

where, $$x^* = \overline{U}_o \, T_L = \frac{\overline{U}_o}{v^2{}_2} \, D \tag{3.11}$$

The above approach and other phenomenological theories (Hinze (1975)) describe the turbulent diffusion of heat and mass into the flow by following a marked 'fluid lump' which maintains its identity as it is carried along by the flow. Any contaminant contained in these elements, such as heat or tracer molecules is assumed to diffuse through the turbulent movements of these elements which is adequately described by some characteristic properties of the flow. When a tracing material of the same physical properties as the flow is introduced into the flow, its turbulent diffusion process is exactly the same as that of the fluid lumps. Such a diffusion is completely described by the flow characteristics and is independent of the

properties of the diffused material (neglecting the molecular diffusion). However, when the introduced material has different physical and dynamical properties than that of the flow, it will resist following the random movements of the fluid lumps. Consequently, its diffusion process will depend upon its properties as well as the flow characteristics. An example of such problem is the turbulent diffusion of large discrete particles into turbulent flows. The diffusion of discrete heavy particles was extensively studied theoretically and experimentally in order to develop a relationship between the particle diffusion coefficient and the fluid lump coefficient (Soo (1967) & Hinze (1975)). Such relationship is a function of the particle properties and the diffusion time. Another approach was proposed to describe the diffusion of the particles as a random-walk process. McComb (1974) proved that the random-walk approach gives the same results as that of Taylor's theory for the diffusion of small particles in homogeneous turbulence. He went further more and expressed the diffusion coefficient in terms of Eulerion variables.

When a relatively concentrated polymer solution is injected into the core of a turbulent pipe flow, two factors will affect its turbulent diffusion process into the flow. The first of these factors is the changes in the flow structure due to the drag reducing effects of the polymer. The second is that the viscoelastic properties and the relaxation time effect of the polymer solution lumps or aggregates tend to suppress the response of the polymer lumps (or aggregates) to follow the random movements of the fluid lumps. This implies that the polymer injected has a different eddy diffusion coefficient (D_p) from that of the fluid (D_f). Kalashnikov & Kudin (1973) observed that polymer aggregates behaviour at high frequency variations in velocity is similar to that of solid particles.

A number of investigators (Smith et al (1969), Sidahmed & Grisky (1972), McConaghy & Hanratty (1977), and Virk (1977) have established that in turbulent pipe flow of homogeneous polymer solution the fraction reduction in heat and mass transfer is roughly the same magnitude as that of the friction reduction. These results suggest that an analogy between mass, heat and momentum transfer (Kale (1977), Virk (1977)). Accordingly, in order to consider the effect of the changes in the flow structure due to the drag reducing effect of polymer, the eddy diffusivity of the fluid (D_f) was made dimensionless as:

$$D^+_f = \frac{D_f}{u^* d} \tag{3.12}$$

where u^* is the friction velocity

d is the pipe diameter

By analogy with the expressions relating the eddy diffusion coefficient of discrete heavy particles with that of the fluid, the relationship between the injected polymer eddy diffusion coefficient D_P and that of the fluid lump D_f is:

$$D^+_P = D^+_f f_1(c) \tag{3.13}$$

where $D^+_P = \frac{D_P}{u^* d}$

and $f_1(c)$ is an experimentally determined function which is assumed to consider the viscoelastic effects in resisting the diffusion process which is basically a function of the polymer type and concentration.

3.3 THE EXPERIMENTAL TECHNIQUE

In order to study the diffusion of the injected polymer solution into the pure water flow, a salted polymer solution was injected into the flow just upstream from the test section of the first pass of the pipe flow rig described in chapter II. Samples of the flow were taken at different radii across the pipe section using a sampling system which will be discussed later in this section. The electrical conductivity of each sample was measured and the results were fed through the data logger to the computer. Polymer concentrations were calculated from the calibration curves and a least-squares fit of the results was used to give smooth concentration profiles as a function of the radius. This procedure was repeated for a number of pipe sections along the pipe at different distances downstream of the injector.

3.3.1 The Sampling System and the Polymer Concentration measurements technique

A sectional view of the sampling system is shown in figure (3.1). The system consisted of a Perspex flange, a sample collecting assemblage, and a digital micrometer traverse system. The Perspex flange was 26.8 mm I.D, 65 mm O.D. and 20 mm thickness. The inner diameter of the flange was 0.8 mm larger than the inner diameter of the pipe in order to substitute for the size of the sampling tube, which allowed the withdrawal of flow samples from the wall. A side hole was drilled in the flange through which the sampling tube passed. The sampling tube was made of a stainless tube of 0.85 mm I.D. and 1.2 mm O.D. On the top of the tube, a stainless steel hypodermic needle tube of 0.5 mm I.D. and 0.8 mm O.D. was fitted. The needle tube was bent through 90° in order to make the tip of the sampling tube facing the flow. The length of the needle tube in the direction

of the flow was 10 mm. The solution sample passed through the needle down to the sampling tube where it was collected as appropriate. The sampling tube was fitted into a brass tube and soldered together as shown in figure (3.1). The above assemblage was contained in a brass casing which is fixed to the Perspex flange and sealed against leakage by a rubber O-ring. At the end of the brass casing, a digital micrometer-traverse system was fixed. By moving the stem of the micrometer, the whole assemblage moves inside the casing against the spring action as shown in figure (3.1). By this way the sampling tube could be positioned along the diameter of the pipe flow with an accuracy of 0.001 inch using the micrometer screw. The outlet of the sampling system was fitted with a valve to control the sampling flow rate. The sampling system was carefully aligned with and flanged to the pipe at the required distance downstream the injector.

During the concentration measurement experiments, the test section tubing of the first pass was replaced with a set of six pipe sections identical to the removed one. The six pipe sections were 2.0, 2.0, 1.0, 0.5, 0.25, 0.25 meters long and their total length was the same as the removed section. These pipe sections were flanged together in such a way that they would give the required distance between the sampling system and the injector with the minimum possible number of sections. This sort of organization allowed us to measure the polymer concentration at a number of cross sections of different distances downstream from the injector.

The electrical conductivity of the collected samples were measured using a conductivity cell which was connected to a direct reading conductivity meter. When the cell is immersed in the sample solution and the meter is switched on, the specific conductivity of the solution is indicated immediately on the meter panel.

The conductivity cell consisted essentially of two parallel and laterally insulated electrodes. The electrodes were made of two platinum foils of 10 x 10 mm^2 each. The platinum foils were mounted on two parallel glass surfaces and facing each other. The two electrodes were enclosed in a glass casing which was provided with enough holes to allow the measured solution to cover the two electrodes completely and to fill the gap between them.

The cell was connected to a direct reading conductivity meter made by Portland Electronics Ltd., Series 300, model P.335. The meter has ten operating ranges, each range is accurate to within 1.5% of its full scale. The lowest of these ranges is 0-1.0 μ.mho and the highest range is 0-30 mmho. This wide range of the instrument allowed us to measure the specific conductivity of high salt concentrations (- 2%). The meter was also supplied with a temperature compensator to compensate the temperature difference effect on the conductivity measurements.

The conductivity measurement equipment was calibrated using salt solutions, Polyox salt solution and separan-salt solutions all diluted with tap water to the required concentration. In order to cancel the effect of temperature variation on the electrical conductivity of the solution, the relative electric conductivity which is defined as the ratio of the electric conductivity of the salt solution to that of the tap water (i.e. zero slat concentration) is calculated. The calibration results were fed to the computer in the form of relative conductivity as a function of the salt concentration. A least squares fit for the calibration results is calculated and stored in EMAS (Edinburgh Multi Access System). Sample of these results are given in table (3.1).

The use of electric conductivity as a means to measure the polymer concentration in the samples is prefered and highly recommended due to its simplicity and its high accuracy. A relatively concentrated solution of sodium chloride (NaCl) is usually used as a tracer material in turbulent diffusion studies in water flows. (Groenhof (1970)).

The sodium chloride solution is highly recommended as a tracing material because it has a very high schmidt number which means that the effect of the molecular diffusion of the tracing material is negligible. The molecular Schmidt number for NaCl-water solution at 15^{o}c is about 750 (Groenhof (1970)).

The effect of the common salt (NaCl) on the efficiency of the polymer solutions as drag reducers was studied and will be presented in the next chapter. The results of our study and that of White (1969) showed that the addition of salt to solutions of polyox WSR-301 and separan AP-30 does not affect their drag reducing properties up to salt concentration of 4%. The only observation was that the salt slightly affected the shear viscosity of separan AP-30 solutions. Sea water was used as a solvent for polyox and showed the same results as that of polyox solved in water.

Realizing the fact that the NaCl is most unlikely to modify the behaviour of the drag reducing solutions, it had been used as a tracer material in many investigations. Bryson et al (1971) used NaCl solution of concentration 0.5% to study the dispersion in drag reducing polyox flow. Both Hand & Williams (1973) and Arunachalam & Fulford (1971) used NaCl solution in their adsorption measurements in dilute polymer solutions.

3.3.2 Experimental Procedure

The above discussed sampling system was carefully aligned with and flanged to the pipe section at the required distance downstream from the injector. The water flow rig discussed in chapter II was adjusted to work in the open loop flow mode. The water flow rate was adjusted to the required value and was monitored during the experiment on a digital voltmeter screen (DISA digital voltmeter model 55D31). The digital voltmeter read the output of the pressure transducer system which is connected to the orifice meter as discussed in chapter II. The salted polymer solutions were injected into the flow at the required flow rate. The polymer flow was controlled by adjusting the speed of the DC motor using the variac of the DC supply (for more details see chapter II).

When the steady state condition of the flow was reached, samples from the flow were withdrawn at different positions in the cross section starting from one side of the tube moving towards the other side in equidistant steps, then moving back towards the starting side by the same way in different positions. By this way of sampling any variation of the experimental conditions will be distributed among the whole experimental results. For each sample, the electric conductivity was measured immediately before collecting the next. Consequently we ensure that the conductivity of all the samples were measured at the same temperature as the flow. The temperature of the flow was measured at the flow outlet many times during the experiment to ensure that it remained constant.

Samples of water were collected before and after the experiment. An average value for the conductivity of water was calculated.

Before collecting any sample, the sampling tube was positioned in the required radial position using the micrometer and was kept bleeding for enough time in order to ensure that nothing was left in the sampling tube from the previous sample and that the collected sample belonged to the required positon. The sampling flow rate was adjusted so that only liquid from the immediate neighbourhood of the sample tube tip would be withdrawn.

At the end of the experiment we had the following experimental data:

- The distance of the measurement section down-stream from the injector
- The flow rates of both the water and the polymer
- The concentration of the salt and the polymer in the injected solution
- The electric conductivity of the water measured during the experiment
- A number of electric conductivity measurements as a function of distance from the wall

The above procedure was repeated for a number of cross sections at different distances from the injector in order to monitor the development of the diffusion process of the injected solution. The experimental conditions were kept unchanged throughout the experiments of each polymer solution.

3.3.3 Data Processing

The data of each experiment, which contain the experimental results of conductivity at a cross section in the flow, were fed into EMAS. A computer program was written in FORTRAN IV in order to process the data. The following calculations were carried out:

- From the calibration results stored in EMAS, the salt concentration was calculated. Then, the polymer concentration was calculated from the known value of polymer to salt ratio in the injected solution.
- The radial position corresponding to each result was calculated from the measured distance relative to the pipe wall.

At the end of this stage, the measured polymer concentration profile as a function of the radial distance in the cross section was calculated.

The best fit of the polymer concentration results was calculated using the least squares fit method. This was followed by integrating the fitted results over the cross sectional area to calculate the average polymer concentration.

3.4 DISCUSSION OF THE RESULTS

The discussion in this section will be carried out as follows:

1. The concentration measurement results of the injected solutions into both the centreline and the wall of the pipe flow.
2. Analysis of the concentration measurement results to calculate the eddy diffusivity of the injected solutions into the pipe flow core.
3. The experimental results of the eddy diffusivity.

3.4.1 Concentration Measurement Results

This section presents our experimental concentration profile measurements for both centreline and wall injection. In centreline injection, we present the results of the different polymers. Separan AP-30 and Polyox WSR-301. In order to compare the diffusion of the injected polymer solution with that of Newtonian flow, a salt solution was injected into the centreline of a pipe flow. On the other hand only one polymer solution was injected into the wall of the pipe flow. Its concentration profile will be discussed in a separate subsection here. But first, let us discuss the results of centreline injection.

3.4.1.1 Centreline Injection Results

Since the turbulent diffusion from a point source in a pipe of turbulent shear Newtonian flow is well established, a salt solution was injected into the centreline of the water pipe flow to test the experimental set-up and to compare the polymer diffusion with that of Newtonian flow. The salt solution was injected into the flow using an injector similar to that of figure (2.7), but of 1.1 mm ID and 1.5 mm O.D. to act as a point source. Three concentration profiles of the tracing material at 8.5, 18.1 and 27.7 pipe diameters downstream from the injector were measured. The results are shown in figure (3.2) which indicates that the tracing material becomes homogenously distributed in the flow at a distance of 30 pipe diameters from the injector. These results are in good agreement with those obtained by Quramby & Anand (1969).

As we discussed in chapter I, the concentration profiles of the injected polymer solutions by themselves are of great importance in this investigation. These concentration measurement results were used to correlate the development of the drag reduction achieved by injection with that of the polymer concentration in the flow. This correlation will be discussed in detail in the next chapter.

Two kinds of polymer were injected into the core of the water pipe flow using the centreline injector shown in figure (2.7). The two polymers were chosen from two different families in order to universalize the conclusions of the research. Separan AP-30 and Polyox WSR-301 each at concentrations of 1000 wppm and 3000 wppm were used. The separan solutions were injected into the flow at Reynolds number of about 3.7×10^4 and the polyox solutions were injected at $Re \simeq 4.5 \times 10^4$. The salt was kept at a constant concentration of 0.25% in the separan solutions and of 0.2% in the polyox solutions.

The results of the separan solutions are shown in figures (3.3), (3.4), (3.5) and (3.6). Figure (3.3) shows the polymer concentration profiles for a separan solution of 1000 wppm at an average polymer concentration of 5.5 wppm. The results show a suppression of the turbulent diffusion of the injected polymer solution. The complete homogenity of the injected polymer solutions was reached at a distance of $x/d \simeq 135$ from the injector which is nearly 4 times the distance when injecting the salt solution. The results of the 3000 wppm separan solution are presented in figure (3.4). The results show that the homogenity of the injected solution was not reached at even after 230 pipe diameters downstream from the injector. These results support the suggestion that the viscoelastic properties of the injected polymer solutions entangle its turbulent diffusion process.

Figures (3.5) and (3.6) show the development of the polymer concentration along the pipe length downstream the injector at different radial locations in the pipe cross section for both 1000 and 3000 wppm concentration of separan AP-30 respectively. These results clearly indicated the slow diffusion process of the injected solution and its dependence on the concentration of the injected polymer solution.

The results of injecting polyox WSR-301 solutions of concentrations 1000 and 3000 wppm are presented in figures (3.7), (3.8), (3.9) and (3.10). These results support the primary conclusions drawn from the separan injection results. Figure (3.7) shows the polymer concentration profiles of 1000 wppm injected solution concentration and at an average concentration of 4.5 wppm. The homogenity of the injected polymer solution is shown to be achieved at a distance longer than 200 pipe diameters from the injector. The results of injecting a 3000 wppm

polyox concentration are shown in figure (3.8). A bigger suppression in the turbulent diffusion is exhibited indicating the effect of the viscoelastic properties of the injected solutions. As shown in figure (3.8) the homogenity of the injected solution with the flow was not observed at a distance $x/d \simeq 250$ from the injector. In both figures (3.9) and (3.10) the dimensionless relative polymer concentrations c/Cav were plotted against the distance from the injector at different radial locations for the two polyox solutions, 1000 and 3000 wppm respectively. These two figures exhibited the slow development of the polyox concentration towards the homogenity.

As we discussed before, the salt was dissolved in the polymer solution to act as a tracing material in the injected fluid. We have assumed that the polymer and the salt diffuse together. Consequently, the polymer concentration of each sample is related to the injected solution. Such assumption was taken into consideration by most of investigators as a fact that both the polymer and the tracing material diffuse together (Wetzel et al (1969), Walters & Wells (1972) and Ramu & Tullis (1976)). Now, we have to justify this assumption.

The turbulent diffusion of a substance released from a point source can be described by the super position of two processes.

1. A large-scale motion of the instantaneous centre of gravity of the fluid lump containing the foreign matter by the random motion of the turbulent flow.
2. A small-scale motion of the foreign material in the fluid lump relative to the instantaneous centre of gravity, caused by the molecular diffusion and the high frequency variations of the flow field.

In turbulent pipe flow, the eddy diffusivity is about 100 times the molecular diffusivity at Re - 4 x 10^4 (Quarmby & Anand (1969) and Sheriff & O'Kane (1970)), when the tracing material has a molecular Schmidt number $\simeq$ 1.0. In such flows, the molecular diffusion is negligible and the process is dominant by the turbulent diffusion i.e., the large-scale motion of the instantaneous centre of mass of the diffused fluid lump. However, the decrease in the molecular Shmidt number, increases the influence of the molecular diffusion on the process by causing a spread out of the fluid lump.

The molecular Schmidt number of the sodium chloride (NaCl) - water solution is about 750 (Groenhof (1970)) which means that it has a negligible molecular mass diffusivity of about 1.3 x 10^{-3} the kinematic viscosity of the solution. Therefore, NaCl solution is considered as a ideal tracing material in turbulent diffusion studies. On the other hand, the molecular diffusivity of the polymer in the solution was estimated as 1.0 x 10^{-3} that of the kinematic viscosity for dilute Polyox WSR-301 solutions (Fruman & Tulin (1976)). Therefore, the molecular motion of both the polymer and the salt are of the same order of magnitude which is about 10^{-5} to 10^{-4} the turbulent diffusion at the Reynolds numbers of interest in this investigation.

Due to the inertia difference between the polymer and the salt molecules, there could be a possibility of separation between the salt molecules and the polymer molecules mesh by the small eddies. Such process would be resulted in a difference in the diffusion of both the polymer and the salt. However, due to the low energy content of such small eddies, the resulting motion is considered to be of the same order of magnitude of the molecular motion, or at least, of the scale of the dissipative eddies. Since, the scale of the dissipative eddies is about two orders of magnitude less than that of large eddies

responsible for the turbulent diffusion, the influence the small motion caused by the small eddies on the diffusion process is very small and could be neglected as the influence of the molecular diffusion.

Finally, the small-scale motion caused by the molecular diffusion and by the effect of the small scale eddies on both the polymer and the salt molecules could be neglected and the diffusion process is represented by the large-scale motion of the turbulent field. Then, the assumption proposed before that both the polymer and the salt acting as a tracing material diffuse together is practically applicable.

3.4.1.2 Wall Injection Results

In the wall region, the diffusion process is primarily dominated by the molecular diffusion. The molecular diffusivity of polymers decreases with increasing the concentration, and consequently, the difference between the molecular diffusivities of the polymer molecules and the salt (NaCl) increases. The diffusion of salt and polymer at these high concentrations in the wall region will be doubtful. For this reason, the concentration profiles were measured only for one polymer solution just to demonstrate the diffusion of the polymer solution when injected into the wall.

The results of injecting a polyox solution of 1000 wppm are shown in figure (3.11). The polymer concentrations at different radial positions in the cross section were plotted as a function of the distance from the injector. The polymer concentration at the wall exhibited the slow diffusion process near the injector and faster as the distance from the injector increases. This behaviour was due to the increase in the molecular diffusivity with the decrease in the concentration of the polymer at the wall. The most interesting feature of the results was the fast increase in the polymer concentration at the radial position named 0.9 such that it reaches about five times the average concentration at a distance of 20 pipe diameters from the

injector, then the concentration levels off slowly keeping the polymer concentration higher than the average over the whole length of the cross section. Such a development in the polymer concentration was very similar to the development of drag reduction by injecting concentrated polymer solutions into the wall region (this will be discussed in detail in chapter V). The results also showed the slow development of the polymer concentration in the core of the pipe such that the concentration was maintained less than 0.1 of the average value up to 50 pipe diameters downstream from the injector.

3.4.2 Analysis of the Experimental Data

The turbulent diffusion process was considered only in the core of the pipe flow where the flow is uniform with velocity $\overline{U}_o$ and the turbulence is supposed to be homogeneous and isotropic. LDA velocity measurements in drag reducing solutions (Logan (1972) and Rudd (1971)) confirmed that such an assumption is also applicable in the core of polymer solution pipe flow.

When a solution is injected continuously from a point source at the pipe axis, the spread of the injected solution at a certain distance downstream from the source could be expressed as: (Hinze (1975))

$$C = C_o \cdot \exp\left(-r^2 / 2.\overline{y^2}_2(t)\right) \qquad (3.14)$$

and,

$$C_o = \frac{q.C_p}{2\pi\overline{U}_o \overline{y^2}_2(t)} \qquad (3.14a)$$

C, is the concentration of the diffusing substance at the radial distance r in the cross section, q is the flow rate of the injected solution and C_p is the concentration of the diffused substance in the injected solution.

The conditions to which equation (3.14) applies are not strictly applicable in the present experiments and the analogy could be approximately true. For example, a point source was not used and there is no applicable modification for the effect of the finite size source (Flint et al (1960)), the velocity is not uniform in the central region and the eddy diffusivity is not constant across the pipe section. Therefore, it was necessary to modify the above analysis to include only the peak concentration of the concentration profile data.

From equation (3.14.a), the relationship between the peak concentration and its axial position from the source is given by:

$$C_o = \frac{q \cdot C_p}{2\pi \bar{U}_o y^2{}_2(t)}$$

Since,

$$y^2{}_2(t) = \frac{2D_p}{\bar{U}_o} (x - x^*) = \frac{2D_p}{\bar{U}_o} \Delta x$$

$$\frac{C_o}{C_p} = \frac{q}{4\pi D_p \Delta x}$$

Hence,

$$D_p = \frac{q}{4\pi} \cdot \frac{1}{C_o/C_p} \cdot \frac{1}{\Delta x} \qquad (3.15)$$

The dimensionless eddy diffusivity will be:

$$D_p^+ = \frac{D_p}{u^* d} = \frac{q}{4\pi d^2} \cdot \frac{1}{u^*} \cdot \frac{1}{C_o/C_p} \cdot \frac{1}{\Delta x/d} \qquad (3.16)$$

From the above equation, the eddy diffusivity of the polymer solution was calculated using the measured values of C_o/C_p, q and Δx.

Since Δx is not a direct measurement data and it is calculated by calculating the value of x^* from equation (3.11), the eddy diffusivities were calculated by successive approximations as following.

A preliminary value of D_p was calculated by substituting $\Delta x = x$ into equation (3.15). The first approximated value of x^* was calculated from equation (3.11) using the preliminary value of D_p. The Lagrangian velocity of the particle was taken to be that of the fluid at the reduced wall shear stress. This assumption is based on the fact that the eddy diffusivity is not sensitive to the value of x^* especially when the measurements are carried out at long distances from the point source such as in this investigation.

The resulting value of x^* was used to calculate an improved value of D_p using equation (3.15). Further approximations of x^* and D_p could be calculated by this way until a constancy in the calculated values was found. It was found that the difference between the first and the second approximation was only a few percent.

Equation (3.15) could be used in another form to determine the eddy diffusivity of the injected solutions. As we know, the average polymer concentration is defined as:

$$C_{av} = \frac{q \cdot C_p}{\frac{\pi}{4} d^2 \bar{U}_{av}} \qquad (3.17)$$

Substituting into equation (3.15), the result will be:

$$D_p = \frac{d\bar{U}_{av}}{16} \cdot \frac{1}{C_o/C_{av}} \cdot \frac{1}{\Delta x/d} \qquad (3.18)$$

The dimensionless eddy diffusivity D_p^+ is:

$$D_p^+ = \frac{D_p}{u^* d} = \frac{\bar{U}_{av}}{u^*} \cdot \frac{1}{16} \cdot \frac{1}{C_o/C_{av}} \cdot \frac{1}{\Delta x/d} \qquad (3.19)$$

3.4.3 Eddy Diffusivity Results

Using equation (3.16) or (3.19), the eddy diffusivity of the Newtonian Flow was calculated using the concentration profiles of the salt-water solution injected from a point source in the centreline of the pipe flow. Three values were calculated from the three concentration profiles measured. An average value was calculated and listed in table (3.2). The table represents our results compared with other previous investigations to measure the eddy diffusivity in the centre-line of the pipe flow. An average value for the eddy diffusivity in the core of the pipe flow is estimated to be:

$$D_f^+ \simeq 4.0 \times 10^{-2} \qquad (3.20)$$

which is independent on the flow Reynolds number.

The polymer concentration at the centreline of the pipe flow relative to the injected concentration is shown in figures (3.12) and (3.13) as a function of the distance from the source. The salt-water solution concentration is also shown in these two figures for comparison. Figure (3.12) shows the results of the separan solutions and the polyox results are shown in figure (3.13). Both figures showed a large scatter in the polymer solution results which increases with increasing the concentration of the injected solutions. Comparing these results with that of salt-water solution, a clear indication that a large suppression in the turbulent diffusion of the injected solutions are shown in these figures. Such a suppression is suggested to be partially due to the reducing effect of the polymer solutions to the transfer of heat, mass and momentum, and partially due to the viscoelastic properties of the injected polymer which make the polymer lumps (or aggregates) resist following the movements of the fluid lumps.

In order to investigate the effect of the viscoelastic properties on the diffusion of the injected polymer solutions, the effect of the polymer molecules on the flow structure was taken into consideration by calculating the diffusivity at the reduced value of the shear stress. This assumption is based on the fact that the complete analogy between mass, heat and momentum transfer is also held in drag reducing solutions (Virk (1977)).

The dimensionless eddy diffusivities of the polymer solutions were calculated from equation (3.16) or (3.19) as discussed before. The local values of the friction velocity were calculated using the local drag reduction measurements as a function of the distance from the injector (this will be discussed in detail in the next chapter) at the same experimental conditions as that of the polymer concentration measurements.

The dimensionless eddy diffusivity of the injected polymer solutions were represented in two ways in order to investigate the dependence of the diffusion process on the viscoelastic properties of the solution. The results were represented, firstly as a function of the distance from the injector and secondly, as a function of the polymer concentration.

Figure (3.14) present the dimensionless eddy diffusivity D^+_p of the separan AP-30 solutions injected into the centreline region of the pipe flow at different distances from the injector. The results of three polymer concentrations are shown in comparision with the water diffusion results. The results showed that the suppression in the turbulent diffusion decreased away from the injector. In spite of the scatter in the results specially for the 5000 wppm solution, the results could be represented by a straight line for each solution as shown in figure (3.14).

The results of dimensionless eddy diffusivity of the injected polyox solutions are presented in figure (3.15). Two polymer solutions were injected at concentrations 1000 and 3000 wppm, both contained NaCl at concentration 0.2%. The results showed a suppression in the turbulent diffusion compared with water diffusion even at the reduced value of the wall shear stress.

The representation of the dimensionless eddy diffusivity of the diffused polymer solutions as a function of the local polymer concentration is shown in figures (3.16) and (3.17). The results of separan solutions were presented in figure (3.16). An interesting agreement emerged among the results of the three different concentrated solutions injected into the flow, which gave an indication that the dimensionless eddy diffusivity is solely dependent upon the polymer concentration in the range of 5 - 2000 wppm. The results can be approximated by a straight line of:

$$D^{+}_{p} = 2.8 \times 10^{-2} (C)^{-0.4} \qquad (3.21)$$

C is the local concentration of the polymer solution in wppm

This result showed that with increasing the concentration of the polymer solution, its turbulent diffusivity decreases due to the increase of the viscosity and the relaxation time. The increase in the viscoelastic properties increases the resistance of the polymer lumps to follow the turbulent movements of the fluid lumps. This effect could be considered as an analogy of the inertia effect on the turbulent diffusion of heavy particles.

Figure (3.17) represents the results of the polyox solutions as a function of the local concentration. The suppression in the turbulent diffusivity is shown to be independent of the local concentration in the range of (5 - 150) wppm. The dimensionless

eddy diffusivity in this range can be approximated by:

$$D^+_p = 0.85 \times 10^{-2} \qquad (3.22)$$

This is compared with the value of $D^+_f = 4.0 \times 10^{-2}$ of the turbulent diffusion of a tracing material which follow exactly the movement of the fluid lumps. The constant turbulent diffusion of the polyox solutions could be explained by the fact that the changes in the viscosity and relaxation time of the polyox solutions in this rang of concentration is small. Such suppression in the turbulent diffusion was reported by Jin Wu (1972).

TABLE 3.1

CALIBRATION RESULTS OF THE CONDUCTIVITY METER

RUN 1		RUN 2		RUN 3	
c wppm salt	σ_r	c wppm salt	σ_r	c wppm salt	σ_r
5000	67.1	5000	64.6	5000	69.6
4000	54.6	2500	33.7	2500	38.2
3000	41.6	1250	18.4	1500	23.4
2500	34.4	1000	15.6	1000	16.1
2000	28.3	500	8.5	800	13.2
1500	22.7	250	4.72	700	11.7
1200	18.5	150	3.36	600	10.2
1000	15.8	100	2.57	500	8.6
800	12.7	90	2.44	400	7.1
600	9.8	70	2.220	300	5.6
500	8.4	60	2.034	250	4.81
400	7.0	50	1.861	200	4.10
300	5.6	40	1.714	150	3.38
250	4.84	20	1.370	100	2.64
200	4.10	10	1.193	80	2.26
180	3.80	5.	1.105	70	2.11
150	3.34	2.5	1.059	60	1.96
120	2.87	1.0	1.0340	50	1.880
100	2.57	0.5	1.0210	40	1.660
80	2.381	0.25	1.0126	30	1.502
60	2.058	0.125	1.0084	22.5	1.391
50	1.885			20.0	1.370
40	1.726			15.0	1.289
30	1.549			10.0	1.203
25	1.474			5.0	1.1196
20	1.381			2.5	1.071
15	1.297			1.0	1.0389
12.5	1.2478			0.5	1.0290
10	1.1947			0.25	1.0150
8	1.637				
6	1.1327				
4	1.0929				
2	1.0580				
1	1.0355				

$\sigma_r = \sigma / \sigma_{water}$

Run 1 NaCl - water solution

Run 2 NaCl - polyox WSR-301 solution

C_p/C salt = 1.0

Run 3 NaCl - Separan AP-30 solution

C_p/C salt = 1.0

TABLE 3.2

Ref.	Re x 10^{-3}	Fluid	Transfer of	P_r or S_c	D/du^*
Hinze (Laufer data)	500	Air	momentum	-	3.5×10^{-2}
Brinkworth & Smith	46-346	Air/water	-	-	3.2×10^{-2}
Bladwin & Walsh	280-640	Air	Heat	0.71	3.0×10^{-2}
Johnk & Hanratty	18-71	Air	Heat	0.71	4.0×10^{-2}
Groenhof	25-75	Water	NaCl	750	4.0×10^{-2}
Sheriff & O'Kane	13-130	Air	No	0.77	4.4×10^{-2}
Quarmby & Anand	20-130	Air	No	0.77	3.4×10^{-2}
Towle & Sherwood	25-180	Air	CO_2	0.95	3.3×10^{-2}
Present study	45	Water	NaCl	750	4.0×10^{-2}

CHAPTER IV

DRAG REDUCTION BY INJECTING POLYMER SOLUTIONS INTO THE CENTRELINE OF A PIPE FLOW

4.1 INTRODUCTION

While it is generally agreed that the polymer molecules or aggregates causing the turbulent drag reduction exert their main influence in the near wall region, the region including the viscous sublayer and the buffer zone of the flow where both the turbulent energy production and dissipation are maximum, the evidence for this tends to be rather indirect. Such indirect evidence was discussed in some detail in chapter I. An attempt was made by Wells & Spangler (1967) to obtain direct evidence that the existance of the polymer in the wall region is necessary for drag reduction. They injected polymer solutions into both the centreline and the wall of a water pipe flow. Their results showed that drag reduction occurs when the polymer reaches the near wall region. However, the results were only qualitative and limited to about 20 pipe diameters downstream from the injector. But recently Vlegaar & Tels (1973-a,b) injected relatively concentrated polyacrylamide (Separan AP-30) solutions of 5000 wppm into the core of a small pipe water flow. They reported that while the injected polymer was forming a polymer thread and remained intact for more than 200 pipe diameter downstream from the injector, a large drag reduction was obtained higher than that of the homogeneous solution at the same Reynolds number and average polymer concentration over the cross section. They described this as a new mechanism to produce drag reduction by thread forming polymer solutions which interact with the large eddies in the core of the pipe flow. These results contradict ~~with~~ the principal concepts of drag reduction.

Other results were reported by Stenberg et al (1977-a,b), where they injected concentrated polyox solutions at concentrations 2,000 and 10,000 wppm respectively at the entrance of a water pipe flow via an impeller mixer. They reported that polymer solutions with poor mixing gave the same results of Vlegaar and Tels but, with good mixing of the injected solution with the water flow by the mixer, the normal results of homogeneous solutions were obtained. The contradictory results of the drag reduction produced by injecting concentrated polymer solutions into the core of pipe flow raises some questions:

Is there a polymer turbulence interaction at the core of the flow i.e. outside the near-wall region? If so, does such interaction produce drag reduction?

Is it necessary for the polymer to be in the near wall region in order to obtain drag reduction? And if so where should it be?

As we discussed before, these questions cannot be answered by such indirect experimental evidence obtained from the homogeneous solution studies. In order to find out satisfactory answers to the above questions and to reveal the contradictions due to drag reduction results by injecting concentrated polymer solutions into the core of water pipe flows, we carried out experiments to monitor the development of the drag reduction resulting from the centreline injection of a relatively concentrated polymer solution into the core of a water flow.

In this chapter, we will discuss the drag reduction results of injecting relatively concentrated polymer solutions into the centreline of a 26 mm diameter water pipe flow. Two polymer solutions, polyethylene oxide (Polyox WSR 301) and polyacrylamide (Separan AP-30) at different concentrations, were used. The effect of different parameters on the drag reduction by polymer injection will be discussed. At the end of this chapter we will discuss the results of correlating the development of drag reduction along the tube length with that of polymer concentration

at different radial location in the cross section along the test section length. But first we have to discuss some of the experimental technique details and the processing of the data.

4.2 EXPERIMENTAL PROCEDURE AND DATA PROCESSING

In chapter II, we described the experimental set up which was mainly a two passes water pipe flow. The test section was six metres long in the first pass and four metres long in the second pass. The first pass was supplied with 18 pressure taps which were arranged in such a way that they covered the whole length of the test section in the first pass. Such a large number of pressure taps allowed us to study carefully the development of the drag reduction over more than 220 pipe diameters downstream from the injector. The test section of the second pass was supplied with only two pressure taps to monitor the drag reduction at the end of second pass. The pressure taps were connected to a DISA low-pressure transducer via a group of scanning valves which allowed us to measure the pressure drop between any two pressure taps in the test section.

The output of the DISA low-pressure transducer was an analogue D.C. voltage proportional to the pressure difference applied to the transducer. The output voltages from the pressure transducer were recorded on paper tape using a Solartron data logger system. The system included a digital voltmeter model LM 1440.2, a paper tape punch machine model LP 1655 which was driven by a punch drive unit model LU 1718, and typewriter machine model LX 1654 which was driven by a typewriter drive unit LU 1469. The system has a number of operating ranges covering a wide range of voltage measurements. The system allows an accurate result of five figures reading. Throughout the whole experiments the range 30 volt was used which allowed us to obtain measurements as accurate as 0.001 volt which was corresponding to a pressure drop of 0.1 mm water head. The recorded pressure drop data results were fed into EMAS where the necessary computer programs were written for processing on ERCC (Edinburgh Regional Computing Centre) digital computer to calculate an average value for the local friction factor at points midway between successive pairs of pressure taps.

The centreline injector described in chapter II and shown in figure (2.7) was used throughout the experiments to inject the polymer solutions into the centreline of the fully developed region of the water pipe flow. The injector was flanged to the flow system at an enough distance downstream from the entrance providing over one hundred pipe diameters to ensure the full development of the flow.

The flow rate of the water was measured by a DISA low-pressure transducer connected to the orifice flow meter and monitered during the experiment on the display of a DISA digital voltmeter as mentioned before.

The drag reduction measurement experiments were carried out at the open flow mode of the water flow system as described in chapter II. The experiments were performed at the following steps:

- The water flow rate was adjusted for the required value of the flow rate which was monitored during the experiment on the digital voltmeter display to ensure that the steady state conditions were kept during the experiment.
- When the experimental conditions reached the steady state values of flow rate and temperature, the pressure drop measurement data were recorded in a sequence of records. Each record contained ten random values of the pressure drop between two pressure taps which were averaged to a mean value used in calculating the local friction factor at the midway point between the two pressure taps. In order to obtain a good average value for the pressure drop measurements, the output of the transducer system had been averaged electronically over a time period of 1.0 seconds before it was fed into the data logger system.

- Then the polymer solution was injected and its flow rate was adjusted to the required value by adjusting the input voltage to the driving motor as we have described in chapter II. The polymer flow rate was measured during the experiment time by measuring the distance travelled by the piston in the cylinder and the time taken to travel the distance.
- The water flow was then readjusted to maintain the same value as that in the water flow measurement, mentioned above. The value was monitored on the digital voltmeter display during the experiment to ensure that it was maintained constant throughout the experiment.
- When the steady state condition of both polymer and water flow rate and the flow temperature were reached, the pressure drop measurements were recorded by the same way as in the water flow measurements mentioned above.

At the end of the experiment, we had two groups of pressure drop measurement records, the first group contained the data of the water flow measurements in certain sequence, while the other group contained the pressure drop measurement of the flow with polymer injection in the same sequence as that in the first group.

The pressure drop measurements recorded on the paper tape were then fed into EMAS for further processing of the data. Beside the pressure drop records, the other parameters of the experiment were fed into EMAS. These parameters are the water flow rate Q_w, the polymer flow rate Q_p, the water viscosity ν and the concentration of the injected polymer solution C_p.

The data were processed on the ERCC digital computer to calculate an average value of the pressure drop and consequently the local friction factor at the midway point between successive pairs of pressure taps for both the water flow and the flow with polymer injection. Hence, the local percentage drag reduction was calculated at this mid point as:

$$\% \text{ DR} = \left(\frac{f_w - f_p}{f_w}\right) \times 100$$

or as,

$$\% \text{ DR} = \left(\frac{\Delta p_w - \Delta p_p}{\Delta p_w}\right) \times 100$$

where, p_w and p_p are the pressure drop between a successive pair of the pressure taps for both water flow and the flow with polymer injection respectively.

The average concentration of the polymer solution over the pipe cross section was calculated as:

$$C_{av} = \left(\frac{Q_p}{Q_w + Q_p}\right) \times c_p$$

4.3 DISCUSSION OF THE EXPERIMENTAL RESULTS

The experimental results of our investigation of the drag reduction by injecting relatively concentrated polymer solutions into the centreline of a water pipe flow are presented and discussed below in the following order.

1. The development of the drag reduction with the distance downstream the injector.
2. The effect of the salt concentration in the injected polymer solution on both the development and the asymptotic value of the drag reduction.

3. The effect of the average polymer concentration on the drag reduction achieved by injecting the polymer solutions into the core of the pipe flow.
4. The aging effect of the injected polymer solutions on the drag reduction.
5. The effect of the flow Reynolds number on the drag reduction by polymer injection.
6. The second pass drag reduction results.
7. Comparison with other experimental results.

4.3.1 The development of Drag reduction

In order to check the effect of the injection process on the local friction factor, water solutions were injected instead of polymer solutions. The local friction factor at different sections downstream the injector for the flow with and without water injection are shown in figure (4.1). The results were indistinguishable from each other which indicated that the injection of a water into the core of the flow does not affect the friction factor value of the flow. Consequently, any changes in the friction factor of the flow with polymer injection would be considered as an effect of the polymer solution only.

Two different polymers, Separan AP-30 and Polyox WSR-301, of different concentrations of 500, 1000, 2000, 3000 and 5000 wppm were injected at different flow rates into the centreline of a water pipe flow. Representative results are shown in figures (4.2) to (4.8). In these figures the local percentage drag reduction at different locations downstream from the injector were plotted against their distance from the injector. The general feature of the results as shown in the figures is the gradual building up of the drag reduction from a negative value just downstream the injector to an asymptotic

value at a distance downstream from the injector. Such a gradual building up of the drag reduction with the distance is very similar to that of the polymer concentration in the near-wall region as discussed in chapter 3 and shown in figures (3.5), (3.6), (3.9) and (3.10). The similarity in the development of both the drag reduction and the polymer concentration near the wall supported the assumption that the influence of the polymer happens mostly in the near-wall region as we will discuss at the end of this chapter.

The drag increase observed just downstream the injector was found to be independent on the injection flow rate and slightly dependent on the concentration of the injected solutions. This effect is believed to be due to the introduction of a viscoelastic solution into a fully developed flow which disturbs the flow structure in the core region. Such disturbance causes an increase in the friction factor of a value ranging from 3% to 6% at distance of $x/d \simeq 6$ from the injector. The drag increase was also observed to die out with the distance downstream from the injector due to the decrease in the concentration of the injected solution and the building up of the drag reduction as the polymer reached the wall region. The value of the drag increase and the distance downstream where the drag increase vanished are slightly dependent on the concentration of the injected solutions and independent, within the experimental error , of the injection flow rate. The drag increase associated with polymer injection was also observed before by Wells and Spangler (1967) when they injected solutions of guar gum (1000 wppm) and copolymer of polyacrylamide and polyacrylic (100 wppm) into the centreline of a pipe flow. Maus & Wilhelm (1970) observed an increase in the friction factor of about 200% at the injection point which was quickly demolished downstream the injector when they injected polyox WSR-301 solutions (2000 wppm) into the wall of a water pipe flow.

From the drag increase observed just downstream the injector and over a distance of 15 pipe diameters, one can conclude that polymer turbulence interaction in the core of the pipe flow does not produce a drag reduction but it produces a drag increase due to the high viscosity of the solution and the disturbance of the flow structure caused by the viscoelastic effects of the polymer solutions introduced into the flow.

As the drag increase dies outway downstream the injector the drag reduction builds up to an asymptotic value. The developing distance downstream from the injector is highly dependent upon the concentration of the injected solution and the polymer type. The effect of the concentration of the injected solutions on the developing distance could be clearly seen if we compare figures (4.5), (4.6), (4.7) and (4.8) with each other. Such comparison showed that the local drag reduction reached its asymptotic value at a distance 110, 170, 220 and more than 220 pipe diameters respectively downstream from the injector for polyox solutions injected at concentrations of 500, 1000, 3000 and 5000 wppm respectively. The same results were obtained for Separan AP-30 solutions. Comparison of figures (4.2), (4.3) and (4.4) with each other showed that the asymptotic value of the local drag reduction were reached at distances 100, 150 and 200 pipe diameters from the injector for polymer concentrations of 1000, 2000 and 3000 wppm injected into the core of the pipe flow. These results support the assumption made before by a number of investigators that drag reduction by polymer injection whether into the core of the pipe flow or into the wall region is highly dependent on the diffusion process of the injected solutions (Wells & Spangler (1967), Ramu & Tullis (1976) and Fruman & Tulin (1976)).

The development of the local drag reduction is shown to be dependent on the aging of the injected solutions. Such dependence was clearly observed when we compared the results of fresh polymer solution of 1000 wppm polyox WSR-301 (of one day age) shown in figure (4.6) with the results of the same solution after being aged for three weeks which is shown in figure (4.9). The results indicated that the aged solutions developed faster than the fresh solution but it has an asymptotic value for drag reduction less than that of the fresh solutions. Experimental evidence showed that the drag reduction by polymer injection depends on the diffusion process of the injected solutions (as discussed in chapter I). Since, the turbulent diffusion of the injected solution depends on its viscoelastic properties which was found to be relaxed with aging. Then, a faster development in the local drag reduction was expected due to the faster diffusion process of the aged solution than fresh ones. More detailed discussion will be presented later in this chapter.

The asymptotic value of the local drag reduction is shown to be a function of the average polymer concentration in the flow and the age of the injected solution. For fresh polymer solutions i.e. solutions of age less than one week (as we will discuss later), the asymptotic drag reduction is a unique function of the average polymer concentration C_{av} and seems to be independent on the injection flow rate and the concentration of the injected solutions.

4.3.2 The Influence of the Salt Concentration Content on the Drag Reduction by Polymer Injection

The effect of salt concentration on the drag reduction of non-ionic polymers such as polyethylene oxide have been discussed before. Hoyt & Fabula (1964) investigated the effect of using sea water as a solvent

for polyethylene oxide polymers. Their results were very similar to those obtained with water as a solvent. White (1969) and Shin (1965) reported that the presence of the salt in the homogeneous solutions of non-ionic polymers to the extent typical of the world oceans has little or no effect on the drag reduction observed. On the other hand, Monti (1973) investigated the effect of NaCl on the effectiveness of an ionic polymer solution (polyacrylamide AP-273) to reduce the friction and the heat transfer. His results showed a decrease in the effectiveness of the polymer to reduce the heat transfer and the friction with the increase of the salt concentration.

As we mentioned before, small quantities of the common salt ($\simeq$ 0.2 - 0.25% NaCl) were added to the injected polymer solutions to act as a tracer for the diffusion measurements. In order to investigate the effect of the salt on the diffusion process of the polymer solutions and its effectiveness as drag reducers, different solutions of Polyox WSR-301 and Separan AP-30 at different polymer and salt concentrations were injected into the centreline of the water pipe flow. For each polymer concentration the salt concentration was increased by mixing a concentrated polymer solution with salt-water solution and used within one hour. The local drag reduction measurements were carried out and plotted as a function of the distance from the injector. Representative results are shown in figures (4.10) and (4.11).

Figure (4.10) presents the results of three solutions at different salt concentrations (0, 5000 and 20,000 wppm of NaCl) of the same polymer concentration (1000 wppm of Separan Ap-30). These were typical results of Separan solutions with and without NaCl additives. The results showed a faster development of the Separan solutions with and without NaCl additives. The results showed a

faster development of the Separan solutions towards the asymptotic value with NaCl additives. However the asymptotic value was not affected by the presence of the salt in the Separan solutions. The faster development of the local drag reduction with the NaCl additives described an increase in the turbulent diffusion process of the injected solution. The increase in the turbulent diffusivity of the separan solutions with salt additives is believed to be due to the decrease in the viscoelastic properties of these solutions with the addition of NaCl.

The decrease in the viscoelastic properties of separan solutions with NaCl additives was observed before by Ayyash (1978) when he investigated the effect of NaCl additives on the damping of bubble pulsation in drag reducing solutions. He reported that the NaCl additives relaxed the viscoelastic effects of the separan AP-273 solutions on the damping of the bubble pulsation. Such effect was also observed in the decrease of the shear viscosity of Separan solutions with the NaCl additives, and the decrease in the extensional viscosity reported by Morgan (1971) when they added NaCl to an orifice flow of separan solutions.

The results of the above investigations and the turbulent diffusion results discussed in chapter 3 are in agreement with the above results which showed that the addition of salt to Separan solutions resulted in an increase in the local drag reduction development.

The results of the influence of the salt additives on the development of the local drag reduction by injecting Polyox solution are shown in figure (4.11). In this figure, the results of four solutions of 1000 wppm polyox WSR at salt concentrations 0, 5000, 20,000 and 40,000 wppm respectively are presented. The results indicated that the addition of NaCl to Polyox solutions affect neither

the development of the local drag reduction by polymer injection nor its asymptotic value. The unaffected development of the local drag reduction with the addition of NaCl suggests that the viscoelastic properties of the non-ionic polymer solutions are not affected by the presence of the salt in the solution.

The effect of NaCl concentration on the asymptotic value of the local drag reduction for both Polyox WSR-301 and Separan AP-30 are shown in figure (4.12). The results of both polymers showed the independence of the asymptotic drag reduction upon the salt concentration in the solution. These results indicate that the effectiveness of Polyox WSR-301 and Separan AP-30 as drag reducers were not affected by the addition of NaCl at such high concentrations of 4%.

The results of the polyox solutions are in general in agreement with all previous experimental results which showed that non-ionic polymer solutions are not affected by the NaCl additives. On the other hand our results using Separan AP-30 solutions showed an agreement with previous results concerned with the changes of their viscoelastic properties, and a disagreement with the results of Monti (1973) which showed a reduction in the effectiveness of the Separan AP-273 as a drag reducer with NaCl additives.

In order to cancel any probable effects of the salt in the results and to keep the experimental conditions of both drag reduction and turbulent diffusion measurements as similar as possible, the salt concentration was kept constant in the injected polymer solution throughout the whole experimental investigation.

4.3.3 The Effect of the Average Polymer Concentration in the Flow on the Drag Reduction by Polymer Injection

As Shown in the previous section, the local drag reduction develops increasingly with the distance from a negative value just downstream from the injector to an asympototic value away from the injector. The results showed that the asymptotic drag reduction is a function of the average polymer concentration in the flow. These results are presented in figures (4.2) to (4.9). They showed that for the same injected polymer solution, the increase in the polymer average concentration in the flow does not affect the development of the local drag reduction towards the asymptotic. However, the drag reduction at any distance in the developing part increases with the increase in the average polymer concentration by a percentage approximately the same as the increase in the asymptotic drag reduction. This increase is due to the increase of the polymer diffused into the supposed critical region near the wall, where polymer-turbulence interaction produces drag reduction, as a result of increasing the injected polymer flow rate.

In figure (4.13), the asymptotic drag reduction results of different Separan AP-30 solutions injected into the centreline of the water pipe flow were plotted as a function of the average polymer concentration in the flow. The results show that the asymptotic drag reduction is a unique function of the average polymer concentration and independent of the concentration of both the polymer and the salt in the injected solutions.

The results of the asymptotic values of the local drag reduction of Polyox WSR-301 are shown, in figure (4.14), as a function of the average polymer concentration in the flow. These results confirmed the evidence shown in the Separan results presented in figure (4.13)

which indicated that the asymptotic values of the local drag reduction is a unique function of the average polymer concentration and is independent of the concentration of both the salt and the polymer concentration in the injected solutions.

The most remarkable observation found in these results was the large values of the drag reduction achieved by such very low values of the average polymer concentrations and low values of Reynolds numbers. This remarkable high drag reduction was found in both Polyox and Separan solutions by the injection into the centreline of the pipe flow and was reported before by Vleggaar and Tels (1973). They found that the injection of 5000 wppm solution of Separan AP-30 gave a higher value of drag reduction than that obtained by homogeneous solutions at the same experimental conditions. These impressive results were more pronounced at low values of Reynolds number and polymer concentration.

A comparison of the drag reduction achieved by injecting concentrated polymer solutions with that of homogeneous solutions are shown in figures (4.15) and (4.16). The results shown in the two figures indicated the high drag reduction achieved by the injection of the polymer solutions into the water flow. Such results exhibited the fact that the injection technique resulted in an increase in the polymer's efficiency as drag reducers. This high efficiency of the drag reduction resulting by injection could lead to assume that the so-called "heterogeneous" drag reduction is different from that of homogeneous solutions. The dye visualization of Vleggaar and Tels showed that the injected polymer solutions formed a thread which remained intact over the test section length. This observation and the large degree of drag reduction achieved compared with the homogeneous solutions, made them assume that the polymer thread affects the large eddies which is mainly in

the core of the pipe flow. However the observation of our results showed that the development of the local drag reduction towards an asymptotic value along the test section length is very similar to the development of the polymer concentration in the near wall region, and the asymptotic value of the local drag reduction was reached when the polymer concentration reached an asymptotic value in this region. The similarity in the development of both the local drag reduction and the polymer concentration in the near-wall region indicated that there are no basic differences between the heterogeneous and the homogeneous drag reduction. The drag increase by injecting the polymer solutions observed downstream from the injector and maintained for about 15 pipe diameters confirmed the fact that the polymer-turbulence interaction in the core of the pipe flow, if any, can not produce a reduction in the friction. Why then, does injecting the polymer solutions achieve a large degree of drag reduction?

In order to explain the high drag reduction achieved by injecting solutions into the flow, we have to consider the experimental evidence that polymer aggregates or agglomerations are a common feature in the drag reducing solutions at least in the concentrated polymer solutions. This fact is widely accepted among the drag reduction research workers as we have discussed before in chapter I. It is also known that the turbulent diffusion of a foreign matter introduced into the turbulent flow is achieved by following the random movements of fluid lumps of sizes comparable to the turbulence integral length scales (Hinze (1975)), which is also controlled by the parameters of the turbulence in the flow. When the concentrated polymer solutions were injected into the flow they diffused into the flow by following the turbulence movements in the flow. Due to the viscoelastic properties of the polymer solutions, the polymer reached the critical region near the

wall, where polymer-turbulence interactions produce a drag reduction, in the form of concentrated polymer solution lumps which have sizes of comparable dimensions to that of fluid flow lumps responsible for the diffusion process. Hence it was expected to find concentrated polymer strands of dimensions compared with the turbulence scales in the flow and even larger. Stenberg et al (1977-a,b) dye visualization and Schlieren photographes of concentrated polyox WSR-301 (2000 and 10,000 wppm) injected into a mixing chamber at the inlet of a pipe flow demonstrated the presence of such polymer strands which split into finer and finer strands downstream. The polymer in these polymer lumps is in the form of agglomerations. The size of these agglomerations are ranging from as large as the size of the polymer lumps to as small as individual molecules. The presence of such super-molecular agglomerations in the critical region near the wall causes a substantial increase in the drag reduction efficiency of the polymer over that of the individual polymer molecules or the small aggregates as in the homogeneous solutions.

The influence of polymer agglomerations on the efficiency of polymer solutions as drag reducers could be explained by considering the principal aspects of the drag reduction phenomenon. As we discussed in chapter I, it is generally accepted that drag reduction occurs when some characteristic scale such as length, time or energy of the polymer molecule becomes of comparable dimensions with the corresponding scale of the turbulence. Increasing both the flow Reynolds numbers and the polymer concentration in the flow increases the drag reduction achieved due to the increase of polymers molecules interact with more turbulence eddies. Eventually the state of saturation is reached where all the turbulence eddies are influenced by the presence of the polymer molecules (or aggregates) and then the maximum

drag reduction is obtained. Thus, it can be contemplated that the scales associated with the polymer aggregates are larger than those for individual molecules. Therefore, polymer aggregates will exhibit a larger drag reduction in flows characterized by lower turbulence scales than those required for the individual molecules. As a result, for turbulent flows of sufficiently low shear stress the influence of polymer agglomerations is more pronounced while at higher shear stress both polymer molecules and aggregates co-operate to reach the maximum drag reduction.

In the light of the above discussion, the differences between the drag reduction by injecting the concentrated polymer solutions into the flow and that of homogeneous polymer solutions could be explained. The injection of the concentrated solutions into the flow resulted in the presence of the polymer as super molecular aggregates in the near wall region. The size of these polymer agglomerations could be larger than the turbulence largest eddies responsible for its diffusion into the wall region. Due to the large scales associated with these super molecular agglomerations, most of the scales of the turbulence are influenced resulting in the achievement of the higher drag reduction. At low Reynolds number and large tube diameter, where the wall shear stress is small, the difference between the drag reduction by the polymer injection and that of the homogeneous solutions is large and more pronounced. As the wall shear stress becomes lower the difference became larger and larger with the disappearance of the onset wall shear stress of drag reduction by polymer injection as reported before by Vleggaar & Tels (1973-a,b) and confirmed later on by Stenberg et al (1977-a,b), and as exhibited in our results (more detailed discussion will be presented later in this chapter). This could be explained by the fact that polymer

molecules are present as super molecular aggregates or entanglements which are bounded together by some physical bounds and break-up under shearing such solutions. This sort of molecular entanglements were found in polymer solutions, especially in concentrated and freshly prepared ones. Therefore, when the concentrated solutions were injected into the flow, the agglomerations were broken up into a smaller and smaller aggregates by the shearing action of the turbulence eddies of the flow. Consequently, the size of the polymer aggregates would be of the same size as the turbulent eddies in flow and would result in a polymer-turbulence interaction at any Reynolds number. As a result one should expect that drag reduction by injecting concentrated polymer solutions would set in with the turbulence onset in the flow.

4.3.4 The Influence of Aging the Injected Solutions on The Drag Reduction

The above discussions revealed the fact that the viscoelastic properties of the injected polymer solutions affect both the development and the asymptotic value of the local drag reduction by polymer injection. In chapter III the turbulent diffusion of the injected solutions was found to be dependent on its viscoelastic properties while the drag reduction efficiency of the injected solutions is believed to be dependent on the polymer agglomerations in the flow.

The effect of aging the polymer solution was investigated by Brennen & Gadd (1967). They reported that the viscoelastic effects on the pitot tube reading in dilute polyox solutions disappeared after storing the solution for several days, but the effectiveness of these solutions as drag reducers was not affected. White (1968) results showed that aged polymer solutions (30 wppm Polyox WSR-301) for 17 days gave an increase in the onset shear stress. He postulated this effect

to be due to the presence of polymer aggregates which disappeared with aging the polymer solution. Fabula (1966) measurements of turbulence in polyox solutions behind a grid revealed some anomalous ragged signal which was believed to be due to the presence of polymer agglomerations in the flow. He found that the raggedness of the signal disappeared with aging the polymer solutions. Granville (1968) found that the viscoelastic properties of Polyox solutions disappeared with aging while their drag-reducing efficiency did not. In order to explain that and to distinguish between the viscoelastic nature of these solutions and their drag reducing ability, he postulated that the solution viscoelasticity is stored in the molecular entanglements which slowly dispersed with aging and stirring while the drag reducing ability is stored in the polymer molecules which was not affected by aging.

In order to investigate the influence of aging the injected solutions on the drag reduction achieved by the injection technique, two Polyox WSR-301 solutions (500 and 1000 wppm) were stored to age for several days. The polymer solutions of different ages were injected into the centreline of the water pipe flow. The local drag reduction was measured and the results were plotted as a function of the distance downstream from the injector. Representative experimental results are shown in figures (4.6) and (4.9). Figure (4.6) shows the results of injecting fresh polymer solution of 1000 wppm concentration (one day after the usual preparation procedure mentioned in chapter II), while, figure (4.9) represents the results of an identical solution aged for three weeks and injected at the same experimental conditions of the fresh solution experiments. It is not difficult to see the remarkable relaxation of the viscoelastic properties influence on the development exhibited by the aged solution results shown in figure (4.9).

A more detailed comparison between fresh and aged polymer solution results are shown in figures (4.17) and (4.18). The results of both the two polymer concentration (500 and 1000 wppm) exhibited a faster development of the local drag reduction and asymptotes at lower values in the aged than in the fresh solutions. The fast development of the local drag reduction is believed to be due to the decrease in the viscoelastic properties of the aged polymer solutions, which resulted in an increase in the turbulent diffusion of these solutions (as we have discussed in chapter III). The relaxing of the influence of the viscoelastic properties on the behaviour of aged polymer solutions was experimentally demonstrated by a number of investigators as discussed above. This relaxed effect is thought to be due to the dispersion of the polymer entanglements in the solution with aging. Consequently, the aged solutions are expected to be less entangled and the formed agglomerations are easier to be torn off by the eddying motion to smaller and smaller sizes, as they are introduced into the turbulent flow, than fresh solutions. The high level of drag reduction achieved by polymer injection is demonstrated by the presence of super-molecular aggregates in the flow. Hence, the drag reduction by injecting aged polymer solutions is lower due to the presence of smaller polymer aggregates than in fresh solutions.

As shown in figure (4.18), The results of one day aged solution and that of one week aged are indistinguishable and the differences are within the experimental error. This result is in agreement with the viscosity measurements of concentrated Polyox solutions (Ramu & Tullis (1976)). They reported that the viscosity decreased by about 2% within 8 days and the aging effect was found to accelerate after 10 days.

4.3.5 The Effect of Reynolds Numbers on the Drag Reduction by Polymer Injection

The effect of varying the flow Reynolds numbers on the drag reduction by polymer injection was studied before by Vleggaar & Tels (1973-b) and Stenberg et al (1977-a,b). These investigations revealed that the drag reduction by injecting concentrated polymer solutions into the flow is higher than that in homogeneous solutions. The difference was found to be larger and larger as the flow Reynolds number gets smaller. The most interesting result obtained was the disappearance of the critical shear stress of the drag reduction onset. Hence, drag reduction by polymer injection was found to occur in all turbulent Reynolds numbers. Both Vleggaar & Tels and Stenberg et al observed the disappearance of the onset point for drag reduction by the injection of concentrated polymer solutions into the flow.

The effect of Reynolds number was investigated in this study to demonstrate its influence on the drag reduction by polymer injection. The results for the local drag reduction as a function of the distance from the injector were plotted for different flow Reynolds numbers. In figure (4.19), which shows the results at $Re = 2.8 \times 10^4$, represents an example of the results obtained at different flow Reynolds numbers. The results are very similar to that measured at $Re = 4.5 \times 10^4$ presented before. In figure (4.20) the asymptotic value of the local drag reduction as a function of the average polymer concentration in the flow is shown in comparision with the homogeneous solution results of Goren and Norbury (1967). The results shown in figure (4.20) exhibited a large difference between the drag reduction by polymer injection and that resulted in homogeneous solutions at such low Reynolds number.

Figure (4.21) represents the results of the asymptotic local drag reduction by injecting Polyox WSR-301 solutions of concentration 1000 wppm at different Reynold numbers. The results were plotted on Prandtl-von Karman coordinates which is a linear plot of $\frac{1}{\sqrt{f}}$ against the logarithim of Re $\sqrt{f}$. Such a plot produces a straight line between $\frac{1}{\sqrt{f}}$ and Re$\sqrt{f}$ with a slope (A) which is related by Prandtl to the von-Karman constant (k) by the relation (Schlichting (1960)).

$$A = \frac{2.3}{\sqrt{2}} \frac{1}{k} \tag{4.1}$$

Available data of Newtonian flows are in good agreement with equation (1.1). Drag reducing polymer solution flows also describe a straight line in Prandtl-Karman co-ordinates with slope increasing progressively with the polymer concentration until the maximum drag reduction is reached. (Virk (1971) Goren & Norbury (1967) and Peterson et al (1973)). It was found also that these straight lines intersect with that of the Newtonian flow at the onset point which is independent of the polymer concentration. These experimental observations could suggest a similar relation to that of Prandtl-Karman to describe the flow parameters. Virk (1970), in the light of his three-layer model, derived the following relation:

$$\frac{1}{\sqrt{f}} = (4.0+\delta) \log_{10} (Re\sqrt{f}) - (0.4+\delta\log_{10}(\sqrt{2}\, dw^*)) \tag{4.2}$$

and

$$W^* = u^*_{cr}/\nu \tag{4.3}$$

where, u^*_{cr} is the wall shear stress at drag reduction onset, d is the pipe diameter and δ is the slope increment which is related to the upward shift in the logarithimic region of the mean velocity profile in drag reducing solutions (ΔB) by the equation:

$$\delta = \frac{\Delta B}{\sqrt{2} \log_{10} (u^*/u^*_{cr})} \tag{4.4}$$

The above relation is bounded between two extremes; the Prandtl-Karman Law of Newtonian flows (equation 1.1) and the maximum drag reduction asymptote of Virk (equation (1.3)).

Water flow data in figure (4.21) showed a good agreement with Prandtl-Karman Law (equation (1.1)). Polymer (Polyox WSR-301, 1000 wppm) injection results at average polymer concentrations of 1.0, 3.0, 5.0, 8.0, 10.0, and 20.0 wppm respectively are shown in figure (4.21). The results were described by straight lines where all of them intersected with the line representing Prandtl-Karman Law at the same point. The intersection point represents the drag reduction onset flow conditions (Virk (1975) Goren & Norbury (1967)). The onset drag reduction conditions were found to be 9.2 and 240 for $\frac{1}{\sqrt{f}}$ and $Re\sqrt{f}$ respectively which corresponds to a critical Reynolds number of 2.3×10^3. This value of the Reynolds number showed that the drag reduction was established with the beginning of the turbulent flow region. This result is in agreement with what we have mentioned before that the drag reduction by injecting [illegible] concentrated polymer solutions is characterized by the disappearance of the onset point. The onset wall shear stress was found to be 0.065 N/m^2 which is considered very small compared with the onset data of homogeneous polymer solution Table (4.1) present our drag reduction parameters in comparision with other previous results in both homogeneous polymer solution and polymer injection studies. From the table, the most dramatic difference between drag reduction by injecting concentrated polymer solutions into the flow and that of the homogeneous solutions is the low value of the onset wall shear stress associated with polymer injection.

Virk (1970) found that the slope increment δ proportions with the square root of the polymer concentration. Later, Virk (1971) found that $\delta/c^{\frac{1}{2}}$ is a characteristic parameter of the polymer type and molecular weight and its value is a measure of the efficiency of the polymer as drag reducer. As we see in table (4.1) there is no difference between the $\delta/c^{\frac{1}{2}}$ values for drag reduction by polymer injection and that for homogeneous solutions. This could be explained by the fact that the parameter is a unique function of the molecular characteristics (Virk (1975)) and represent the efficiency of the polymer molecules to reduce the frictional drag as they are involved in interaction with the flow eddies. While the onset point represents the range of the turbulence scales that interact with the polymer molecules or aggregates. As the earlier the onset occurs, the wider the range of the turbulent scales that interact with the polymer. Therefore, at high Reynolds numbers, where the turbulence scales are of comparable dimensions with those of polymer molecules, the influence of the presence of the polymer aggregates in the flow is small. At low Reynolds numbers, the turbulence scales are small to be involved in interaction with the polymer molecules. Consequently, the polymer turbulence interactions are dominated by the super molecular polymer clusters which bring more turbulent scales to interact with resulting in a high drag reduction.

The same experimental results presented in figure (4.21) were plotted in the normal way as the friction factor against the flow Reynolds number and shown in figure (4.22)

4.3.6 The Second Pass Drag Reduction Results

In the previous sections, we showed that the drag reduction by injecting concentrated polymer solutions into the flow exhibited higher values than those reported for homogeneous polymer solutions at the same experimental conditions. Then we discussed the hypothesis that polymer agglomerations play an important role in the drag reduction by polymer injection. In the following discussion we will present the drag reduction results measured near the end of the second pass of the pipe flow described in chapter II. These results monitored the drag reduction at a distance of 350 pipe diameters from the injector and after passing a U-turn at the end of the first pass.

Figures (4.23) and (4.24) present the drag reduction results of the second pass for Separan AP-30 and Polyox WSR-301 respectively in comparision with the asymptotic drag reduction results. The results of the second pass drag reduction exhibited lower values than those of the asymptotic local drag reduction. The difference was found to be about 10% of the asymptotic value. In general, the results showed that the difference was slightly larger in Separan results than that in Polyox results. Since Separan solutions are characterized by their high resistance to mechanical degradation (Peterson et al (1973)), we believe that the lower drag reduction of the second pass was not due to mechanical degradation of the polymer molecules in the solution. It was also not due to changes in the polymer concentration in the flow cross section because of the experimental evidence presented before that the development of the drag reduction reached its maximum asymptotic value as the polymer concentration became homogeneously distributed in the flow.

These results strongly supported the hypothesis introduced to explain the drag reduction results by injecting concentrated polymer solutions into the water flow. Since polymer molecules in such super-molecular agglomerations are bounded together by some weak physical bonds (Lumely (1977) and Dunlop & Cox (1977)). Such polymer agglomerations are expected to split into smaller aggregates by the eddying motion in turbulent shear flow. This observation was noted by Stenberg et al (1977-a,b) when they found that the concentrated polymer solutions injected into the flow formed a small visible strands which split-up into finer and finer strands downstream and eventually disappeared.

The second pass drag reduction results indicated that the size of the polymer agglomerations is getting smaller and smaller downstream from the injector by the shearing action of the eddies in the flow. Since polymer agglomerations play an important role in drag reduction by polymer injection, especially at low Reynolds number, the drag reduction decreases as the size of the agglomerations decreases with the shearing action of the turbulence in the flow. Figure (4.20) presents the second pass drag reduction results at a lower Reynolds number ($Re - 2.8 \times 10^4$) which confirmed the other results of figures (4.23) and (4.24) of Separan and Polyox at Reynolds number 3.7×10^4 and 4.5×10^4 respectively.

4.3.7 Comparison with Other Experimental Results

In the foregoing discussion, we showed some comparisons between our results and other previous results. These comparisons revealed the high drag reduction achieved by polymer injection compared with that achieved in homogeneous polymer solutions at the same experimental conditions. The results presented in figures (4.15), (4.16) and (4.20) showed that even the lower drag reduction of the second pass

was larger than the homogeneous solution results. At lower Reynolds numbers the exhibited difference increases as we discussed before. Experimental evidence discussed in this section suggested the presence of super molecular agglomerations which are assumed to be responsible for the high drag reduction level achieved by injecting concentrated polymer solutions into the flow.

One of the remarkable observations of figure (4.15) was the drag reduction results obtained by Vleggaar and Tels (1973). Their results by polymer injection exhibited lower values than our results of the asymptotic value and the second pass drag reduction value. The difference could be attributed to the fact that our results represent the maximum value by which the local drag reduction development asymptotes, while Vleggaar & Tels results were average values for the local drag reduction over the distance between 50 to 150 pipe diameters downstream from the injector where the drag reduction was still developing and did not reach its asymptotic value.

In order to compare the drag reduction by polymer injection results with that of homogeneous solutions at different Reynolds number, our results of an average polymer concentration of 8.0 wppm were plotted in figure (4.25) in comparison with some results of homogeneous Polyox WSR-301 solutions. The homogeneous solution results were calculated from the data present in table (4.1) at the same experimental conditions as those of our experiments. As we noticed in the data tabulated in table (4.1), the results in figure (4.25) clearly showed that the only dramatic difference between the drag reduction by polymer injection and that exhibited in homogeneous solutions was the early drag reduction onset in the case of the polymer injection. The slope of the straight lines describing the results seemed to be the same for both polymer injection and homogeneous

solution results. These results strongly confirmed the assumed hypothesis that polymer agglomerations play the important role in the high drag reduction achieved by polymer injection as we have discussed before.

The effect of the early drag reduction onset on the drag reduction value at any Reynolds number, after the onset, could be clearly observed in figure (4.25). The difference in drag reduction between the homogeneous and injection results is observed to be large as the difference between their onset points is large and as the Reynolds number at which the comparision is made is small. While the difference is getting smaller as the Reynold number increased.

It is relevant to mention here, that the low value of the onset wall shear stress by Goren & Norbury (1967) was obtained by injecting polymer solutions of concentration 675 wppm into the wall of 2 inch pipe diameter water flow. In spite of the careful polymer solution preparation which minimized the possibilities for the formation of super-molecular agglomerations, it is believed that their onset results could be affected by the presence of small polymer aggregates. They reported that the drag reduction results by injecting such relatively concentrated solutions were much better than those obtained in homogeneous solutions. They attributed the difference to the improved mixing technique used to prepare the injected solutions.

Comparison between our results and the other available results of drag reduction by polymer injection is shown in figure (4.26). The general feature of the result was its low onset shear stress which is usually found to be corresponding to the Reynolds number of which the flow changed from laminar to turbulent (Re $\simeq$ 2100 - 3000) or very near to that value of the Reynolds number. Consequently, the onset wall shear stress exhibited in flows with polymer injection would be affected

by the pipe diameter as well as the polymer characteristics and the method of solution preparation. This result is observed in the onset wall shear stress results shown in figure (4.26) and presented in table (4.1). A value of 0.13 N/m^2 onset wall shear stress was obtained by the results of Ramu & Tullis when they injected concentrated Polyox solutions into the wall shear stress into the wall of 12 inch diameter pipe flow, while the onset wall shear stress results of Stenberg et al were corrosponding to 0.3 and 0.25 N/m^2 for pipes of 0.78 cm and 1.03 cm diameters respectively. As listed in table (4.1), our results with polymer injection into water pipe flow of diameter 2.6 cm exhibited an onset wall shear of 0.064 N/m^2.

In this section we have discussed the differences between the drag reduction by polymer injection and that of homogeneous solutions. The comparision was carried out over the whole Reynolds number range investigated. In the following discussion, an attempt to reveal the differences between drag reduction by polymer injection and that of homogeneous solutions at the same Reynolds number will be carried out.

Virk (1967), in an attempt to develop a correlation between the polymer concentration and the drag reduction, defined a characteristic intrinsic concentration as:

$$\{C\} = DR_m \Big/ \lim_{C \to 0} (DR/C) \qquad (4.5)$$

where, DR_m is the maximum drag reduction for a given Reynolds number and $\lim_{C \to 0} (DR/C)$ is the intrinsic drag reduction. The drag reduction data was found to fit an empirical equation which was first proposed by Virk (1966) and later modified by Little et al (1975) into the form:

$$\frac{DR}{DR_m} = \frac{1}{1 + C/\{C\}} \qquad (4.6)$$

In this equation, there are two empirical parameters DR_m and {C} characterizing the polymer solution. The maximum drag reduction DR_m represents the upper limit which can be obtained by increasing the polymer concentration, while the intrinsic polymer concentration {C} is the concentration level at which the drag reduction reaches half the maximum drag reduction DR_m. The maximum drag reduction divided by the intrinsic concentration, $DR_m/\{C\}$ is a measure of the efficiency of the polymere because it represents the drag reduction per unit concentration.

In order to use equation (4.6) to fit the experimental results, Little et al (1975) proposed a rearrangement which leads to a straight line relation between $\frac{C}{DR}$ and C as:

$$\frac{C}{DR} = \frac{\{C\}}{DR_m} + \frac{C}{DR_m} \qquad (4.7)$$

A plot of C/DR versus the concentration C was found to be successfully described by the above equation (see figure (4.27). The intercept value at C/DR = 0 yields the intrinsic concentration {C}, while, the intercept value at C = 0 yeilds the value of $\frac{\{C\}}{DR_m}$. Hence, the maximum drag reduction DR_m could be calculated by dividing {C} by $\{C\}/DR_m$, or from the slope of the straight line.

In figure (4.27) our drag reduction by polymer injection results were plotted as Cav/DR versus Cav at different flow Reynolds numbers. All the results were found to be successfully described by straight lines each represents the data of a certain Reynolds number. The results exhibited a constant value of the intrinsic concentration independent of the flow Reynolds number. While the maximum drag reduction DR_m was found to decrease as the flow Reynolds number decrease which was observed in the increase of the straight line slopes ($1/DR_m$) with the decrease in the flow Reynolds number.

These results are in general agreement with the experimental evidence which indicates that the maximum drag reduction is a function of the flow Reynolds number, while the intrinsic concentration is a purely polymeric parameter.

In figure (4.28) we present a comparison between our results of injecting Separan AP-30 into the flow and other previous experimental results. The results of the intrinsic concentration, maximum drag reduction and $DR_m/(C)$ which is considered as a measure of the polymer efficiency as a drag reducer were tabulated in table (4.2). The results showed the increased polymer efficiency, with polymer injection, which is caused by both changes in the intrinsic concentration and the maximum drag reduction.

The results of Polyox solutions were plotted in figure (4.29) and calculated values of the intrinsic concentration, maximum drag reduction and the polymer efficiency are included in table (4.2). They are in agreement with that of figure(4.28) of Separan AP-30 which indicated that polymer injection resulted in a higher maximum drag reduction, and lower values for the intrinsic polymer concentration than those of homogeneous polymer solutions. Hence an increase in the efficiency of the polymer solution.

The decrease in the intrinsic concentration associated with the drag reduction by polymer injection indicated that the polymer concentration required to achieve a certain value of drag reduction is smaller than that required in homogeneous solutions. Since the polymers used in the investigation were commercial types with a wide range of molecular weight distribution around an average value, we thought that the super-molecular agglomeration formed in the flow with injection help in shifting the size distribution of the polymer molecules and aggregates to higher values and consequently most of the polymer molecules take part in the polymer-turbulence interaction.

4.4 DRAG REDUCTION - POLYMER CONCENTRATION CORRELATION

In the previous sections of this chapter, we discussed the drag reduction by injecting concentrated polymer solutions into the centre-line of a water pipe flow. The discussion revealed the presence of a similarity between the drag reduction development with the distance downstream the injector and that of the polymer concentration near the wall. Such similarity in drag reduction and polymer concentration near the wall suggested that there could be a relation between the drag reduction and the polymer concentration at a certain region near the wall. In this section, we will introduce an analysis used to predict the drag reduction from the polymer concentration measurement results discussed in chapter III. A comparison between the predicted large reduction development and the experimentally measured results discussed in this chapter indicated that the critical shear region, where polymer becomes effective in reducing wall friction could be estimated. The results of this investigation will be presented and disucssed in this section.

The analysis is based on the assumption that the drag reduction achieved is a function of the polymer concentration in a narrow region in the flow not in the whole flow. The assumption is supported by the experimental evidence exhibited by the drag reduction results. This evidence could be understood from the results which showed that the most affected region of the flow by the presence of the polymer is near the solid boundaries (for more details see chapter I). More direct evidence was given by injecting the polymer solutions into the flow. The results of injecting the polymer into the wall exhibited drag reduction just downstream the injector, while, the injection into the core of the flow resulted in a drag increase when the polymer was still in the core and the drag reduction started to build up as the polymer reached the wall region as we have discussed in this chapter.

In chapter III, we discussed the results of the polymer concentration measurement of the injected polymer solutions into the centreline of water pipe flow. The results are plotted in figures (3.3) and (3.4) for Separan AP-30 and in figures (4.7) and (4.8) for Polyox WSR-301, both at concentrations 1000 and 3000 wppm respectively. The polymer concentration measurement results near the wall were replotted in large scales and shown in figures (4.30), (4.31) (4.32) and (4.33) in order to increase the accuracy of the next calculations.

As we suggested before, the influence of the polymer molecules or aggregates is mainly confined to a narrow region, where polymer-turbulence interactions are most effective in reducing the wall friction. The drag reduction achieved is produced by the amount of the polymer in this critical region. Then, it is a reasonable inference that the amount of drag reduction at any distance x/d from the injector will be determined by the local polymer concentration c(x,r) averaged over the width of the critical region to give the polymer concentration $\bar{c}$ in this region. It is also reasonable to infer that the magnitude of this local drag reduction will be equal to that measured in a pipe flow with homogeneous polymer solution or with a uniformly dispersed polymer solution of concentration $\bar{c}$ (i.e. a flow in which $c(x,R) = C_{av} = \bar{c}$).

In the pipe flow studied in this work, the critical region was supposed to be an annulus somewhere near the pipe wall with a centroid radius r_m and thickness Δr. The polymer concentration c of the annulus was taken as the averaged value over the range from $(r_m - \frac{\Delta r}{2})$ to $(r_m + \frac{\Delta r}{2})$ which was calculated from the least squares fit of the polymer concentration profiles shown in figures (4.30) to (4.33).

Since the local drag reduction was found to reach the asymptotic value as the concentration of the injected polymer solutions became uniformly distributed in the flow, and the magnitude of the asymptotic drag reduction is a unique function of the average polymer concentration in the flow (see figures (4.13) and (4.14)). The magnitude of the drag reduction which is supposed to be achieved as a result of a polymer concentration $\bar{c}$ over the annulus, was taken the asymptotic drag reduction at an average concentration C_{av} equals to $\bar{c}$.

At first stages of our analysis we assumed $\Delta r = 0$ and varied the annulus position from $r_m/R = 1.0$ to 0.75 in equal steps of 0.05. The results of the two Separan AP-30 are presented in figures (4.34), (4.35) and the Polyox WSR-301 results are shown in figure (4.36) and (4.37). Each of the four figures contains two sets of results for different annular radial positions r_m in the flow. First, the annular mean concentration $\bar{c}$ is shown as a function of the distance x/d from the injector for various values of r_m. Second, figures (4.13) and (4.14) have been used to relate $\bar{c}$ to the local drag reduction for Separan AP-30 and Polyox WSR-301 respectively, and the resulting predicted drag reduction for each annulus is plotted as a function of x/d for each r_m. Comparable measured values, under the same experimental conditions, are also shown in the figures of the four polymer solutions. The results clearly indicated that there is good agreement between the predicted local drag reduction of an annulus at $r_m = 0.90$ R and the experimentally measured values.

Further steps were taken to give the analysis more physical interpretation and to define the thickness of the critical region. The thickness of the annulus was taken as $\Delta r = 0.05R$ and the results of the four polymer solutions are presented in figures (4.38), (4.39), (4.40) and (4.41). The results also exhibited good agreement between the predicted local drag reduction of the 0.9R anulus and the experimentally measured values.

The thickness of the annulus was increased further to 0.1, 0.15 0.20 of the pipe radius R. The results were plotted in the same way as in figures (4.34) to (4.41) in which all the results showed a good agreement between the predicted results of the 0.9R annulus and the measured values. The results obtained by varying the annulur thickness Δr indicated that changing Δr of the 0.9R annulus has little effect on the agreement. The deviation of the calculated results from that experimentally measured was calculated and the standard deviation σ of each plot was obtained. The results of the standard deviation of an annulus thickness of $\Delta r/R = 0.00$ and r_m varied from $r_m/R = 1.0$ to 0.75 are presented in figure (4.42), which indicated that the good agreement between the experimental and the predicted results is obtained at $r_m/R = 0.90$ where the lowest standard deviation values were found for the four polymer solutions tested. In figure (4.43) the standard deviation results calculated for the annulus $r_m/R = 0.9$ with various thicknesses $\Delta r/R$ ranging from 0.00 to 0.20. The results showed that the good agreement is good for $\Delta r/R$ up to 0.15, but pooner as Δr increases more than 0.15R. (McComb & Rabie (1978)).

In conclusion, we can suggest that polymer molecules (or aggeegates) have their maximum influence on the flow near a radius of 0.9R with a thickness of 0.05 - 0.15R. These results correspond to a region of dimensionless distances from the wall extending from $y^+ = 00$ to $y^+ = 100$. In this region, where most of the turbulent energy production and dissipation occurs, the most dramatic changes due to the presence of the polymer in the flow were found (see chapter I). More discussion about the importance of this region in the flow will be found in the next chapter.

TABLE 4.1

EXPERIMENTAL DATA FOR THE ONSET WALL SHEAR AND THE SLOPE INCREMENT FOR POLYOX WSR-301

M x 10^{-6}	d cm	c range wppm		τ_w^* N/m^2	$\delta/c^{\frac{1}{2}}$	Reference
3.7	0.27	30	H	2.9	2.92	Liaw (1968)+
4.7	0.22	0.29 - 2.2	H		7.8 ± 0.3	Shin (1965)+
5	5.08	2 - 50	H	0.27 ± 0.05	5.0 ± 4.0	Goren & Norbury (1967)
4.5	2.0	2 - 40	H	0.45	4.7 ± 0.2	McNally (1968)+
5.3	0.46	1 - 30	H	-	3.9 ± 0.5	Virk (1966-1971)+
5.3	0.95	1 - 30	H	0.7 ± 0.15	4.7 ± 0.2	
5.5	0.85	10 - 100	H	0.71 ± 0.15	4.6 ± 0.3	
6.1	6.42	20 - 500	H	0.35 ± 0.1	3.3 ± 0.7	
5	0.78	50	I	0.28 ± 0.02	2.2 ± 0.5	Stenburg et al (1977-a)
5	1.03	10 - 50	I	0.25 ± 0.05	3.8 ± 1.0	
4	4.13	3 - 9	W	0.2 ± 0.05	2.2 ± 0.2	Maus & Wilhelm (1970)
4	30.5	2 - 6	W	0.13 ± 0.02	6.5 ± 0.5	Ramu & Tullis (1976)
5	2.6	1 - 20	CL	0.064 ± 0.005	6.1 ± 1.2	Present Work

I Drag reduction results by injecting concentrated polymer solutions into water flow

W Wall injection results

CL Centre line injection results

H Results of homogeneous polymer solutions

\+ Data taken from Virk (1975)

TABLE 4.2

Polymer	M x 10^{-6}	Solution	(C) wppm	$\%DR_m$	$\%DR_m/(C)$	Reference
Separan AR30*	3.0	Homogeneous	4.0	36.0	9	Whitsitt (1968)
	3.0	C.L. Injection	3.0	50	16.7	Vleggaar & Tels (1973)
	3.0	Asymptotic	2.0	69.0	34.5	Present work
		Second pass	2.1	63.0	30.0	
Polyox WSR-301**	5.3	Homogeneous	1.5	58.0	39.0	Virk (1975)
	4.5	Homogeneous	1.25	60.0	43.0	McNally (1968)
	5	Asymptotic	0.65	72.5	111.5	Present work
	5	Second pass	0.95	68	71.5	C.L. Injection
	5	Maximum DR +	0.50	74	148	Present work
	5	Second pass +	0.65	68	105	Wall injection
	5	Maximum D.R. ++	0.30	76.5	255	
	5	Second pass ++	0.70	69.5	99	

* Separan results are at Re = 3.7×10^4, except that of Vleggaar & Tels was at Re = 5.25×10^4

** Polyox WSR-301 results all at Re = 4.5×10^4

\+ Results of the wall injection Cp = 500 and 1000 wppm

++ Results of the wall injection Cp = 3000 wppm

CHAPTER V

DRAG REDUCTION BY INJECTING POLYMER SOLUTIONS INTO THE WALL REGION OF A WATER PIPE FLOW

5.1 INTRODUCTION

In chapter IV, we discussed the drag reduction by injecting relatively concentrated polymer solutions into the centreline of a water pipe flow. The results clearly showed that the frictional drag was increased over the water flow value in the region up to 15 pipe diameters from the injector where the polymer was still in the core of the pipe flow. This result indicated that polymer-turbulence interaction in the core, if any, is not responsible for the drag reduction. Then, the local drag reduction increasingly developed to an asymptotic value when the injected solutions became uniformly distributed in the flow. The similarity between the development of the local drag reduction and that of the polymer concentration near the wall suggested that the local drag reduction could be related to the polymer concentration in a region somewhere near the wall. McComb & Rabie (1978) found that such correlation indicated that polymer molecules (or agglomerations) exert their main influence on the flow near a radius of 0.9 R which is corrosponding to a region which extends from $y^+ = 0$ up to $y^+ = 100$.

In this chapter, we will discuss the drag reduction results by injecting the polymer solutions into the wall region of the pipe flow. Fortunately, drag reduction by injecting polymer solutions into the wall region has received much more attention than centreline injection. Most of these investigations were carried out by ejecting the polymer solutions into the wall region of a flat plate to study the economic and the possible drag reduction applications in external flow. Some

of these investigations were carried out by injecting the polymer solutions into the wall region of a pipe flow mostly to study the effectiveness of the injection techniques. In spite of the dependence of the drag reduction upon the injection techniques used, a general agreement among the results obtained was shown (as we discussed in chapter I). The dependence of the wall injection results upon the injection technique is in fact a dependence upon the diffusion process of the polymer into or out of the most effective region.

As a complementary study of our investigation, we injected relatively concentrated Polyethylene oxide (Polyox WSR-301) into the wall region of the water pipe flow discussed in chapter II. Three polymer concentrations were used, 500, 1000 and 3000 wppm. In the following sections we will discuss our experimental results. More concern will be given to the importance of the wall region in drag reduction.

5.2 DISCUSSION OF THE RESULTS

The experiments were carried out in the 26 mm diameter water pipe flow system described in chapter II and previously used in centreline injection experiments. The only change was the replacement of the centreline injector with the wall injector described in chapter II and shown in figure (2.8). The injector was designed to deliver the polymer solutions into the wall region with the minimum possible disturbance to the flow and as close to the wall as possible.

The experimental procedure and the data processing were exactly the same as used in the centreline injection experiments and discussed in chapter IV. Only polyethylene oxide (Polyox WSR-301) was used throughout this part of the investigation in three relatively concentrated solutions of 500, 1000 and 3000 wppm.

The results of injecting the polymer solutions into the wall will be discussed in this section in the following order.

1. The development of the drag reduction with the distance downstream from the injector.
2. The effect of the average polymer concentration.
3. The results of the second pass.
4. Comparison with other results.
5. The influence of the bursting process on the drag reduction development.

5.2.1 Drag Reduction Development with the Distance Downstream

In chapter IV we found that the local drag reduction develops from a negative value just downstream from the injector, increasing with the distance until it reaches an asymptotic value. The turbulent diffusion study discussed in chapter III indicated that the local asymptotic drag reduction is reached when the injected solutions become homogeneously distributed in the flow.. Representative results of polymer solutions wall injection are shown in figures (5.1), (5.2) and (5.3) in comparison with the centreline injection results at the same experimental conditions. These figures exhibit the differences between the development of the local drag redcution of the centreline injection and that of the wall injection. The most remarkable difference is the fast development of the local drag reduction of the wall injection to a higher value than the asymptotic value of the centreline injection. Then the local drag reduction slowly decreased until the centreline injection asymptotic value is attained downstream. The difference between the wall injection maximum drag reduction and the centreline asymptotic value was found to increase with the concentration of the injected solutions. The results also showed that the distance at which the local drag reduction by wall injection reaches the centreline injection asymptotic value was increased with increasing the concentration of the injected solutions.

A comparision was carried out between the local drag reduction results of a wall injection of 100 wppm Polyox WSR-301 solution shown in figure (5.2) and the development of polymer concentration at different location in the cross section shown in figure (3.11). The comparison indicated the presence of a similarity between the development of the local drag reduction and that of the polymer

concentration at r = 0.90 R. In this region the polymer concentration was found to build up rapidly to higher values than the average polymer concentration. Then, the polymer concentration slowly decreased to the average concentration in the flow.

As we discussed before, the presence of the polymer molecules or aggregates in the most effective region near the wall may be responsible for the observed drag reduction in polymer solutions. The results obtained by injecting the polymer solutions into the wall confirmed the conclusions we derived by the results of the centreline injection discussed in chapter IV. The results of the wall injection exhibited that the presence of the polymer near the wall, and not at the wall itself, is necessary for the drag reduction. In spite of the maximum polymer concentration observed in the wall region just downstream from the injector, the local drag reduction was found to be less than half the maximum value obtained by the wall injection. This result completed the picture obtained by the centreline injection results indicating that the drag reduction is totally represented by the polymer in the most effective region which was found to extend from $y^+ = 00$ to $y^+ = 100$. The importance of this region could be demonstrated by the fact that most of the turbulent energy generation and dissipation are localized in this region (Hinze (1975)).

The high levels of the local drag reduction by injecting polymer solutions into the wall of pipe flows over that achieved when the injected solutions became homogeneously distributed in the flow was observed earlier by Walters & Wells (1971) and Ramu & Tullis (1976). Walters & Wells injected Polyox WSR-301 solutions of concentrations 1000 and 5000 wppm through porous wall into the pipe flow. Their results showed a decrease in the local drag reduction with the

distance downstream. They envisaged this effect to be due to the shear degradation of the polymer solution. Ramu & Tullis injected the polymer solutions (Polyox WSR-301 of concentrations varied from 100 to 2400 wppm) using 30° inclined holes to the main stream direction drilled in the pipe wall. Their local drag reduction results showed a maximum just downstream the injector and rapidly dropped off to a constant value downstream. This maximum local drag reduction by wall injection could be attributed to the increase of the polymer concentration in the most effective region above the average value in the flow. Such increase in the polymer concentration was observed in the development of the polymer concentration in the 0.9 R region (see figure (3.11)). As the polymer diffused outwards into the core of the flow, the local drag reduction dropped off to a constant value. The location at which the local drag reduction asymptotes was found to be consistent with the location where the polymer becomes uniformly distributed across the flow.

The differences in the rate of the development of the local drag reduction between our results presented in figures (5.1), (5.2) and (5.3) and other wall injection results could be attributed to the type of the injector, the angle of injection and the concentration of the injected solutions. These factors, in fact, affect the diffusion process of the polymer into and out of the most effective region. Ramu & Tullis (1976) and Walters & Wells (1971) results showed a maximum local drag reduction just downstream from the injector. This may be due to the large angle of injection used (90° in the porous wall injector used by Walters & Wells and 30° used by Ramu & Tullis). A large angle of injection allows the polymer to be delivered into the most effective region. Our results exhibited a developing part after the injector. This is attributed to the small angle of injection used (8° to the main stream direction).

The local drag reduction results by injecting the polymer solutions into the wall region of the flow were characterized by oscillatory scatter. McComb & Rabie (1978) related such oscillatory variation in the wall friction to the phenomenon of turbulent bursts as we will discuss later in this chapter.

5.5.2 The Effect of the Average Polymer Concentration

In chapter IV, the asymptotic value of the local drag reduction by polymer centreline injection was found to depend only on the average polymer concentration in the flow. The results were higher than those obtained by homogeneous polymer solutions. The differences were more impressive at low Reynolds numbers and at low polymer concentration in the flow. The comparision between the local drag reduction of centre-line injection and that of wall injection showed that the drag reduction by wall injection has a maximum slightly higher than the asymptotic value of the centreline injection. The difference increased with the increase in the concentration of the injected polymer solution (see figures (5.1), (5.2) and (5.3)).

The maximum local drag reduction results by injecting concentrated polymer solutions into the wall region of the flow are presented figure (5.4) as a function the average polymer concentration in the flow. The results showed a slight increase over the asymptotic value of the centreline injection shown in figure (4.14). The results of injecting 3000 wppm Polyox WSR-301 solution exhibited higher drag reduction values than those of 500 and 1000 wppm solutions. A comparision between the 3000 wppm solution results and those of 500 and 1000 wppm solution are present in figure (5.5). The comparison showed a difference of about 7% which would clearly be observed if we compared the results of the local drag reduction presented in figures (5.2) and (5.3). The large degree of drag reduction, exhibited by the 3000 wppm, could be attributed to the larger polymer agglomerations present in concentrated polymer solutions than those present in the less concentrated ones (500 and 1000 wppm).

The dependence of the maximum local drag reduction on the concentration of the injected solutions was not observed in the asymptotic local drag reduction results by centreline injection. This result could be attributed to the longer time taken by the polymer, injected in the centreline, to reach the most effective region near the wall. As we discussed in chapter III, we found that the higher the concentration of the injected solutions, the longer the time taken to reach the near wall region. During the time of the diffusion the large polymer agglomerations would be broken into smaller and smaller aggregates by the eddying motion of the flow (Gadd (1965-a) and Stenberg et al (1977-a). The long shearing time taken by higher concentrated polymer solutions resulted in more deagglomeration of the larger aggregates initially present in these solutions. Eventually, they reach the near-wall region in comparable sizes to those resulting from the injection of less concentrated solutions. The resulting size of the agglomerations is assumed to be comparable to that of the eddies responsible for their diffusion (see chapter IV). As we will discuss in the next section, the results of the second pass drag reduction are independent on the injected solution concentration. This result is consistent with the suggestion that for long shearing times the resulting agglomeration sizes are independent on the size of the initially present ones. On the other hand, the short times taken by the polymer solutions injected into the wall region to reach the most effective zone give no chance for the large agglomerations to breakup into smaller. A similar hypothesis was suggested before by Cox et al (1974) to explain their time dependent drag reduction results of a rotating disc in freshly prepared polymer solutions.

5.2.3 The Second Pass Drag Reduction Results

The drag reduction results of the second pass achieved by centreline polymer injection showed lower values than those of the asymptotic. The result was envisaged to be due to the deagglomeration of the supermolecular clusters by shearing stresses of the flow near the wall. In figures (5.4) and (5.5) we present the second pass drag reduction results of the wall injection. The wall injection results showed an agreement with the centreline results discussed before in chapter IV. The difference between the maximum and the second pass drag reduction values of the wall injection were found to be slightly less than those of the centreline injection results. In spite of the fact that the values of the maximum drag reduction achieved by the 3000 wppm polymer solutions were higher than those of the 500 and 1000 wppm solutions, their second pass drag reduction results have the same values (see figures (5.4) and (5.5)). Such results could suggest that as the polymer agglomeration sizes increase they become easier to break into smaller ones. Eventually, the resulting smaller aggregates have sizes independent of that initially present in the flow. This suggestion could explain the independence of the asymptotic value of the centreline injection results on the concentration of the injected polymer solutions. These results are in agreement with those of Cox et al (1974) which showed that the steady state drag reduction of a rotating disc were independent on the grain size of the polymer powders, added to the water and assumed to represent the initial size of the large polymer agglomerations.

5.2.4 Comparison

The discussion carried out in chapter IV revealed the high degree of drag reduction achieved by the injection of concentrated polymer solutions into the flow. The high drag reduction by polymer injection

was found to be due to the low onset wall shear stress. Such low onset wall shear stress is attributed to the presence of super-molecular polymer agglomerations in the flow. Their sizes are assumed to be comparable to those of the turbulent eddies responsible for the diffusion of the injected solutions.

The results of the wall injection showed complete consistancy with those of the centreline injection with a slight increase in the maximum drag reduction over that of the asymptotic drag reduction by centreline injection. The higher drag reduction by wall injection is envisaged to be due to a higher polymer concentration in the most effective region above the average concentration or to be due to the large sizes of agglomerations reaching this region or to both.

The plot of C_{av}/DR against C_{av} was found to give a straight line with two parameters characterizing the efficiency of the polymer solution. The intrinsic concentration {C}, which is the polymer concentration required to achieve 50% of the maximum possible drag reduction DRm, exhibited a lower value for centreline injection results than that of homogeneous solution results. The maximum possible drag reduction DR_m also showed higher value for injection results. The parameter $DR_m/\{C\}$ is considered as a measure of the polymer efficiency as drag reducers. The results presented in table (IV.2) indicated that the centreline injection resulted in higher efficiency in reducing the frictional drag of the flow.

The wall injection results were plotted in the same way in figures (5.5) and (5.6) as $C_{av}/\%DR$ against C_{av}. The results exhibited a slightly lower value of the intrinsic concentration (0.5 wppm) than that of centreline injection results (0.65 wppm). The maximum possible drag reduction was also slightly higher (74%) than that found in the centreline injection (72.5%). Consequently wall injection has a

higher efficiency ($DR_m/\{C\}$ = 148) than that shown by centreline injection ($DR_m/\{C\}$ = 111). The wall injection results were presented in table (IV.2) for comparison with others. As shown in figure (5.5) the 3000 wppm polymer solution give higher efficiency ($DR_m/\{C\}$ = 255) than that of the 500 and 1000 wppm polymer solutions. Such high efficiency produced by the 3000 wppm polymer solution support the hypothesis discussed before in chapter IV that, the increase in the drag reduction efficiency by polymer injection is a result of the polymer aggregation influence on the flow.

The second pass drag reduction results exhibited the same increase observed in all wall injection results (see table 4.2), but with a remarkable increase in the scatter of the results compared to that of the centreline injection results.

5.2.5 The Influence of the Bursting Process on the Drag Reduction Development

An interesting observation was found in the local drag reduction produced by injecting concentrated polymer solutions into the wall region of a turbulent water flow. An oscillatory scatter was observed to characterize the local drag reduction results by wall injection. Such oscillatory character was not detected in the centreline injection results (see figures (5.1), (5.2) and (5.3)). We think this may be related to the phenomenon of turbulent bursts (Kim et al (1971), Corino & Brodkey (1969) and Rao et al (1971)).

At first, these oscillatory character variations in the wall friction reduction results by wall injection were thought to be random scatter due to some experimental errors. However, after inspection of many sets of data, it seemed clear that this was a quasi-cyclic process and its magnitude is larger than any experimental error encountered during the study.

Representative results of the local drag reduction by wall injection are present in figures (5.7), (5.8) and (5.9). The figures show typical plot of the local drag reduction results by centreline and wall injection. The results of the wall injection exhibited slight "over-shoots" in the mean local drag reduction value. Such over-shoots in the local wall friction are consistent with the usual picture of the polymer acting in the near-wall region of the flow.

In order to understand the nature of the oscillatory character in the wall friction, it is necessary to understand the physical interpretation of the turbulent structure in the near-wall region.

Visual studies of the turbulent boundary layers of Kline et al (1967) and Corino & Brodkey (1969) revealed the presence of well-organized spatially and temporally dependent motions within the so-called "the laminar sub-layer". These motions lead to the formation of low-speed streaks in the region very near the wall. In fact, these streaks are formed by the streamwise vorticity observed in the sub-layer region. The stretching and compressing of the spanwise vortex elements in the region very near the wall lead to locally high and low speed zones respectively in the spanwise direction. These low-speed streaks gradually lift-up moving away from the wall as they move downstream over a long streamwise extent. Once the low-speed streak has reached some critical distance from the wall, it turns much more sharply outward away from the wall, but still moving downstream.

The rapid lifting of the low-speed streak creates an instantaneous inflexional velocity profile which often leads to a rapid growth of an oscillatory motion. The very rapid growth of the oscillation ends with the break-up of the streak which is violently ejected outward towards the core of the flow. The whole stages described above represent

the so-called bursting process. The bursting process, which ends with the abrupt ejection of the fluid from the wall region into the flow outside the near-wall region, is followed by an inward flow from the core main stream into the wall in a so-called 'sweep event' or sometimes 'fluid inrush phase'. During the very short time of the sweep event the inrushing fluid from the turbulent core replaces the outward bursting fluid which is thought to be responsible for the initiation of the next burst (Offen & Kline (1975)).

The above described sequence of events repeat itself in space and time, but not periodically at one place in time nor at one time in space. Such a quasi-cyclic process creates the repetitive nature of the flow patterns near the wall which is our main concern in this section.

Two possible explanations could be introduced to discuss the oscillatory character variations of the wall friction reduction produced by injecting the polymer solutions into the wall region of the water pipe flow (see figures (5.7), (5.8) and (5.9). First, there could be some structural instability in the flow due to the non-Newtonian nature of the fluid being injected. Such instabilities occurred occasionally during our experiments. But they were much smaller in magnitude than this effect which tend to occur only at very low injection flow rates. Second, the turbulent bursting process could be modulating the outward diffusion of the polymer from the wall. Such modulation in the polymer outward diffusion could occur as a result of the violent ejection of the low-speed streaks from the buffer zone into the core region and the subsequent sweep process. During these two events, high polymer concentration fluid was ejected from the near-wall region into the core of the flow by the burst ejection event which was replaced by low polymer concentration in-rushing from the turbulent core. The result would be a less polymer

content zone near the wall producing less frictional reduction effect. Since, the turbulent bursts are of periodic nature in both the time and space, their marked effect on the produced wall friction reduction were expected to be observed in quasi-periodic manner in space or time. This was supported by the general oscillatory shape of local drag reduction as a function of the distance (see figures (5.7), (5.8) and (5.9)). Thus, the second idea seemed more likely and was tested as follows.

Consider the oscillatory part of the drag reduction curves in figures (5.7), (5.8) and (5.9). Let the distance between successive crests be L_x (i.e. the analogue of the wavelength for a regular periodic function but of course L_x is a random variable). If the oscillations are due to the turbulent bursts, the mean value of L_x should be related to the mean time between bursts T_B. Thus,

$$T_B = \langle L_x \rangle / U_B \qquad (5.1)$$

where U_B is the streamwise mean velocity of the large-scale burst structures and $\langle\ \rangle$ denotes an ensamble mean (or averaging) value.

We evaluated $\langle L_x \rangle$ from three or four cycles of each pressure curve (as in figure (5.7)) and from seven such curves in all. The velocity U_B was taken to be $0.8\ U_o$, where U_o is the centreline mean velocity (Offen & Kline (1975) and Brown & Thomas (1977)). The result was:

$$T_B = 0.41 \pm 0.06 \text{ sec} \quad \text{(predicted from drag reduction curves)}$$

In order to check this, we used the laser anemometer to measure the autocorrelation of the streamwise fluctuating velicity, $R_{11}(\tau)$. Individual (i.e. single - realization) values of T_B were obtained from the first cycle of $R_{11}(\tau)$ curve as we will discuss in the next chapter (Kim et al (1971)). Then, 49 such curves were used to form an ensemble average, with the result:

$$T_B = 0.43 \pm 0.05 \text{ sec.}$$

The agreement between the two values of T_B suggests quite strongly that the oscillations exhibited in the local drag reduction results of wall injection are evidence of interaction between the injected polymer solution and the turbulent bursts. This effect may be particularly relevent to the long held view that the polymers reduce drag by stabilising the wall layer with a consequent reduction in the bursting rate as we discussed in chapter I.

CHAPTER VI

LASER DOPPLER ANEMOMETER MEASUREMENTS

6.1 INTRODUCTION

The use of the convensional techniques to measure the velocity distribution, the turbulent intensity and the turbulance structure in drag reducing flows have been found to have serious errors. Pitot tube measurements were subjected to anomalous errors due to the non-Newtonian properties of the polymer solutions, for example, Smith et al (1967) demonstrated that measurements in identical flow situations using various size pitot tubes yield different results. Hot-film and Hot wire sensors suffer more serious errors especially, in turbulence structure and intensity measurements. In addition to the difficulty in calibration due to the changes of the heat transfer characteristics associated with drag reducing flows, they exhibited anomalous ragged signals which were attributed to the presence of polymer agglomerations in the flow. (Fabula 1966). Bubble tracing is an extremely tedious process and suffered large uncertainties (see Donohue et al (1972) and Offen & Kline (1975)).

Recently, a new technique, the laser doppler anemometer (LDA), has been developed and shown to be reliable in making measurements of the mean velocity, the turbulence intensity and turbulence structure. The main advantages of the LDA are:

1. It is not dependent on the rheological or intensive properties of the working fluid.
2. It does not require the insertion of external probes into the velocity field, i.e. it is a non-interfering instruments. Therefore, it is possible to measure the mean and axial fluctuating velocities in the near-wall region.

Due to these advantages, the LDA is considered a very promising technique for the turbulence structure measurements in the near-wall region. The importance of this region has been experimentally demonstrated in both the Newtonian (Corino & Brodkey (1969) and Kim et al (1971) and the drag reducing flows (Donohue et al (1972), and Hanratty et al (1977)). The laser doppler anemometer was first used in drag-reducing flows by Goldstein et al (1969), Rudd (1971) and Chung & Graebel (1972) almost at the same time. The measurements of Goldstein et al were only in the centreline of a 14 mm diameter pipe flow. Rudd's measurements were the most comprehensive results which were the first to exhibit an increase in the streamwise intensities and decrease in the spanwise intensities. Chung & Graebel (1972) used a 12 mm diameter pipe. Their measurements were limited to the pipe core due to the large size of the laser probe volume. The results showed that the axial turbulent intensities were substantially reduced compared with that of the water flow. Logan (1972) used the LDA to measure the Reynolds stresses in a 12.7 mm square pipe flow. His results verified Rudd's results which showed an increase in the axial turbulence intensity near the wall. Kumor & Sylvester (1973) measured the mean and the fluctuating velocity of drag reducing flow over a flat plate. They have offered no water results which allows us to verify the system performance and to detect the changes associated with the polymer additives. Reischman & Tiederman (1975) measured the mean and turbulent intensity of the streamwise velocity component in a channel flow. Their results do not confirm the hypothesis of Virk et al (1970) that the mean velocity profile in the buffer region will follow their proposed "ultimate profile". They showed that the distinct peak of the turbulent intensity near the wall disappeared in drag reducing solutions and distributed over a much wider range of y^+.

Mizushina & Usui (1977) measured the mean and turbulent velocity profiles and the bursting period in drag reducing pipe flow (25.4 mm diameter) using LDA. Their results shows a substantial suppression of the turbulent intensity near the wall. However these results exhibit a great unreliability due to the large size of the laser probe volume (0.8 mm in the direction normal to the wall).

In this chapter, we will present the results of our measurements using the laser doppler anemometer in water pipe flow with and without the injection of concentrated polymer solutions into the centreline and the wall regions. The discussion in this chapter will start with the laser doppler anemometer technique used. This will be followed by discussing the experimental results of the influence of the polymer on mean velocity profile, streamwise turbulent intensity, autocorrelation of the streamwise fluctuating component and the streamwise energy spectrum.

6.2 THE EXPERIMENTAL TECHNIQUE

Considerable development of the laser doppler anemometer has been achieved since the initial measurements of Yeh & Cummins (1964). They deomonstrated the use of the doppler shift to measure the velocity of small particles in the flow. They heterodyned the scattered light from the moving particles illuminated by the laser beam with the unscattered light on a photomultiplier (PM) tube. The resulting signal, which is the difference in the frequency between the scattered and unscattered lights, was directly proportional to the particle velocity. Such arrangement is known as "the reference beam mode". In this system, the laser beam is split and the two resulting beams focused into the measuring point. One of the two beams is directed to the photo detector (usually termed the reference beam). The other beam (the illuminating beam) is much more intense. The scattered light from the measuring point is collected and focused on the detector to heterodyne with the reference beam. The doppler frequency shift f is related to the velocity of the scattering particles u as:

$$f = (2u \sin \theta/2)/\lambda \qquad (6.1)$$

where, λ is the wave length of the illuminating laser beam and θ is the angle between the reference and the illuminating beams.

Rudd (1968) introduced a new model in which the two incident laser beams cross at the measuring point to produce a set of interference fringes. The scattered light from the particles crossing the fringes is collected and focused on the photo detector. The observed scattered light is explained as the amount of light blocked by the particles as they cross the bright fringes. The velocity of the scattering particle is related to the time taken to pass a bright fringe to the next, hence, to the frequency of the scattered light. The resulting relationship is:

$$f = \frac{(2u \sin \theta/2)}{\lambda}$$

where θ is the angle between the two incident beams.

The above arrangement is known as the real fringe pattern. The relationship between the velocity of the scattering particle and the frequency of the scattered light is the same as that of the doppler shift (reference beam) arrangement. Rudd showed that the laser is not essential to produce the interference fringes, but is generally preferable due to its brightness and spatial coherence.

The main advantage of the real fringe configuration, as compared to the heterodyning, is that they are quite simple to align and are not so sensitive to small vibrations (Mazumder & Wankum (1970).

Lading (1971) showed that there is no difference in the results obtained by the real fringe mode and the doppler shift. He found that the doppler shift is independent of the direction of detection, but as the angle of detection increases, the doppler signal deteriorates. The best signal-to-noise ratio was found to be obtained when the two laser beams are the same and the direction of detection is along the bisector of the angle between the two beams. Mozumder & Wankum (1970) found that for low scattered intensity the fringe method has better signal to noise ratio while the reference beam and the interference fringe modes give comparable results when the intensity of the scattered light is high and the angle of detection is small. Their results showed that the signal broadening in the real fringe mode is small and independent of the diameter of the receiving aperature. They concluded that the real fringe mode is advantageous as long as the signal power can be appreciably increased by increasing the receiving aperature area.

Durst & Whitelaw (1971) studied the optimization of the optical arrangements. They discussed the differences between the real fringe mode and the heterodyning mode arrangements and best situations for the use of either arrangement. Abbiss et al (1974) discussed the different optical arrangements of the LDA and their best accuracy in measurements for specified situations.

Generally, the real fringe mode seem to offer the most advantages and hence became the most popular. In nearly all practical situations they provide a better signal-to-noise ratio than do the heterodyne schemes (Durani & Greated (1977)). It also offers easy alignment.

A fundamental limitation of the laser doppler anemometer is the signal broadening or what is usually termed the ambiguity noise of the doppler anemometer signal. This noise was found to be due to:

1. The finite transit time of particles through the scattering volume.
2. The turbulent velocity fluctuations across the scattering volume.
3. The mean velocity gradient in the scattering volume.
4. The electronic noise of the photo detector and the signal processing system.
5. The optical noise introduced by the diffractive and refractive beam perturbations, coherence degradation and the laser hum.

This noise is white and Gaussian due to the independent nature of the noise sources. The influence of the ambiguity noise on the turbulence measurements was studied by a number of investigators. George & Lumely (1973) estimated the dimensionless wave number at which the turbulence-to-ambiguity ratio is unity for a number of different applications. These estimates showed that the possibility of measuring dissipation spectra in high-speed flows using Doppler velocimeters is quite remote. Berman & Dunning (1973) verified experimentally the laser-Doppler ambiguities predicted by George &

& Lumley (1973). They measured the turbulence power spectra for water pipe flow. They demonstrated that the power spectral density can be obtained up to wave numbers as large as those for hot-wire film anemometers after accounting for the LDA signal ambiguity noise.

A large number of investigators studied theoretically and experimentally the different sources of the LDA signal broadening (Edward et al (1971), George (1975), Owen & Rogers (1975) and Adrian et al (1975). Different corrections were suggested to make corrections for removing the doppler ambiguity (Bokemeier & Feige (1975) and Berman & Dunning (1973)). It was also suggested by a number of investigators that the use of a frequency-tracking device could reduce the level of the ambiguity noise (George & Lumley (1973), Durrani & Greated (1977) and Durst (1975). The signal-to-noise ratio enhancement in the frequency tracker is achieved by passing the optical anemometer signal through a narrow band-pass filter and by the integration of the discriminator voltage output. However, such improvement in the signal-to-noise ratio is on the expense of eliminating some of the high frequency part of the turbulence spectrum.

Durst (1975) showed that the ambiguity noise due to the finite life time of the scattering particles in the measuring volume could be decreased by increasing the number of the fringes observed by the PM tube. Shaughnessy & Morton (1977) suggested that the electronic shot noise in the detector could be minimized by making the scattered light flux reaching the detector large in order to reduce the gain required for producing a usable signal.

Since the ambiguity noise is uncorrelated, it was suggested by a number of investigators that cross-correlation of two LDA velocity signals independently obtained at the same measuring point achieve a large reduction of the ambiguity noise (George & Lumley (1973) and van Maanen et al (1975)). The results of van Maanen et al

(1975) showed an impressive decrease in the ambiguity noise after making cross correlation to the output of two frequency trackers measuring the same point. The results also indicated that the LDA ambiguity noise is completely eliminated when the output of the two LDA signals measuring the same point is completely independent.

However, careful design and alignment of the optical arrangement and proper signal processing system could minimize greatly the ambiguity noise. Some successful attempts to measure the turbulence energy spectra have been carried out (McComb et al (1977), Van Maanen et al (1975) and Berman & Dunning (1973)). The results of McComb et al (1977) showed that LDA could provide a more satisfactory technique for measuring the turbulent energy spectra in polymer solutions.

In the following two sections we will discuss the optical arrangement and the signal processing of the laser doppler anemometer used in our investigation to measure the mean velocity, the turbulent intensity, autocorrelation, bursting time and the energy spectral density in a turbulent flow with polymer injection.

6.2.1 The Optical Arrangement

In the foregoing discussion, the real fringe mode arrangement was found to be easy to align and the signal to noise ratio is usually better than the reference beam mode system. One of the greatest advantages of the real fringe mode is the very high spatial resolution that could be achieved with a good singal-to-noise ratio. As the laser probe volume becomes small, the intensity of the scattered light decreases. The use of the real fringe method with the scattered light collected along the bisector of the two beams, would result in a good signal-to-noise ratio at large angles between the two beams. Due to these advantages, the real fringe mode of arrangement was used.

The optical arrangements of the LDA which is shown in figure (6.1) was mounted on a steel plate (200 cm x 15 cm x 1 cm) which is considered as the base of the optical arrangement, is provided with 8 levelling screws in order to adjust the level of the steel plate. The optical bench (2.0 m long), on which all the laser optics were mounted, rested on a number of rollers which in turn mounted on the steel plate. These rollers provided an easy traversing motion of the optical bench on the steel plate. The optical bench was traversed over a short distance (10 cm) in the horizontal direction by the movement of a threaded rod through a nut fixed in the steel plate. The distance travelled by the optical bench was measured by a micrometer which has an accuracy of $\pm$ 0.001mm.

A 5 mw continuous He-Ne gas laser (Spectra Physics, model 120) was used to produce the light beam which was subsequently split into two parallel beams in a horizontal plane and of equal intensity by a beam splitter (Precision Devices Malvern). The distance between the two parallel beams was kept at 24.5 mm. The two beams, then, were focused by a lens of focal length of 51 mm to form an interference fringe pattern at their point of intersection, representing what we call the measuring probe or the probe volume. The angle between the two beams was $\theta = 28^{\circ}$ which resulted in a fringe spacing of 1.3 μm. The probe volume dimensions were 31, 130 and 32 μm in the streamwise, radial and spanwise directions respectively with 25 fringes in the measuring volume. For this configuration the doppler frequency f_D was 760 KHz for a velocity of one metre per second.

The scattered light from the probe volume was collected by a collecting lens of 121 mm focal length which was counted on the front of the photomultiplier (DISA 55L 12). The photomultiplier was mounted along the bisector of the two intersecting beams which is the direction of the maximum intensity of the scattered light (Blake & Jesperson (1972)). The collected light was focused on a small pin hole of 0.1 mm diameter in the front of the PM tube in order to restrict the light to that scattered from the measuring volume. A very narrow band-pass optical filter, which was centred on 633 nm (the wavelength of the He-Ne laser light), was provided as an integral part of the PM tube housing in order to ensure that all light waves striking the photocathode have a wave length of the laser light. Thus, the background light effectively blocked which resulted in a reduction of the photomultiplier noise due to the presence of the white daylight mixed with the laser scattered light. The power supply of the photomultiplier was DISA high voltage power supply type 55L 15. The output signal was then fed to the signal processing section of the LDA system for analysis to detect the doppler frequency.

Because of the low concentration of the scattering particles in the flow, it was found necessary to seed the flow to increase the signal-to-noise ratio. Fresh milk was found to provide an inexpensive and also a good supply for the required scattering particles. The milk was injected into the suction side of the centrifugal pump (see chapter II) via a hypodermic needle using a constant head tank. It was homogeneously mixed with the flow by the pump. Its flow rate was controlled by varying the level of the milk supply tank. An Excellent signal-to-noise ratio was obtained at milk concentration of 100 wppm. The average fat particle size is approximately 0.3 μm with about 10^{14} particles per litre of milk (George & Lumley (1973)). Then, the particle concentration was approximately 10^{7} particles per c.c.

The optical system was arranged at the required distance downstream from the injector in such a way that the two beams and the centreline of the pipe flow were in the same plane, and the bisector of the two beams, which is in the direction of the optical bench axis, is normal to the centreline of the pipe flow. The laser probe volume was traversed along the horizontal diameter inside the pipe flow cross section from one wall to the other.

6.2.2 The LDA Signal Processing Technique

A number of signal processing techniques have been used successfully fo analysing the photodetector signal in order to extract the instantaneous frequency of the doppler signal. The choice of a particular technique depends on the flow conditions, or more specifically on the scattered radiation. For highly seeded flows where there are a large number of scattering particles in the probe volume, the doppler signal is continuous. The wave analysing or the frequency tracking techniques are usually employed. On the other hand, when the doppler signal is not continuous, different techniques are used such as individual realization of the doppler burst signal (McComb & Salih (1977-a,b) and photon correlation techniques.

The frequency tracking technique was used for analysing the LDA signal. It offers the advantages of converting the doppler frequency into an analogue DC voltage output proportional to the instanteneous velocity. It is also suggested that the use of a frequency tracking device can reduce the level of the ambiguity noise associated with the doppler signal as we discussed before.

As shown in figure (6.1), the output signal from the photomultiplier was fed to a frequency tracker (Communications & Electronics Ltd. model HF & LF), through a wide band pre-amplifier. In the frequency tracker, the photomultiplier signal was bandpass filtered. The filter

cutoff freqeuncy was adjusted to be close to the mean doppler frequency, and the filter bandwidth was made large to accommodate the doppler signal frequency variations due to the turbulence effects. The band pass filtered signal then, is separated into two orthogonal modulated frequency components by mixing the signal with two orthogonal output components of voltage-controlled oscillator (VCO). The input voltage to the VCO is a feed back averaging of the instanteneous analogue voltage output. The two orthogonal frequency modulated components are filtered in a narrow bandpass intermediate filter (IF) which is usually tuned around the centre frequency of the doppler signal. Then, the two components are differentiated. The last stage is mixing each component with the differentiation of the orthogonal one. The subtraction of the resulted two signals gives an analogue DC voltage proportional to the instantaneous frequency of the doppler signal (Durrani et al (1973) Wilmshurst & Rizzo (1974) and the technical drawings of the E & C frequency tracker, model HF & LF). The tracker is also capable of working as a frequency analyser when it operates on the sweep mode. The frequency spectrum of the doppler was displayed on x, y oscilloscope (Hewlett Packard, model 130C) to check the effectiveness of the bandpass filtering of the signal.

The output of the frequency tracker was fed into a digital voltmeter (DISA, type 55 D 31) where the instantaneous voltage was averaged over 10 sec. in order to calculate the value of the mean velocity of the flow. It was also fed to RMS voltmeter (DISA, type 55 D 35) which was also averaged over 10 sec. in order to calculate the intensity of the fluctuating component of the flow velocity. The instantaneous output was also fed to a tape recorder (Racal Thermionic, model store 4D) in order to record the signal on a magnetic tape for further analysis as we will discuss later. The speed of the tape recorder was 15 inch/sec which allows us to record a signal of fluctuations up to 5 K

The recorded signal was replayed at the same recording speed and the output was fed to a signal conditioner (DISA, 55 D 26) to act as a low-pass filter with a cutoff frequency of 2.5 KHz. The low pass filtering of the signal was suggested by a number of investigators to remove the high frequency ambiguity noise associated with the signal (McComb et al (1977) and George & Lumley (1973)). The output of the signal conditioner was then fed to a correlator (Hewlett-Packard model 3721 A) in order to measure the turbulence autocorrelations and the bursting time. The low pass filtered signal from the signal conditioner was also digitized at a sampling rate of 5000 samples/sec. using a PDP 8 mini-computer. The digitized data were then fed into EMAS where the turbulent energy spectrum was calculated using the Fast Fourier Transformation method (FFT) (Allan (1977) and Dickson (1978)).

6.3 DISCUSSION OF THE RESULTS

In this section, we will discuss the results of the LDA measurements during the injection of drag reducing polymer solutions into the centreline and the wall of a water pipe flow. The object of such measurements was to detect the possible changes in the flow structure due to the presence of the polymer molecules in the flow, and to know whether these changes were due to the presence of the polymer molecules in the flow, or if they were an effect of the drag reduction which was found to be localized in the near-wall region (see chapters IV and V). The measurements were taken at a number of cross sections of different distances downstream from the injector. These cross sections were as near as 8 pipe diameters from the injector, where the injected polymer solution was still in the core, and the drag was increased, and as far as 2^{14} pipe diameters from the injector, where the injected polymer became homogeneously distributed and the asymptotic drag reduction was obtained. Only one run of measurements

were carried out at section of 41 pipe diameters downstream from the injector during the injection of the polymer solution into the wall region. At this section the drag reduction was about 62.5% and there was no polymer in the core of the flow (see chapter III). The discussion will be carried out on:

- the mean velocity profiles,
- the streamwise turbulent intensity profiles,
- the time of the turbulent bursts,
- the streamwise turbulence autocorrelations, and
- the streamwise turbulent energy spectrum.

In order to check the LDA performance and to detect the changes in the flow structure due to the presence of the polymer in the flow, three runs of measurements were carried out on the water flow without polymer injection.

6.3.1 The influence of the polymer on the mean velocity profiles

Measurements were carried out in turbulent pipe flow of water in order to check the established standard character of the pipe flow. All the mean velocity profiles were measured from one wall to the other. Figure (6.2) shows the measurements made at three slightly different Reynolds numbers. The results show a good agreement with the universal law:

$$U^+ = 2.5 \ln y^+ + 5.5 \qquad (6.2)$$

In the buffer region ($y^+ \simeq 6$ to $y^+ \simeq 30$), the results show a good agreement with the proposed hypothesis of Van Driest that the eddy viscosity is dampened close to the wall. In this region the velocity distribution could be expressed as (Quarmby & Anand (1969)).

$$\frac{dU^+}{dy^+} = \frac{1-y^+/R^+}{1+E(y^+)} \qquad (6.3)$$

and, $$E(y^+) = \tfrac{1}{2}\{1 + 4k^2 y^{+2} (1 - \exp(- y^+/A^+))^2\}^{\frac{1}{2}} - \tfrac{1}{2} \qquad (6.4)$$

where k is Von Karman constant = 0.4 and A^+ is the Van Driest damping constant which is usually taken as 26 (Spalding (1973)). A similar expression was suggested by Deissler (1954) to describe the velocity distribution in this region as:

$$\frac{dU^+}{dy^+} = \frac{1}{1 + n^2U^+y^+ \{1-\exp(-n^2y^+)\}} \qquad (6.5)$$

He found that with n = 0.124 his expression approaches the universal law (equation (6.2)) at $y^+ \simeq 26$.

On the other hand, the universal law as well as Van Driest's model fails to describe faithfully the velocity in the central region of the pipe (see figure (6.2)). Various methods for correcting such deficiency have been proposed. Some investigators use expressions that combine the wall region eddy viscosity expression of Van Driest and the Reichardt's expression for the centre portion of the pipe flow. (Hussain & Reynolds (1975), Tiederman & Reischman (1976) and McConaghy & Hanratty (1977)). Others modify the velocity profile obtained by the universal law (equation (6.2)) by using the "law of the wake" (Ramu & Tullis (1976) and Dimant & Porch (1976)). The velicity profile in the core of the pipe flow could be expressed as:

$$U^+ = U_1^+ + U_2^+ \qquad (6.6)$$

where; U_1^+ is given by the universal law (equ. (6.2)), and U_2^+ is given by the "law of the wake" which is described by Coles' wake function as:

$$U_2^+ = \frac{\pi}{2k} \{1 - \cos(\pi y^+/R^+)\} \qquad (6.7)$$

where, $\pi = 0.67$ is a universal constant for pipe flows (Dimant & Porch (1976). The results shown in figure (6.2) are in good agreement with "law of the wake" modification.

Six runs of measurements were carried out during the injection of the polymer solutions (Polyox WSR-301 , C_p = 1000 wppm) into the centreline of the pipe flow. These runs were taken at different cross sections downstream from the injector. Before taking the LDA measurements of each run, the local drag reduction was measured along the pipe flow (as described in chapter IV) in order to calculate the local friction velocity u^* at the section of measurements. The results of the mean velocity profiles at different cross sections downstream the injector are shown in figure (6.3). The results were normalized using the local friction velocity u^* and the kinematic viscosity ν of the water at the flow temperature. It was realized that the use of the local viscosity to normalize the data would not result in a change in the mean velocity profiles because the maximum polymer concentration variation (at the section of x/d = 8.0 from the injector) is from the water near the wall to 110 wppm at the centreline. The maximum variation in the viscosity will be about 10% from the water viscosity (from the viscosity data of Polyox WSR-301 present in Ayyash (1978) and Ramu & Tullis (1976)). This viscosity variation was getting smaller and smaller with the distance downstream from the injector such that at the next cross section the viscosity variations decreased to less than 4%.

The velocity profile at the section of 8.0 pipe diameters downstream from the injector shows an interesting result. At this section, the injected polymer solution was still in the core region of the flow and there was an increase in the frictional drag. In spite of the presence of the polymer in the core of the flow, there were no detectable changes in the mean velocity profile, even in the core region. As the drag reduction built up downstream from the injector, changes in the mean velocity profiles were observed in the turbulent

core as well as in the near wall region (see figure (6.3)). Such result clearly indicated that these changes are effects of the drag reduction, which was found to be mainly confined in the near wall region (see chapters IV and V).

The mean velocity measurements shown in figure (6.3) confirm the existence of three regions in drag reducing turbulent flow. These three regions are the viscous sublayer, the polymer interactive region which is sometimes known as the elastic sublayer, and the turbulent core region. The results shows that the thickness of the viscous sublayer is the same as that of the Newtonian flow. This result is in agreement with recent LDA measurements by Kumar & Sylvester (1973) and Reiscman & Tiederman (1975) which indicated that there were no detectable changes in the non-dimensional thickness of the viscous sublayer. This result is in direct contrast to some of the previous data such as those of Rudd (1972) which showed thickening in the viscous sublayer. However, Rudd's data near the wall are questionable because his measurements were carried out in a square duct where the secondary flows in the corners would affect the results near the wall.

The polymer interactive layer which is a layer similar to buffer zone in the non drag-reducing flows. This region was found to extend from $y^+ \simeq 11.6$ which is the point of intersection of Virk's ultimate profile with the universal law (equ. (6.2)). The mean velocity distribution in this region was found to be described by:

$$U^+ = C \ln y^+ + D \qquad (6.8)$$

where, C is the slope of the straight line describing the mean velocity data in the sime-log plot of U^+ against y^+, and D is constant. The values of the constants C and D were calculated for each profile by fitting the mean velocity data in this region by straight line (as that of equ. (6.8)). The results are presented in table (6.1).

The mean velocity results in this region shown in figure (6.3) and the values of the slope C presented in table (6.1) indicated that the slope of the mean velocity is a function of the drag reduction. This result does not confirm the hypothesis of Virk et al (1970) which proposed that the mean velocity distribution in this region (the elastic sublayer) is universal and described by:

$$U^+ = 11.7 \ln y^+ - 17 \qquad (6.9)$$

However, the results confirm Van-Driest hypothesis which postulates that the mean velocity distribution in this region is not unique, but characterized by a variable Von Karman constant ($k_p = \frac{1}{C}$) which is a function of the polymer concentration. The results also shows an agreement with the results of Reischman & Tiederman (1975) using LDA technique. They reported that their mean velocity data in this region does not follow the ultimate profile of Virk. They reported a value of 7.7 for the slope in this region at 40% drag reduction level instead of the value of 11.7 of Virk. It was also reported by Ramu & Tullis (1976) that the mixing length in the polymer interactive layer is a function of the drag reduction. Their results showed that k_p varied from 0.4 for non drag reducing flows to 0.086 at the maximum possible drag reduction which is described by the ultimate profile of Virk ($k_p = 0.0855$).

In the turbulent core region, a noticeable change in the slope of mean velocity distribution was observed in addition to the well-known upward shift (see figure (6.3)). At low and moderate values of drag reduction (less than 40%) the changes in the slope of the mean velocity in the turbulent core were small such that it could be neglected. Thus, it shows an agreement with previous results and with the mean velocity models which postulate that the mean velocity profile in the core region is just shifted upward and parallel to the Newtonian profile.

This is clearly demonstrated in the velocity profile measured at 40 pipe diameters from the injector. This result indicated that the influence of drag reduction extends from the near-wall region to modify the turbulence structure in the turbulent core region which was exhibited by the slight change in the Von Karman constant. (This will be discussed later in this chapter). With the increase in the drag reduction level, the influence of the drag reduction, caused by the presence of the polymer in the most effective region, became more pronounced in modifying the turbulence structure in the core such that it was difficult to distinguish between the polymer interactive region and the turbulent core. This is usually associated with an increase in the thickness and the slope of the mean velocity distribution in the polymer interactive region. As a result the turbulent core region becomes smaller and smaller with an increase in the influence of the drag reduction in this region which was observed in an increase in the mean velocity profile slope. The result is demonstrated in the mean velocity profiles at 76 and 100 pipe diameters from the injector where the drag reduction values were 46% and 57% respectively. Further increase in the drag reduction level approaching the asymptotic drag reduction of Virk, as the conditions of the velocity profiles measured at x/d = 190 and 214 respectively, the polymer interactive layer demonated the whole cross section and the mean velocity distribution approached the ultimate profile of Virk. Then, the turbulent core disappeared (as in the mean velocity profile at x/d = 214 where the % DR = 67.0), or started to disappear (as exhibited in the profile measured at x/d = 190 where the % DR = 65%). This result completed the picture indicating that further increase in the drag reduction increases its influence on the structure of the core region such that at high drag reduction levels the effect is as much as that on the polymer interactive layer and the two layers become one layer.

In general, the mean velocity profile results in the turbulent core region show good agreement with the previously reported results. Kumor & Sylvester (1973) measured the mean velocity profiles of a turbulent boundary layer over a flat plate submerged in a drag reducing polymer solution (Separan AP-30) tunnel, using the LDA technique. Their results showed a substantial increase in the mean velocity distribution in the turbulent core region at relatively high drag reduction levels. They reported a value of 5.6 for the slope in this region (compared with the Newtonian value of 2.5) at a drag reduction level of 49% while at 30% drag reduction they found that the slope was 2.7. Comparing these values with those of our results presented in table (6.1) showed a good agreement. However, none of the other LDA measurements in drag reducing flows did not show such increase in the slope of the mean velocity distribution in the turbulent core. Presumably, because of the moderate drag reduction levels at which these measurements were carried out. In spite of the noticeable scatter associated with the measurements using conventional techniques such as pitot tubes, the results are in agreement with those obtained using LDA.

The mean velocity profile, during the injection of polymer solution into the wall region of the flow, was measured at a distance 41.0 pipe diameters downstream from the injector. At this section, the polymer solution was found to be mainly confined in the near-wall region while, the core was still free of the polymer (see figure (3.11)). The drag reduction at this section was 62%. The results of the mean velocity profile measurements at this section are shown in figure (6.4). The results of the mean velocity profile measurements at this section are

shown in figure (6.4). The results clearly indicated the presence of the above discussed three layers. The viscous sublayer showed no difference from that found in the centreline injection results. The velocity distribution in the interactive layer exhibited the same features discussed before. It supported the centreline results in this region which indicated that the velocity distribution does not follow the ultimate profile of Virk. The slope of the velocity profile in this region was found to be consistent with the values calculated from the velocity profiles measured during the centreline injection (see table (6.1)). The turbulent core region exhibited an interesting slight increase in the slope of the mean velocity profile. Its value was found to be in agreement with the values exhibited by the profiles measured during the centreline injection. This result showed that the influence of the drag reduction extend to affect the flow in the turbulent core, although, it was found to be almost free of the polymer.

6.3.2 The Effect of the Polymer on the Turbulent Intensity

The root-mean-square values of the axial fluctuating velocity were measured in both the water and the flow with polymer injection. The axial turbulent intensity results $u`$ were normalized using the friction velocity $u^*$. The normalized data $u`^+$ were plotted as a function of the distance from the wall y normalized with the pipe radius R, or as a function of y^+ ($y^+ = y.\ u^*/\nu$) in the near wall region.

The results of turbulent intensity measurements in water flow are shown in figure (6.5). They show good agreement with the recent measurements of Lawn (1971) which were carried out in a turbulent air pipe flow using the hot wire anemometer. The plot of the turbulent intensity results near the wall as a function of y^+ are presented in figure (6.6). The results showed a distinct peak of $u`^+_{max} = 2.8$ at $y^+ \simeq 15$. These results showed good agreement with the previous LDA measurements of Rudd (1972) and Reischman & Tiederman(1975) which

showed that the peak of the axial turbulent intensity occurs at $y^+ = 10 - 20$. However, the results of both Rudd and Logan exhibited as high values for the turbulent intensity peak as $u`^+_{max} = 4.3$ and 3.5 respectively while Reischman & Tiederman results exhibited a peak of $u`^+_{max} = 2.8$ (compared with a value of 2.6 exhibited by Luafer's (1953) results). Presumably, these high values reported by Rudd and Logan could be due to the effect of secondary flows in the square ducts they used, while the measurements of Reischman & Tiederman were carried out in a channel flow of high aspect ratio.

The turbulent intensity profiles during the injection of the polymer solution (Polyox WSR-301, C_p = 1000 wppm) into the centreline of the pipe flow are shown in figure (6.7). The profiles shown in this figure were measured at sections of 8, 40, 76, 100 and 214 pipe diameters from the injector. In order to detect the changes due to the effect of the polymer in the flow, the results are shown in comparison with that of the water. The turbulent intensity in the near wall region were plotted as a function of the dimensionless distance y^+ in figure (6.8).

As shown in both figures (6.7) and (6.8), the turbulent intensity profile at x/d = 8 exhibited slightly lower values compared with that of the water flow due to the slight increase in the shear velocity u^*. In the core region, there were no noticeable changes in the turbulent intensity in spite of the high polymer concentration in this region. This supported the previous results of the mean velocity profiles which showed that changes in the flow structure resulted as an effect of the drag reduction. As the drag reduction built up downstream from the injector, the changes in the turbulent intensity became observable as shown in figures (6.7) and (6.8). Both figures showed that the changes were set on in the near-wall region where, the polymer molecules or aggregates exert their main influence to reduce the frictional drag, and extended to the core region as the drag reduction level increased.

The turbulent intensity profiles of distances x/d = 40, 76, 100 and 214 where, the local drag reduction values of 26.5%, 46.%, 57.% and 67.% respectively, clearly demonstrate the development of the changes in the turbulent intensity with the increase in the drag reduction. At low and moderate values of drag reduction (i.e. %DR< 40.), an increase in the turbulent intensity was found to be confined to the region near the wall as demonstrated by the profile measured at x/d = 40 (see figures (6.7) and (6.8). Such increase was found to extend over the region of y^+ up to 250 with a distinct peak of $\hat{u}^+_{max}$ = 3.2 (Compared with the value of 2.8 found in water flow). At x/d = 76, where the drag reduction increased to 46%, the effect extends from the near wall region to the core of the flow and a slight increase in the turbulent intensity observed (see figure (6.7)). The maximum turbulent intensity, which was observed as a distinct peak in water flow and in low levels of drag reduction, increased slightly ($\hat{u}^+_{max}$ = 3.3) but distributed over a wider region of y^+. With further increase in the drag reduction, the increase in the turbulent intensity became more pronounced even in the core region. The maximum turbulent intensity increased more ($\hat{u}^+_{max}$ = 3.5 and 3.8 at drag reduction levels of 57% and 67% respectively) and the region of the maximum turbulent intensity became wider and wider (see figures (6.7) and (6.8)).

These results showed that the turbulent intensity increased with the drag reduction and the changes which were found to be confined to the near wall region at low drag reduction levels, extended to the core region at high drag reduction. The maximum turbulent intensity was also found to increase and the distinct peak distributed over a pronounced wider region. The results are in agreement with the results of Rudd (1972), Logan (1972) and Chung & Graebel (1972) which showed a pronounced increase in the turbulent intensity near the wall. Both

the results of Rudd and Chung & Graebel exhibited maximum turbulent intensity of about two times the value for the water flow while Logan results showed a value of 1.3 for the water flow results (compared with a value of 1.2 exhibited by our results at approximately the same drag reduction level). The results of Rudd (1972) and Logan (1972) showed no changes in the turbulent intensity of the core region. The results of Reischman & Tiederman (1975) showed that the turbulent intensity distinct peak of the water flow results disappeared and the maximum values of u'^{+} were distributed over a much wider range of y^{+}. These results are in general agreement with our results which showed that the drag reduction is associated with an increase in the thickness of the region of the maximum turbulent intensity.

The turbulent intensity results during the injection of polymer solution into the wall region of the flow are shown in figures (6.9) and (6.10) in comparison with water flow results. The results are consistant with the turbulent intensity results measured in flows with polymer injection at the centreline and shown in figures (6.7) and (6.8)

6.3.3 The Effect of the Polymer on the Turbulent Bursts

As we discussed before in chapter I, IV and V, the polymer molecules or aggregates were found to exert their main influence on the flow in the near-wall region. Recent studies have shown that turbulent structure in the near wall region is dominated by a special structure made up of "streaks" and bursts (Kline et al (1967), Corino & Brodkey (1969) and Kim et al (1971)). These wall-layer streaks result from the inflow - outflow fluid motion caused by streamwise counter-rotating 'Towensend' eddies. The resulting vortex compression and stretching at the wall leads to regions of high speed and low speed streaks. The low speed streaks of this structure periodically lift away from the

wall into the buffer region, where they oscillate and are violently ejected away from the near-wall region. The periodic ejection of the fluid bursts from the wall layer and their interaction with the outer-flow are believed to be the major factor in the generation and maintenance of the turbulence (Kim et al (1971)).

In the light of these two studies, the conclusion which could be suggested was that polymer molecules or aggregates would affect, in some way, the turbulent structure in the near-wall region by reducing the rate of the turbulent bursts. Hence, the production of the turbulence is reduced which directly leads to a reduction in the dissipation rate and lower friction factor. The effect is attributed to the high resistance of the polymer solutions to elongational strains, (see chapter I) which is thought to suppress the vortex stretching motions during the streak formation and the bursting process.

Kim et al (1971) reported that the bursting process has a characteristic signature on the instanteneous velocity fluctuations in the near wall region. They showed that the auto-correlation of the axial turbulent velocity could be used to measure the interval time between bursts as the time delay between the peaks of the auto-correlation curve. Their average bursting time using this technique showed a good agreement with their visual observation results using hydrogen-bubble as well as dye technique. Einstein & Li (1956) were the first to use this technique to measure the life-period of the sublayer using the auto-correlation of the wall pressure signal. Strickland & Simpson (1975) noticed that auto-correlations taken over a long averaging time show no discernible peaks. On the other hand, auto-correlations taken over a short averaging time display distinct peaks. The auto-correlation technique has been used by a

number of investigators to measure the interval time between bursts (Meek & Baer (1970), Mizushina & Usui (1977) and Achia & Thompson (1977)).

In this investigation, the bursting time was measured by a short averaging and long delay time auto-correlation of the streamwise fluctuating velocity using HP correlator model 3721A. Figure (6.11) shows typical auto-correlation curves of the axial turbulent velocity at different levels of drag reduction. The bursting was measured as the time delay to the re-rise positive maximum of the $R_{uu}(\tau)$ curve. Since, the variation of the bursting time from sample to sample using short averaging time auto-correlation is some what large. It was suggested to calculate the bursting time as an average of a number of different samples. Strickland & Simpson (1975) showed that the average time of only 26 individual bursting times gave a reasonable value for the mean bursting period Mizushina & Usui (1977) reported that the average value of 20 samples agreed well with that of 100 individual samples. In the present work the bursting time was calculated as an average of more than 30 bursting time values calculated at different radial locations in the cross section. Each was calculated as an average of more than 20 individual sample results. Figure (6.12) shows the results of the average time interval between bursts as a function of the distance from the wall y^+. The results showed that it was possible to detect the marked signature of the bursting process on the instanteneous velocity of the flow even in the core region using the short averaging time auto-correlation technique. However, the effect of the bursting process on the flow near the wall is pronounced such that the bursting time could be easily measured in the region of y^+ up to 500. This is in agreement with previously reported results of Rao *et al* (1971) which showed that the average bursting time $\overline{T}_B$ appears to be constant across most of the boundary layer.

The results of the bursting time of water flow and flows with polymer injection are shown in table (6.2). The results of water flow presented in table (6.2) showed good agreement with the previous results in Newtonian flows. These results indicated that the bursting time $\overline{T}_B$ when correlated with outer flow parameters $\overline{U}_o$ and δ exhibited a constant value independent of the flow Reynolds number. Rao et al (1971) found that $\frac{\overline{T}_B \overline{U}_o}{\delta} = 5 \pm 2$, $\overline{U}_o$ is the free stream velocity of the flow (the centreline velocity in the case of pipe flow) and δ is the boundary layer thickness (the pipe radius R). The bursting time results of water flow when correlated with wall parameters of the flow (shear velocity u^* and the kinematic viscosity ν) are in agreement with previously reported results. Corino & Brodkey (1969) visual observation results in water pipe flow ($R_e = 2 \times 10^4 - 5.5 \times 10^4$) showed that $\frac{T_B u^{*2}}{\nu} = 243$, while the results of Meek & Baer (1970) in a pipe flow using hot-film probe auto-correlation ($R_e = 0.5 \times 10^4 - 20 \times 10^4$) showed that $\frac{T_B u^{*2}}{\nu} = 325 \pm 40\%$.

The bursting time results of water flows with polymer injection, presented in table (6.2), showed a substantial increase over that of water flow even at the same wall shear stress. Such dramatic increase in the dimensionless time interval between bursts T^+_B ($T^+_B = \frac{T_B u^{*2}}{\nu}$) was found to increase with the drag reduction. These results are in agreement with Achia & Thompson (1977) results using laser hologram interferometer which showed that the dimensionless bursting time T^+_B was increased in drag reducing polymer solution over the water flow value. They found that this increase was by a factor almost equal to the increase in the dimensionless streak spacing of drag reducing solutions over that of the Newtoian flow value. However, the results of Donohue et al (1972) measurements using dye visualization technique showed that bursting time has the value of the water flow at the

reduced wall shear stress (i.e. T^+_B is constant). The results of Meek & Baer (1970) and Thomas et al (1973) auto-correlation measurements at the pipe wall with hot-film anemometers in drag-reducing flows exhibited bursting time values equal to that of water flow at the same wall shear stress. However, these results subjected to some doubt owing to the use of hot-film probes in drag reducing flows.

On the other hand, all the experimental results of the streak spacing measurements in drag reducing flows showed that its dimensionless values λ^+ ($\lambda^+ - \frac{\lambda u^*}{\nu}$) were larger than the value of the Newtonian flow ($\lambda^+ = 100$) where λ is the streak spacing (see chapter I). The non dimensional spanwise spacing of the low-speed streaks was found to increase with the increase in the drag reduction.

The results discussed above, showed that the main influence of the drag reducing additives on the flow is to suppress the formation of the streaks in the wall region and the eruption of the turbulent bursts. Such effect leads to a stabilization of wall layer in the presence of drag reducing additives as compared with that of the Newtonian flows, resulting in a decrease in the production of turbulence.

As we discussed before, the suppression of the streak formation and the rate of the turbulent bursts is attributed to the high resistance of the polymeric additives to stretching (see chapter I). This effect is clearly demonstrated in the large increase of the streak spacing observed in drag reducing flows suggesting a much lower stretching and compressing of the counter-rotating spanwise vortices in the viscous sublayer. Stretching can also be postulated to occur during the low-speed streak lift-up and during the rapid growth of the oscillatory motion which ends with the breakdown and the violent ejection of the low speed streaks from the wall into core of the flow. Low-speed streak lift-up is probably triggered by large vortical motions of the

sweep event which follows the burst ejection (Offen & Kline (1975)). This effect causes a rapid stretching of the lifted-up streak, since fluid elements are convected away from the slow moving flow in the wall layer to the faster-moving bulk of the flow. The suppression of the bursting rate could be due to the high resistance to such stretching motions offered by the presence of drag reducing polymer additives in this region.

6.3.4 The Effect of the Polymer Additives on the Streamwise Turbulent Velocity Auto-correlation

Auto-correlation of the streamwise turbulent fluctuations were carried out mainly to examine the changes in the life time of the turbulent eddies with the drag reducing polymer additives. It was also intended to investigate whether these changes in the turbulent structure are associated with the drag reduction or with the presence of the polymer additives in the flow without drag reduction.

The results of the auto-correlation measurements of the centreline turbulent fluctuations are shown in figure (6.13). In this figure, the auto-correlation coefficient $R_{11}(\tau)$ results measured in the flows with polymer injection into the centreline region at two different locations of 8 and 214 pipe diameters downstream from the injector, and in the flow with wall injection are shown in comparison with water results. The importance of the comparison presented in this figure lies in the experimental conditions at which these measurements were carried out. The results of 8 pipe diameters downstream from the centreline injector were measured in a region where the polymer was still high concentrated but there was no drag reduction. On the other hand, the results of the flow with the wall injection were measured at 41 pipe diameters downstream from the injector where there was no sensible polymer concentration in the core region of the flow but there was a high level of drag reduction (62%).

As shown in figure (6.13), the auto-correlation coefficient of the streamwise turbulent fluctuations in water flow vanished after a time delay of less than 10 ms indicating that the life time of the largest turbulent eddies in the centreline of the water flow was less than 10 ms. Comparing this with that measured at x/d = 8 downstream from the injector, where there was a drag increase and the polymer concentration was about 100 wppm, we can see that there was no change in the life time of the big eddies. However, the results showed a slight increase in the life time of the medium size eddies which is thought to be a result of the different properties of the polymer solution than those of the water. The opposite side of the picture is shown by the results measured during the injection of the polymer into the wall region. These results exhibited a large decrease in the decay rate of the auto-correlation coefficient $R_{11}(\tau)$ in the core region where the polymer concentration was so small to be detected. This result indicated that the life time of the turbulent large eddies was substantially increased in the core region of the flow as a result of the changes in the turbulence structure in the near wall not due to the polymer-turbulence interaction in the core region. The measurements of the auto-correlation coefficient at x/d = 214 where the polymer concentration at the centreline was about 5 wppm and the drag reduction level was 67%, showed an increase in the life time of the streamwise large eddies of the flow.

The above discussed results could suggest that the large increase in the life time of the large turbulent eddies in the core region are associated with the drag reduction effect which is resulted from the polymer-turbulence interaction in the near wall region (as discussed in the previous section of this chapter). These results are consistant with the experimental evidence in Newtonian flow which showed that the turbulent structure in the whole boundary layer of the flow is governed by that in the near-wall region. The results also suggest that the

presence of the polymer outside the most effective region does not change the life time of the large eddies.

Figure (6.14) present the auto-correlation coefficient results measured at r/R = 0.5. At this radial location in the flow cross section, the polymer concentration at x/d = 8 downstream from the centreline injector was approximately the same as that of x/d = 41 downstream the wall injector. The only difference was the drag reduction level (-2.5% for centreline injection at x/d = 8. and 62% for wall injection at x/d = 41). For the results of the x/d = 8 from the centreline injector there were no detectable changes from that of the water flow at this location, while the results of the wall injection exhibited large increase in the life time of the turbulent eddies. These results are in complete agreement with the results measured at the centreline and shown in figure (6.13). The results also indicated that the increase in the drag reduction level increases the change in the life time of the turbulent eddies. This is clearly demonstrated by the increase in the time delay at which the auto-correlation coefficient vanished with the increase in the drag reduction level as shown in figures (6.13) and (6.14).

Near the wall, where the drag reduction is associated with the presence of the polymer additives in this region, the changes in the life time of the turublent eddies are resulted from the polymer-turbulence interaction in this region. The auto-correlation coefficient $R_{11}(\tau)$ results measured at r/R = 0.85 and r/R = 0.88 are shown in figures (6.15) and (6.16) respectively. These results exhibited the same changes observed in both the results measured at the centreline and that obtained at r/R = 0.5.

The increase in the life time of the turbulent eddies are in good agreement with the previous results reported by Buston & Glass (1974) using an electrochemical mass-transfer technique to measure the instantaneous velocity gradient in the wall region. Their auto-correlation results indicated that polymer additives increase the turbulence macroscales of the flow. Fortuna & Hanratty (1972), Fortuna & Eckelmann (1972) and Hanratty et al (1977) using the electrochemical technique reported results which showed that the most dramatic changes due to the drag reducing polymer additives were in the spatial correlation coefficients and the turbulent scales. These results exhibited a substantial increase in the turbulent length scales in both the spanwise and the streamwise directions.

The observed increase in the turbulent time and length scales observed in our measurements and in previous results are consistent with the observed increase in both the length and time scales of the bursting process proviously discussed.

6.3.5 The Influence of the Polymer Additives on the Turbulent Energy Spectra

In the foregoing discussion carried out in this chapter, we found that the changes in the structure of the turbulent flow are associated with the drag reduction which resulted due to the polymer additives interaction with the flow structure in the near-wall region. It was very interesting to find that there were no detectable changes in the flow structure when the polymer additives were outside the near-wall region. In this section, we will discuss the results of the turbulent energy spectrum measured in water flow and flows with polymer injection.

As we discussed before, the analogue output of the frequency tracker was recorded in a magnetic tape. The recorded signal was played back and the output signal was low pass filtered (cut-off frequency 2.5 KHz) to reduce the effect of the ambiguity noise associated with the LDA signal. Then, the signal was digitized using PDP 8 mini-computer and the data fed into ERCC digital computer to calculate the Energy Spectra using the Fast Fourier Transformation method (Allan (1977)).

The results of the turbulent energy spectra in the centreline of the flow are shown in figure (6.17). The results showed that there was no difference between the water results and that measured at x/d = 8 downstream from the centreline injection, where the local polymer concentration was high and there was an increase in the frictional drag. On the other hand, the comparison of the turbulent energy spectrum measured in the centreline during the injection of the polymer solution into the wall region and that of the water flow showed a substantial shift of the spectrum of the flow with polymer injection towards lower frequencies. In spite of the undetectable polymer concentration on the core region at x/d = 41 from the wall injector, pronounced changes in the turbulent energy spectrum were found. The above two comparisons indicated that the changes in the turbulent energy spectrum of the core region of the flow were associated with the drag reduction, not the presence of the polymer additives in this region. These results are in complete agreement with the results discussed in this chapter which indicated that the polymer additives interaction with the turbulent eddies outside the near wall region, if any, does not produce any changes in the turbulent structure of the flow. The results also indicated that the polymer additives interaction with the flow structure in the near wall region (as discussed

in section 6.3.3) does change the in the whole boundary layer even when the polymer additives are localized only in the near-wall region (the viscous sublayer and the buffer zone).

Figure (6.18) also showed the results of the turbulent energy spectrum of the core region measured at x/d = 100 and 214 downstream from the centreline injector. These results exhibited a similar shift towards the low frequency end to that observed during the injection of the polymer solutions into the wall region. The shift of the turbulent energy spectrum towards lower frequences indicates an increase in the size of the turbulent scales. This confirmed the results of the auto-correlations of the axial turbulent velocity fluctuations which showed that the drag reduction is associated with an increase in the life time of the turbulent eddies. According to the hypothesis of Kolmogoroff (Hinze (1975)) which postulates that the turbulent energy dissipation decreases with the increase of the length scale of the turbulence, the observed suppression of the smallest eddies of the turbulence resulted in a reduction of the rate of the dissipation of the turbulent energy.

The reduction of the rate of the dissipation of the turbulent energy is believed to be an effect of the reduced turbulent energy production. This suggestion is supported by the experimental results which showed that the changes in the rate of the turbulent dissipation 'ε' outside the near-wall region is associated with the drag reduction not the presence of the polymer additives in this region.

Figure (6.18) shows the turbulent energy spectrum results as a function of the wavenumber k ($k = \frac{2\pi f}{U}$; f is the frequency in H_z). The data was normalized using the turbulent intensity u' and the pipe

diameter d. The normalized turbulent energy spectrum $E(k)/u^2.d$ which is shown as a function of the non-dimensional wavenumber k.d indicated that the drag reduction is associated with a suppression the small eddies of the turbulence and an enhancement of the large eddies of the turbulent structure in the core region.

The turbulent energy spectrum results measured in the core region and shown in figures (6.17) and (6.18) were re-normalized using Kolmogoroff variables. Such type of normalization allows us to compare the turbulent energy spectra at the same wall shear stress. The turbulent energy spectrum E(k) results were normalized as,

$$E(\bar{k}) = E(k)/\nu^2 . k_d \qquad (6.10)$$

where ν is the local kinematic viscosity , $k_d = (\varepsilon/\nu^3)^{\frac{1}{4}}$, the Kolmogoroff turbulent dissipation wavenumber and ε is the rate of the dissipation of the turbulent kinetic energy. The wavenumber was normalized as:

$$\bar{k} = k/k_d$$

The local rate of the turbulent energy dissipation ε was estimated from the spectral curves by fitting tangents of slope - 5/3 by eye. The best fit values of E(k) and k were then substituted in the formula describing the inertial subrange of the spectrum:

$$E(k) = K . \varepsilon^{3/2} . k^{-5/3} \qquad (6.11)$$

where K = 0.55 in outer layers of shear flows and = 0.51 in the inner layers (Bradshaw (1967)). Lawn (1971) found that a value of 0.53 for the constant K gave an estimate of the dissipation rate ε in a pipe flow and for $0<r/R<0.9$ in a good agreement with the data of Bradshaw for other shear flows. This method is based on the assumption that an inertial subrange exists in the energy spectrum. The existence of the inertial subrange in the turbulent power spectral results is clearly

demonstrated by the existence of a region in which the spectrum results varied as $k^{-5/3}$ (see figures (6.17) to (6.23)).

In normalizing the results using Kolmogoroff's variables, the water viscosity was used instead of the solution viscosity. As discussed before in this chapter, the highest polymer concentrations in the LDA set of measurements were at the centreline of the section at x/d = 8 from the centreline injector and at the wall of the section of x/d = 41 from the wall injector. At the section of x/d = 8, the polymer concentration was about 110 wppm while at the section of x/d = 41 from the wall injector the spectrum measurements were carried out at r/R = 0.85 where the polymer concentration was estimated to be less than 100 wppm. Since the viscosities of Polyox WSR-301 solutions of concentrations up to 100 wppm were very little different from that of water, it was expected that the use of water viscosity in normalizing the spectrum results would give a little difference. This effect was discussed by McComb et al (1977). They reported that the use of the solvent (water) viscosity in normalizing their spectrum results gave a very little difference than when they used the polymer solution viscosity for concentrations up to 100 wppm.

Figure (6.19) present the power spectral density of the turbulence at the centreline of the flow normalized using Kolmogoroff variables. The normalized results showed that the high wavenumber part (the inertial subrange and the dissipative range) of the flow with drag reduction exhibited no difference than that of the water flow. This indicated the high wave number part of the turbulent energy spectrum of the drag reducing flows is the same as that of the water flow at the reduced wall shear stress. On the other hand, the results showed a substantial enhancement of the low wave number part of the turbulent energy

spectrum (energy containing eddies region). These results showed that at the same wall shear stress, the most dramatic change in the turbulent energy spectrum were the enhancement of the energy containing eddies while there were no change in the structure of the inertial subrange and the dissipatiive eddies.

In the near wall region, the measurements were carried out in two radial locations, at r/R = 0.75 and 0.85. The turbulent energy spectral density results are shown in figures (6.20), and (6.21) for r/R = 0.75, and (6.22) and (6.23) for r/R = 0.85. The turbulent energy spectrum measured at r/R = 0.75 and normalized using the RMS of the local axial turbulent fluctuations u` and the pipe diameter d is shown in figure (6.20). The results show that, in flows exhibiting drag reduction, the high wavenumber part of the turbulent energy spectral curve were suppressed in comparison with that of the water while the low wave number part showed a substantial enhancement. These results are in full agreement with that measured in the centreline of the flow (see figure (6.18)). When these data were normalized using Kolmogaroff variables and plotted in figure (6.2), they exhibited the same features observed in the turbulent energy spectrum results measured at the centreline of the flow (see figure (6.19)). The high wavenumber (inertial subrange and the dissipation range) part in flows exhibiting drag reduction showed no difference from that of the water flow. While, the low wavenumber part of the spectrum (energy containing eddies range) showed an increase over that of the water flow.

The turbulent energy spectrum results measured at r/R = 0.85 exhibited the same features observed in the spectrum results measured at the centreline and at r/R = 0.75. The spectrum data when normalized using 'u`' and 'd' shown in figure (6.22) are in agreement with that of (6.18) and (6.20) for centreline and r/R = 0.75 respectively.

They also showed both qualitative and quantitative agreement when normalized using Kolmogoroff's variables (as shown in figure (6.23)) with those measured at the centreline and at r/R = 0.75 and shown in figures (6.19) and (6.21) respectively.

For more quantitative comparison, table (6.3) shows the rate of the turbulent dissipation and the dissipative length and time scales for the water flow and flows with polymer injection. The results showed a reduction in the rate of the turbulent energy dissipation in both the centreline and the near-wall region. The table also showed an increase in the size and the life time of the turbulent dissipative eddies in both the core region of the flow and the near wall region. The results showed the observed independence of the polymer concentration outside the most effective region near the wall. The results obtained x/d = 8 from the centreline injector showed no difference from that of the water flow even in the core region where the polymer additives was concentrated. On the other hand, substantial changes were found in the core region at x/d = 41 from the wall injector where there were no polymer additives.

The above discussed results showed an agreement with both the results of Kowalski & Brundrett (1974) and that of McComb et al (1977). Kowalski & Brundrett injected concentrated polymer solution (Polyox WSR-301, 2500 wppm) into the wall region of an open channel flow. Their turbulent energy spectrum results, using a hot film, showed a substantial shift towards lower frequences compared with that of the water. McComb et al (1977) measured the energy spectrum of grid-generated turbulence in drag reducing flows using LDA. When their spectral data were normalized using Kolmogoroff's variables, the results showed no difference in the high wavenumber range than that of the water flow.

However their results showed some attenuation of small-scale (dissipative range) components observed at higher concentrations. On the other hand, our results show disagreement with the results of Chung and Graebel (1972). They measured the turbulent energy spectra in turbulent pipe flow of Polyox WSR-301 (50 wppm, DR = 62 - 70%) using laser doppler anemometer. Their results showed no difference from the turbulent energy spectrum measured in water flow.

Summarizing the above discussions, the experimental evidence shown by the turbulent energy spectrum results indicated that the turbulent energy spectra in flows exhibiting drag reduction do show changes compared with those of water flow. These changes were demonstrated in a suppression of the small turbulent eddies which was observed as a shift of the spectrum curve towards the low frequency end, and in enhancement of the large eddies (see figures (6.17), (6.18), (6.20) and (6.22). When the spectrum data were normalized using Kolmogoroff's variables, the high wavenumber part (the inertial subrange and the dissipative range) showed no changes from that of the water flow. This indicated that the suppression of the small turbulent eddies is of the same scale as the suppression of the wall shear stress such that when they compared them with that of the water results at the same wall shear stress they showed no difference (see figures (6.19), (6.21) and (6.23). These changes in the turbulent energy spectrum were found to be consistent across the whole cross section of the flow, dependent on the drag reduction and completely independent of the polymer concentration outside the near-wall region.

6.4 CONCLUSIONS

The general conclusions that could be drawn from the experimental evidence shown by the results of the LDA measurements present in this chapter are:

1. The presence of the polymeric additives outside the near-wall region does not affect the flow structure neither locally nor as a whole; indicating that polymer - turbulence interactions outside the near wall region, if any, do not cause any significant changes in the structure of the flow.
2. The presence of the polymer additives in the near wall region does cause significant changes in the whole structure of the flow even in the core region when it was free of the polymer additives.
3. The change in the flow structure is demonstrated in,
   (i) The presence of the polymer interactive layer in the mean velocity profile which is characterized by a smaller mixing length constant ($0.4>k_p>0.085$), and in the upward shift of the mean velocity profile in the core region,
   (ii) An increase in the axial turbulent intensities $u`/u^*$ near the wall which extended to the pipe centreline when the drag reduction level increased,
   (iii) A substantial increase in the bursting time and the streak spacing over that of the water flow even at the same wall shear stress, and
   (iv) A suppression in the small scales of the turbulence which resulted in a decrease in the rate of the turbulent energy dissipation and an increase in the size and the life time of the turbulent eddies.
4. The observed changes in the flow structure are thought to be an effect of the polymer additives interaction with the flow structure in the near-wall region (the viscous sublayer and the buffer zone)
5. Such interaction is thought to be in the form of inhibiting the formation of the streaky structure and the eruption of the turbulent bursts, which is attributed to the increased resistance of the vortex structure to stretching by the polymer additives.

TABLE 6.1

CONSTANTS OF THE MEAN VELOCITY PROFILES

Test	x/d	u^* (cm/s)	%DR	$A^{(1)}$	$B^{(1)}$	$C^{(2)}$	$D^{(2)}$
C.L. Inj.	8.0	11.0	-2.5	2.5	5.5	-	-
C.L. Inj.	40.0	9.00	26.5	2.8	8.4	5.9	-2.8
C.L. Inj.	76.0	7.70	46.0	3.6	12.0	6.3	-3.3
C.L. Inj.	100.0	6.90	57.0	3.7	16.5	8.0	-7.8
C.L. Inj.	190.0	6.23	65.0	3.4	24.5	9.7	-12.3
C.L. Inj.	214.0	6.17	67.0	-	-	10.2	-13.5
W. Inj.	41.0	6.72	62.0	3.2	20.0	9.8	-12.6

(1) Mean velocity profile in the core region

$$\overline{U}^+ = A \ln y^+ + B$$

(2) Mean velocity profile in the polymer interaction region

$$U^+ = C \ln y^+ + D$$

TABLE 6.2

BURSTING TIME RESULTS

Test	%DR	u^* cm/s	ν cm^2/s	$\overline{T}_B$ sec.	$T^+_B = \frac{\overline{T}_B . u^{*2}}{\nu}$	$\frac{\overline{T}_B . U_o}{R}$
Water Flow	-	11.0	0.013	0.028	255	5.5
Water Flow	-	9.7	0.011	0.029	248	5.3
Water Flow	-	10.5	0.0145	0.035	266	6.8
C.L. Inj.	-2.5%	11.0	0.015	0.034	274	6.6
C.L. Inj.	26.5%	9.0	0.015	0.094	500	18.0
C.L. Inj.	46%	7.7	0.015	0.175	690	36.0
C.L. Inj.	57%	6.9	0.015	0.25	795	52.5
C.L. Inj.	65.0%	6.23	0.015	0.38	980	83.0
C.L. Inj.	67.0%	6.17	0.015	0.455	1160	102.0
Wall Inj.	62.0%	6.7	0.015	0.43	1280	89.0

TABLE 6.3

THE RATE OF THE TURBULENT DISSIPATION AND THE DISSIPATIVE LENGTH AND TIME SCALES

Test	x/d	%DR	u^* cm/s	ν cm /s	r/R = 0.0			r/R = 0.85		
					ε cm^2/sec^3	$\eta_d x10^3$ cm	$\tau_d x10^3$ sec	ε cm^2/sec^3	$\eta_d x10^3$	$\tau_d x10^3$
Water Flow	-	-	10.5	0.0145	1510.	6.7	3.1	14260	3.8	1.0
C.L. Inj.	8	-2.5	11.0	0.015	1500	6.9	3.1	15070	3.8	1.0
C.L. Inj.	40	26.5	9.0	0.015	-	-	-	9670	4.3	1.3
C.L. Inj.	76	46.0	7.7	0.015	253	10.7	7.7	-	-	-
C.L. Inj.	100	57.0	6.9	0.015	165	12.0	9.5	3840	5.4	2.0
C.L. Inj.	214	67.0	6.17	0.015	157	12.1	9.8	2960	5.8	2.3
Wall Inj.	41	62.0	6.7	0.015	160	12.1	9.7	3670	5.5	2.1

η_d = dissipation length scale = $(\nu^3/\varepsilon)^{\frac{1}{4}}$

τ_d = dissipation time scale = $(\nu/\varepsilon)^{\frac{1}{2}}$

CHAPTER VII

GENERAL DISCUSSION

In this investigation, we studied the drag reduction due to the injection of concentrated drag reducing polymer solutions into both the centreline and the wall of a turbulent shear pipe flow. In addition to the systematic study of the drag reduction by polymer injection, the diffusion of the injected polymer solutions was also studied and the experimental results were discussed in detail in a separate chapter. The flow structure was also studied, using the laser doppler anemometer, through the measurements of the mean velocity and the axial turbulent intensity profiles, the rate of the turbulent bursts, the axial turbulent auto-correlation coefficients, and the turbulent energy spectra. The results were discussed in detail in the previous chapter. The aim of this chapter is to give an overview for the experimental results discussed in the previous chapters and their consistency with each other and with other published results.

Polymer concentration measurements discussed in chapter III showed a large suppression in the turbulent diffusion of the injected solutions compared with diffusion of salt solution into water pipe flow. The difference was large even when they were compared at the same wall shear stress. The suppression of the turbulent diffusion of the injected polymer solutions are in a good agreement with the results of Walters & Wells (1971, 1972), Wu (1972) and Fruman & Tulin (1976). Both Wu (1972) and Fruman & Tulin (1976) injected polymer solutions into the wall region of a flat plate. They reported that polymer additives greatly suppress the turbulent diffusion. Walters and Wells injected the polymer solutions into the wall region of a pipe flow through a porous wall section. Their eddy diffusivity results calculated from the polymer

concentration measurements showed a large suppression which was pronounced near the wall.

In discussing the results of the turbulent diffusion, we attributed the large suppression of the diffusion process to the viscoelastic properties of the injected solutions and their tendency to form super molecular aggregates (see chapter III). The polymer aggregates are thought to behave as solid particles in the turbulent flow in opposing the flow variations, hence, reducing the turbulent diffusion. Such behaviour of the polymer solutions was observed by Kalashnikov & Kudin (1973) when they observed that the anomalous low readings of the pitot tube in polymer solutions was very similar to that caused by the presence of solid particles in a Newtonian turbulent flow. Dye visualization and schlieren photographing technique used by Vleggaar & Tels (1973-a,b) and Stenberg et al (1977-a,b) showed that the existence of these super molecular aggregates is a common feature of the flows with polymer injection.

Drag reduction results due to the injected drag reducing polymer solutions into both the centreline and the wall region of a pipe flow were discussed in chapter IV and V respectively. The experimental results of both centreline and wall injection showed that turbulent flows with polymer injection exhibited much higher drag reduction than that of homogeneous polymer solutions at the same Reynolds numbers. Such high levels of drag reduction by polymer injection were observed before by Walters & Wells (1971) and Vleggaar & Tels (1973-a,b). Vleggaar & Tels injected concentrated polymer solutions into the centreline of a small pipe flow. Their results showed a larger drag reduction than that of homogeneous solutions at the same polymer concentration and Reynolds number. The difference was dramatic at low levels of average polymer concentrations and at low Reynolds numbers.

The larger drag reduction levels observed in the turbulent flows with polymer injection is attributed to the lower values of the onset wall shear stress exhibited in such flows. Table (4.1) showed that the most dramatic difference between the homogeneous polymer solutions and the flows with polymer injection is the low onset wall shear stress, while, the slope ~~///~~ increment δ is the same for both. The results shown in figure (4.21) showed that the drag reduction set in with turbulence in the flow (R_e = 2100 - 3000) and the drag reduction was established over the whole range of the turbulent Reynolds number investigated. The disappearance of the drag reduction onset point in flows with polymer injection was first observed by Vleggaar & Tels (1973) and recently confirmed by Stenberg et al (1977). The effect of shifting the onset point on the observed drag reduction a certain value of Reynolds number or wall shear stress is clearly demonstrated in the comparison shown in figure (4.23). This comparison showed a large difference between the drag reduction by polymer injection and that of homogeneous solutions at low Reynolds numbers (see chapter IV).

Such low value of the onset wall shear stress of drag reduction are believed to be a result of the presence of super molecular polymer aggregates in the flow, which is thought to be as large as the size of the turbulent eddies responsible for the diffusion of the injected solutions. The effect of polymer aggregates on the onset wall shear stress could be observed on the onset wall shear stress results of Whitsitt et al (1969), Hansen & Little (1971), Paterson & Abernathy (1970) and Wang (1972). These results showed that the onset wall shear stress decreased with the increase of polymer concentration. Even the results of Virk (1975), who reported that the onset wall shear stress is independent of the polymer concentration, exhibited lower onset wall shear stress at high polymer concentrations. Such

dependence is presumably a result of the increased polymer aggregates in the solution with the increase of the polymer concentration. The super molecular polymer aggregates are postulated to have much higher length and time scales to interact with the larger scales of turbulence at lower Reynolds numbers (see chapter I and VI).

The hypothesis introduced to explain the larger drag reduction levels obtained with polymer injection is supported by the lower drag reduction levels observed in the second pass section and those observed with aging the injected solutions. The observed lower drag reduction in the second pass section is attributed to the decreased size of the polymer aggregates which is caused by the continuous shearing of these aggregates by the action of the turbulent eddies. Such effect of the turbulent eddies was observed by Stenberg et al (1977) when they found that the visible polymer strands formed with polymer injection were continuously splitted into smaller and smaller downstream with the flow. Experimental evidence discussed before in chapters I, III and IV showed that aging the polymer solutions would result in disaggregation of the super molecular polymer agglomerations due to dispersion of the polymer molecules. The reduced size of the polymer molecular clusters in the aged solutions would cause a reduction of their effectiveness and consequently to lower drag reduction. White (1969) found that aging the polymer solution for several days resulted in an increase of the onset wall shear stress. His results showed that the onset wall shear stress exhibited by fresh polymer solutions is dependent on the polymer concentration. These results showed a complete consistency with our results discussed in chapter IV.

The results of both Vleggaar & Tels (1973-a,b) and Stenberg et al (1977-a,b) raised some questions about the role of the polymer.

turbulence interaction in the core region on drag reduction. These results initially motivated the work of this investigation to reveal the differences between the drag reduction due to the injection of the polymer solutions and that of homogeneous solutions and to investigate the role of the polymer turbulence interactions outside the near-wall region. Experimental results of polymer concentration and local drag reduction along the pipe length measurements showed that the local drag reduction development downstream with the distance downstream from the injector was very similar to the development of the polymer concentration in the near wall region. The local drag reduction results showed a slight increase in the frictional drag just downstream from the centreline injector where the polymer additives were confined to the core region (see chapter IV). On the other hand, when polymer solutions were injected into the wall region, the flow exhibited drag reduction just downstream from the injector. These results indicated that the polymer interactions with the turbulent eddies in the core region, if any, have no influence on the drag reduction and the drag reduction is determined by the polymer concentration in some region near the solid boundaries of the flow.

In chapter IV, we discussed the possible correlation between the drag reduction and the polymer concentration near the wall. The polymer concentration - drag reduction correlation results shown in figures (4.34) to (4.43) could suggest that drag reduction is a function of the average polymer concentration in an annular region with a mean radial distance of 0.9R and a radial width extending to 0.2R. These results gave the evidence that the influence of the polymer additives is mainly confined to the near wall region. This region is thought to include both the viscous sublayer and the buffer zone and presumably a part of the logarithmic region very near to the buffer zone.

The flow structure in this region is quite different from that of the core region. Recent studies of the turbulent boundary layer in Newtonian flows showed, that this region is dominated by an organized streaky structure which is periodically ejected away into the core region of the flow in a quasi-cyclic process known as the bursting process. The observed low-speed streaks are formed in the compressed regions between the counter-rotating vortices spatially organized in the viscous sublayer. These low speed streaks lift up into the buffer zone presumably as a result of the interaction between the streaks and the large vortecal motion of the fluid coming from the core region into the wall during the sweep event. The lifted up streak grows rapidly in both the streamwise direction and the direction normal to the wall. In this stage the vortex structure suffers large extensional strains as the streak moves away from the wall. As it reaches a certain stage, it oscillates very rapidly and the cycle is ended by the breakdown of the whole structure violently ejecting the low-speed streaks away into the core region.

Polymer additives are thought to inhibit the streak formation and the eruption of the turbulent bursts by increasing the resistence of the flow structure to stretching. The increase in the flow resistence to stretching strains allow the micro-vortices in the viscous sublayer to grow large and hence, the streak spacing increases. Polymer additives also affect, by the same way, the rapid growth of the low speed streaks after they have been lifted up from the viscous sublayer allowing them to grow in much slower rates. This large increase in the growing time of the low-speed streaks is thought to be the major factor causing the observed increase in the bursting time $\overline{T}_B$. It seems that the rapid growth of the oscillatory motion of the streak which ends by the breakdown and the ejection of the

low-speed streak could be affected by the increased stretching resistance. This effect is thought to be in the form of stabilizing the response of the streak to the turbulent random oscillations. Such type of boundary layer stabilization was suggested by Landahl (1974, 1977) to explain the increase of the bursting time. Both the increase in the growing time of the low-speed streaks and the stabilization of their response to the imposed turbulent oscillations co-operate in increasing the interval time between bursts. Consequently, the increase in both the streak spacing and bursting time $\overline{T}_B$ resulted in a substantial reduction in the production of the turbulent energy.

During the measurements of the local drag reduction by injecting the polymer solutions into the wall region, an intersting oscillatory scatter of measurement of the local friction factor was observed. The analysis presented in chapter V and in McComb & Rabie (1978) showed that such oscillatory variation of the wall shear stress is related to the bursting process. The turbulent bursting process is thought to modulate the outward diffusion of the polymer from the wall through the burst ejection event and the subsequent sweep event. Both the two events co-operate in lowering the concentration of the polymer in the near-wall region resulting in lower drag reduction. The observed oscillatory variation of the local wall shear stress supports the hypothesis which postulates that the main influence of the polymer additives is to reduce the turbulent energy generation by suppressing the formation of the streaks and the eruption of the turbulent bursts.

One of the main objectives of this work was to investigate the changes in the flow structure and whether the changes associate the local presence of the polymer additives or the drag reduction. Mean velocity and turbulent intensity profiles, bursting time, auto-correlation coefficients and turbulent energy spectrum measurements

were carried out in water flow and flows with polymer injection using LDA. The use of the laser doppler anamometer allowed us accurate measurements free of the serious errors associated with the use of the conventional techniques in drag reducing solutions (see chapters I and V). The measurements carried out at the section of x/d = 8 downstream from the centreline injector where the polymer additives were outside the near wall region and confined to the core region of the flow showed interesting results. The local wall shear stress at this section exhibited a slight increase over the water flow value (i.e. an increase in the frictional drag). The mean velocity and the turbulent intensity profiles at this section showed no detectable changes from the water results even in the core region where the polymer additives were confined (see figures (6.3) and (6.7). Furthermore, the auto correlation coefficient and the turbulent energy spectrum measurements at the centre of the pipe cross-section at this location did not show any sensible changes from the water results (see figures (6.13), (6.17), (6.18) and (6.19). The slight differences are attributed to the slight increase in the local viscosity. These results gave the evidence that the polymer additives interaction with the flow structure outside the near-wall region does produce neither drag reduction nor changes in the local structure of the flow.

On the other hand, the measurements carried out at the section of x/d = 41 from the injector during the injection of the polymer solution into the wall region, showed the other side of the picture. At this section, the polymer additives were confined to the near-wall region while the core region was almost free of polymer additives and the drag reduction was about 62%. Mean velocity and turbulent intensity profiles exhibited an increase in the mean velocity and the turbulent intensity over those of water flow (see figures (6.4),

(6.9) and (6.10). The changes were pronounced near the wall which seems to extend to the core region with the increase in the drag reduction. These results are in general agreement with the previous results. However, the most interesting results were those of the auto-correlation coefficient and the turbulent energy spectrum measured at the centre of this section where the region was considered free of polymer. The auto-correlation coefficient results showed a substantial increase in the life time of the turbulent eddies (see figure (6.13). This is confirmed by the turbulent energy spectrum results which showed a large suppression of the small eddies. This set of results gave the evidence that the changes in the flow structure are associated with the drag reduction not the local presence of the polymer additives outside the near-wall region. The general conclusion of these results is that the observed changes in the flow structure of the drag reducing flows is caused by the polymer additives interaction with the flow structure in the near-wall region and not due to the local interaction between the additives and the turbulent eddies outside the most effective region.

The mean velocity and the turbulent intensity profiles measured during the centreline injections at the sections of x/d = 40, 76, 100, 190 and 214 from the injector showed that, the changes in the flow structure started near the wall and extended to the core region with the increase in the drag reduction level (see figures (6.13), (6.7) and (6.8)). The mean velocity profiles exhibited a continuous change across the whole section. However, they could be approximated by three layers, the viscous sublayer, the polymer interactive layer, and the turbulent core region. The results showed no significant change in the thickness of the viscous sublayer from that of water (y^+ - 11.6).

The mean velocity distribution in the polymer interactive region exhibited a variable Von-Karman mixing length constant ($0.085<k_p<0.4$) which is dependent on the drag reduction. The dependence of the slope of the mean velocity distribution in this region are in disagreement with Virk's hypothesis which postulate that the mean velocity distribution in this region follow a unique ultimate profile. However, these results support the hypothesis of Van Driest (1970) postulating that the mean velocity distribution in this region is characterized by a variable Van Karman constant (k_p) which depends on the flow parameters. In the turbulent core region and at low and moderate drag reduction levels, the mean velocity distribution exhibited a slight increase in the slope in addition to the normal upward shift. This is in good agreement with the results of Kumor & Sylvester (1973) which showed that the mean velocity distribution in the core region exhibits an increasing slope with the increase in drag reduction. The results also showed that at high drag reduction levels, the core region became indistinguishable from the polymer interactive layer such that it disappeared at maximum drag reduction and the whole cross-section is dominated by the polymer interactive layer. This result shows a good agreement with the available results at maximum drag reduction and with the hypothesis of Virk and Van Driest.

The results of the auto-correlation coefficients shown in figures (6.13) to (6.16) indicated that the increase in the life time of the turbulent eddies is a function of the drag reduction and completely independent of the polymer concentration outside the near-wall region. The increase in the life time of the turbulent eddies seems to be the same across the whole cross-section.

The turbulent energy spectrum results shown in figures (6.17) to (6.23) exhibited the same features shown by the auto-correlation results. The results showed a suppression of the small turbulent eddies. Such suppression was found to be across the whole cross-section and independent of the local polymer concentration outside the most effective region. When the data were normalized using Kolmogoroff variables, the turbulent energy spectrum results showed no difference from the water results in the high-wave number part of the spectrum, while, the low wave-number region exhibited a substantial enhancement. This result showed that the small eddies of the turbulent eddies were suppressed compared to those of water flow at the reduced wall shear stress.

The results of both the auto-correlation coefficient and the turbulent energy spectrum indicated that the changes in the turbulence structure in the whole cross-section associate the changes in the flow structure near the wall brought by the polymer additives interaction with the streaky structure and the turbulent bursting process. This is confirmed by the results of the bursting time measurements shown in table (6.2) and the previous results of the bursting time and the streak spacing (see chapter I and VI). The results presented in table (6.2) showed that the interval time between bursts was higher than that of the water flow even when compared at the same wall shear stress. These results are in agreement with those of Achia & Thompson (1977) which showed that both the bursting time and the streak spacing of the drag reducing flows were higher than those of water flow at the reduced value of the wall shear stress.

The increase in both the streak spacing and the interval time between bursts indicated a large suppression of the turbulent bursts in drag reducing flows. The lower number of turbulent bursts in drag reducing flows than that of the water flow at the reduced wall shear stress could suggest a more momentum transport per burst in drag reducing flow. This is possible because of the increase in the scale of the bursts due to the increase of their spanwise dimension and their developing time. However, still the most dramatic change in the flow structure is the suppression of the turbulent energy generation due to the large suppression of the formation of the streaks and the eruption of the turbulent bursts.

CHAPTER VIII

SUMMARY AND CONCLUSIONS

The drag reduction due to injected drag reducing polymer solutions into the centreline and the wall region of a turbulent, water pipe flow was studied. The diffusion of the injected solutions was also investigated. In order to investigate the changes in the flow and the turbulence structure due to the polymer additives, mean velocity and turbulent intensity profiles, bursting time, auto-correlation coefficients and the turbulent energy spectra were measured in both water flow and flows with polymer injection. The measurements were carried out using the laser doppler anemometer technique.

The results of the diffusion of the injected polymer solutions showed a large suppression of the turbulent diffusion. This is thought to be due to the viscoelastic nature of the diffused matter and its tendency to form super molecular agglomerations, which make the polymer additives lag the movement of the turbulent eddies responsible for their diffusion.

The local drag reduction measurements due to the injected polymer solutions into the centreline of the pipe flow indicated that the presence of the polymer additives in the core region does not produce any reduction in the frictional drag. The local drag reduction was found to develop downstream from the injector to an asymptotic level. The development of the local drag reduction was very similar to that of the polymer concentration near the wall. This similarity suggested a correlation between the drag reduction and the polymer concentration near the wall. Such correlations were found by predicting the local drag reduction from the local polymer concentration measurements using the measured drag reduction as a function of the average polymer

concentrations in the flow. This procedure was carried out along the whole test section length, for a number of different radial locations in the cross section and tested in four polymer solutions injected. The results of this correlation showed that the achieved drag reduction is determined by the average polymer concentration in an annular region of radius 0.9R and with a radial width varied from zero to 0.15R. This is corresponding to the region from the wall up to $y^+ = 100$.

The results of the local drag reduction due to injected polymer solutions into the wall region confirmed the conclusions obtained from the centreline injection results. These results showed that drag reduction was achieved just downstream from the injector when the polymer additives were in the wall region. They also showed a similarity between the local drag reduction development and that of the polymer concentration at $r/R = 0.9$. Furthermore, the local drag reduction results exhibited an oscillatory character variation which was found to be related to the ejection of the turbulent bursts and their subsequent sweep events.

The results of the drag reduction due to injected polymer solutions into the centreline and those of the wall injection gave the direct evidence for the importance of the near-wall region in drag reduction. They indicated that the only polymer additives interaction with the flow structure which is responsible for the drag reduction is that with the flow structure in the near wall region. The flow in this region is characterized by the streaky structure and the turbulent bursts. Hence, polymer additives are thought to reduce the frictional drag by suppressing the streak formation and the eruption of the turbulent bursts.

The results of the drag reduction by injecting relatively concentrated polymer solutions into the centreline and into the wall region exhibited higher values than those achieved in the homogeneous

solutions at the same polymer concentration and flow Reynolds number. The difference was found to be much pronounced at low polymer concentrations and Reynolds numbers.

The most interesting result obtained was the low values of the onset wall shear stress which was found to characterize the flows with polymer injection. In such flows, the drag reduction was found to be established over the whole range of the flow Reynold number studied with almost the disappearance of the onset point for drag reduction.

The high drag reduction efficiency observed in the flows with polymer injection is attributed to the low onset wall shear stress values exhibited in these flows. The low values of the drag reduction onset are believed to be caused by the increase in the characteristic dimension of the polymer additives due to the presence of super-molecular polymer agglomerations. The presence of such agglomerations was found to be a common feature in the flows with polymer injection.

The polymer agglomeration hypothesis introduced to explain the high efficiency of the drag reduction by polymer injection is supported by the results of the drag reduction of the second pass of the flow and by those due to injecting aged polymer solutions. The drag reduction results of the second pass were found to be lower than the asymptotic value of the drag reduction by almost 10%. This difference is thought to be the result of the reduced characteristic dimensions of the polymer additives due to the continuous splitting of the super molecular polymer agglomeration into smaller and smaller pieces by the eddying motion of the flow. The drag reduction results by the injection of aged polymer solutions exhibited lower values than those of fresh polymer solutions. This is attributed to the reduced size of the polymer agglomerations by the dispersion of the polymer molecules with aging these solutions.

The flow and the turbulence structure measurements were carried out using laser doppler anemometer. In addition to the many advantages offered by the use of LDA, its results are free of the serious errors which associate the use of the conventional measuring techniques in drag reducing flows. The results of the mean velocity and the turbulent intensity profiles in water flow are in a good agreement with other previous results showing the compatibility of the system.

The results of the mean velocity profile measurements in the flow with polymer injection showed continuous changes across the whole cross section which was found to set in with the drag reduction. However, the mean velocity profile in drag reducing flows could be approximated by three regions, the normal viscous sublayer, the polymer interactive region and the turbulent core region. In the polymer interactive region, the mean velocity distribution exhibited a variable slope depending on the drag reduction level, which increases with the increase in the drag reduction approaching the ultimate profile of Virk at maximum. The results indicated that the mean velocity distribution in the turbulent core exhibited a slight increase in the slope in addition to the normal upward shift. At high levels of drag reduction, both the polymer interactive layer and the turbulent core region became indistinguisable.

The results of the turbulent intensity profile measurements showed that the turbulent intensity in drag reducing flows increased over that of the water flow. The increase was confined to near the wall at low drag reduction values and extended to the core region as the drag reduction increased. The distinct peak of the turbulent intensity observed in water flow results was found to be increased and distributed over a wider range of y^+ with the increase in the drag reduction.

The results showed that when the polymer additives were confined to the core region of the flow, the mean velocity and the turbulent intensity profiles were identical to those of water flow. This result gave the evidence the polymer additives interaction with the turbulent structure in the core region does produce neither drag reduction nor changes in the flow structure.

The results of the auto-correlation coefficient measurement indicated that the drag reduction is associated with an increase in the life time of the turbulent eddies across the whole cross section. The change was found to be independent of the local polymer concentration outside the core region.

The measurements of the turbulent energy spectrum in drag reducing flows confirmed the results of the auto-correlation. The results showed a large suppression of the small eddies of the turbulence structure and an enhancement of the large eddies. The normalization of the spectrum results using Kolmogoroff variables indicated that the suppression of the small turbulent eddies was to the level of those of water flow at the reduced value of the wall shear stress.

Both the auto-correlation coefficient and the turbulent energy spectrum results showed no differences from those of the water flow when the polymer additives were outside the near-wall region. These results gave more evidence for the conclusion derived before that the polymer additives interaction with the flow structure in the core region, if any, does not produce any changes in the turbulence structure, even locally.

The results of the flow and the turbulent structure measurements indicated that the changes in these structures are brought by the polymer additives interaction with the flow structure in the near wall region. These additives are thought to inhibit the streaky

structure and the development of the turbulent bursts resulting in suppression of the streak formation and the eruption of bursts. This hypothesis is supported by the results of the bursting time measurements. These results showed that the interval time between bursts was substantially increased over that of water flow even at the reduced value of wall shear stress.

REFERENCES

ACHIA, B.U., and THOMPSON, D.W., Int. Conf. Drag Reduction, Cambridge, England, BHRA, Paper A4, (1974)

ACHIA, B.U., and THOMPSON, D.W., J. of Fluid Mech., 81, 439, (1977)

ADRIAN, R.J., HUMPHREY, J.A.C., and WHITELAW, J.H., Proc. the LDA Symp., Copenhagen, Denmark, 287, (1975)

ALLAN, J., Mech. Eng. Dept., Univ. of Edinburgh, Edinburgh, Scotland, Research Report, (1977)

ARUNACHALAM, V., and FULFORD, G.D., Chem. Eng. Science, 26, 1065 (1971)

ASTARITA, G., GRECO, G., Jr., and NICODEMO, L., AIChE., 15, 564, (1969)

AYYASH, S.Y., PhD., Thesis, Univ. of Edinburgh, Scotland, (1978)

AYYASH, S.Y., and McCOMB, W.D., Chem. Eng. Science, 31, 169, (1976)

BALAKRISHNAN, C., and GORDON, R.J., Nature, 231, 177, (1971)

BALDWIN, L.V., and WALSH, T.J., AIChE., J., 7, 53, (1961)

BERMAN, N.S., Physics Fluids, 20, 715, (1977)

BERMAN, N.S., and GEORGE, W.K., Physics Fluids, 17, 250, (1974)

BERMAN, N.S., and DUNNING, J.W., J. Fluid Mech., 61, (1973)

BLACK, J.J., Viscous Drag Reduction ed. by Wells, C.S., Plenum Press, N.Y. 383, (1969)

BLAKE, K.A., and JESPERSEN, K.I., NEL Report No. 510, (1972)

BOKEMEIER, V., and FEIGE, N., Proc. the LDA Symp., Copenhagen, 279, (1975)

BRADSHAW, P., NPL Aero. Rep. 1220, (1967)

BRENNEN, C., and GADD, G.E., Nature, 215, 1368, (1967)

BRINKWORTH, B.J., and SMITH, P.C., Chem. Eng. Sci., 24, 787, (1969)

BROWN, G.L., and THOMAS, A.S.W., Physics Fluids, 20, S 243, (1977)

BRYSON, A.W., ARUNACHALAM, Vr., and FULFORDS, G.D., J. Fluid Mech., 47, 209, (1971)

BUSTON, J., and GLASS, D.H., Int. Conf. Drag Reduction, Cambridge, England, Paper A3, (1974)

CESS, R.D., Westinghouse Research Report 8-0529-R-24 (1958)

CHIEN-BANG WANG, Ind. Eng. Chem. Fundam., 11, 546, (1972)

CHUNG, J.S., and GRAEBEL, W.P., Physics Fluids, 15, 546, (1972)

CORINO, E.R., and BRODKEY, R.S., J. Fluid Mech., 37, 1, (1969)

COX, L.R., DUNLOP, E.H., and NORTH, A.M., Nature, 249, 243, (1974)

DAVIDSON, G.A., and McCOMB, W.D., J. Aerosol Sci., 6, 227, (1975)

DAVIES, G.A., and PONTER, A.B., Nature, 212, 66, (1969)

DEISSLER, R.G., NASA Report, TN 3145, (1954)

DEVER, C.D., HARBOUR, R.J., and SIEFERT, W.F., U.S. Patent No.3, 023, 760, (1962)

DIKSON, K.R., Mech. Eng. Dep., Univ. of Edinburgh, Scotland, Rec. Report, (1978)

DIMANT, Y., and POREH, M., Advances in Heat Trans., 12, 77, 1976

DONOHUE, G.L., McLAUGHLIN, D.K., and TIEDERMAN, W.G., Physics Fluids, 15, 1920, (1972)

DONOHUE, G.L., TIEDERMAN, W.G., and REISCHMAN, J. Fluid Mech. 56, 559, (1972)

DRUST, F., Proc. The LDA Symp., Copenhagen, Denmark, 208, (1975)

DRUST, F., and WHITELAW, J.H., Proc. Royal Soc., London, A-324, 157, (1971)

DUNLOP, E.H., and COX, L.R., Physics Fluids, 20, S 203, (1977)

DURRANI, T.S., and GREATED, C.A., Laser Systems in flow measurement, Plenum Press, N.Y. (1977)

DURRANI, T.S., GREATED, C.A., and WILMSHURST, T.H., Opto-electron, 5, 71, (1973)

ECKELMAN, L.D., FORTUNA, G., and HANRATTY, T.J., Nature, 236, 94 (1972)

EDWARDS, R.V., ANGUS, J.C., FRENCH, M.J., and DUNNING, J.W., J. Appl. Phys., 42, 837, (1971)

EINSTEIN, H.A., and LI., H., Am. Soc. Civil Eng., 82, 293, (1956)

ELLIS, H.D., Nature, 226, 352, (1970)

ELLIS, A.T., WAUGH, J.G., and TING, R.Y., Trans. ASME., J. Basic Eng., 92, 459, (1970)

EL'PERIN, I.T., SMOL'SKII, B.M., and LEVENTHAL, L.I., Int. Chem. Eng. 7, 276, (1967)

FABULA, A.G., Doctoral thesis, Pennsylvania State Univ., (1966)

FABULA, A.G., HOYT, J.W., and GRAWFORD, H.R., Bulletin, American Phys. Soc., 8, (1963)

FABULA, A.G., LUMLEY, J.L., and TAYLOR, W.D., Modern develop. in the mech. of contin., Academic press Inc., N.Y., (1966)

FLINT, D.L., KADA, H., and HANRATTY, T.J., AIChE., J. 6, 325, (1960)

FORTUNA, G., and HANRATTY, T.J., AIChE., Symp., No.111, 90, (1971)

FORTUNA, G., and HANRATTY, T.J., J. Fluid Mech., 53, 575, (1972)

FRENKIEL, F.N., J. Aero. Sci., 15, 57, (1948)

FRUMAN, D.H., and TULIN, M.P., J. of Ship Research, 20, 171, (1976)

GADD, G.E., Nature, 202, 463, (1965-a)

GADD, G.E., Nature, 206, 463, (1965-b)

GADD, G.E., Nature, 212, 1348, (1966)

GADD, G.E., Nature, 217, 1040, (1968)

GASIOREK, J.M., CARTER, W.G., Mech of Fluids for Mech. Engs., Blackie & Son, Glasgow, (1967)

GEORGE, W.K., Proc., the LDA Symp., Copenhagen, Denmark, 20, (1975)

GEORGE, W.K., and LUMLEY, J.L., J. Fluid Mech., 60, 321, (1973)

GORDON, R.J., Nature, 227, 599, (1970)

GORDON, R.J., J. Applied Polymer Sci., 14, 2057, (1970)

GOREN, Y., and NORBURY, J.F., Trans. ASME., J. Basic Eng., 89, 814, (1967)

GROENHOF, H.C., Chem. Eng. Sci., 25, 1005, (1970)

GRANVILLE, P.S., U.S. Naval Ship Research and Develop. Centre Tech. Note 118, (1968)

GYR, A., Nature, 219, 928, (1968)

GYR, A., and MUELLER, A., Chem. Eng. Sci., 29, 1057, (1974)

HAND, H.H., and WILLIAMS, H.C., Chem. Eng. Sci., 28, 63, (1973)

HANRATTY, T.J., CHORN, L.G., and HATZIAVRAMIDIS, D.T., Physics Fluids, 20, S 112, (1977)

HINCH, E.J., Physics Fluids, 20, S 22, (1977)

HINZE, J.O., Turbulence, McGraw-Hill, N.Y., (1975)

HOYT, J.W., Proc. 16th Am Towing Tank Conf., 1, 7, (1971)

HOYT, J.W., Trans. ASME., J. Basic Eng., 94, 258, (1972)

HOYT, J.W., Polymers et Lubrification, Paris, p. 193, (1975)

HOYT, J.W., 2nd Int. Conf. Drag Reduction, Cambridge, England, BHRA Fluids Eng., Paper A1, (1977)

HOYT, J.W., and FABULA, A.G., Proc. 10th Int. Towing Tank Conf. Teddington, (1963)

HOYT, J.W., and FABULA, A.G., Proc. 5th Symp. on Naval Hydro. Bergen, Norway, Office of Naval Research, ACR-112, 947, (1964)

HUNSEN, R.J., and LITTLE, R.C., AIChE Symp. Ser. No.111, 93, (1971)

HUSSAIN, A.K.M.E., and REYNOLDS, W.C., Trans. ASME, J. Fluids Eng. 97, 568, (1975)

JOHNK, R.E., and HANRATTY, T.J., Chem. Eng. Sci., 17, 867, (1962)

JOHNSON, B., and BARCHI, R.H., J. Hydronautics, 2, 168, (1968)

KALASHNIKOV, V.N., and KUDIN, A.M., Nature, 242, 62, (1973)

KALE, D.D., Int. J. Heat Mass Trans., 20, 1077, (1977)

KIM, H.T., KLINE, S.J., and REYNOLDS, W.C., J. Fluid Mech. 50, 133, (1971)

KLINE, S.J., REYNOLDS, W.C., SCHRUB, F.A., and RUNSTADLER, P.W., J. Fluid Mech, 30, 741, (1967)

KOHN, M.C., AIChE J, 20, 185, (1974)

KOWALSKI, T., and BRUNDRETT, E., 1st Int. Conf. Drag Reduction, Cambridge, England, BHRA Fluids Eng., Paper C1 (1974)

KUMOR, S.M., and SYLVESTER, N.D., AIChE Symp. Ser., 130, 1, (1973)

LADING, L., Appl. Optics J., 10, 1943, (1971)

LANDAHL, M.T., Proc. 13th Int. Congr. Thear. and Appl. Mechanics, Moscow, P.177 (1973)

LANDAHL, M.T., Physics Fluids, 20, S 55, (1977)

LANDAHL, M.T., and BARK, F.H., Polymeres et Lubrification, Paris, 249, (1974)

LAUFER, J., NACA report 1174, (1953)

LAUFER, Z., JALINK, H.L., and STAVERMAN, A.J., J. Polym. Sci. Chem. Ed., 11, 3005, (1973)

LAWN, C.J., J. Fluid Mech., 48, 477, (1971)

LATTO, B., and SHIN, C.H., Cand. J. Chem. Eng., 48, 34, (1970)

LITTLE, R.C., J. Applied polym. Sci. 15, 3117, (1971)

LITTLE, R.C., HANSEN, R.J., HUNSTON, D.L., KIM, O.K., PATTERSON, R.L., and TING, R.Y., Ind. Eng. Chem. Fundam., 14, 283, (1975)

LOGAN, S.E. AIAA J., 10, 962, (1972)

LOVE, R.H., Hydronautics Inc. Tech. Report 353-2 (1965)

LUMLEY, J.L., Ann. Review Fluid Mech., 1, 1, (1969)

LUMLEY, J.L., Macromol. Rev., 7, 263, (1973)

LUMLEY, J.L., Physics Fluids, 20, S 64, (1977)

MARRUCCI, G., and ASTARITA, G., Ind. Eng. Chem. Fundam. 6, 471, (1967)

MAUS, J.R., and WILHELM, L.R., J. Hydronautics, 4, 35, (1970)

MAZUMDER, M.K., WANKUM, D.L., Applied Optics, 9, 633, (1970)

McCOMB, W.D., Nature, 241, 117, (1973)

McCOMB, W.D., Nature, 251, 598, (1974)

McCOMB, W.D., J. Phys., A., 7, L 164, (1974)

McCOMB, W.D., AYYASH, S.Y., Nature, 262, 47, (1976)

McCOMB, W.D., ALLAN, J., and GREATED, C.A., Physics Fluids, 20, 873, (1977)

McCOMB, W.D., and SALIH, S.M., J. Aerosol Sci., 8, 171, (1977-a)

McCOMB, W.D., and SALIH, (submitted) (1977-b)

NcCOMB, W.D., and RABIE, L.H., Nature, In press (1978)

McCOMB, W.D., and RABIE, L.H., Under Review in Physics Fluids (1978)

McCONAGHY, G.A., and HANRATTY, T.J., AIChE J., 23, 493, (1977)

MEEK, R.L., and BAER, A.D., AIChE J., 16, 841, (1970)

MEISTER, B.J., and BIGGS, R.D., AIChE J., 15, 643, (1969)

METZNER, A.B., and METZNER, A.P., Rheological Acta., 9, 174, (1970)

MILLWARD, A., and LILLEY, G.M., 1st Int. Conf. Drag Red. Cambridge, England, BHRA paper A1, (1974)

MIZUSHINA, T., and USUI, H., Physics Fluids, 20, S 100, (1977)

MONTI, R., Progress Heat Mass Trans., 5, 239, (1972)

MORGAN, D.T.S., Nature, 231, 624, (1971)

MYSELS, K.J., AIChE Symp Ser., 111, 45, (1971)

OFFEN, G.R., and KLINE, S.J., J. Fluid Mech., 70, 209, (1975)

OLDAKER, D.K., and TIEDERMAN, W.G., Physics Fluids 20, S 133, (1977)

OLDROYD, J.G., Proc. 1st Int. Congr. in Rheology, Amsterdam, Holland, Vol. 2, p.130, (1948)

OLIVER, D.R., and BRAGG, R., The Chem. Eng. J. 5, 1, (1973)

OLIVER, D.R., and BRAGG, R., Polymers et Lubrification, Paris, 325, (1974)

OUSTERHOUT, R.S., and HALL, C.D., J. Petroleum Technology, 13, 217, (1960)

OWEN, J.M., and ROGERS, R.H., Proc. the LDA Symp., Copenhagen, Denmark, 89, (1975)

PATTERSON, G.K., and ZAKIN, J.L., AIChE J., 14, 434, (1968)

PATTERSON, G.K., and FLOREZ, G.L., Viscous Drag Reduction, Wells, C.S., Plenum Press, N.Y., 233, (1969)

PATERSON, R.W., and ABERNATHY, F.H., J. Fluid Mech., 43, 689, (1970)

PETERLIN, A., Nature, 227, 598, (1970)

PETERSON, J.P., ZIELINSKI, P.B., and CASTRO, W.E., AIChE Symp. Ser., 130, 82, (1973)

PFENNIGER, W., Northrop Corp. Norair Division Report BLC-179, (1967)

QUARMBY, A., and ANAND, R.K., J. Fluid Mech., 38, 433, (1969)

RAMU, K.L., and TULLIS, J.P., J. Hydronautics, 10, 55, (1976)

ROA, N.K., NARASHIMHA, R., and BADRI NARAYANAN, M.E., J. Fluid Mech., 48, 339, (1971)

REICHARDT, H., ZAMM, 31, 203, (1951)

REISCHMAN, M.M., and TIEDERMAN, W.G., J. Fluid Mech., 70, 369, (1975)

ROLLIN, A., and SEYER, F.A., Cand. J. Chem. Eng., 50, 714, (1972)

RUDD, M.J., Nature, 224, 587, (1968)

RUDD, M.J., AIChE Symp. Ser., 111, 29, (1971)

RUDD, M.J., J. Fluid Mech., 51, 673, (1972)

SAVINS, J.G., Soc. Petroleum Eng. J., 4, 203, (1964)

SCHLICHTING, H. Boundary layer theory, 6th ed., McGraw-Hill, N.Y. (1960)

SEYER, F.A., and METZNER, A.B., Cond. J. Chem. Eng., 45, 121, (1967)

SEYER, F.A., and METZNER, A.B., AIChE J., 15, 426, (1969)

SEYER, W.A., AIChE J., 12, 522, (1966)

SHAUGHNESSY, E.J., and MORTON, J.B., J. Fluid Mech., 80, 129, (1977)

SHERIFF, N., and O'KANE? D.J., INt. J. Heat Mass Trans., 14, 697, (1971)

SHIN, H., Sc.D. thesis, Mass. Inst. Tech., Cambridge, (1965)

SIDAHMED, G.H., and GRISKEY, R.G., AIChE J., 18, 138, (1972)

SHULMAN, Z.P., POKRYVAILO, N.A., KABERDINA, E.B., and NESTEROV, A.K., Proc. 1st Int. Conf. Drag Reduc. Cambridge, England, BHRA, paper A4, (1974)

SMITH, K.T., MERRILL, E.W., MICKLEY, H.S., and VIRK, P.S., Chem. Eng. Sci., 22, 667, (1967)

SMITH, K.T., KEURAGHLIAN, G.H., VIRK, P.S., and MERRILL, E.W., AIChE J., 15, 294, (1969)

SOO, S.L., Fluid Dynamics of Multiphase Systems, Blaisdell, USA, (1967)

SPALDING, D.B., Progress in Heat transfer, 5, 275, (1972)

STENBERG, L.G., LAGERSTEDT, T. SEHLEN, O., and LINDGREN, E.R., Physics Fluids, 20, 858, (1977-a)

STENBERG, L.G., LAGERSTEDT, T., and LINDGREN, E.R., Physics Fluids, 20, S 276, (1977-b)

STRICKLAND, J.H., and SIMPSON, R.L., Physics Fluids, 18, 306, (1975)

TAYLOR, G.I., Proc. London Math. Soc., 20, 196, (1921)

TAYLOR, A.R., and MIDDLEMAN, S., AIChE J., 20, 454, (1974)

THOMAS, L.C., GREENE, H.L., NOKES, R.F., and CHU, M., AIChE Symp. Ser., 130, 14, (1973)

TIEDERMAN, W.G., and REISCHMAN, M.M., Trans. ASME, J. Fluids Eng., 98, 563, (1976)

TING, R.Y., and HUNSTON, D.L., Ind. Eng. Chem. Prod. Res. Dev., 16, 129, (1977)

TOMS, B.A., Proc. 1st Int. Congr. in Rheology, Amsterdam, Holland, Vol. 2 p.135, (1948)

TOWLE, W.L., and SHERWOOD, T.K., Ind. Eng. Chem., 31, 457, (1939)

TULIN, M.P., Proc. 6th Symp. on Naval Hydrodyn. Washington, ONRACR-136, p.3, (1966)

TULLIS, J.P., and RAMU, K.L., Proct. 1st Int. Conf. Drag Red. Cambridge, England, BHRA, Paper G3, (1974)

VAN DRIEST, E.R., J. Aero. Sciences, 23, 1007, (1956)

VAN DRIEST, E.R., J. Hydronautics, 4, 120, (1970)

VAN MAANEN, H.R.E., VAN DER MOLEN, K., and BLAM, J., Proc. the LDA Symp., Copenhagen, 81, (1975)

VIRK, P.S., J. Fluid Mech., 45, 225, (1971)

VIRK, P.S., J. Fluid Mech., 45, 417, (1971-a)

VIRK, P.S., AIChE J., 21, 625, (1975)

VIRK, P.S., MERRILL, E.W., MICKLEY, H.S., and SMITH, K.A., Modern develop. Mech. Cont., Academic Press, Inc., N.Y., (1966)

VIRK, P.S., Merrill, E.W., MICKLEY, H.S., SMITH, K.A., and MOLLA-CHRISTENSEN, J. Fluid Mech., 30, 305, (1967)

VIRK, P.S., and BAHER, H., Chem. Eng. Sci., 25, 118s, (1970)

VIRK, P.S., MICKLEY, H.S., and SMITH, K.A., Trans. ASME, J. Appl. Mech., 37, 488, (1970-a)

VIRK, P.S., and SURAIYA, T., Proc. 2nd Conf. Drag Red. Cambridge, England, BHRA, Paper G3, (1977)

VLEGGAAR, J. and TELS, M., Chem. Eng. Sci., 28, 309, (1973-a)

VLEGGAAR, J. and TELS, M., Chem. Eng. Sci., 28, 965, (1973-b)

WALLACE, J.M., ECHELMANN, H., and BRODKEY, R.S., J. Fluid Mech., 54, 39, (1972)

WALSH, M., Int. Shipbuilding progress, 14, 134, (1967)

WANG, CH-BANG, Ind. Eng. Chem. Fundam., 11, 546, (1972)

WALTERS, R.R., and WELLS, C.S., J. Hydronautics, 5, 65, (1971)

WALTERS, R.R., and WELLS, C.S., J. Hydronautics, 6, 69, (1972)

WELLS, C.S., AIChE J., 14, 406, (1968)

WELLS, C.S., and SPANGLER, J.G., Phys. Fluids, 10, 1890, (1967)

WELLS, C.S., HARKNESS, J., and MEYER, W.A., AIAA, 6, 250, (1968)

WHITE, A., Viscous Drag Reduction, Wells, C.S., ed. Plenum, N.Y., p.297, (1969)

WHITE, A., Nature, 235, 154, (1972)

WHITSITT, N.F., HARRINGTON, L.J., CRAWFORD, H.R., Viscous Drag Reduction, Wells, C.S. ed., p.265, (1969)

WILMSHURST, T.H., and RIZZO, J.E., J. Phys. E., 7, 924, (1974)

WU, J., Viscous Drag Reduction ed. by Wells, C.S., Plenum Press, N.Y., p.331, (1969)

WU, J., AIChE J., 17, 1408, (1971)

WU, J., J. Hydronautics, 6, 46, (1972)

WU, J., and TULIN, M.P., Trans. ASME., J. Basic Eng., 94, 749, (1972)

YEH, Y., and CUMMINS, H.Z., Applied Phys. lett., 4, 176, (1964)

FIGURE CAPTIONS

Figure 2.1 Elevation view of the experimental set-up: (1) Supply tank; (2) Rigid PVC pipe section; (3) Settling Chamber; (4) Orifice meter; (5) Centrifugal pump; (6) Constant level tank; (7) Injection pump; (8) First pass of the test section; (9) Second pass of the test section; (10) Scanning valves, and (11) Polymer injector.

Figure 2.2. Flow diagram of the experimental set-up.

Figure 2.3.a Sectional view of the pressure tap.

Figure 2.3.b DISA low-pressure transducer set-up.

Figure 2.4 The orifice meter.

Figure 2.5 Plan view of the injection pump and driving system .

Figure 2.6 Polymer Injection pump; (1) Pyrex glass cylinder; (2) Assembling flange; (3) 8-through bolts for cylinder head assembly; (4) Cylinder head; (5) Safety valve; (6) Polymer inlet valve; (7) Polymer outlet valve; (8) 3-stud bolts for piston assembly; (9) 3-long-alignming rods; (10) Base; (11) Chain sprocket for power transmission; (12) Thrust bearing; (13) Brass nut; (14) Key; (15) & (17) Flanges for cylinder assembly; (16) 8-through bolts; (18) Threaded rod; (19) Piston; (20) Rubber rings for sealing, and (21) PTFE sealing rings.

Figure 2.7 Centreline injector.

Figure 2.8 Wall injector.

Figure 2.9 Caliberation of the orifice meter.

Figure 4.16 The asymptotic and the second-pass drag reduction results as a function of the average polymer concentration, Polyox WSR-301, in comparison with the homogeneous solution drag reduction results of Goren & Norbury (1967) and those calculated from the data of Virk (1975) and of McNally (1968).

Figure 4.17) The effect of aging the injected polymer solutions on the local drag reduction development; Polyox WSR-301, C_p = 500 wppm, C.L., injection.

Figure 4.18 The effect of aging the injected polymer solutions on the local drag reduction development; Polyox WSR-301, C_p = 1000 wppm, C.L. injection.

Figure 4.19 The development of the local % drag reduction results downstream from the injector at different values of the average polymer concentration, Polyox WSR-301 C_p = 1000, C.L. injection, $R_e = 2.8 \times 10^4$.

Figure 4.20 The asymptotic and the second-pass drag reduction results as a function of the average polymer concentration, Polyox WSR-301, $R_e = 2.8 \times 10^4$ in comparison with the homogeneous solution results of Goren & Norbury (1967).

Figure 4.21 Prandtl-Karman plot of $\frac{1}{\sqrt{f}}$ against $R_e\sqrt{f}$ for water flow and the flow with polymer injection at different values of average polymer concentrations; Polyox WSR-301, C_p = 1000 wppm, C.L. injection.

Figure 4.22 Friction factor f as a function of Reynolds number R_e for water flow at different values of C_{av}; Polyox WSR-301, C_p = 1000 wppm, C.L. injection.

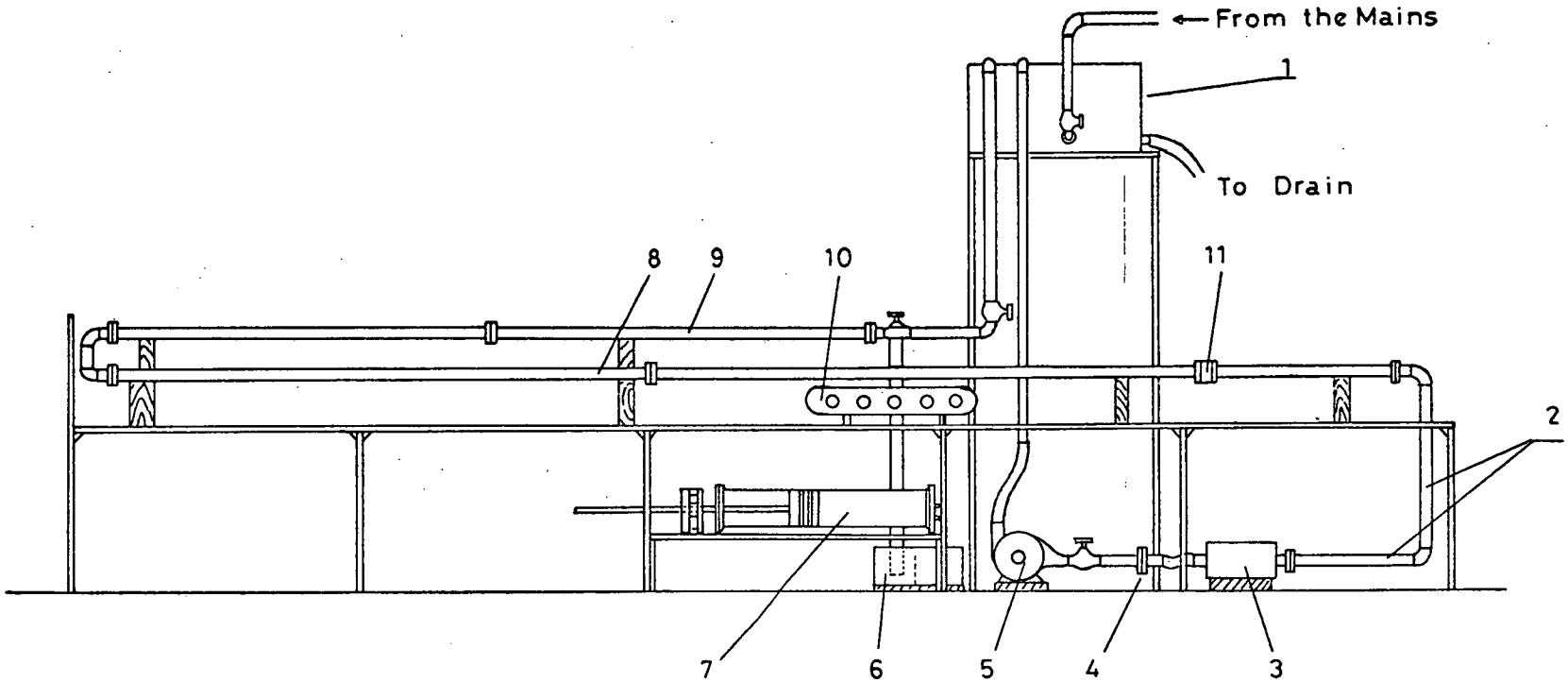

FIG. 2-1 EXPERIMENTAL SET-UP ELEVATION VIEW.

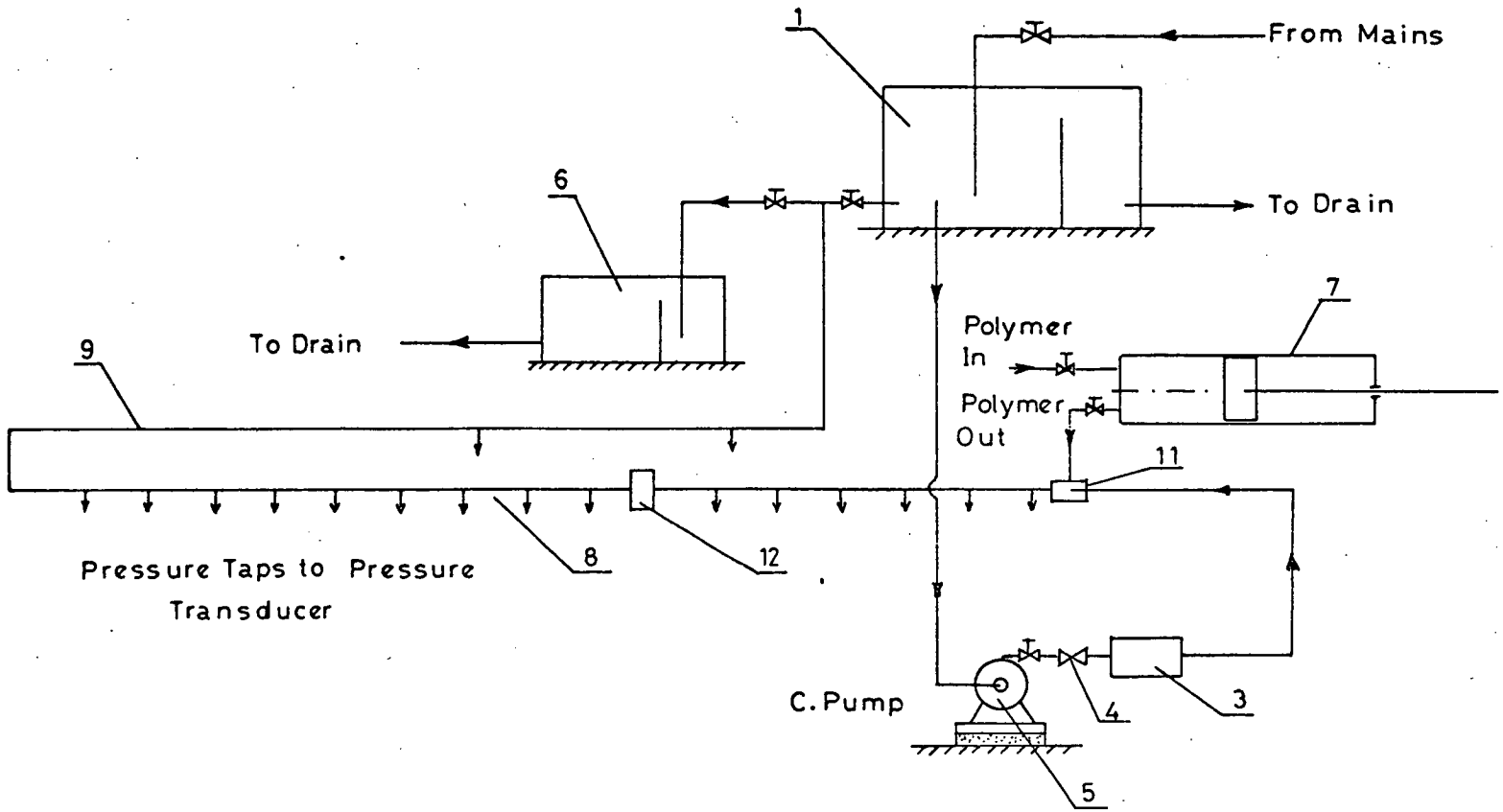

FIG(2.-2) FLOW DIAGRAM OF THE EXPERIMENTAL SET-UP.

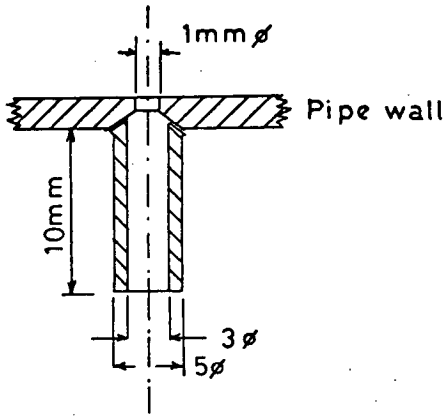

FIG (2-3 a)

SECTIONAL VIEW OF PRESSURE TAP.

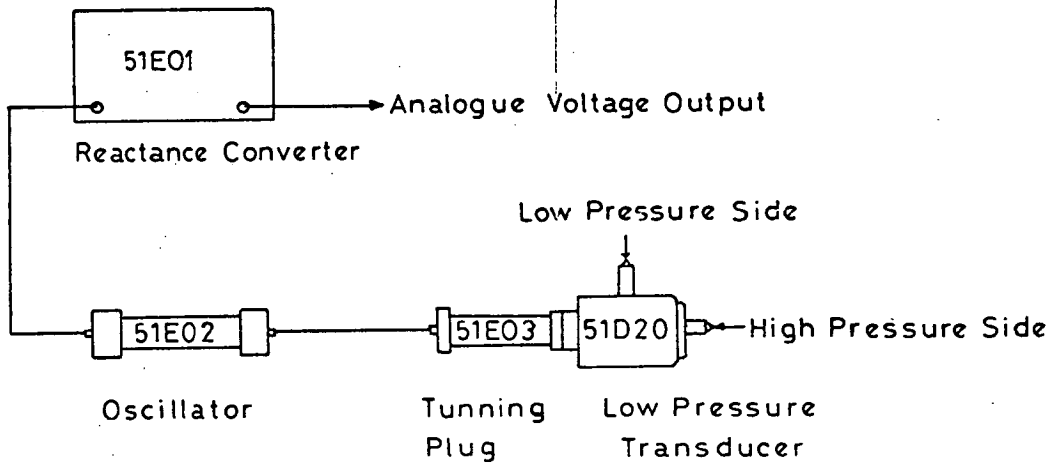

FIG (2 – 3 b)

DISA PRESSURE TRANSDUCER SET-UP.

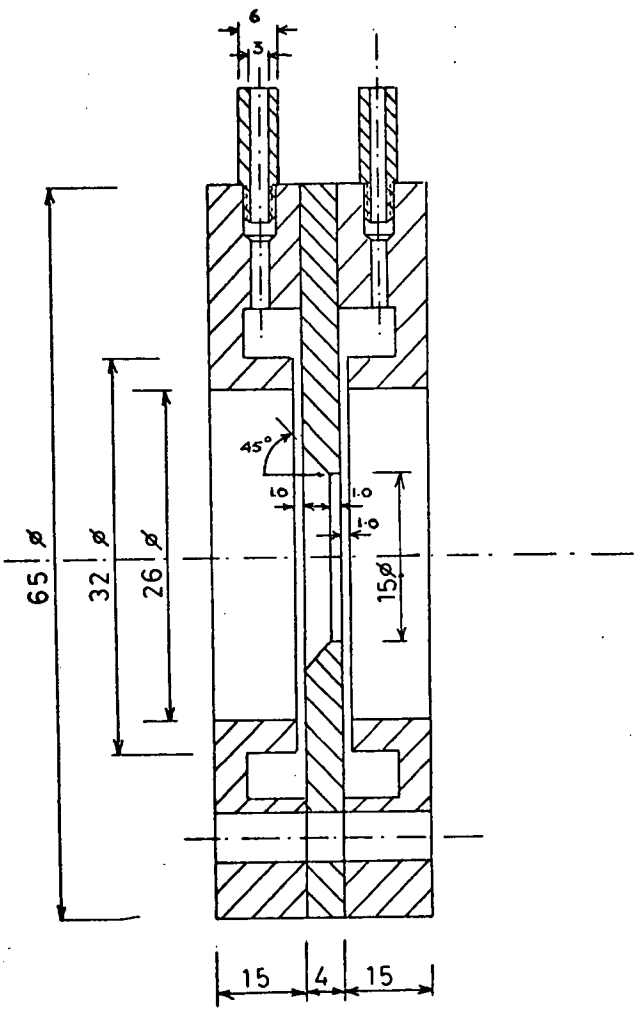

FIG (2–4) THE ORIFICE METER

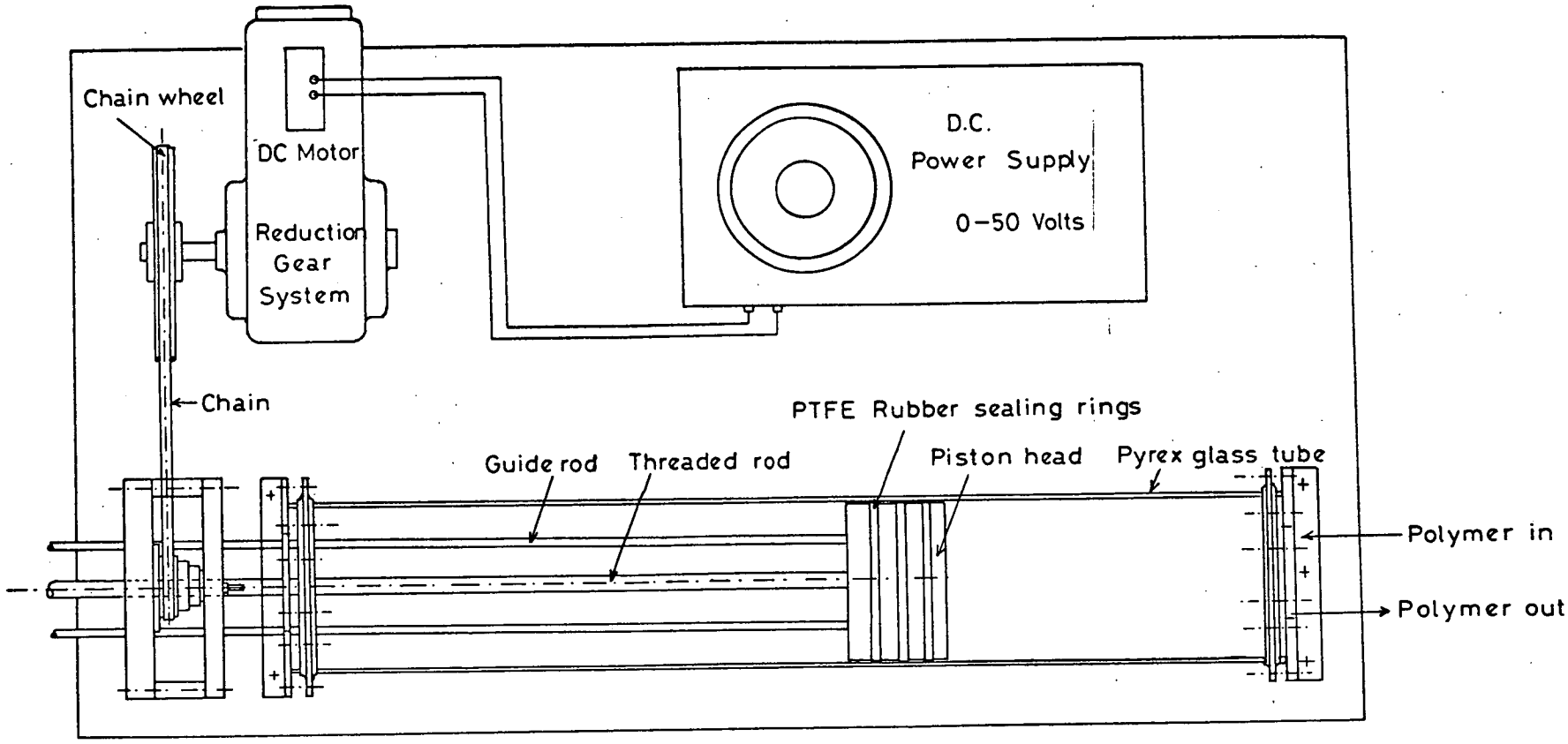

FIG (2-5) PLAN VIEW OF THE INJECTION PUMP AND DRIVING SYSTEM

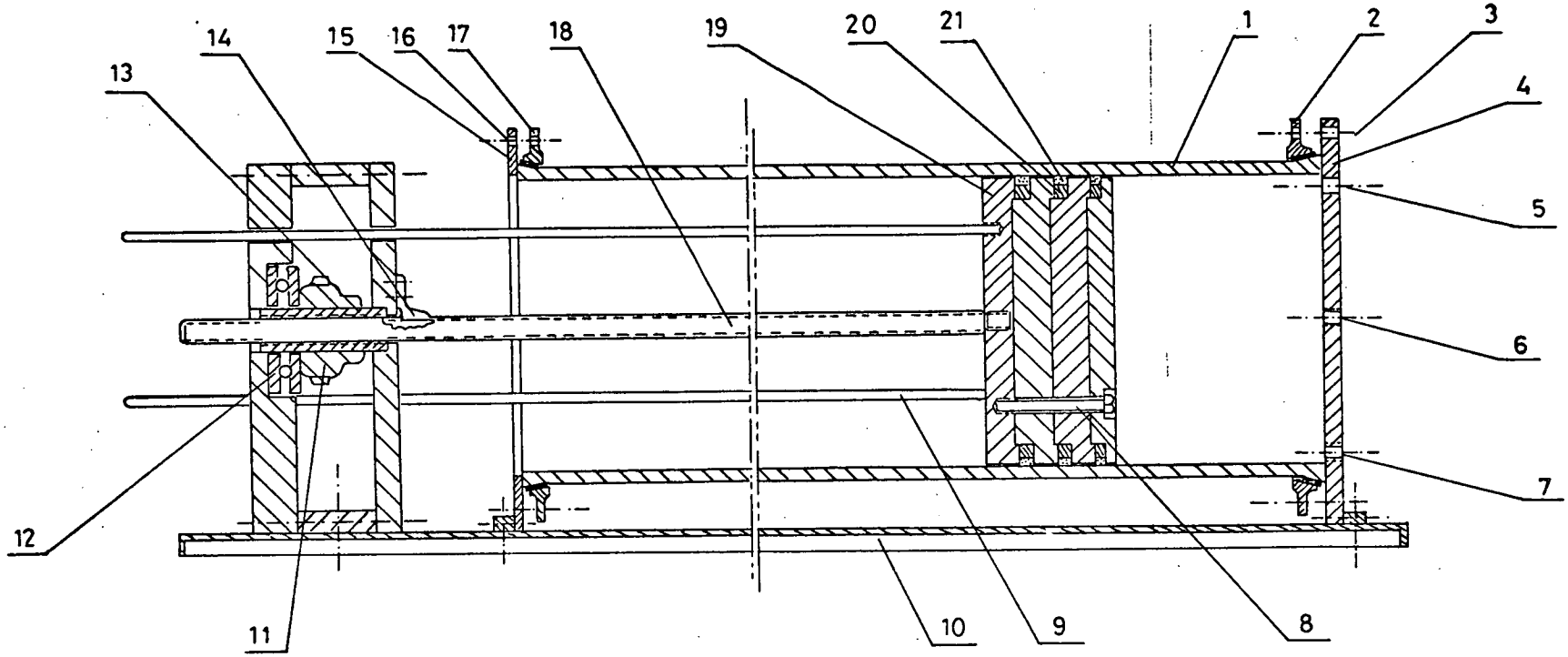

FIG (2 - 6) POLYMER INJECTION PUMP

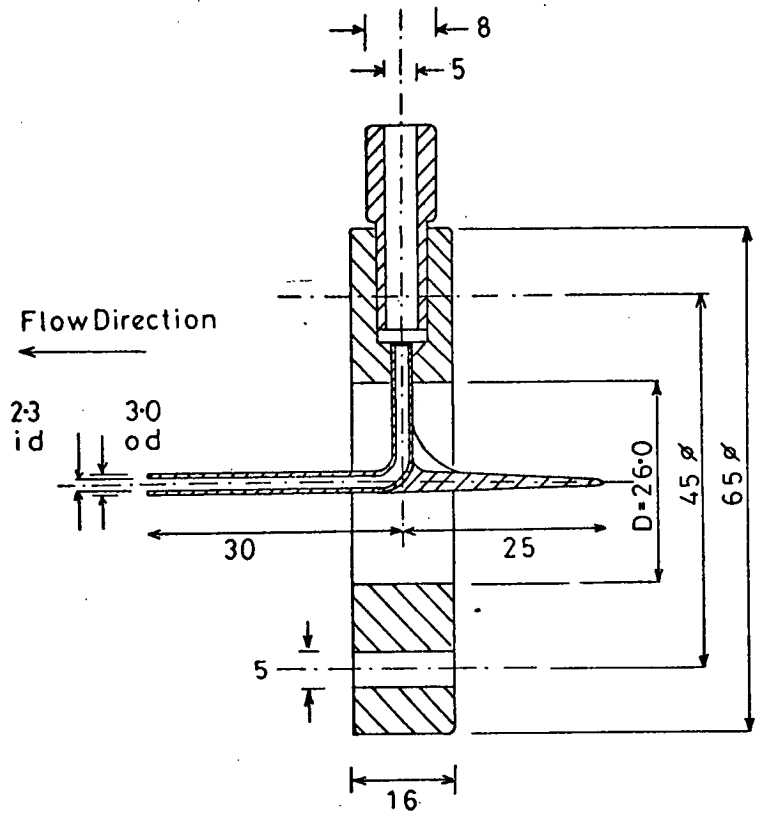

FIG 2-7 CENTRE LINE INJECTOR.

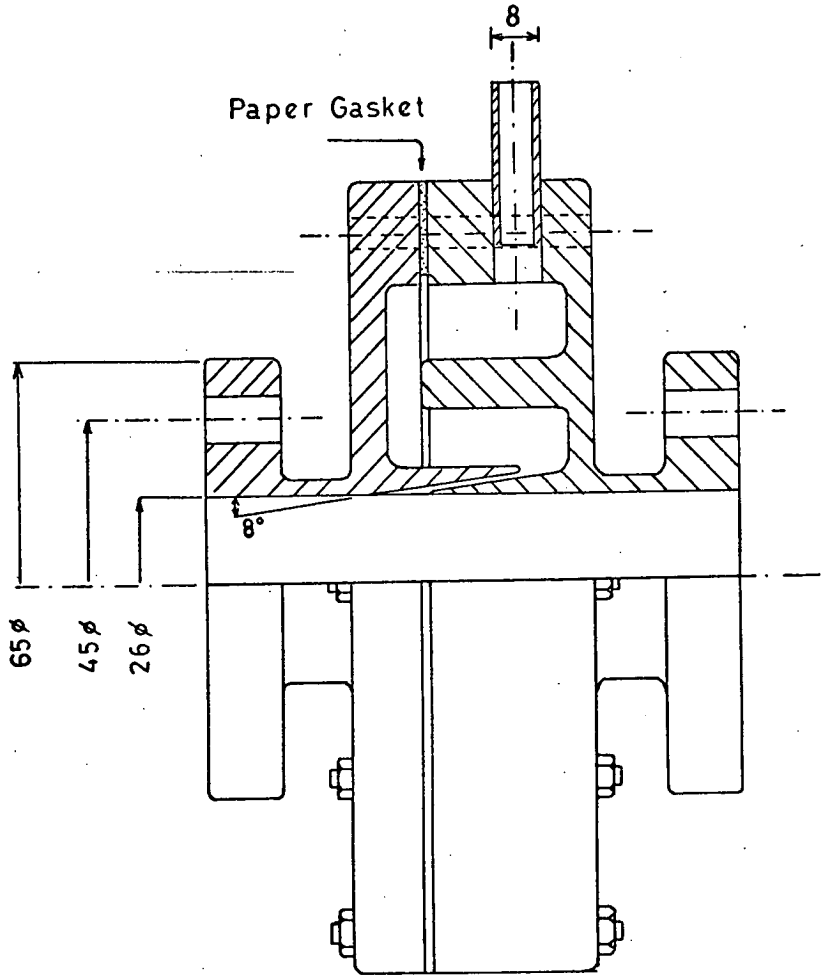

FIG. (2-8) THE WALL INJECTOR.

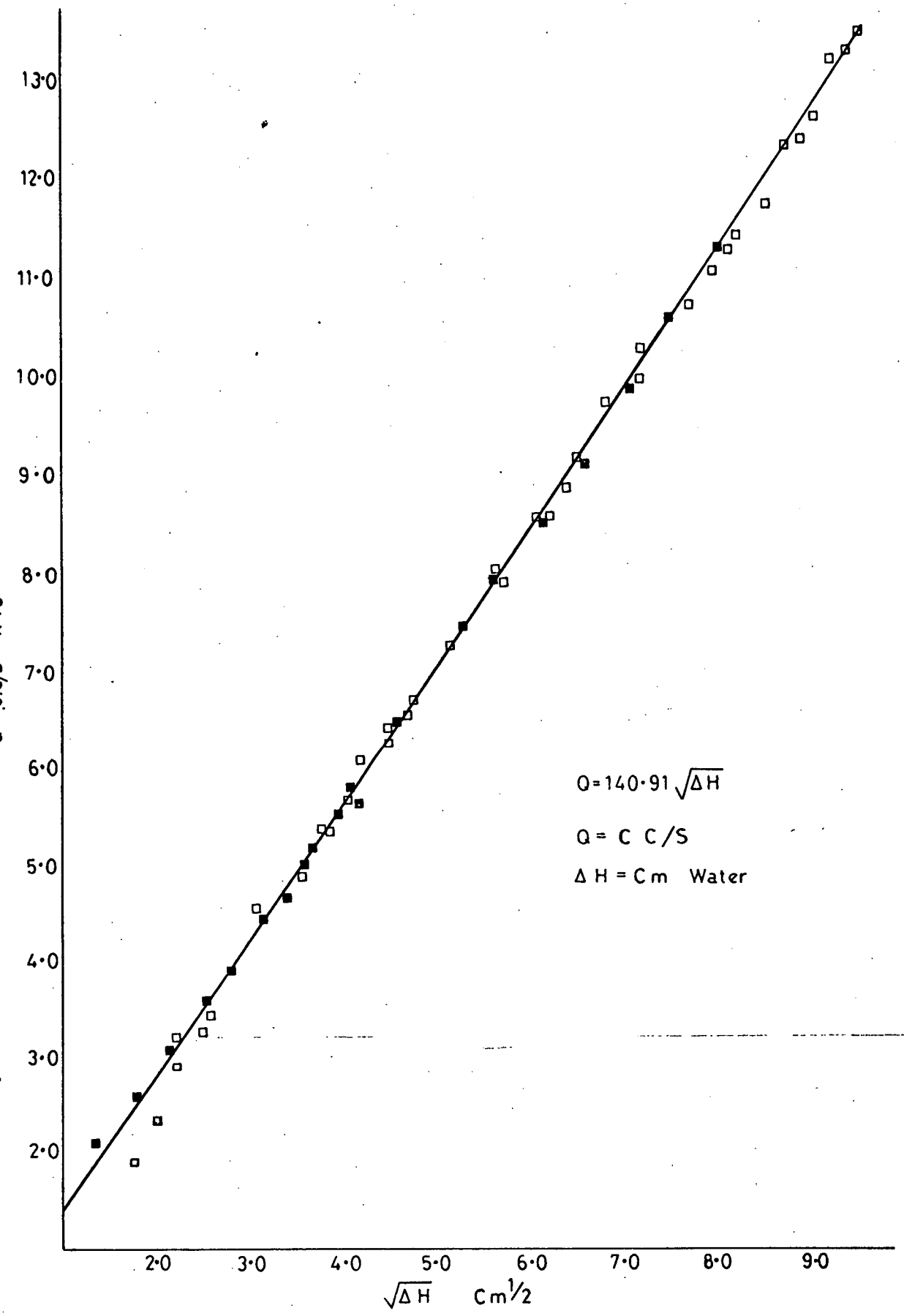

FIG(2·9) Calibration of the Orifice Meter

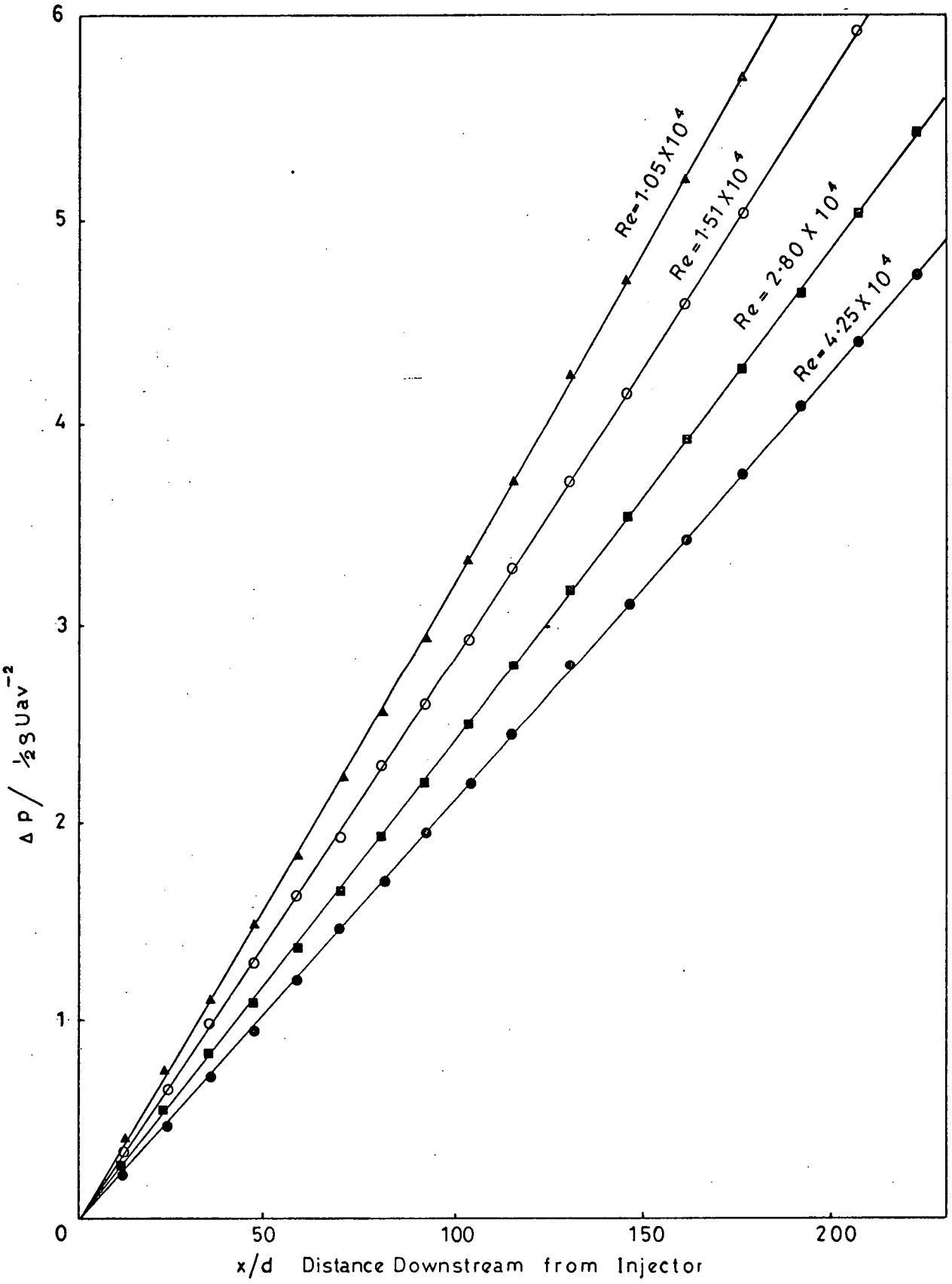

FIG (2 - 10) Mean Flow Development Tests

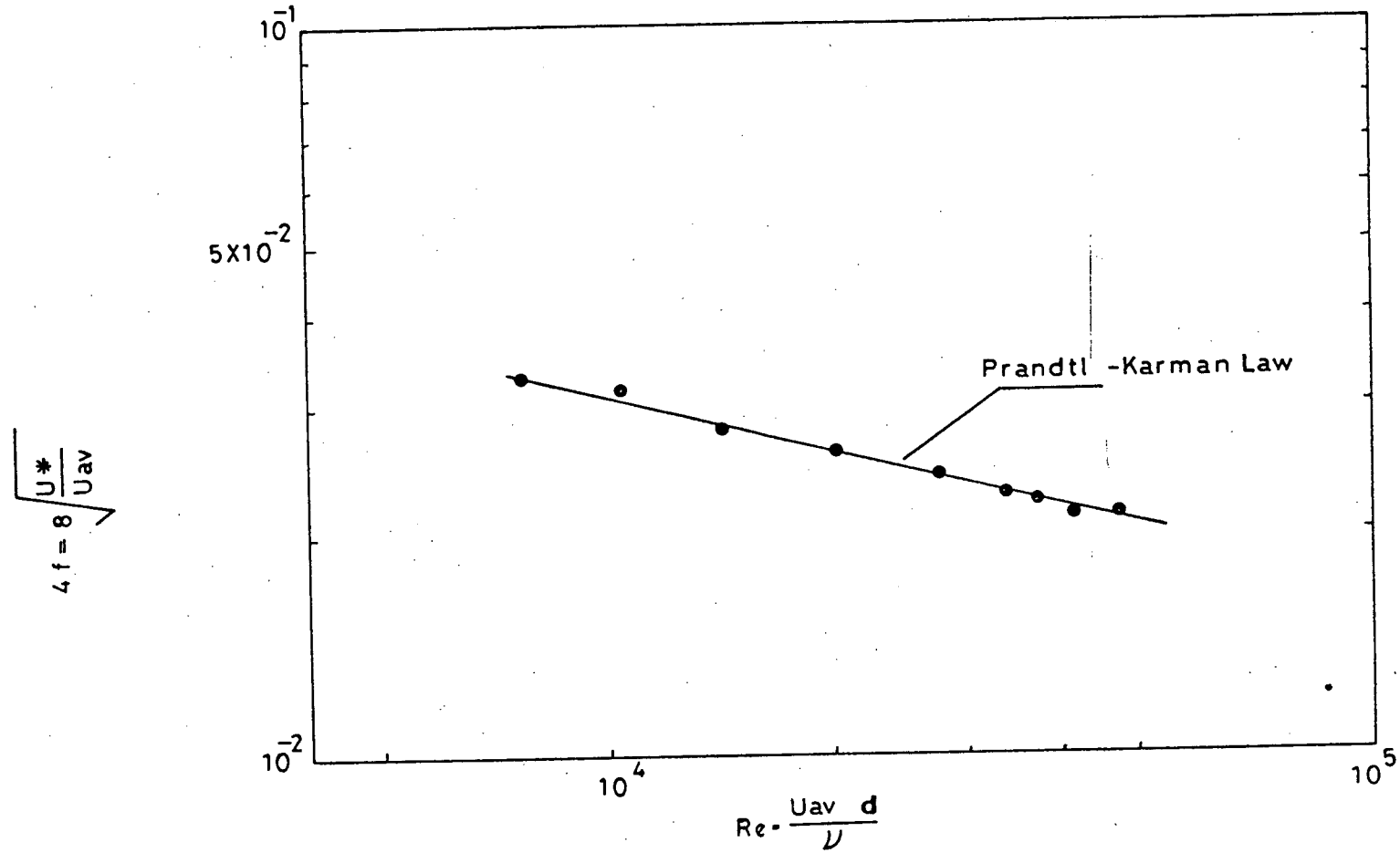

FIG (2 - 11)

The Friction Factor Reynolds Number for Newtonian Flows

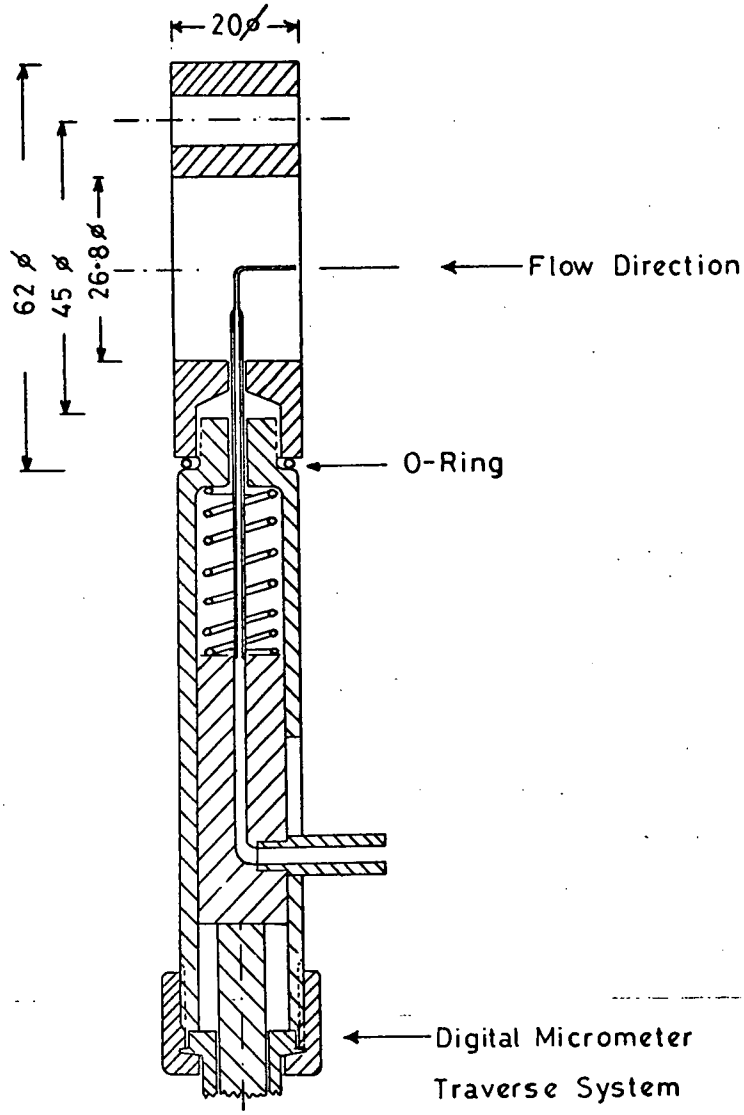

FIG (3 . 1)

THE SAMPLING SYSTEM

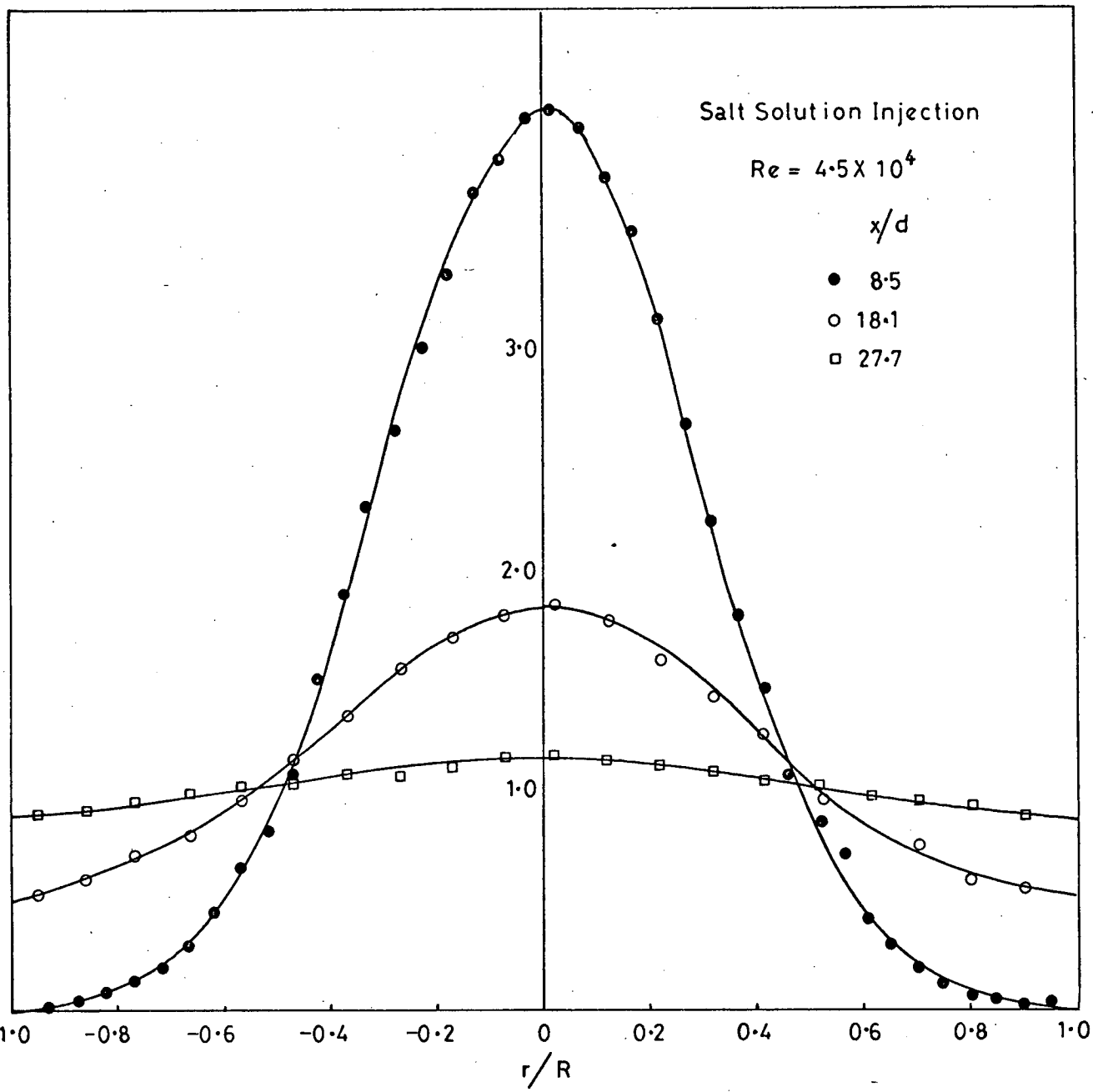
Salt Solution Injection
Re = 4·5 X 10⁴
x/d
8·5
18·1
27·7
3·0
2·0
1·0
-1·0
-0·8
-0·6
-0·4
-0·2
0
0·2
0·4
0·6
0·8
1·0
r/R

FIG (3-2)

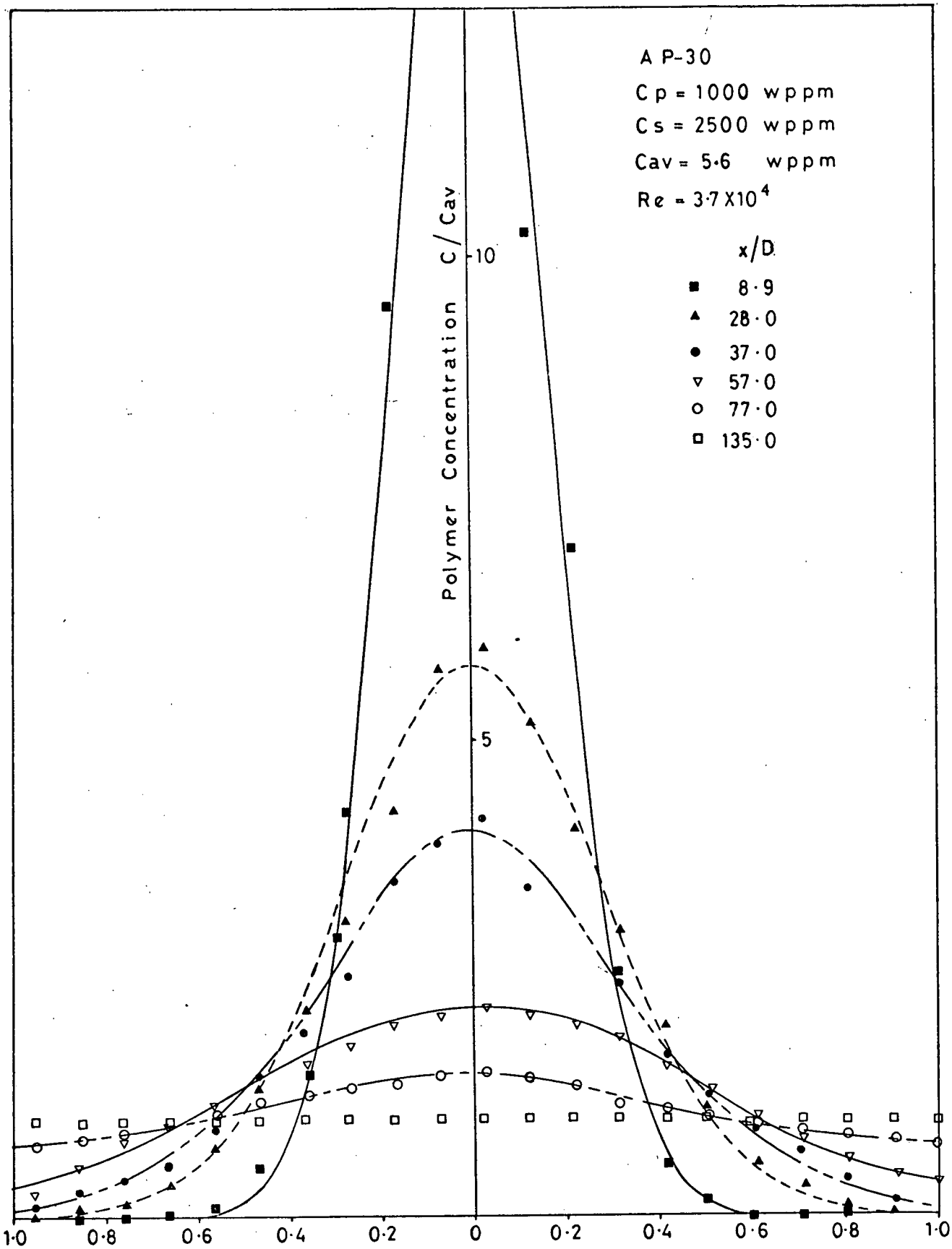

Polymer Concentration Profiles at Different "x/d" from Injector

FIG (3 - 3)

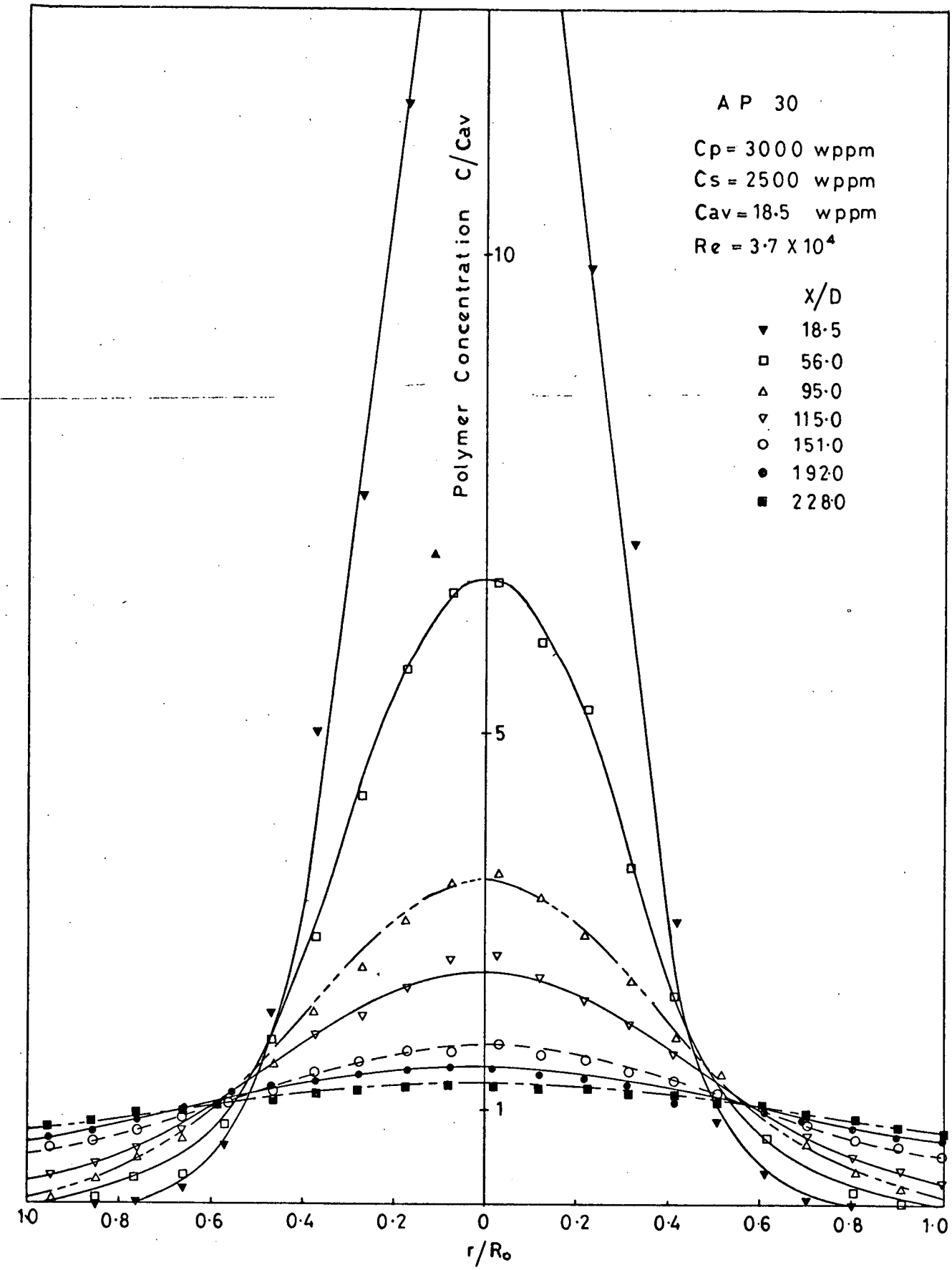

Polymer Concentration Profile Curves at Different x/d from Injector

FIG (3-4)

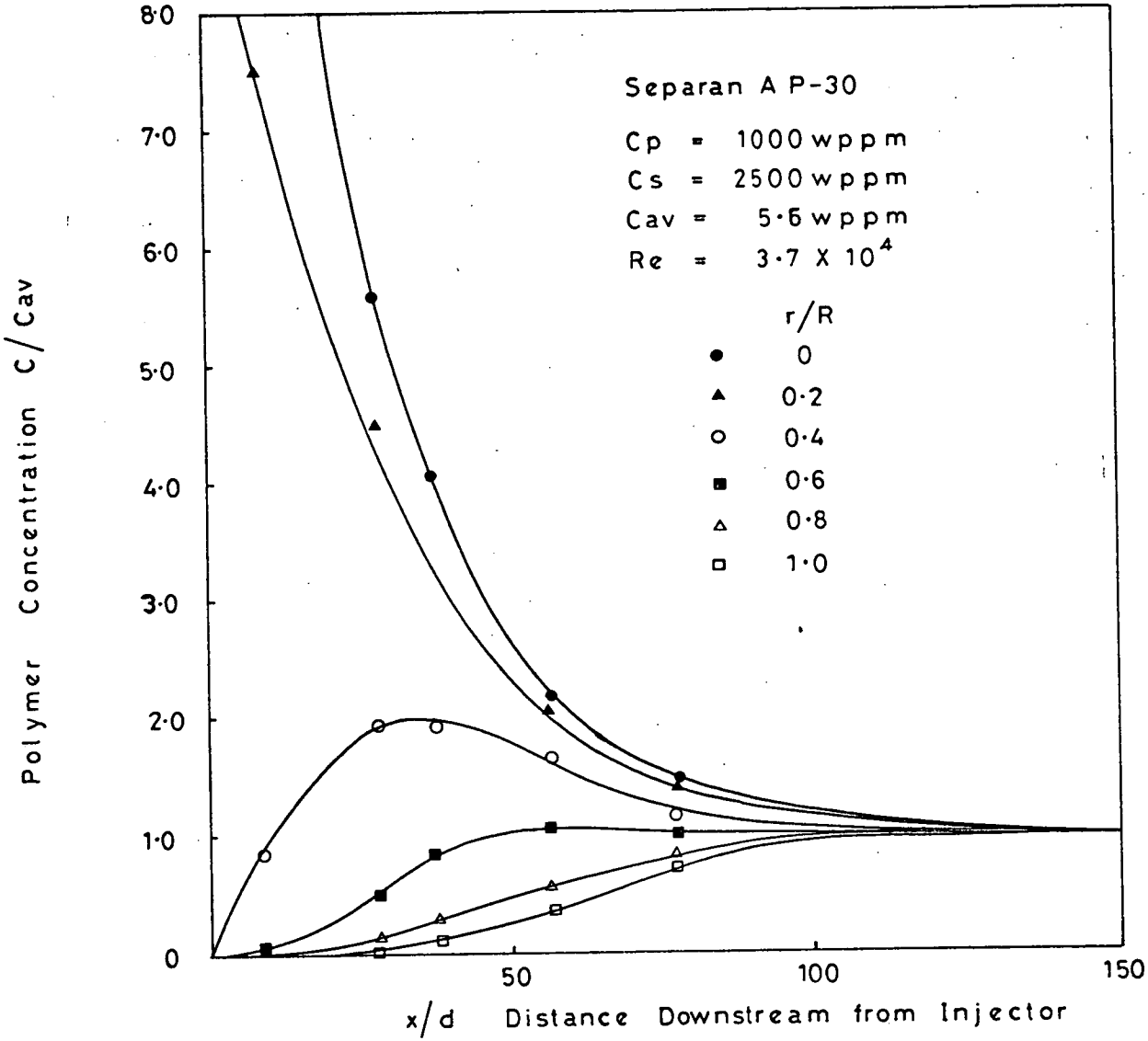
Separan A P-30
Cp = 1000 wppm
Cs = 2500 wppm
Cav = 5·6 wppm
Re = 3·7 X 10⁴
r/R
0
0·2
0·4
0·6
0·8
1·0
Polymer Concentration C/Cav
8·0
7·0
6·0
5·0
4·0
3·0
2·0
1·0
0
50
100
150
x/d Distance Downstream from Injector

FIG (3-5)

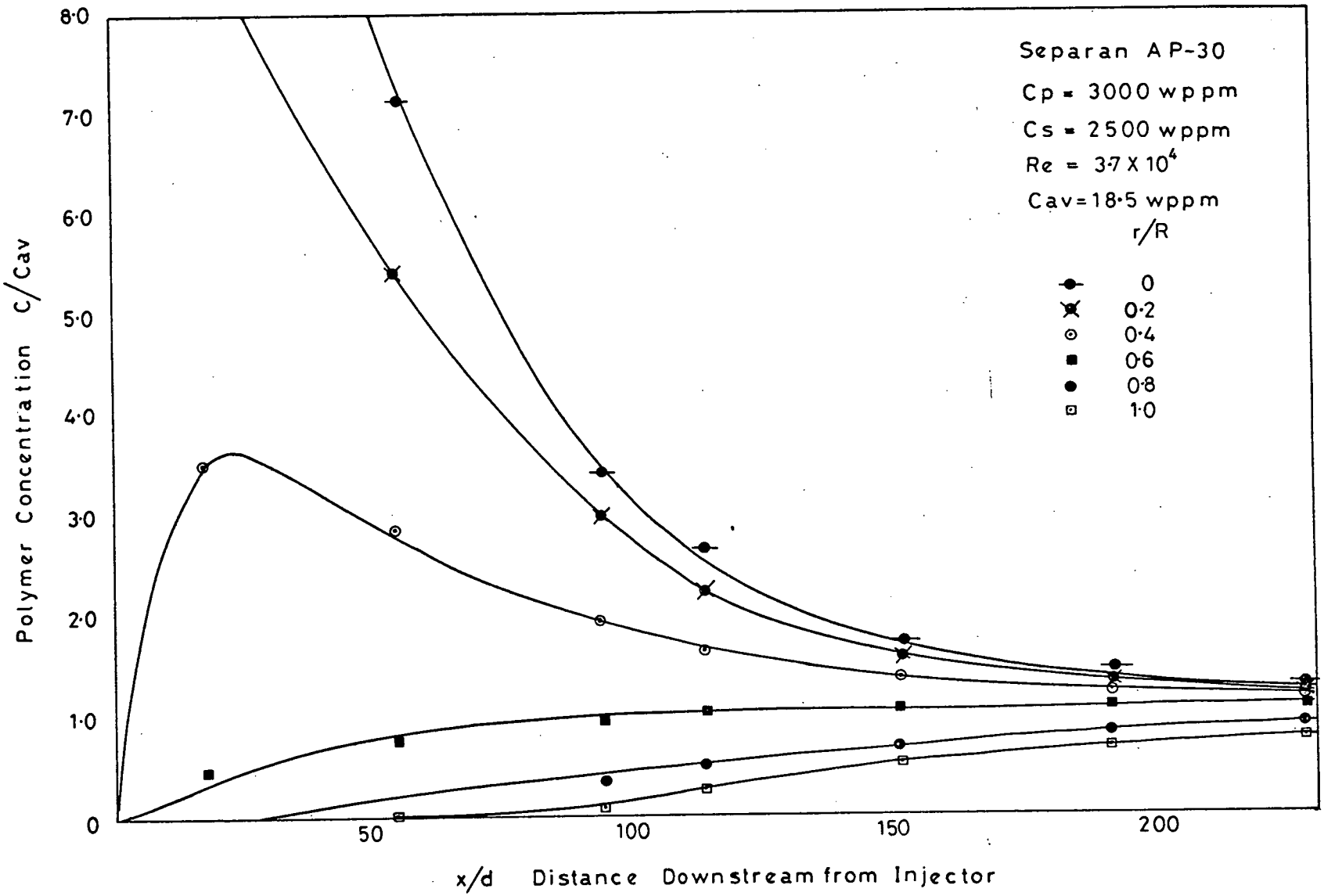
Separan AP-30
Cp = 3000 wppm
Cs = 2500 wppm
Re = 3·7 X 10⁴
Cav=18·5 wppm
r/R
0
0·2
0·4
0·6
0·8
1·0
Polymer Concentration C/Cav
8·0
7·0
6·0
5·0
4·0
3·0
2·0
1·0
0
50
100
150
200
x/d Distance Downstream from Injector

FIG (3-6)

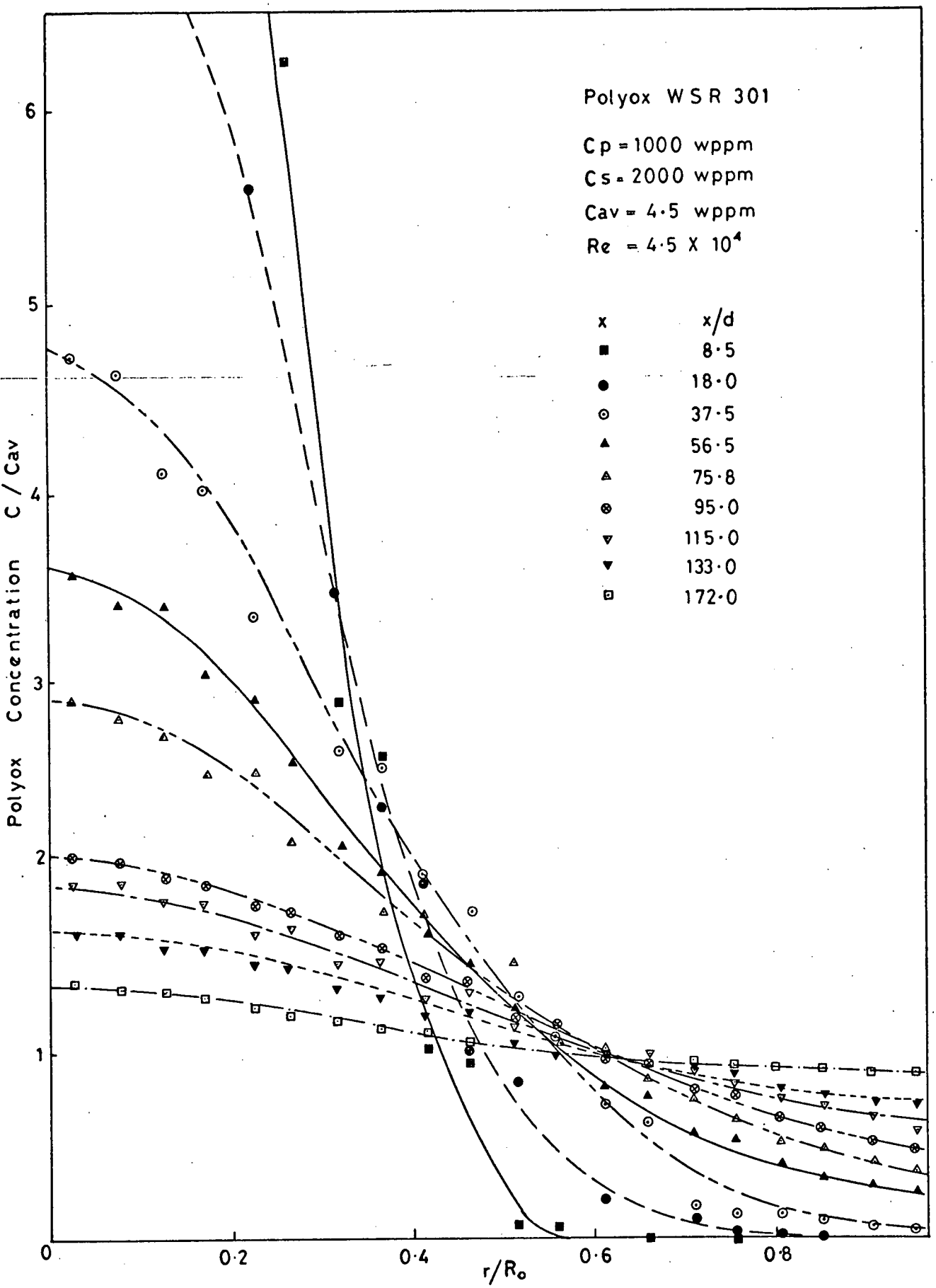
Polyox WSR 301
Cp = 1000 wppm
Cs = 2000 wppm
Cav = 4·5 wppm
Re = 4·5 X 10⁴
x x/d
8·5
18·0
37·5
56·5
75·8
95·0
115·0
133·0
172·0
Polyox Concentration C / Cav
r/Ro
0
0·2
0·4
0·6
0·8
1
2
3
4
5
6

FIG (3 – 7)

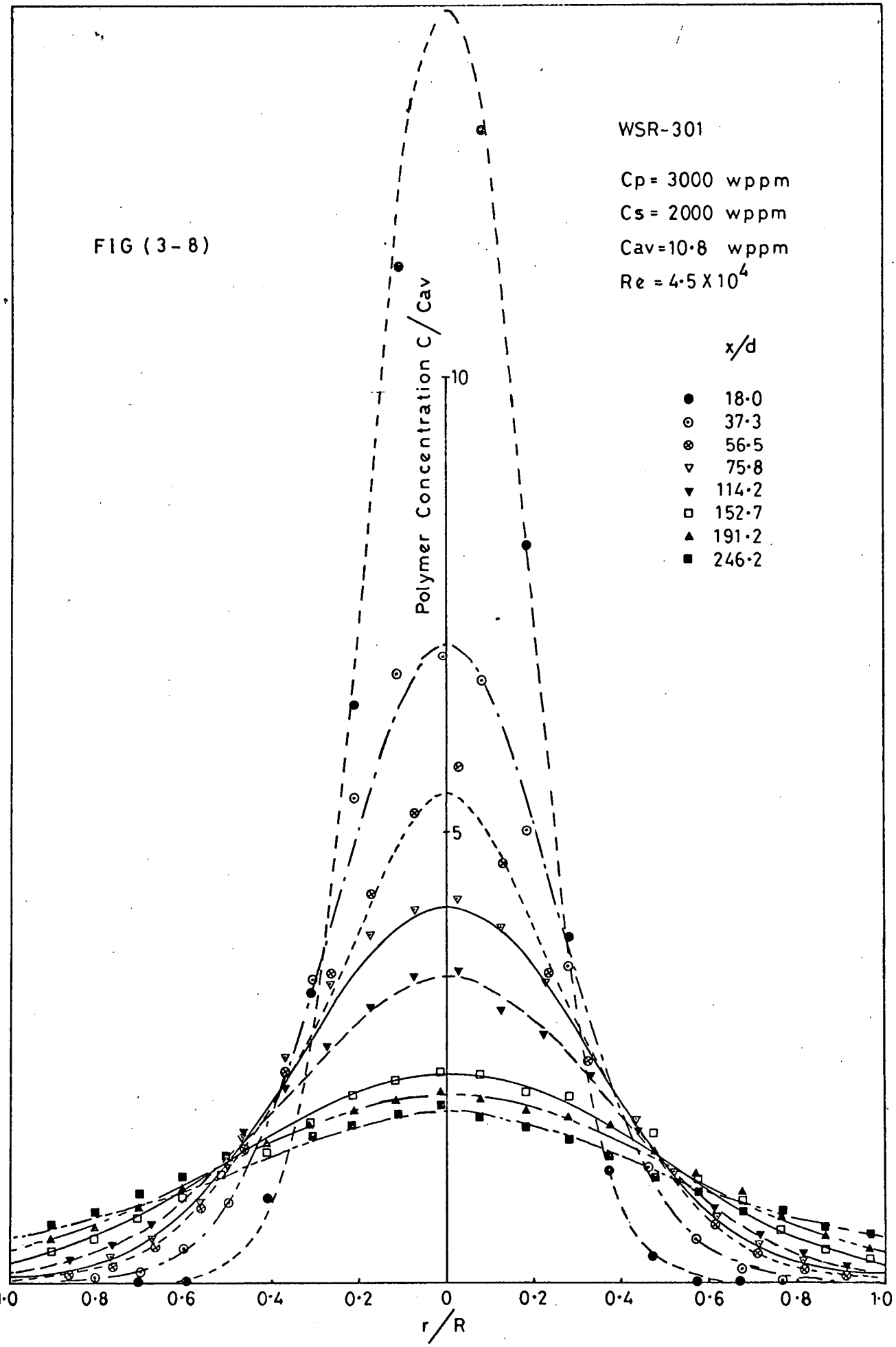
FIG (3-8)
WSR-301
Cp = 3000 wppm
Cs = 2000 wppm
Cav=10·8 wppm
Re = 4·5 X 10^4
x/d
18·0
37·3
56·5
75·8
114·2
152·7
191·2
246·2
Polymer Concentration C/Cav
10
5
1·0
0·8
0·6
0·4
0·2
0
0·2
0·4
0·6
0·8
1·0
r/R

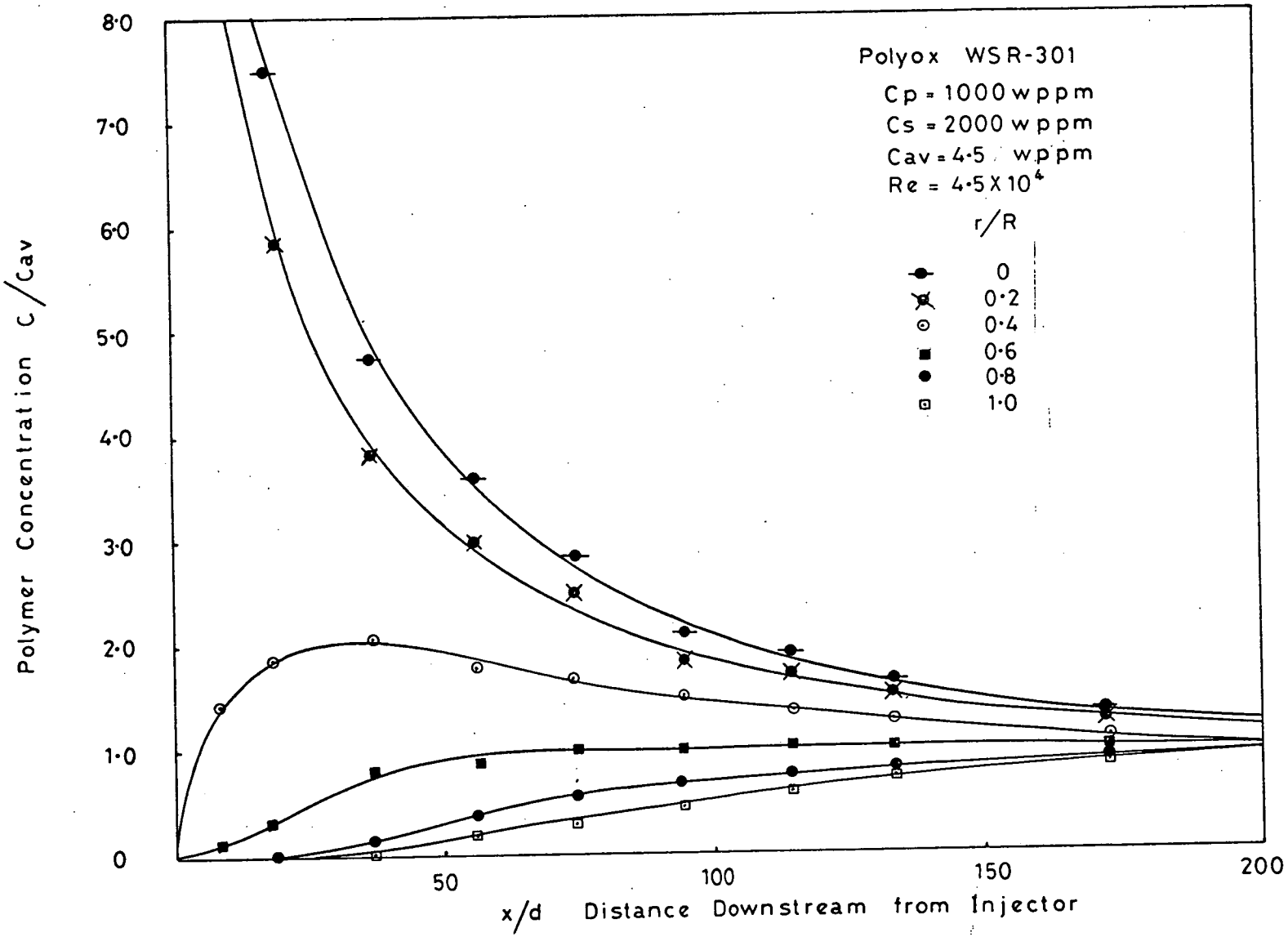
Polyox WSR-301
Cp = 1000 wppm
Cs = 2000 wppm
Cav = 4·5 wppm
Re = 4·5 X 10⁴
r/R
0
0·2
0·4
0·6
0·8
1·0
Polymer Concentration C/Cav
8·0
7·0
6·0
5·0
4·0
3·0
2·0
1·0
0
50
100
150
200
x/d Distance Downstream from Injector

FIG. (3-9)

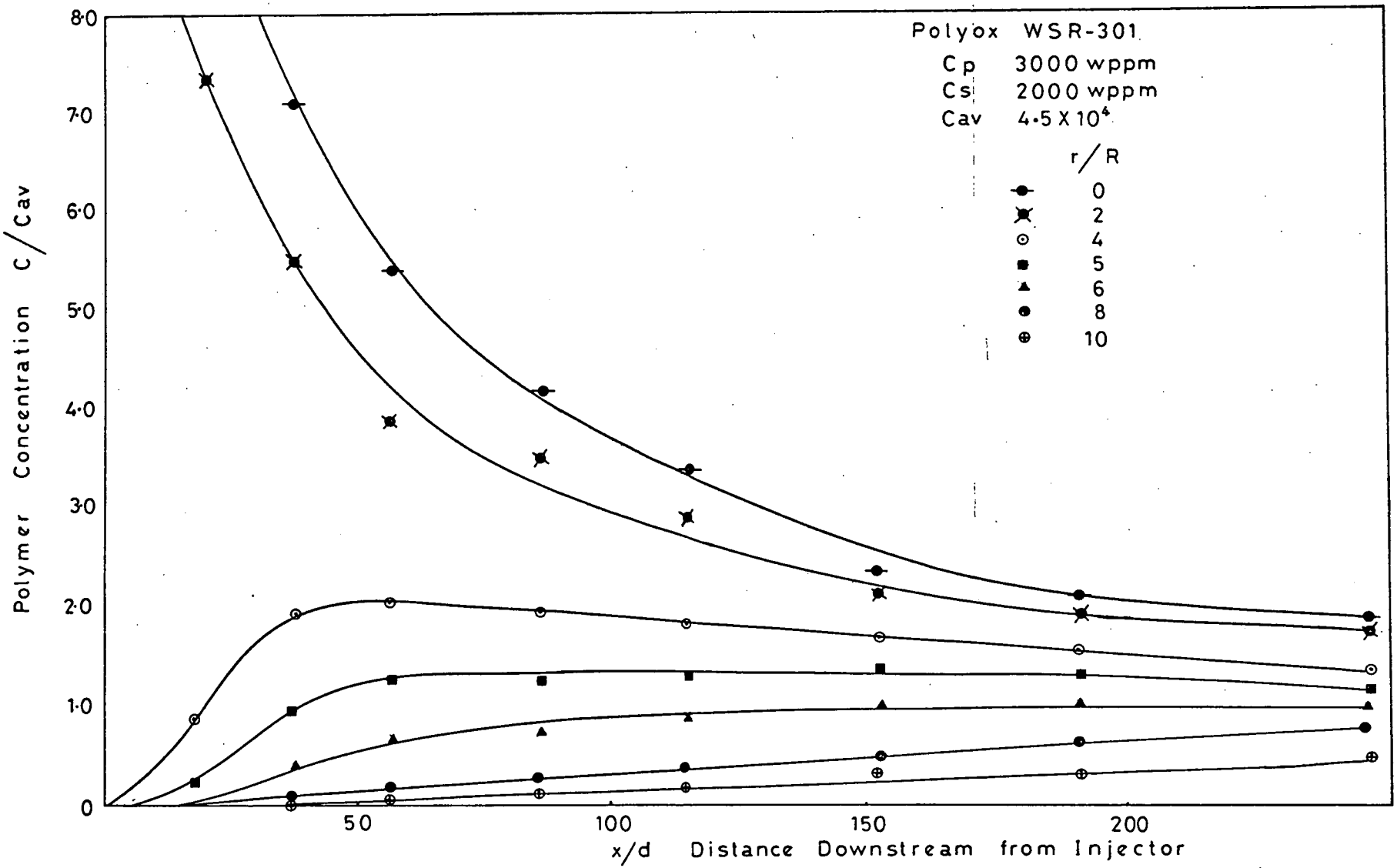
Polyox WSR-301
Cp 3000 wppm
Cs 2000 wppm
Cav 4·5 X 10⁴
r/R
0
2
4
5
6
8
10
Polymer Concentration C/Cav
8·0
7·0
6·0
5·0
4·0
3·0
2·0
1·0
0
50
100
150
200
x/d Distance Downstream from Injector

FIG. (3 - 10)

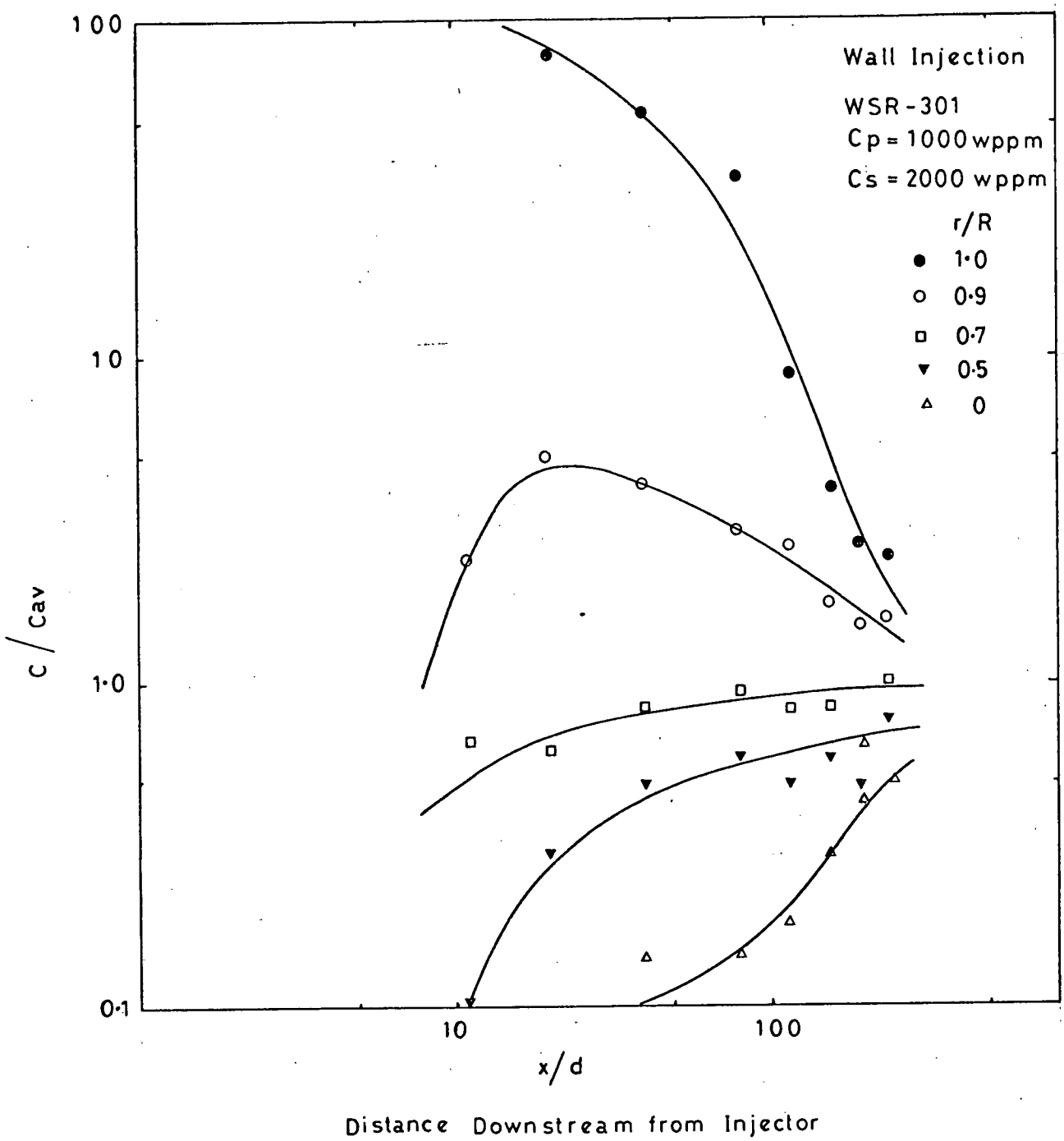
100
10
1·0
0·1
C / Cav
10
100
x/d
Wall Injection
WSR-301
Cp = 1000 wppm
Cs = 2000 wppm
r/R
1·0
0·9
0·7
0·5
0
Distance Downstream from Injector

FIG (3 – 11)

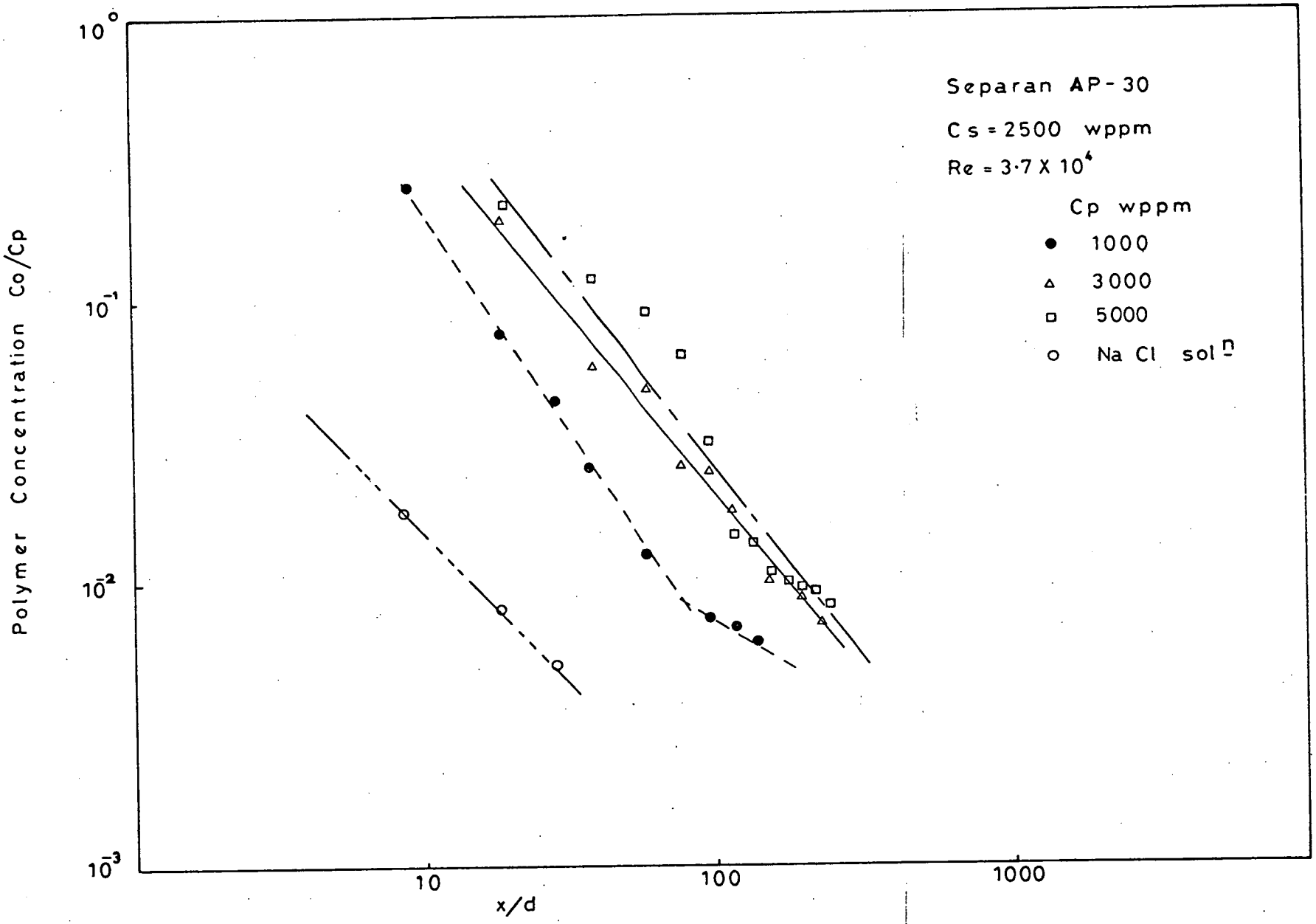
Separan AP-30
Cs = 2500 wppm
Re = 3·7 X 10⁴
Cp wppm
1000
3000
5000
Na Cl soln
Polymer Concentration Co/Cp
10°
10⁻¹
10⁻²
10⁻³
10
100
1000
x/d

FIG (3 - 12)

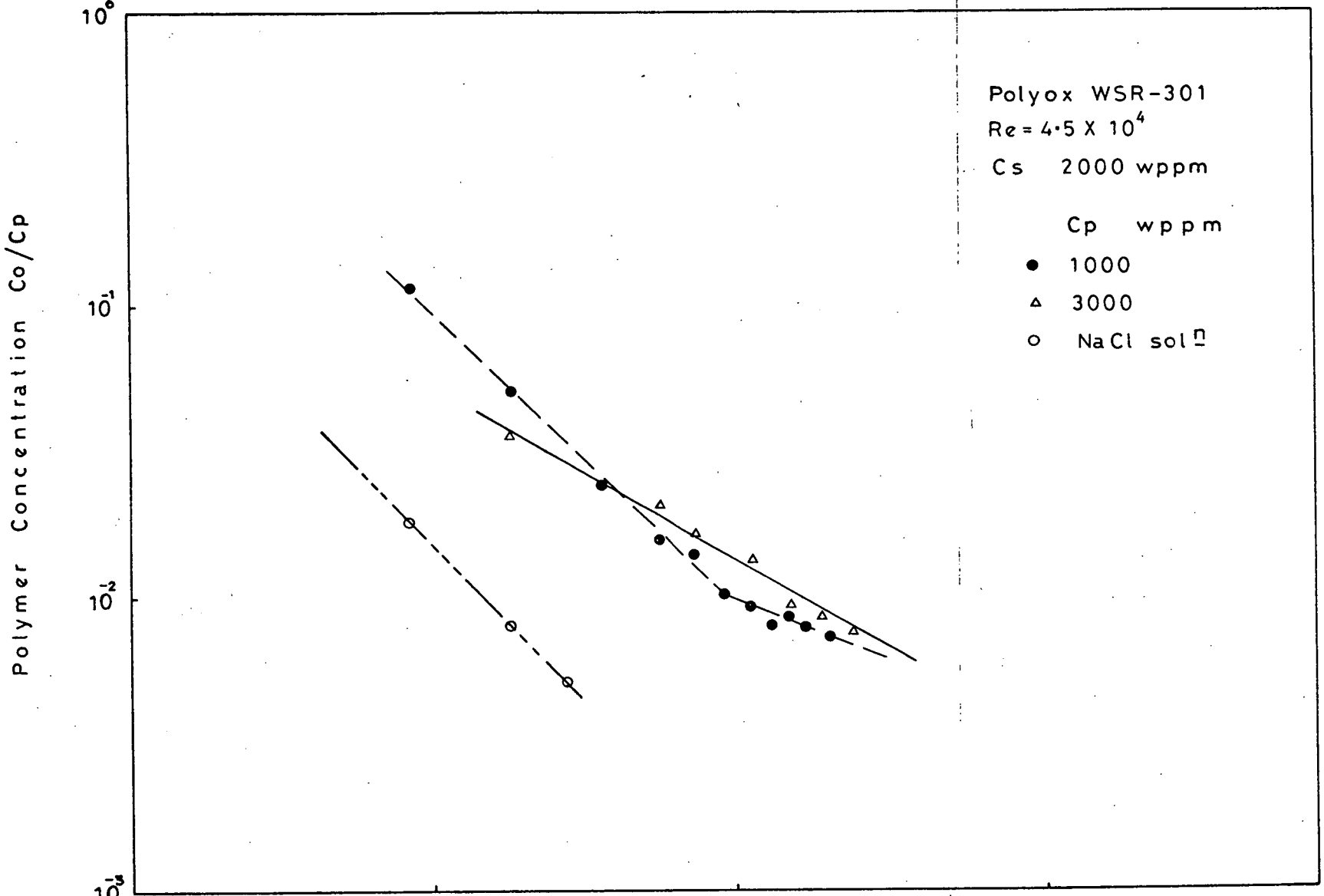
Polyox WSR-301
Re = 4·5 X 10^4
Cs 2000 wppm
Cp wppm
1000
3000
NaCl soln
Polymer Concentration Co/Cp
10^0
10^-1
10^-2
10^-3
10
100
1000
x/d

FIG (3 — 13)

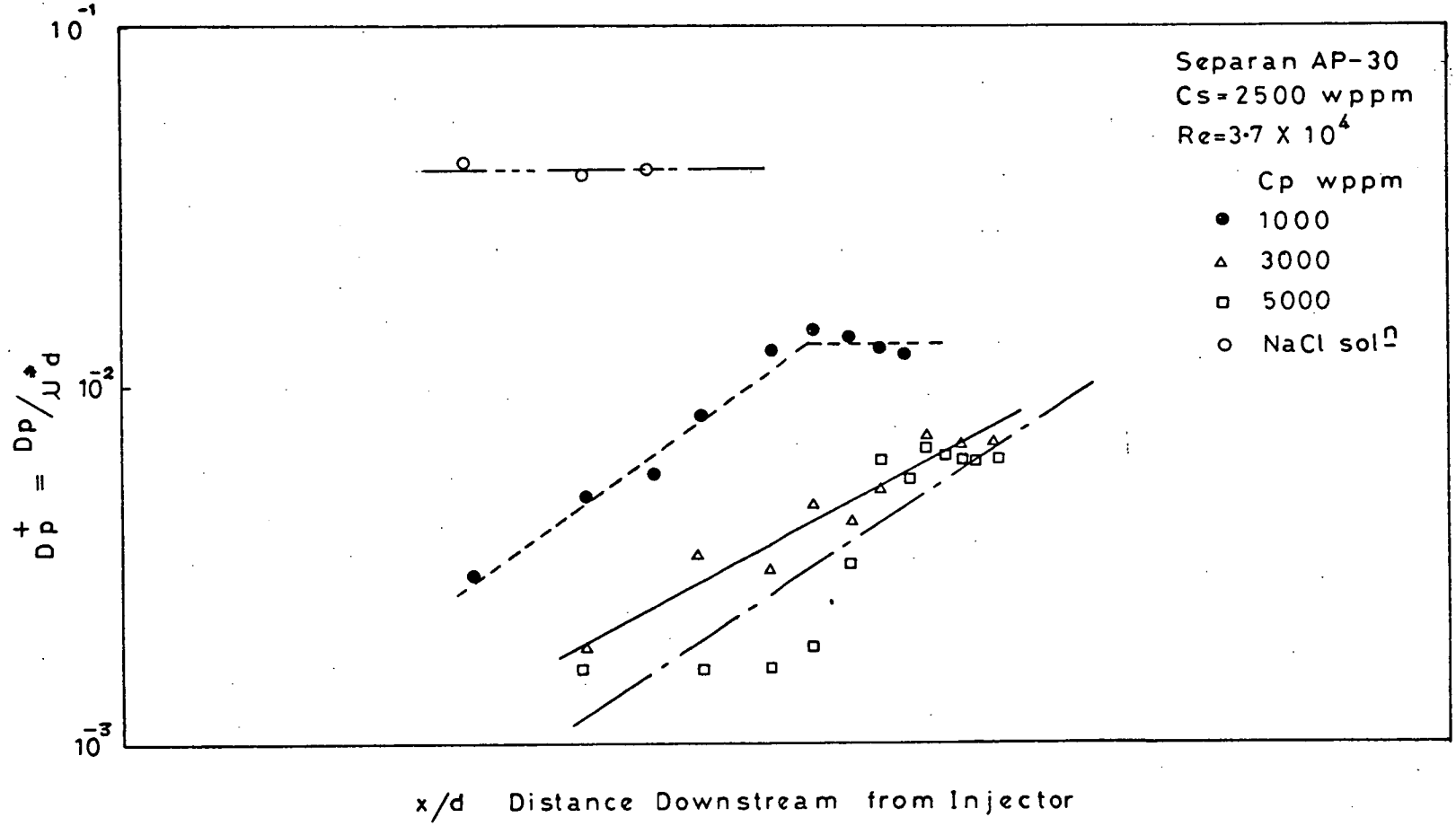
Separan AP-30
Cs = 2500 wppm
Re = 3·7 X 10^4
Cp wppm
1000
3000
5000
NaCl soln
10^-1
10^-2
10^-3
D+p ≡ Dp / ρ u* d
x/d Distance Downstream from Injector

FIG (3 – 14)

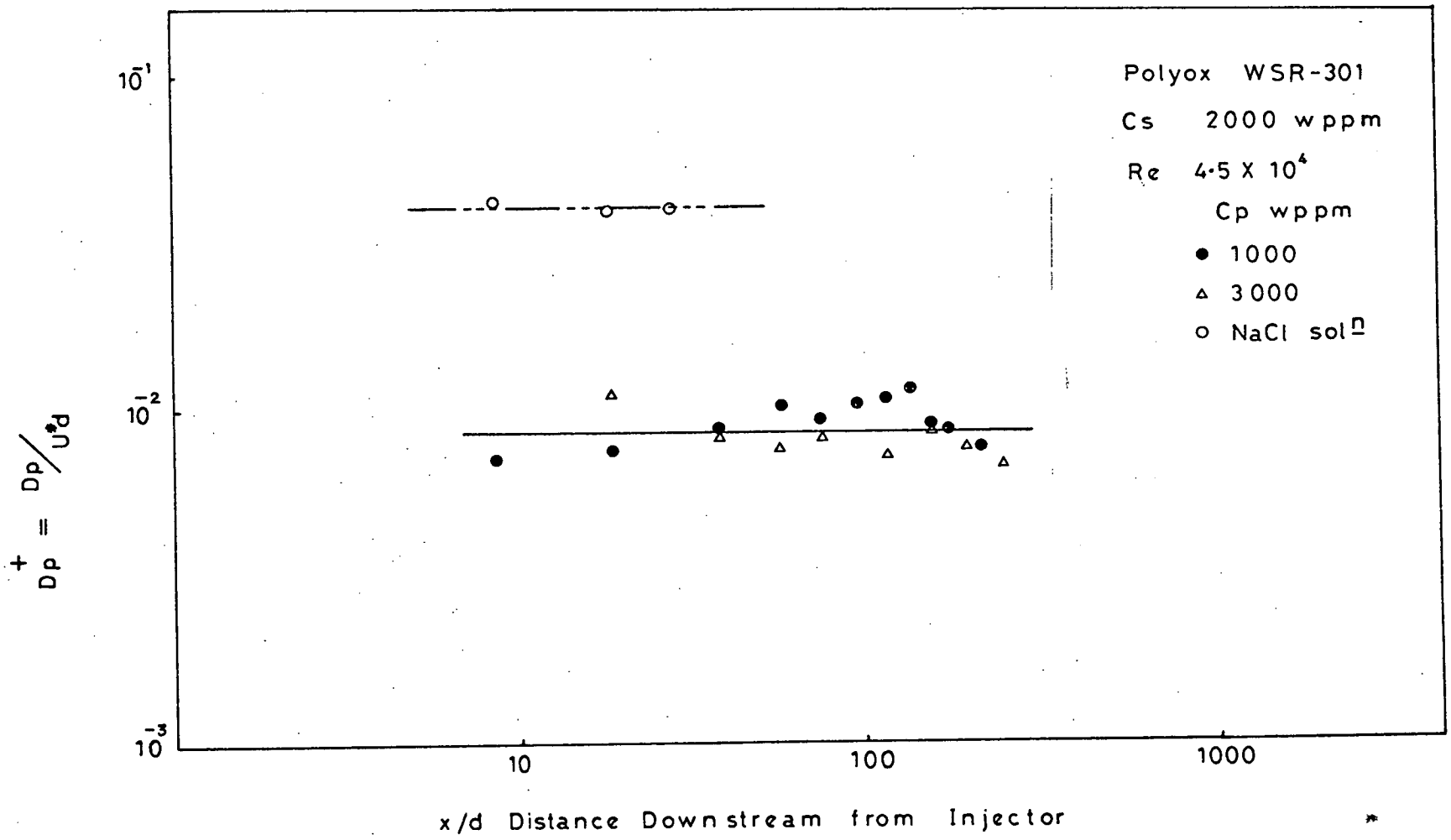
Polyox WSR-301
Cs 2000 wppm
Re 4·5 X 10⁴
Cp wppm
● 1000
△ 3000
○ NaCl solⁿ
10⁻¹
10⁻²
10⁻³
10
100
1000
D⁺p = Dp/U*d
x/d Distance Downstream from Injector

FIG (3 – 15)

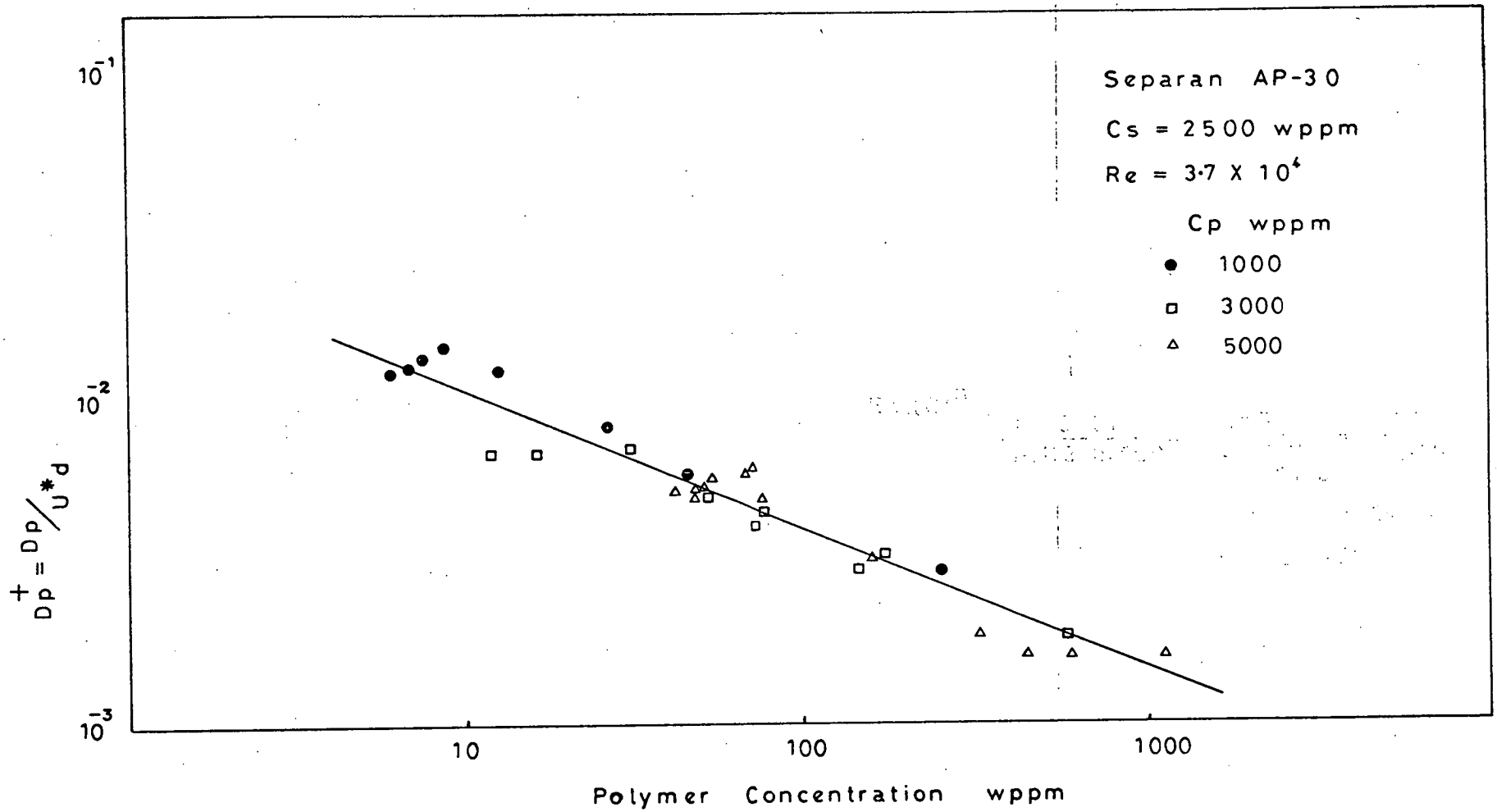
Separan AP-30
Cs = 2500 wppm
Re = 3·7 X 10⁴
Cp wppm
1000
3000
5000
10⁻¹
10⁻²
10⁻³
D⁺p = Dp/U*d
10
100
1000
Polymer Concentration wppm

FIG (3–16)

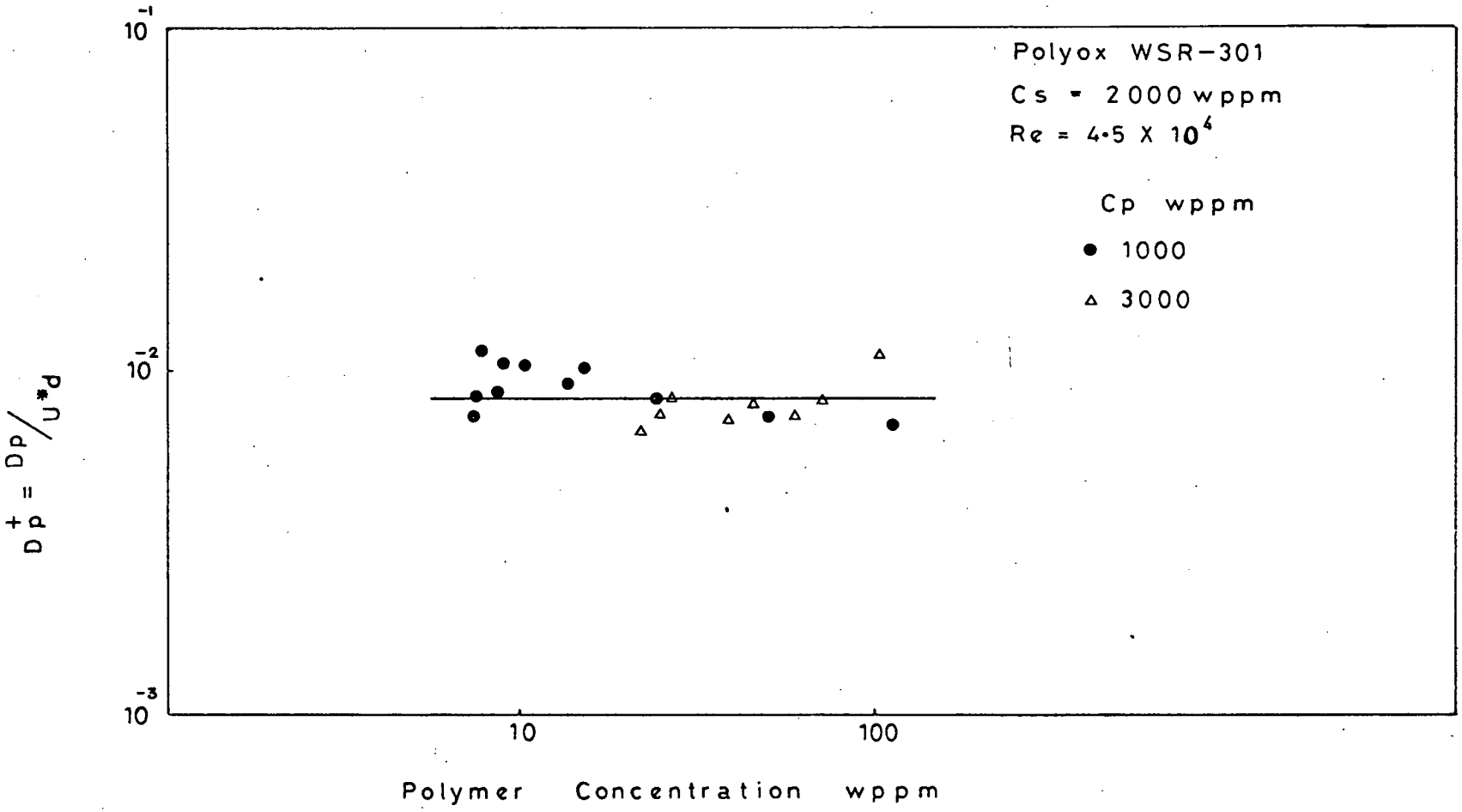
Polyox WSR-301
Cs = 2000 wppm
Re = 4·5 X 10⁴
Cp wppm
● 1000
△ 3000
10⁻¹
10⁻²
10⁻³
D+ = Dp / U*d
10
100
Polymer Concentration wppm

FIG (3 - 17)

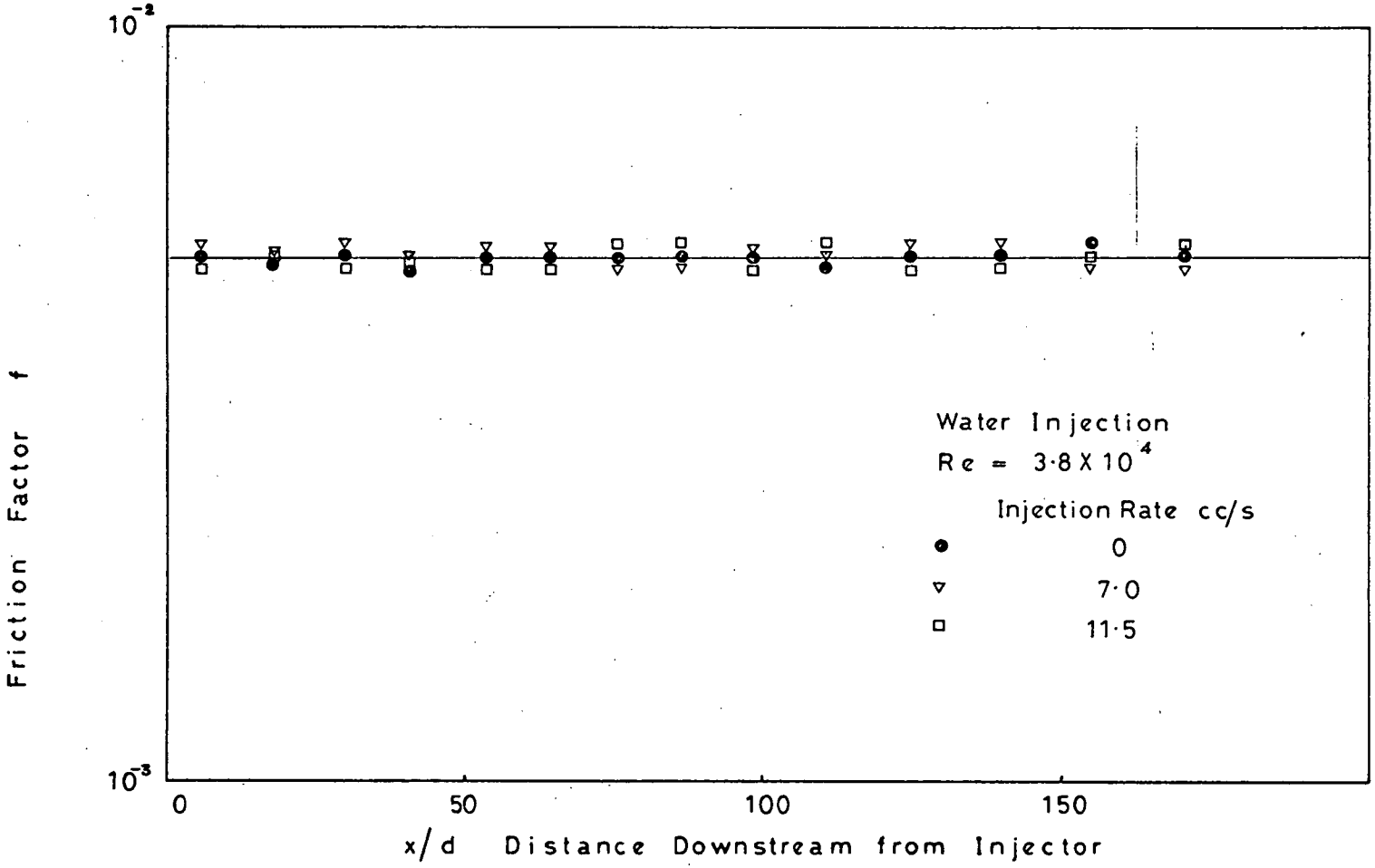
10^{-2}
10^{-3}
Friction Factor f
0
50
100
150
x/d Distance Downstream from Injector
Water Injection
Re = $3{\cdot}8 \times 10^{4}$
Injection Rate cc/s
0
7·0
11·5

FIG. (4 – 1)

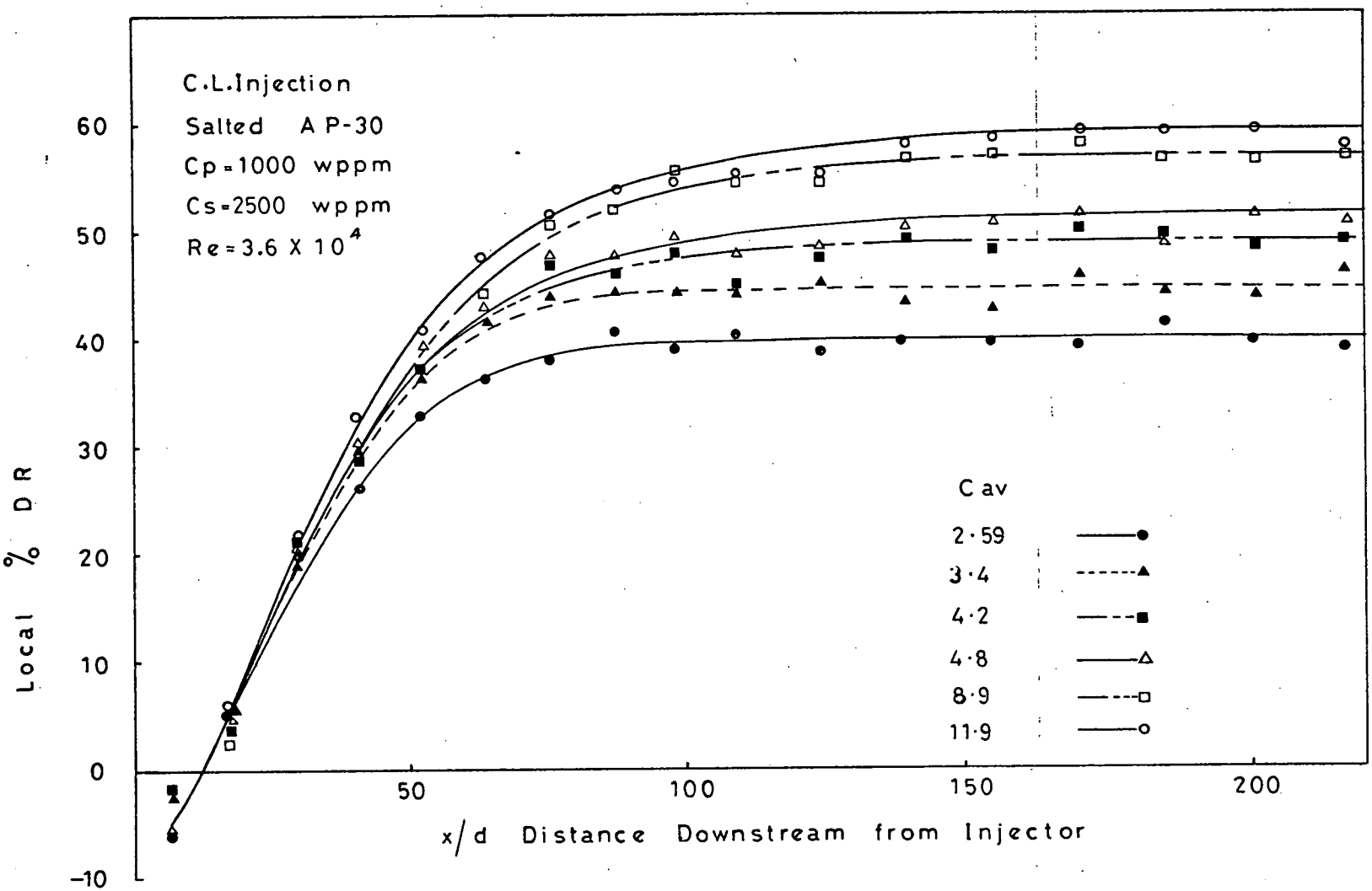
C.L.Injection
Salted A P-30
Cp = 1000 wppm
Cs = 2500 wppm
Re = 3.6 X 10⁴
Local % DR
60
50
40
30
20
10
0
-10
50
100
150
200
x/d Distance Downstream from Injector
C av
2·59
3·4
4·2
4·8
8·9
11·9

FIG (4 - 2)

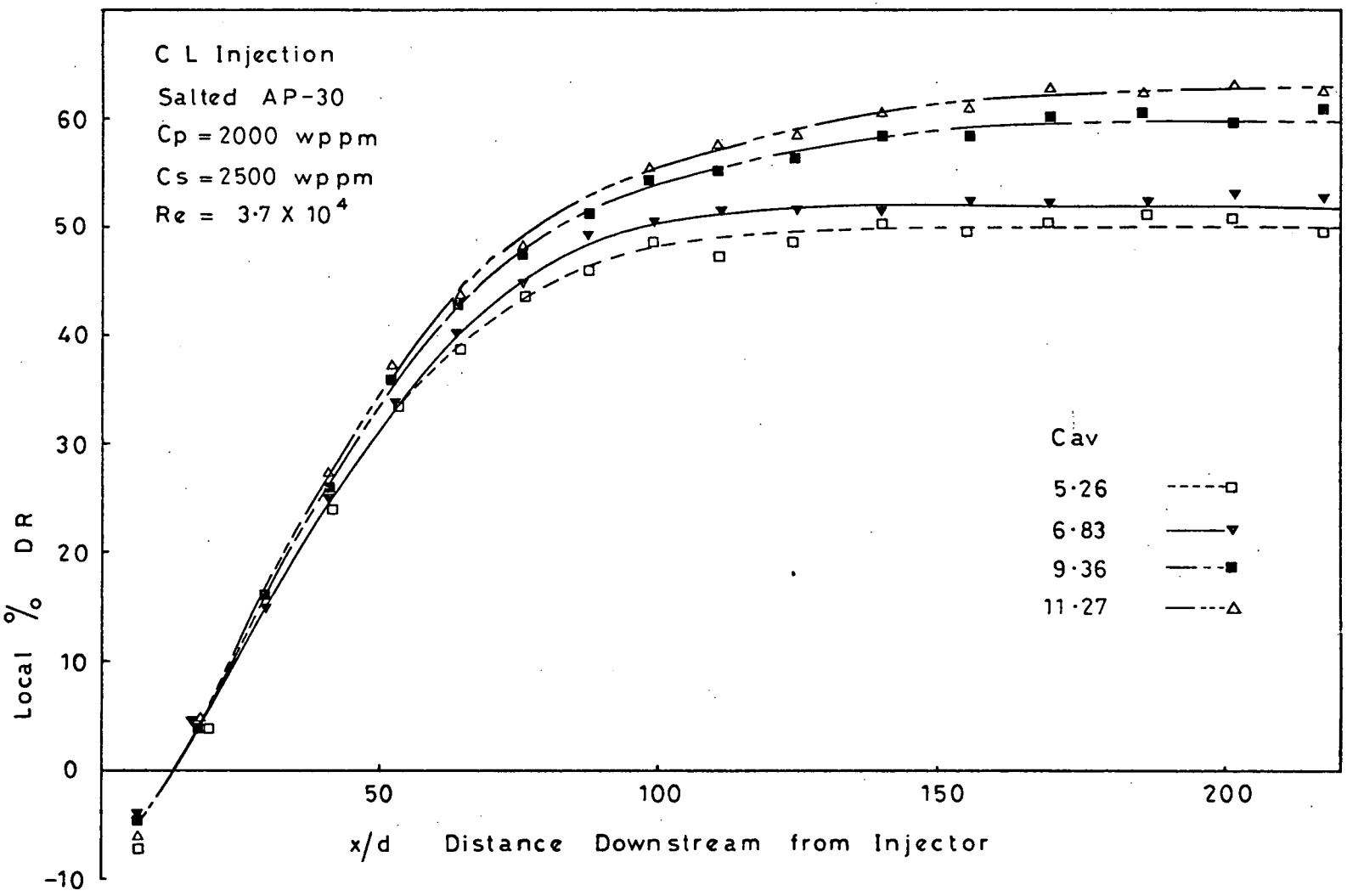
C L Injection
Salted AP-30
Cp = 2000 wppm
Cs = 2500 wppm
Re = 3·7 X 10⁴
Cav
5·26
6·83
9·36
11·27
Local % DR
60
50
40
30
20
10
0
-10
50
100
150
200
x/d Distance Downstream from Injector

FIG (4 – 3)

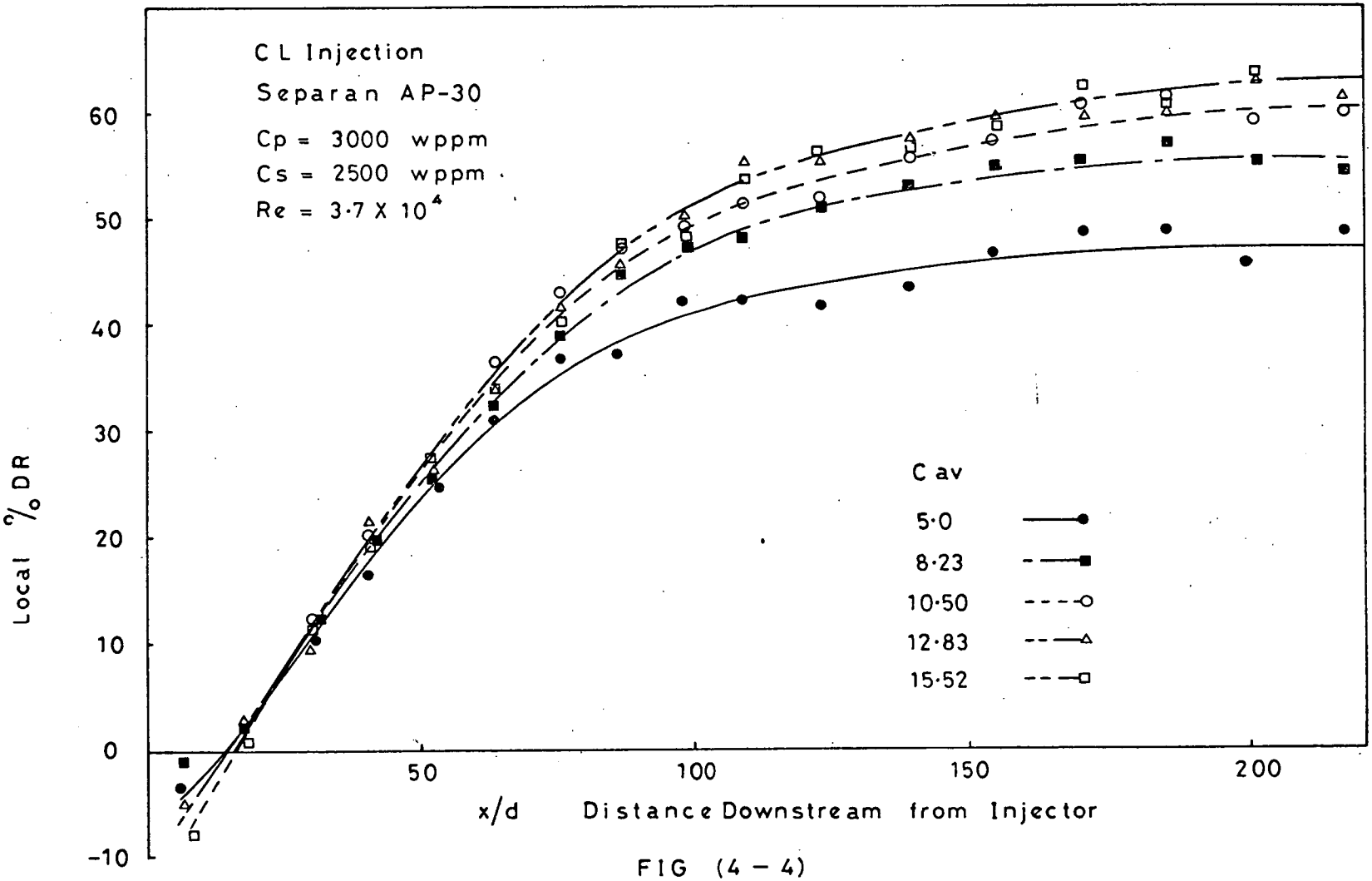
C L Injection
Separan AP-30
Cp = 3000 wppm
Cs = 2500 wppm
Re = 3·7 X 10⁴
C av
5·0
8·23
10·50
12·83
15·52
Local % DR
60
50
40
30
20
10
0
-10
50
100
150
200
x/d
Distance Downstream from Injector

FIG (4 – 4)

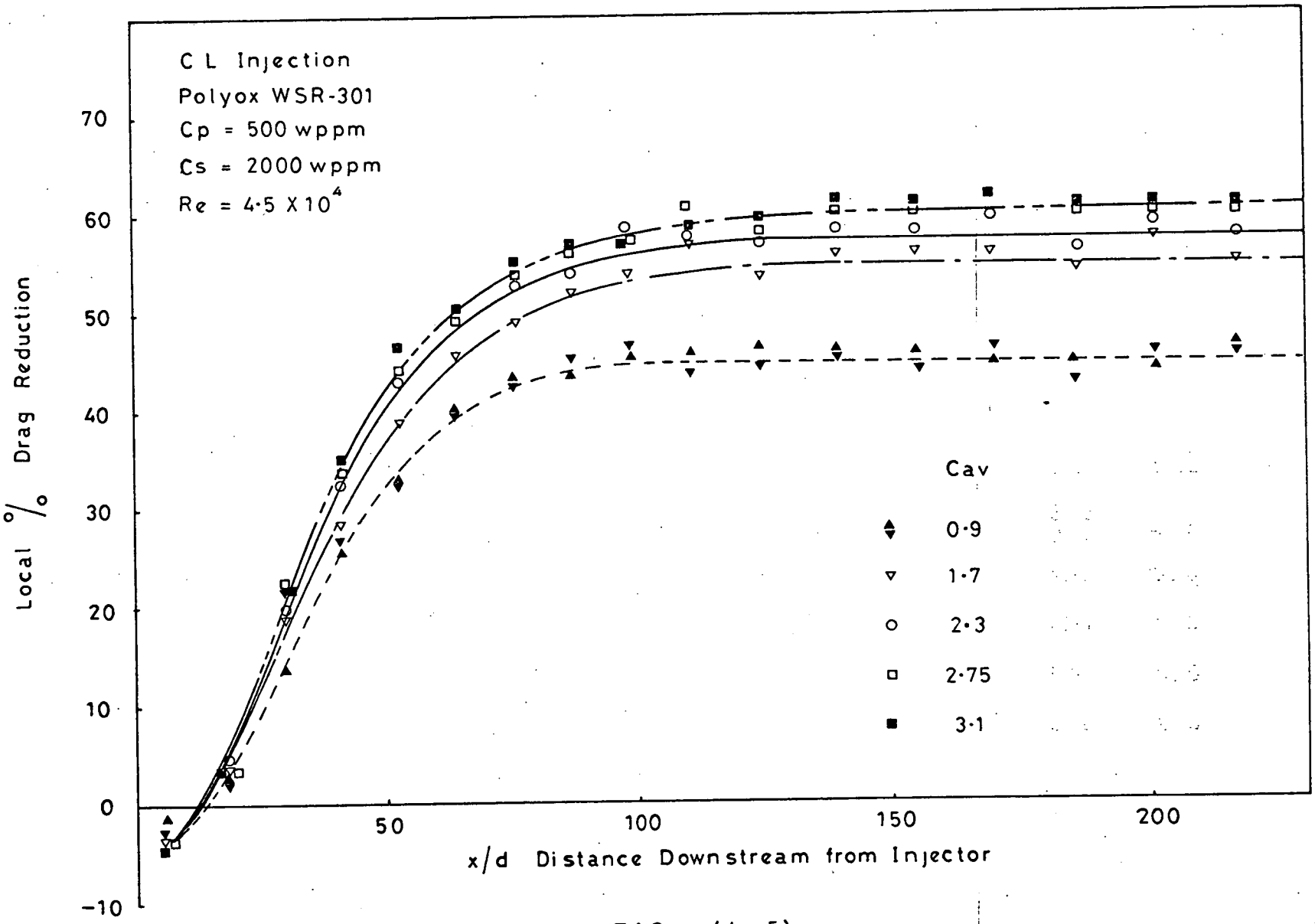
C L Injection
Polyox WSR-301
Cp = 500 wppm
Cs = 2000 wppm
Re = 4·5 X 10^4
Local % Drag Reduction
70
60
50
40
30
20
10
0
-10
50
100
150
200
x/d Distance Downstream from Injector
Cav
0·9
1·7
2·3
2·75
3·1

FIG (4 - 5)

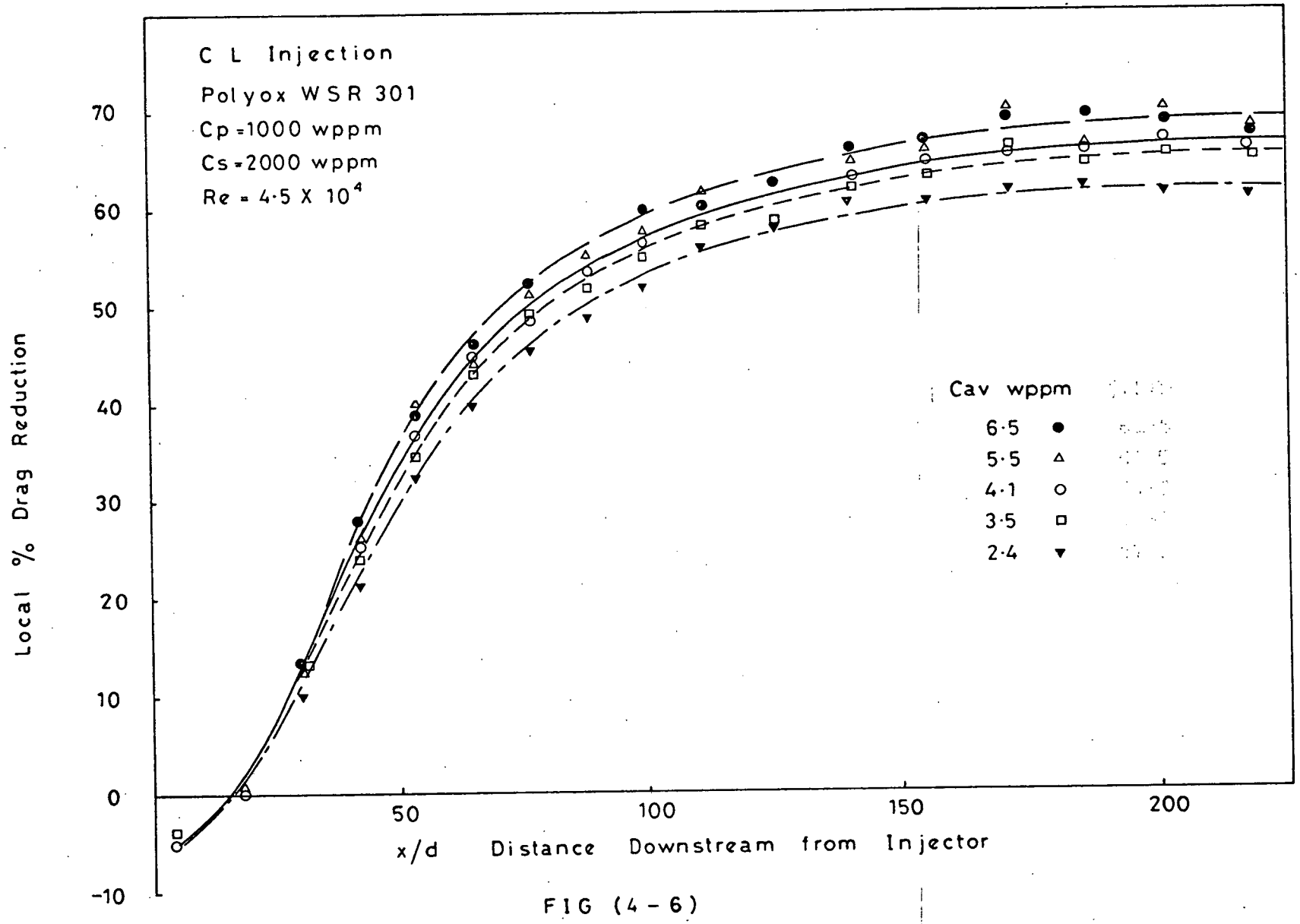
C L Injection
Polyox WSR 301
Cp = 1000 wppm
Cs = 2000 wppm
Re = 4·5 X 10⁴
Cav wppm
6·5
5·5
4·1
3·5
2·4
Local % Drag Reduction
70
60
50
40
30
20
10
0
-10
50
100
150
200
x/d Distance Downstream from Injector

FIG (4 - 6)

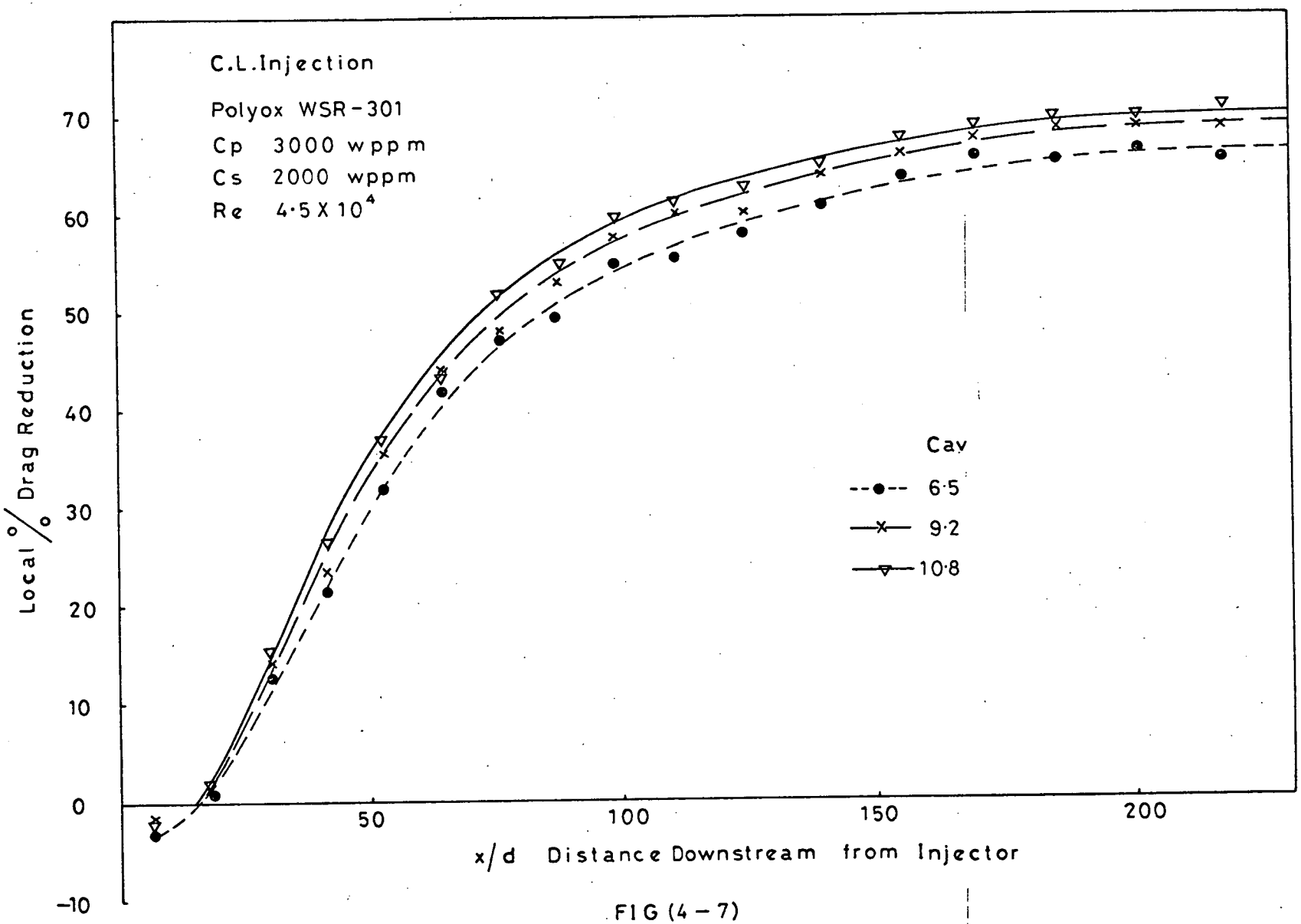
C.L.Injection
Polyox WSR-301
Cp 3000 wppm
Cs 2000 wppm
Re 4·5 X 10⁴
Cav
6·5
9·2
10·8
Local % Drag Reduction
70
60
50
40
30
20
10
0
-10
50
100
150
200
x/d Distance Downstream from Injector

FIG (4 – 7)

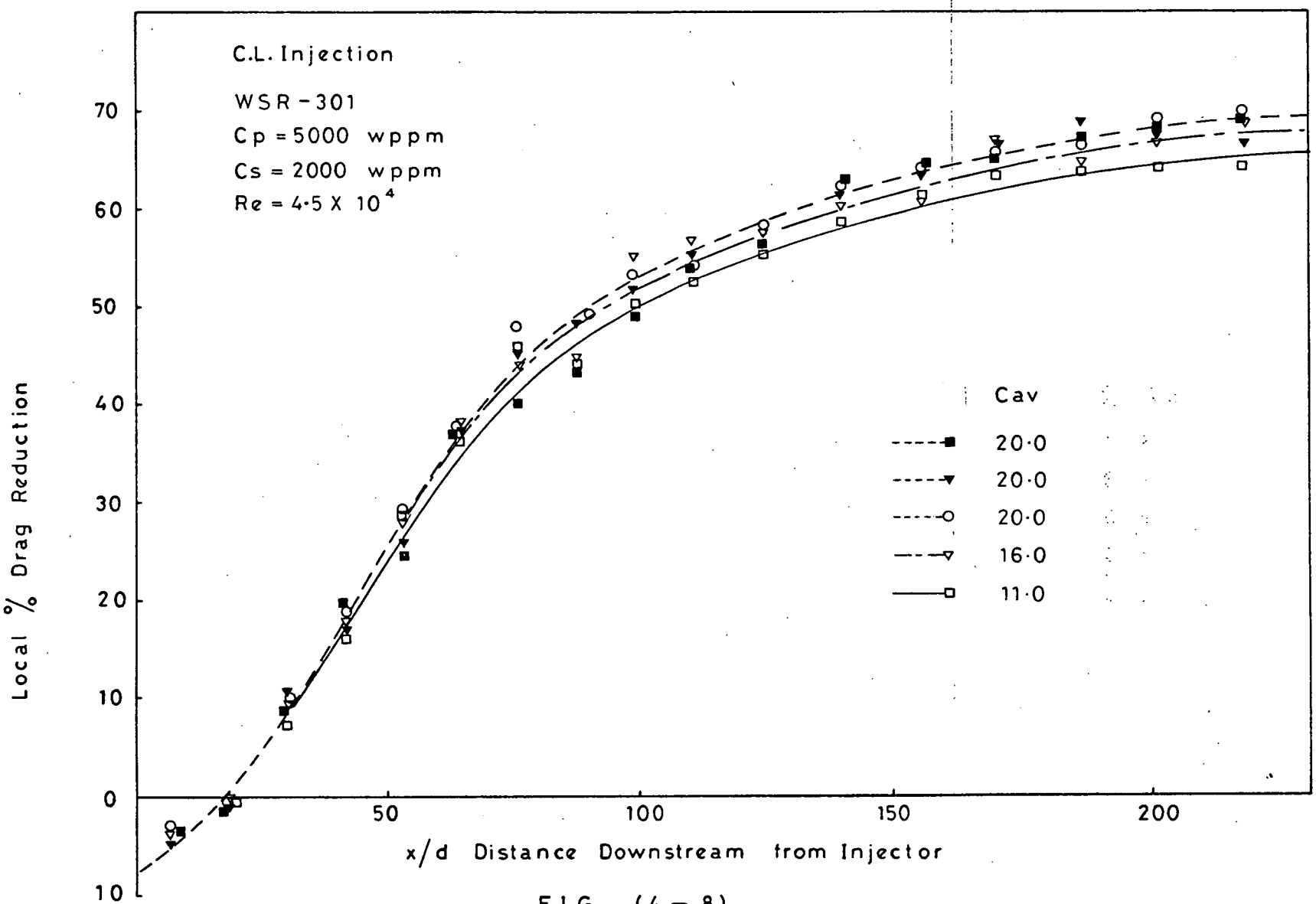
C.L. Injection
WSR-301
Cp = 5000 wppm
Cs = 2000 wppm
Re = 4·5 X 10⁴
Cav
20·0
20·0
20·0
16·0
11·0
Local % Drag Reduction
70
60
50
40
30
20
10
0
10
50
100
150
200
x/d Distance Downstream from Injector

FIG. (4 – 8)

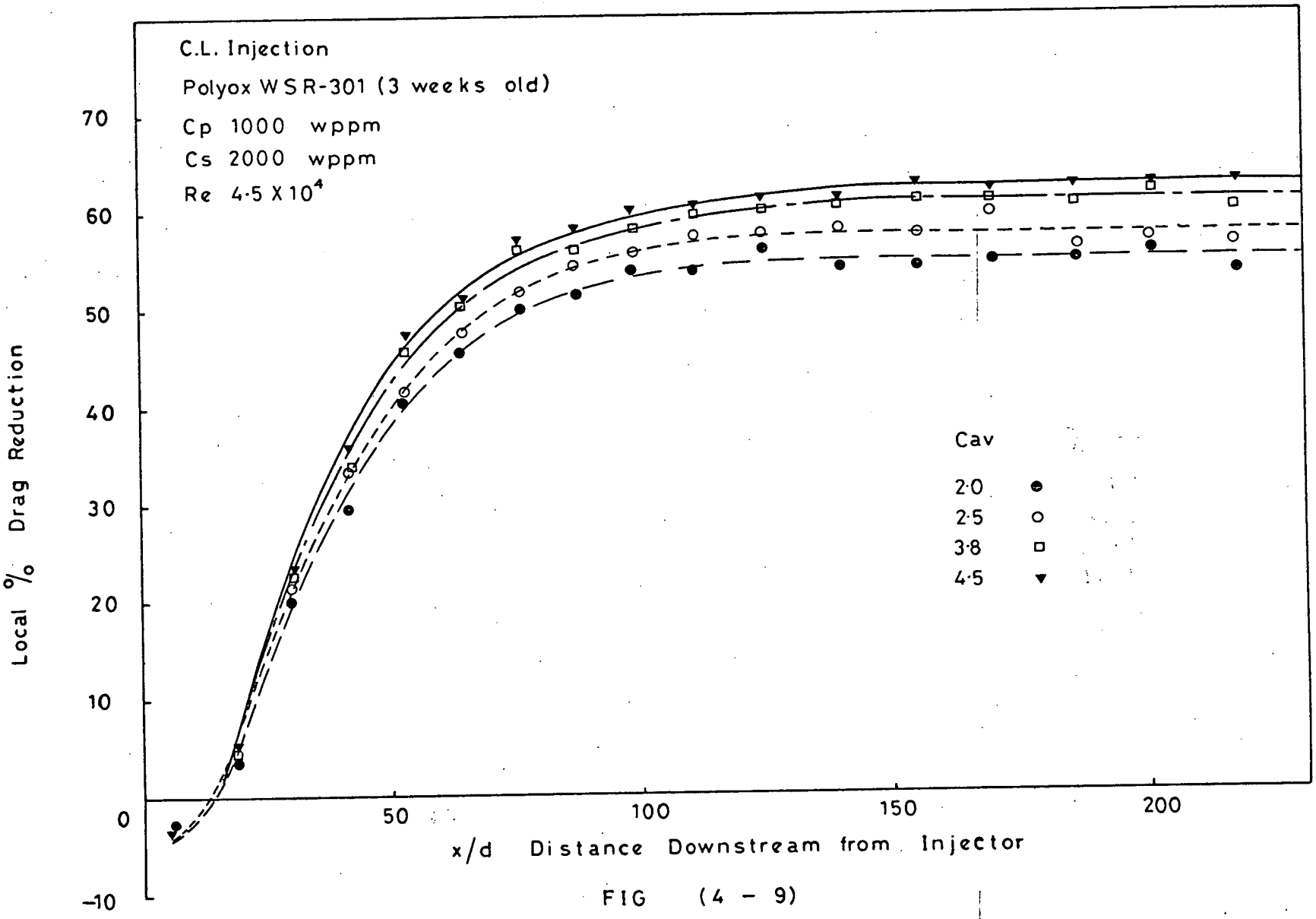
C.L. Injection
Polyox WSR-301 (3 weeks old)
Cp 1000 wppm
Cs 2000 wppm
Re 4·5 X 10⁴
Cav
2·0
2·5
3·8
4·5
Local % Drag Reduction
70
60
50
40
30
20
10
0
-10
50
100
150
200
x/d Distance Downstream from Injector

FIG (4 - 9)

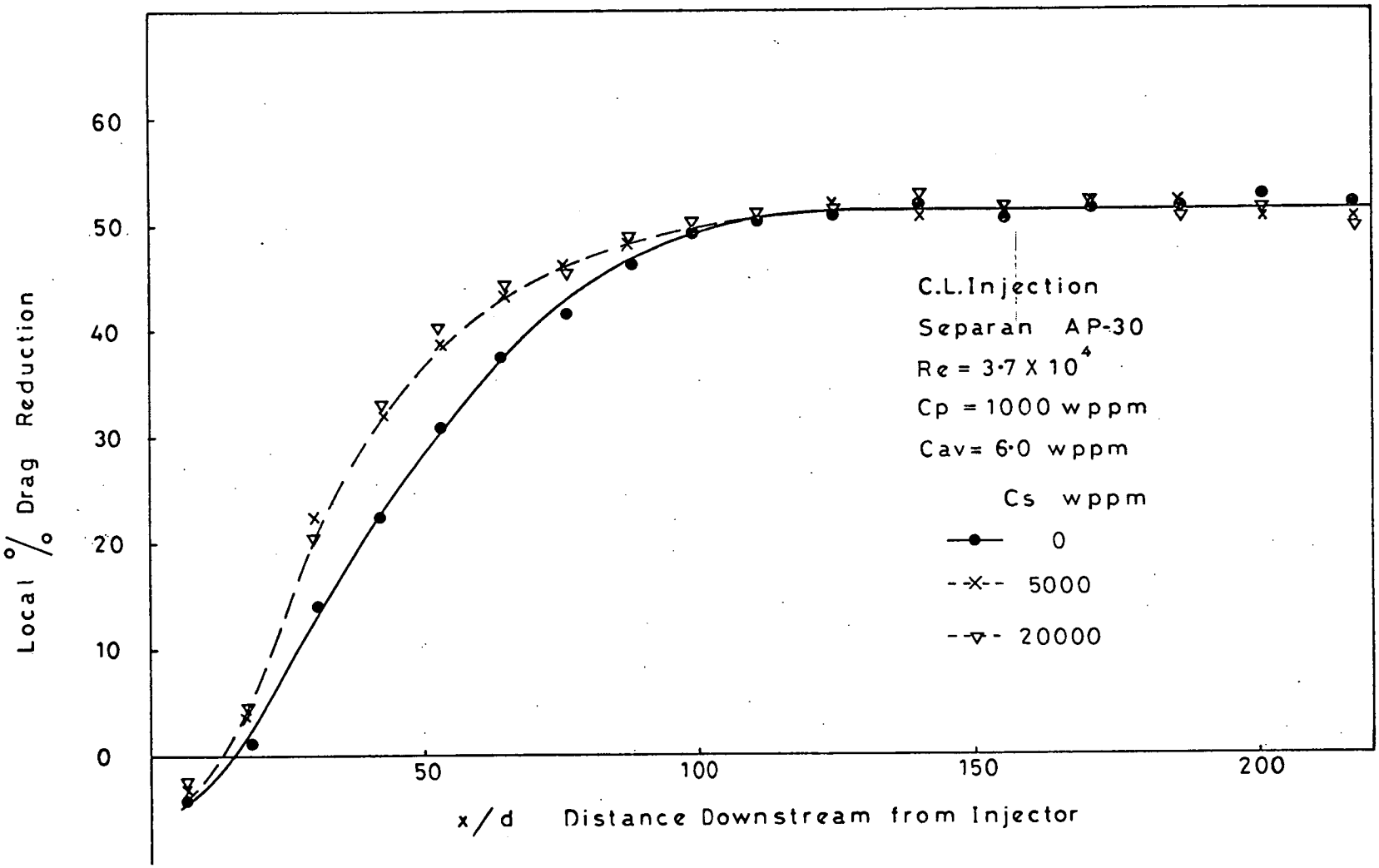
Local % Drag Reduction
60
50
40
30
20
10
0
50
100
150
200
x/d Distance Downstream from Injector
C.L.Injection
Separan AP-30
Re = 3·7 X 10^4
Cp = 1000 wppm
Cav= 6·0 wppm
Cs wppm
0
5000
20000

FIG (4-10)

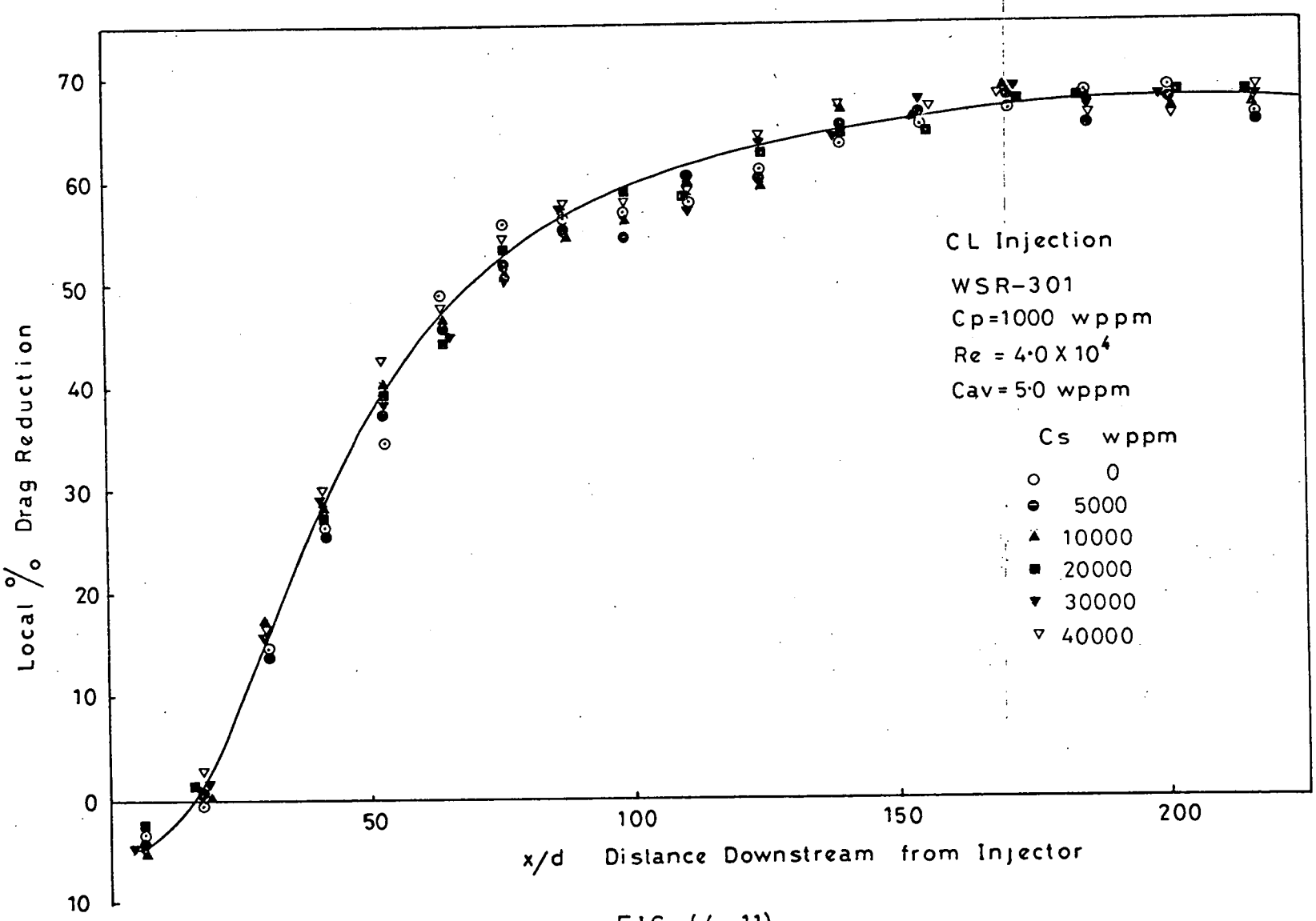
70
60
50
40
30
20
10
0
10
Local % Drag Reduction
50
100
150
200
x/d Distance Downstream from Injector
CL Injection
WSR-301
Cp=1000 wppm
Re = 4·0 X 10⁴
Cav = 5·0 wppm
Cs wppm
0
5000
10000
20000
30000
40000

FIG. (4-11)

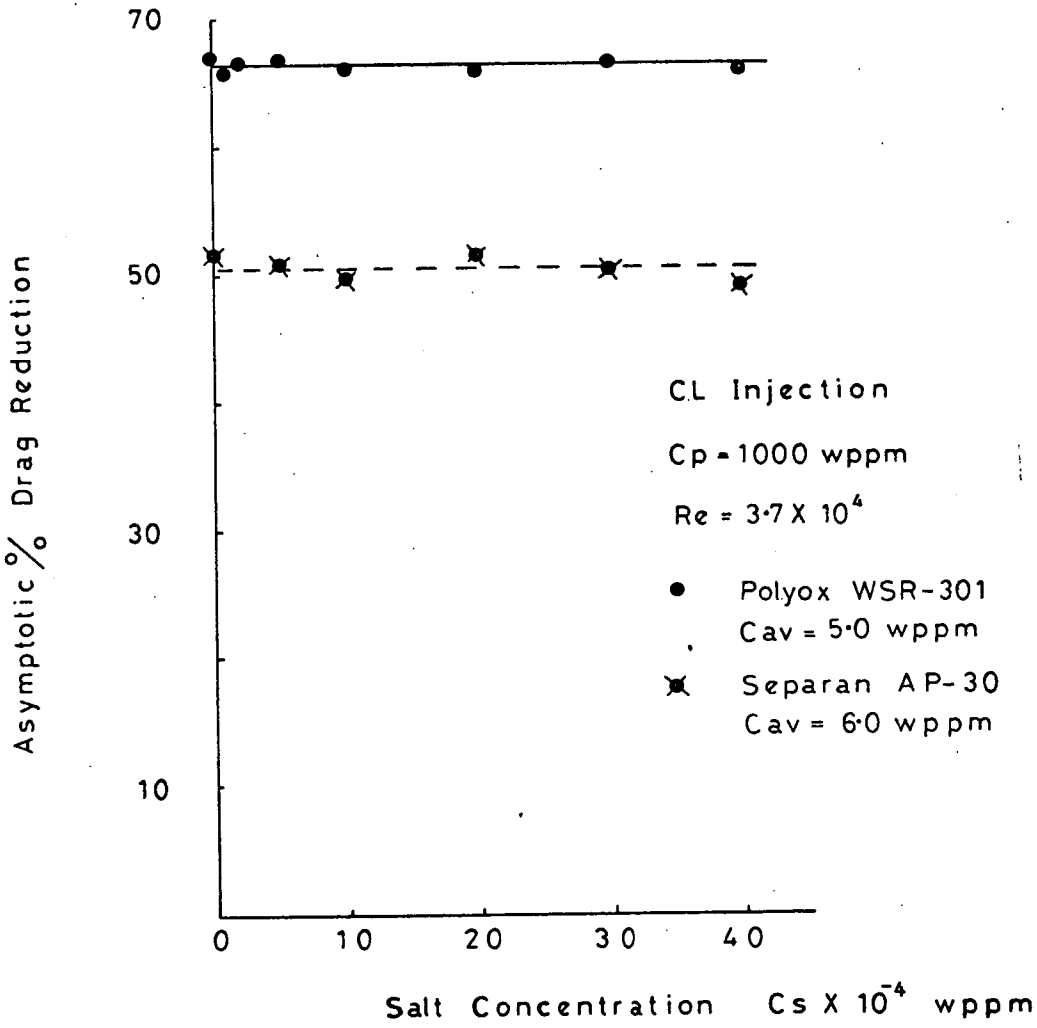
70
50
30
10
Asymptotic % Drag Reduction
0
10
20
30
40
Salt Concentration Cs X 10^-4 wppm
CL Injection
Cp = 1000 wppm
Re = 3·7 X 10^4
Polyox WSR-301
Cav = 5·0 wppm
Separan AP-30
Cav = 6·0 wppm

FIG (4-12)

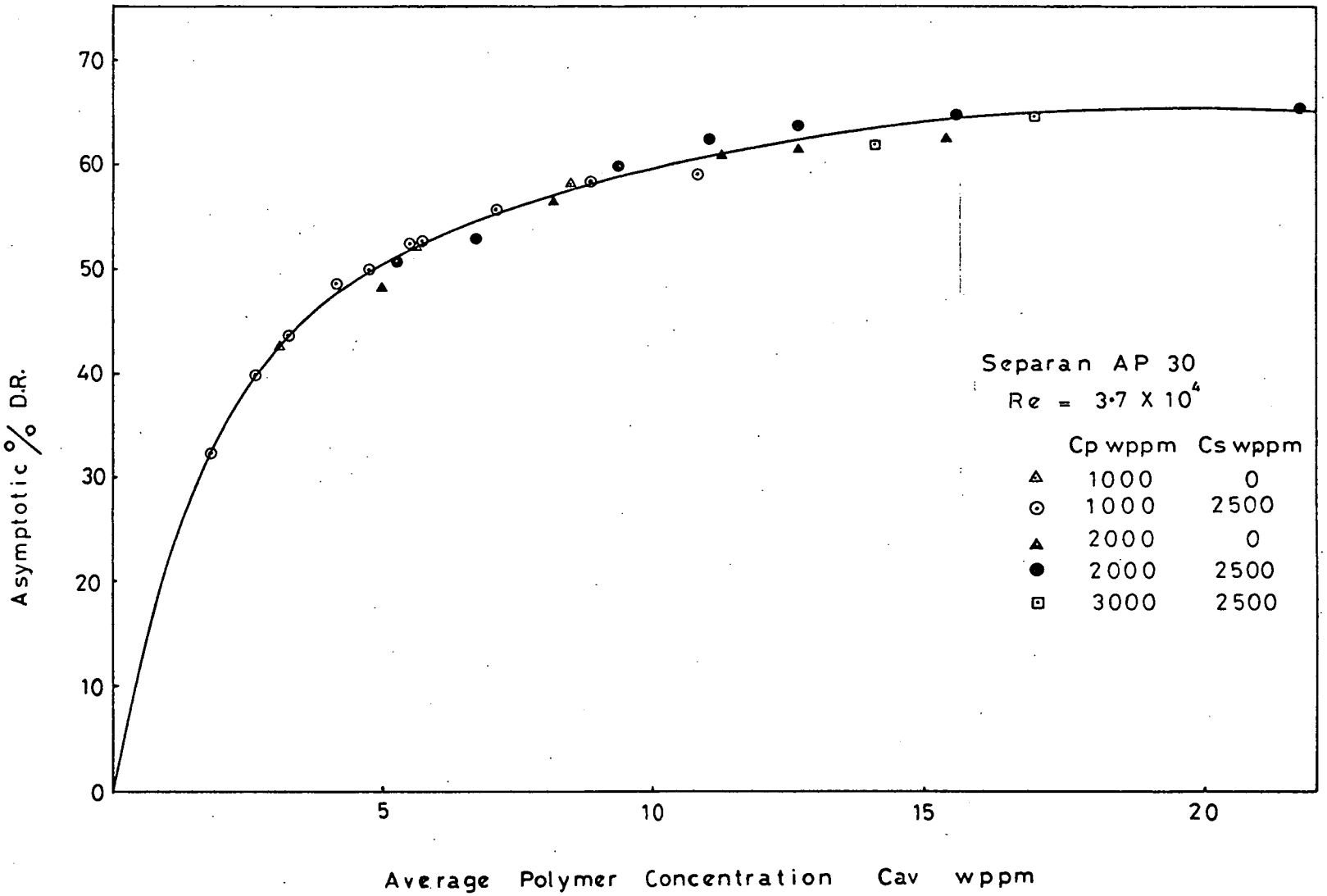
Asymptotic % D.R.
70
60
50
40
30
20
10
0
5
10
15
20
Average Polymer Concentration Cav wppm
Separan AP 30
Re = 3·7 X 10^4
Cp wppm Cs wppm
1000 0
1000 2500
2000 0
2000 2500
3000 2500

FIG. 4 - 13

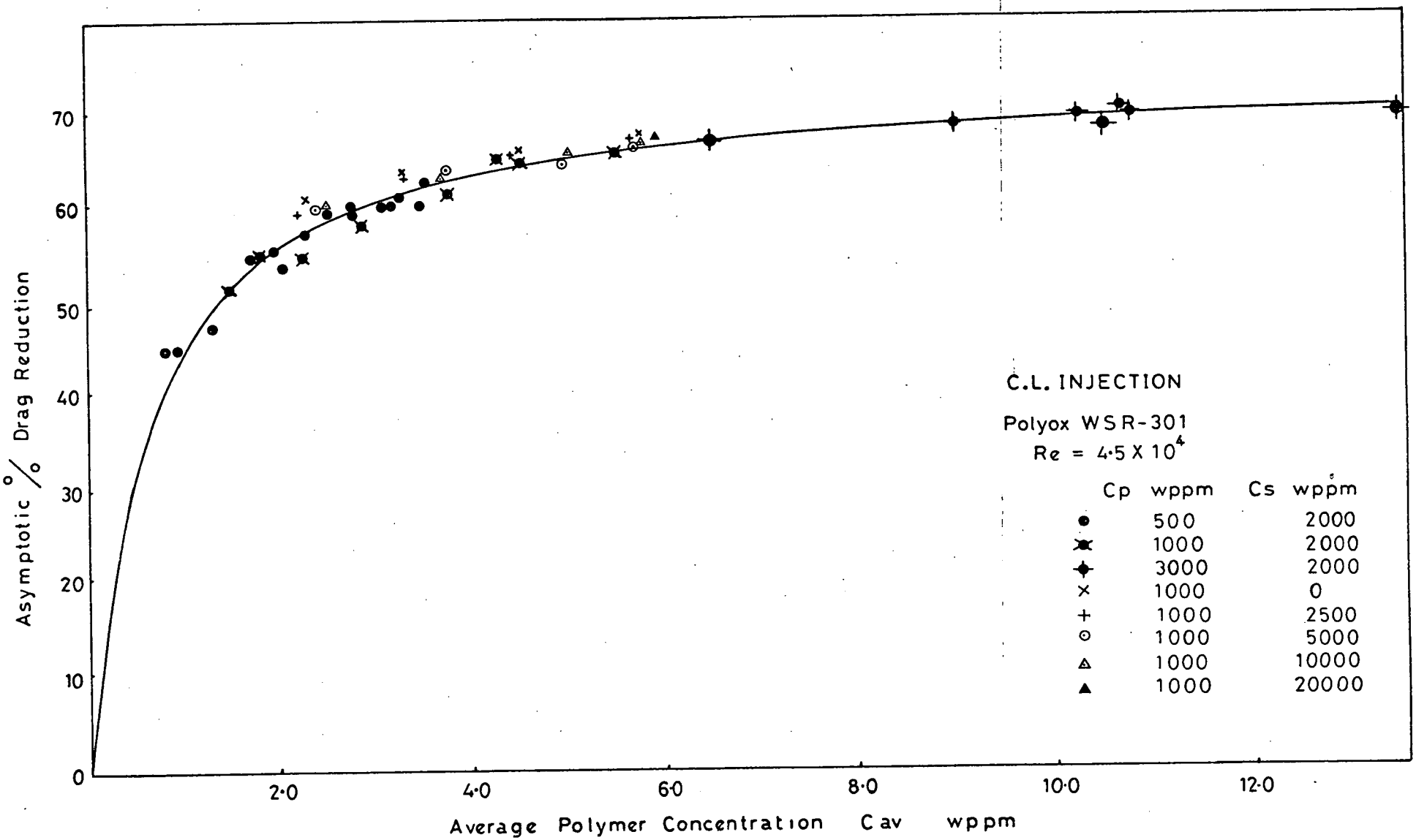
Asymptotic % Drag Reduction
0
10
20
30
40
50
60
70
2·0
4·0
6·0
8·0
10·0
12·0
Average Polymer Concentration Cav wppm
C.L. INJECTION
Polyox WSR-301
Re = 4·5 X 10^4
Cp wppm
Cs wppm
500 2000
1000 2000
3000 2000
1000 0
1000 2500
1000 5000
1000 10000
1000 20000

FIG. (4 – 14)

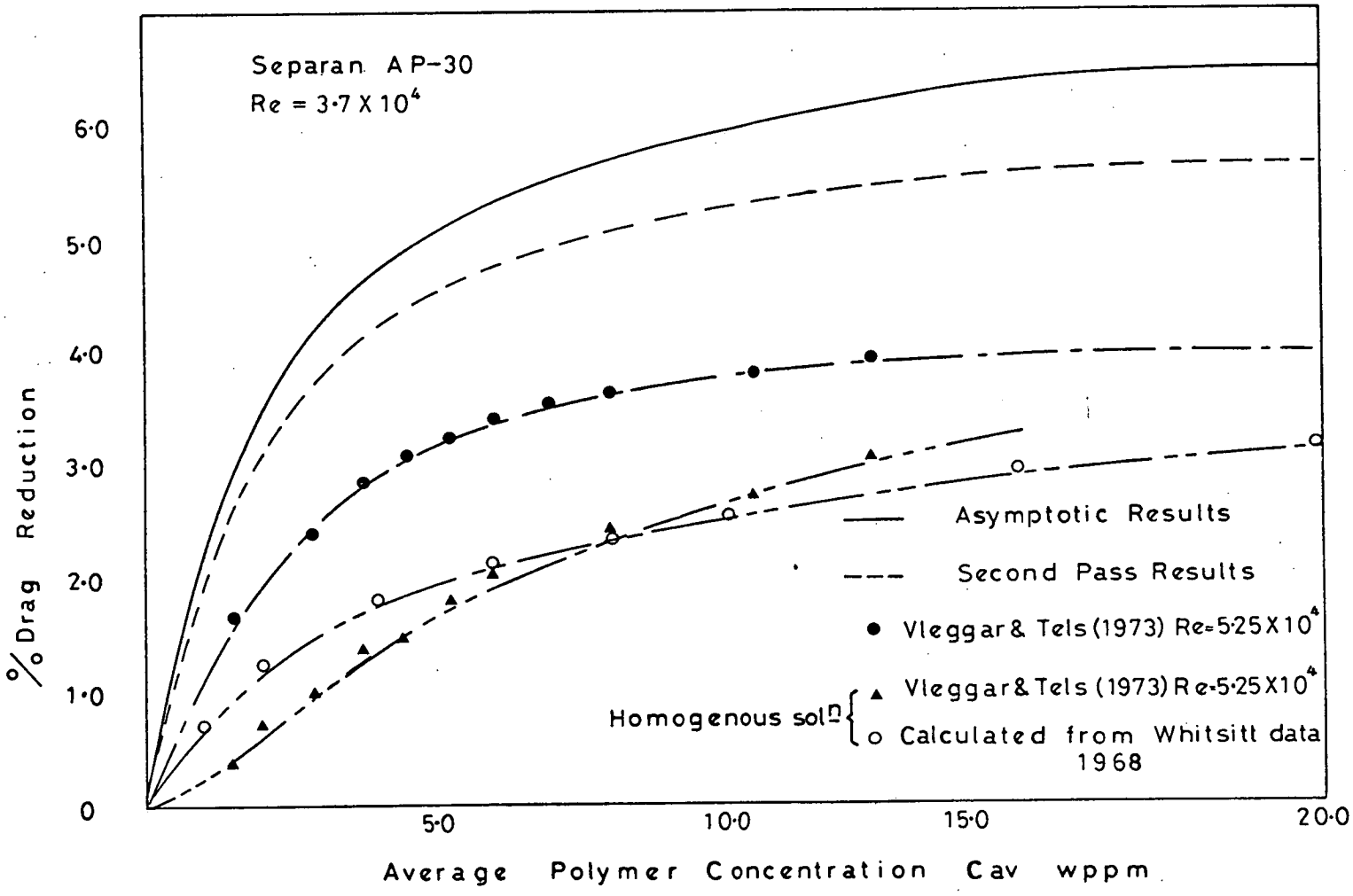
Separan AP-30
Re = 3·7 X 10⁴
6·0
5·0
4·0
3·0
2·0
1·0
0
% Drag Reduction
5·0
10·0
15·0
20·0
Average Polymer Concentration Cav wppm
Asymptotic Results
Second Pass Results
Vleggar & Tels (1973) Re=5·25X10⁴
Homogenous soln
Vleggar & Tels (1973) Re=5·25X10⁴
Calculated from Whitsitt data 1968

FIG (4 - 15)

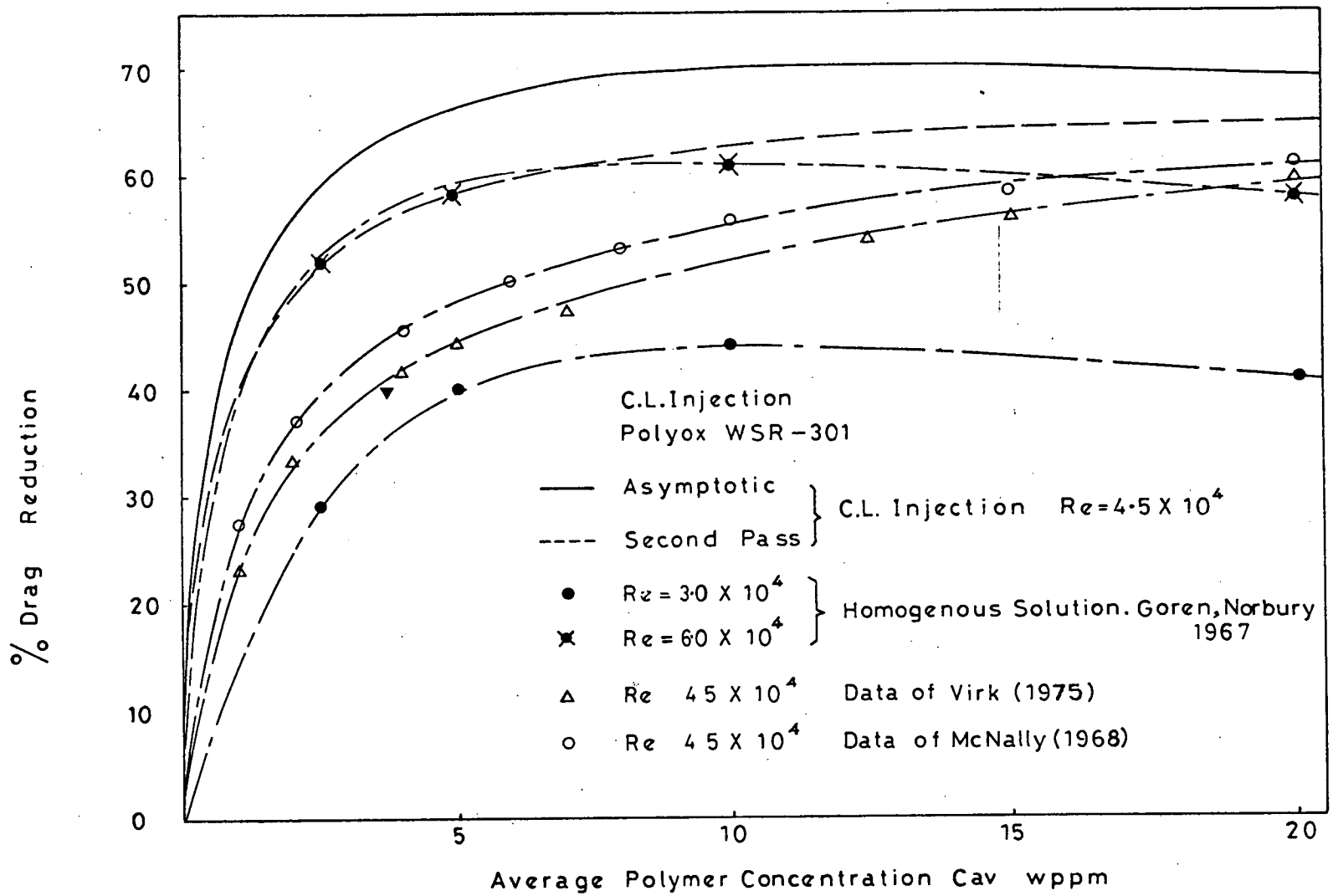
% Drag Reduction
70
60
50
40
30
20
10
0
5
10
15
20
Average Polymer Concentration Cav wppm
C.L.Injection
Polyox WSR-301
Asymptotic
Second Pass
C.L. Injection Re=4·5 X 10^4
Re = 3·0 X 10^4
Re = 6·0 X 10^4
Homogenous Solution. Goren, Norbury 1967
Re 4·5 X 10^4 Data of Virk (1975)
Re 4·5 X 10^4 Data of McNally (1968)

FIG (4-16)

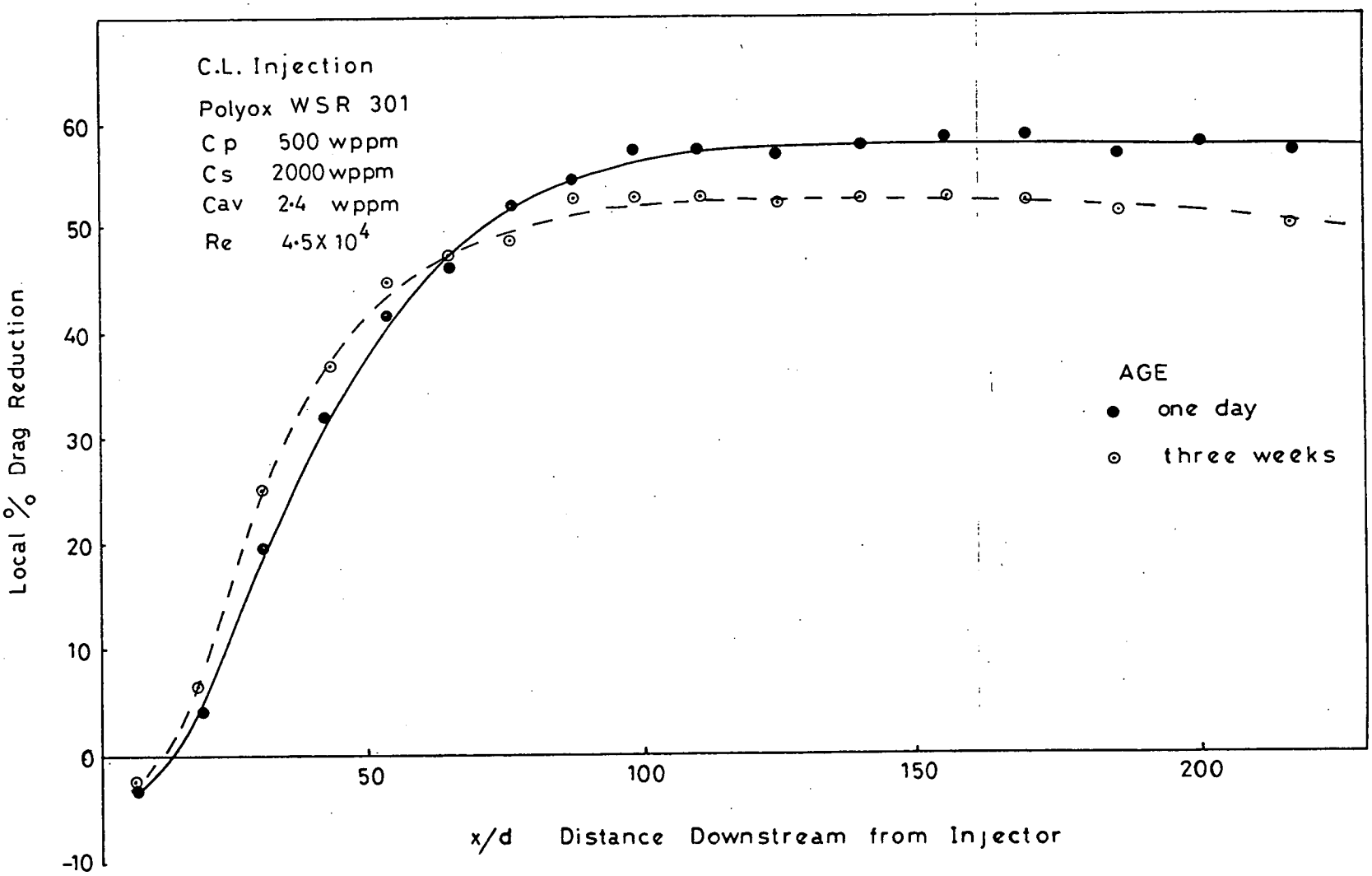
C.L. Injection
Polyox WSR 301
Cp 500 wppm
Cs 2000 wppm
Cav 2·4 wppm
Re 4·5X 10^4
AGE
one day
three weeks
Local % Drag Reduction
60
50
40
30
20
10
0
-10
50
100
150
200
x/d Distance Downstream from Injector

FIG. (4 – 17)

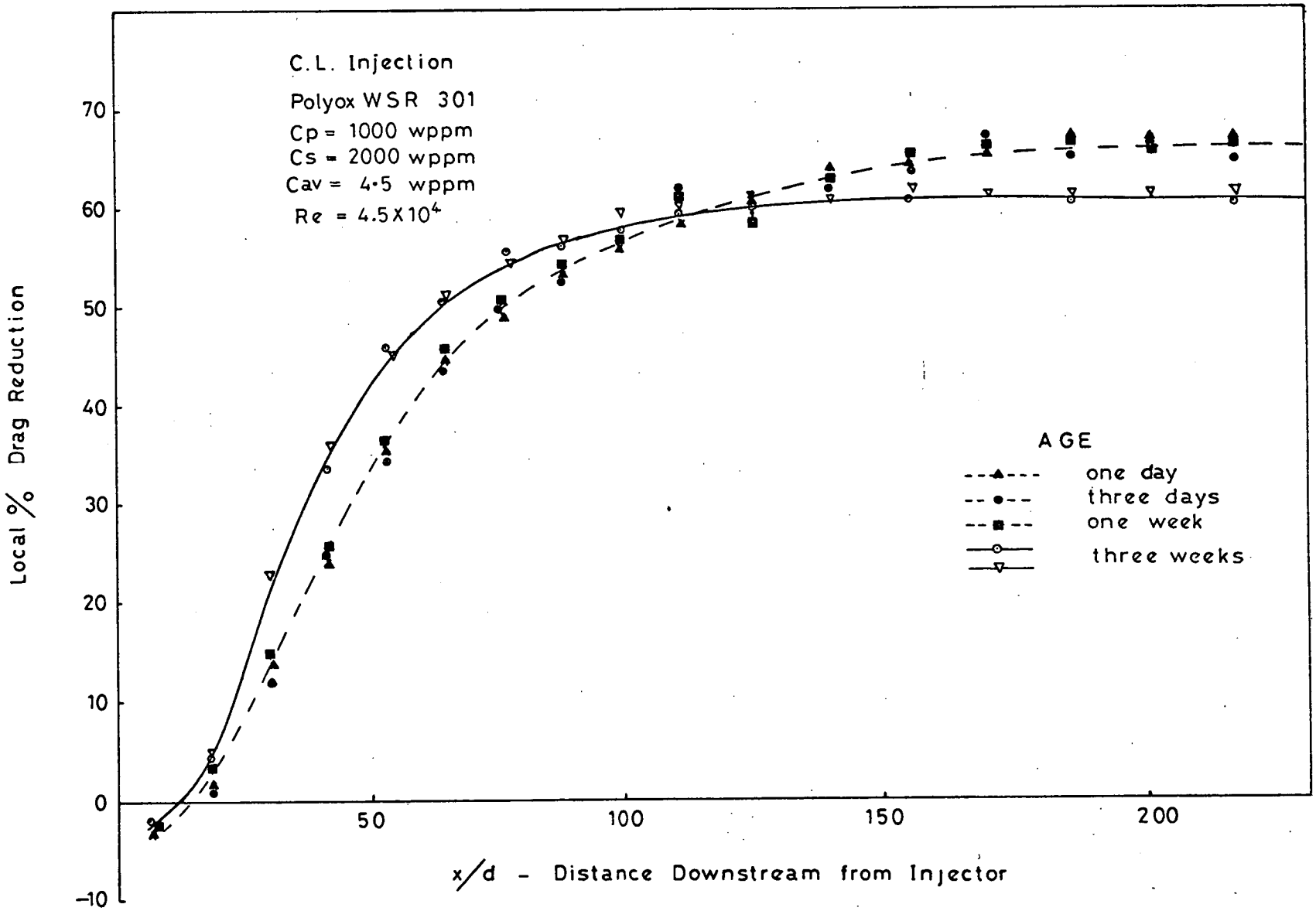
C.L. Injection
Polyox WSR 301
Cp = 1000 wppm
Cs = 2000 wppm
Cav = 4·5 wppm
Re = 4.5X10⁴
AGE
one day
three days
one week
three weeks
Local % Drag Reduction
x/d - Distance Downstream from Injector
70
60
50
40
30
20
10
0
-10
50
100
150
200

FIG (4 - 18)

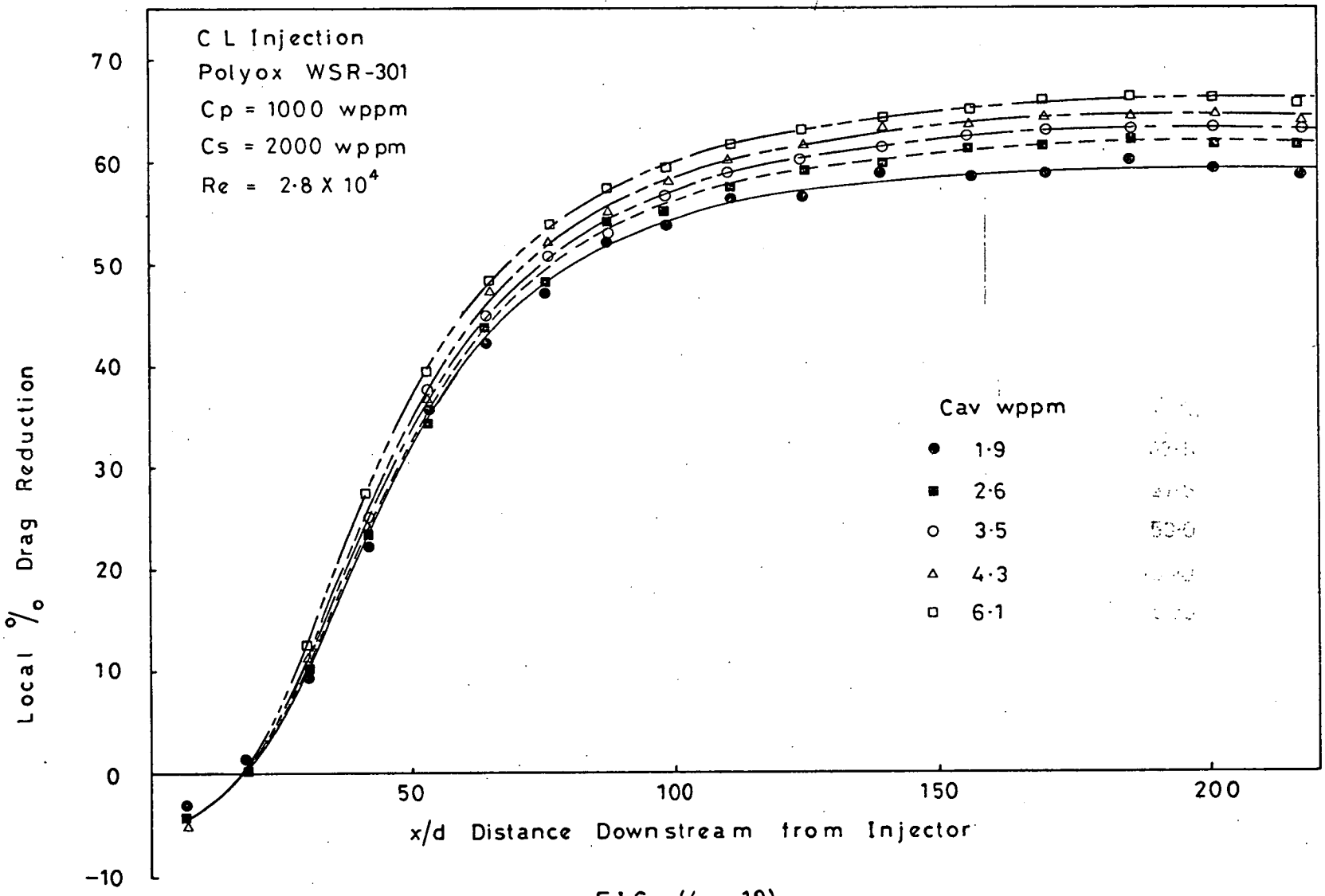
C L Injection
Polyox WSR-301
Cp = 1000 wppm
Cs = 2000 wppm
Re = 2·8 X 10⁴
Cav wppm
1·9
2·6
3·5
4·3
6·1
Local % Drag Reduction
x/d Distance Downstream from Injector
70
60
50
40
30
20
10
0
-10
50
100
150
200

FIG (4 - 19)

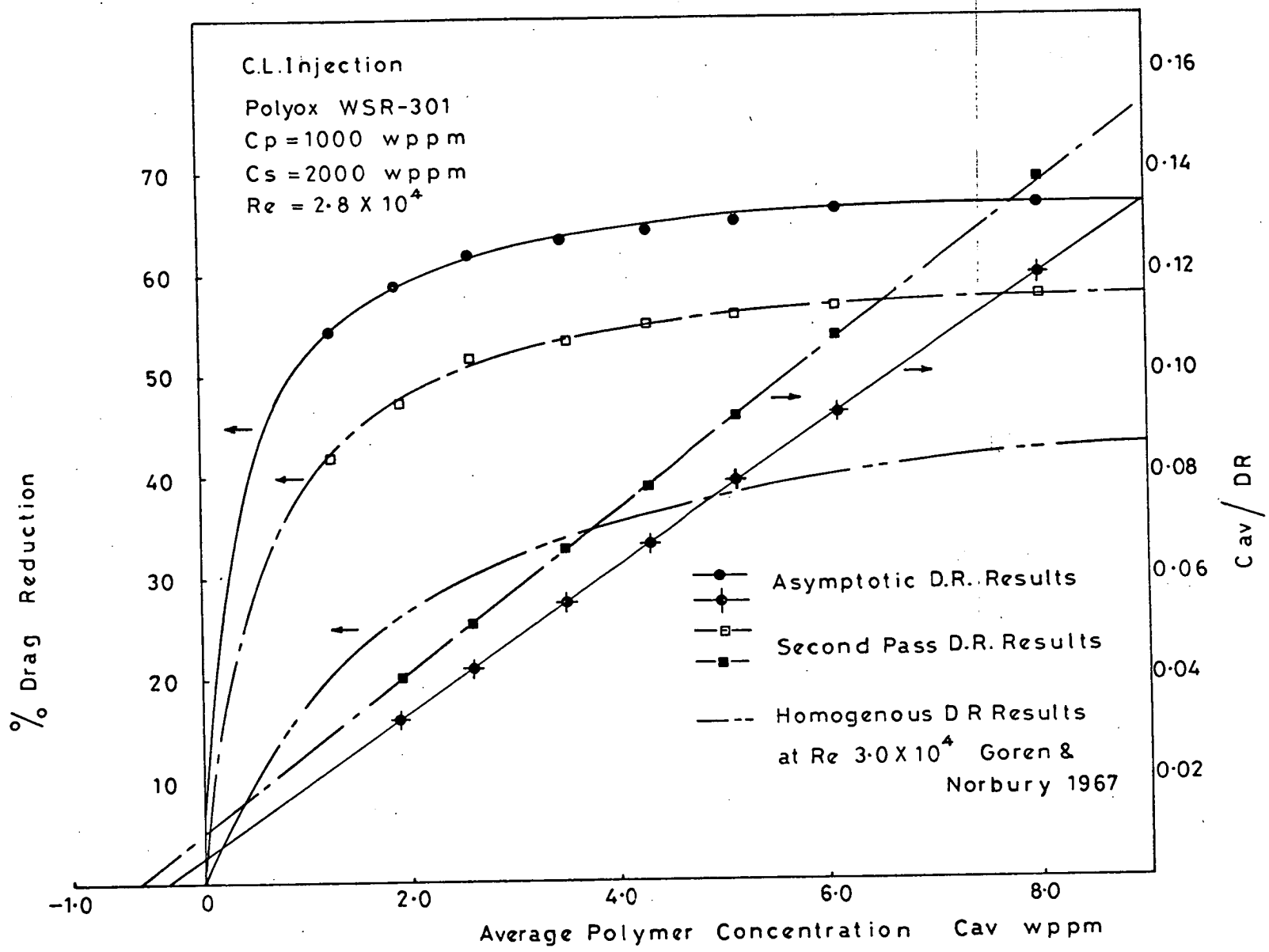
C.L. Injection
Polyox WSR-301
Cp = 1000 wppm
Cs = 2000 wppm
Re = 2·8 X 10⁴
% Drag Reduction
Cav / DR
Average Polymer Concentration Cav wppm
Asymptotic D.R. Results
Second Pass D.R. Results
Homogenous D R Results
at Re 3·0 X 10⁴ Goren & Norbury 1967
70
60
50
40
30
20
10
0·16
0·14
0·12
0·10
0·08
0·06
0·04
0·02
−1·0
0
2·0
4·0
6·0
8·0

FIG (4 – 20)

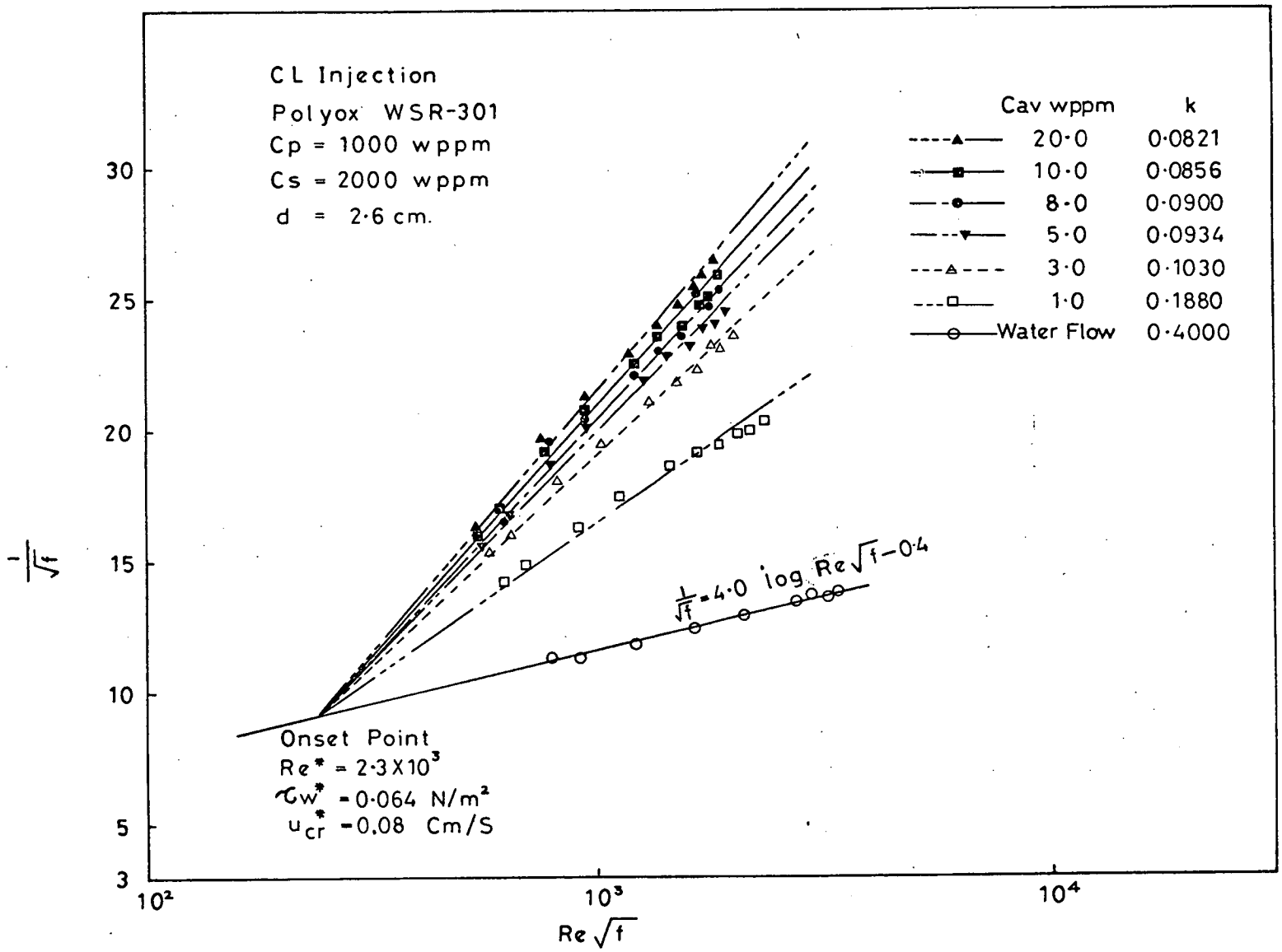
CL Injection
Polyox WSR-301
Cp = 1000 wppm
Cs = 2000 wppm
d = 2·6 cm.
Cav wppm k
20·0 0·0821
10·0 0·0856
8·0 0·0900
5·0 0·0934
3·0 0·1030
1·0 0·1880
Water Flow 0·4000
$\frac{1}{\sqrt{f}} = 4.0 \log Re\sqrt{f} - 0.4$
Onset Point
$Re^* = 2.3 \times 10^3$
$\tau_w^* = 0.064$ N/m²
$u_{cr}^* = 0.08$ Cm/S
30
25
20
15
10
5
3
10^2
10^3
10^4
$-\frac{1}{\sqrt{f}}$
$Re\sqrt{f}$

FIG (4 – 21)

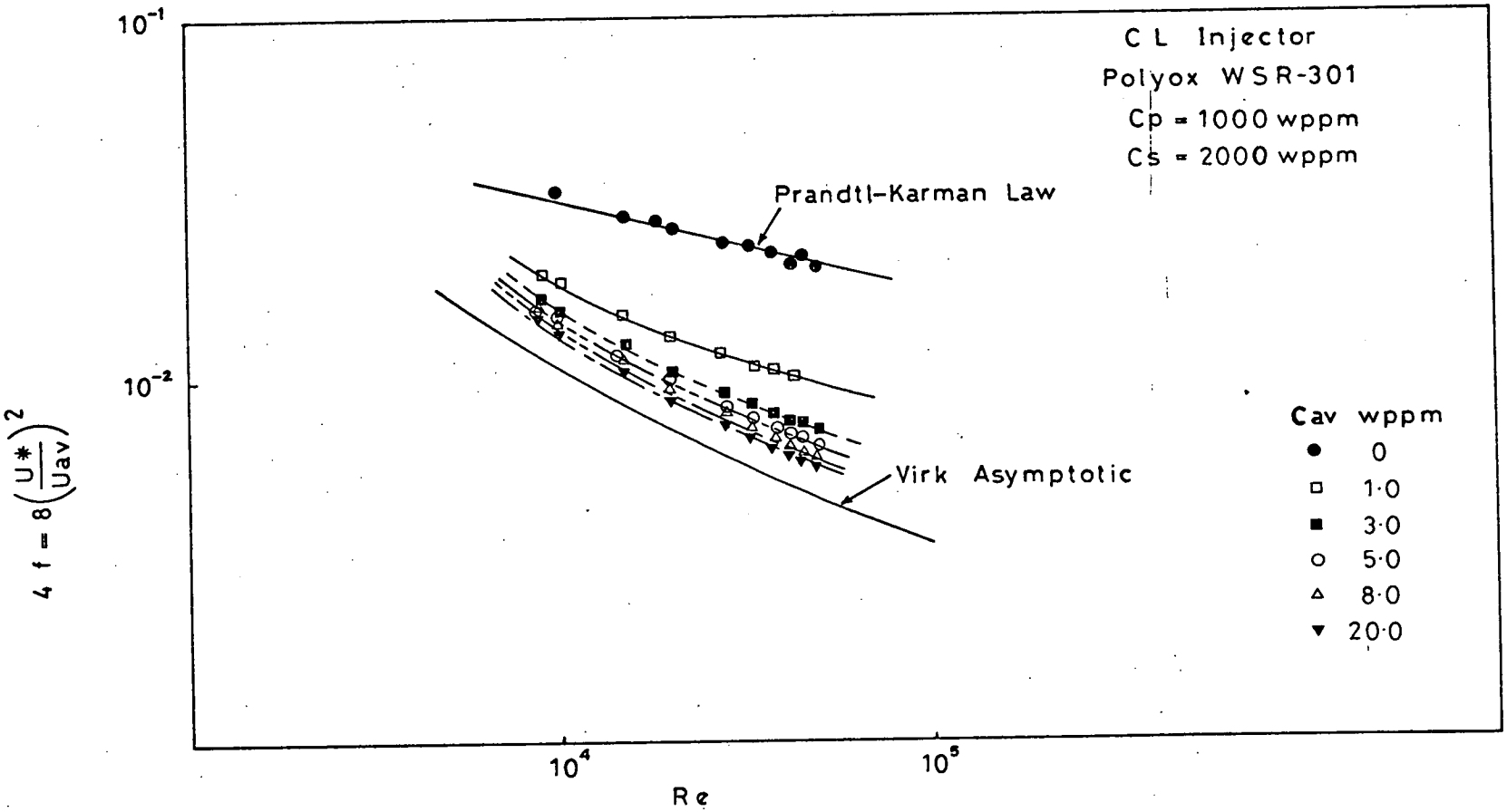
C L Injector
Polyox WSR-301
Cp = 1000 wppm
Cs = 2000 wppm
Prandtl-Karman Law
Virk Asymptotic
Cav wppm
0
1·0
3·0
5·0
8·0
20·0
10^{-1}
10^{-2}
10^{4}
10^{5}
Re
$4f = 8\left(\frac{U*}{Uav}\right)^2$

FIG (4 – 22)

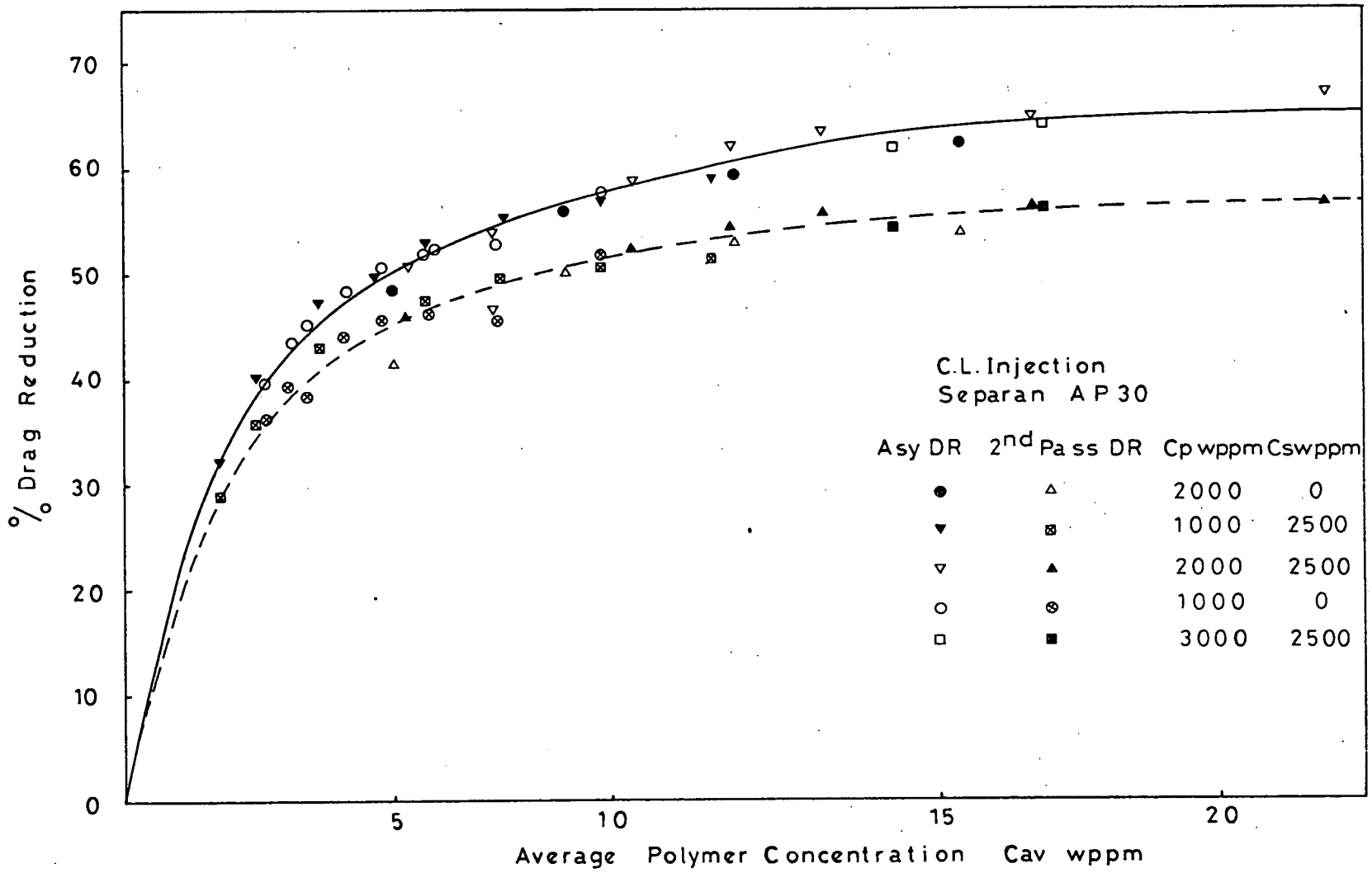
% Drag Reduction
0
10
20
30
40
50
60
70
5
10
15
20
Average Polymer Concentration Cav wppm
C.L. Injection
Separan AP 30
Asy DR
2nd Pass DR
Cp wppm
Cs wppm
2000 0
1000 2500
2000 2500
1000 0
3000 2500

FIG (4 – 23)

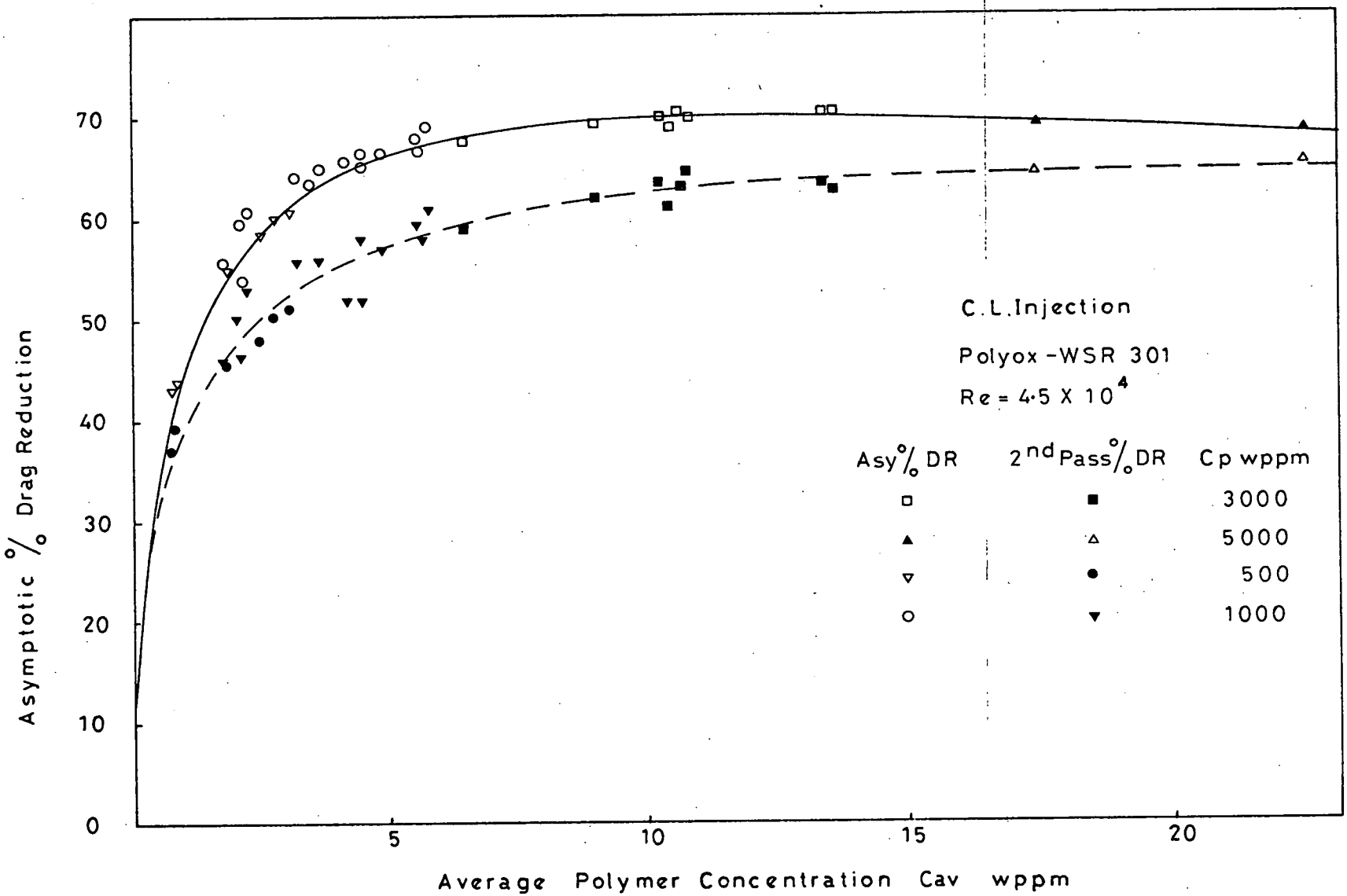
Asymptotic % Drag Reduction
0
10
20
30
40
50
60
70
5
10
15
20
Average Polymer Concentration Cav wppm
C.L.Injection
Polyox -WSR 301
Re = 4·5 X 10^4
Asy% DR
2nd Pass% DR
Cp wppm
3000
5000
500
1000

FIG (4 - 24)

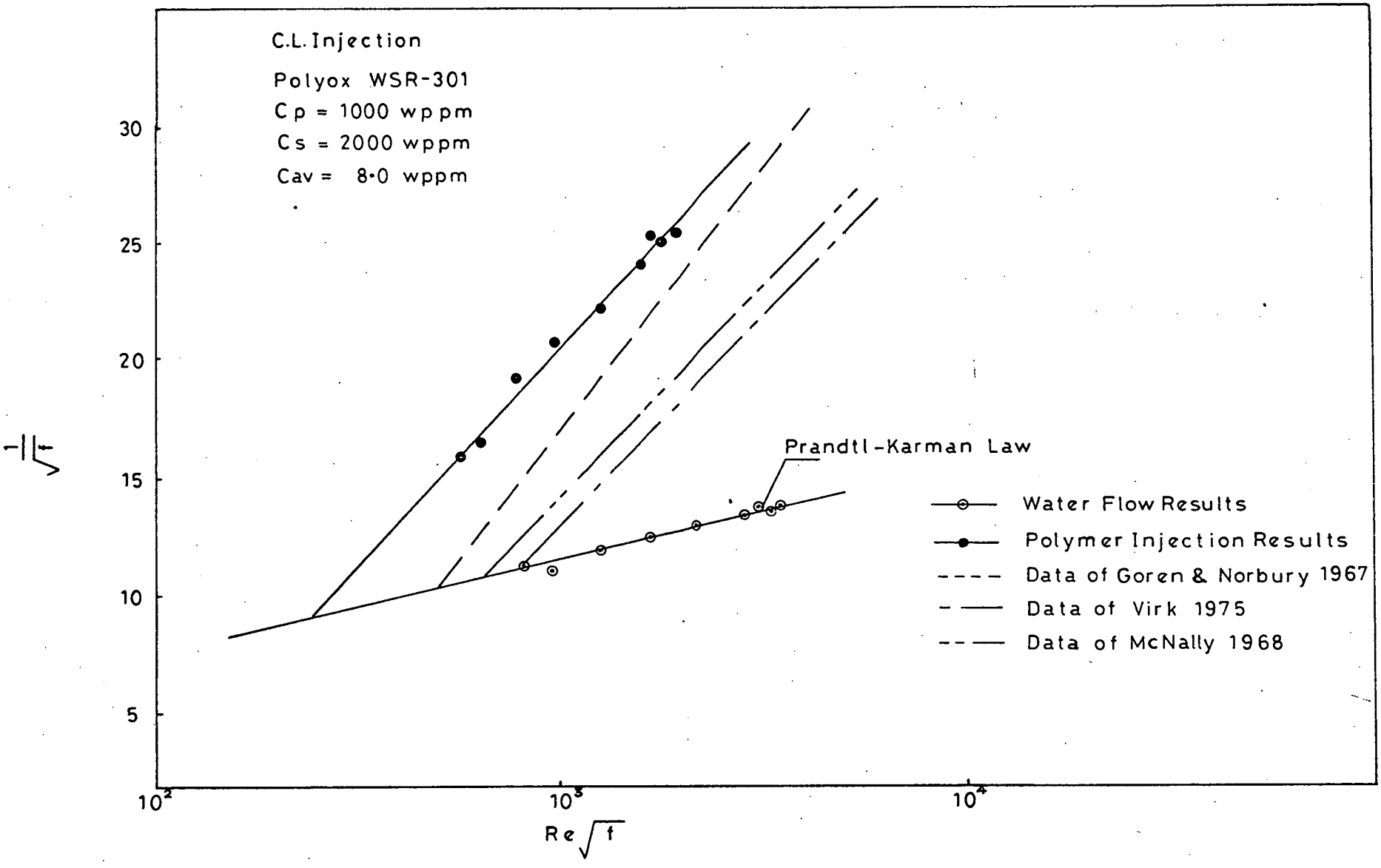
C.L. Injection
Polyox WSR-301
Cp = 1000 wppm
Cs = 2000 wppm
Cav = 8·0 wppm
Prandtl-Karman Law
Water Flow Results
Polymer Injection Results
Data of Goren & Norbury 1967
Data of Virk 1975
Data of McNally 1968
30
25
20
15
10
5
10^2
10^3
10^4
$\frac{1}{\sqrt{f}}$
$Re\sqrt{f}$

FIG (4 - 25)

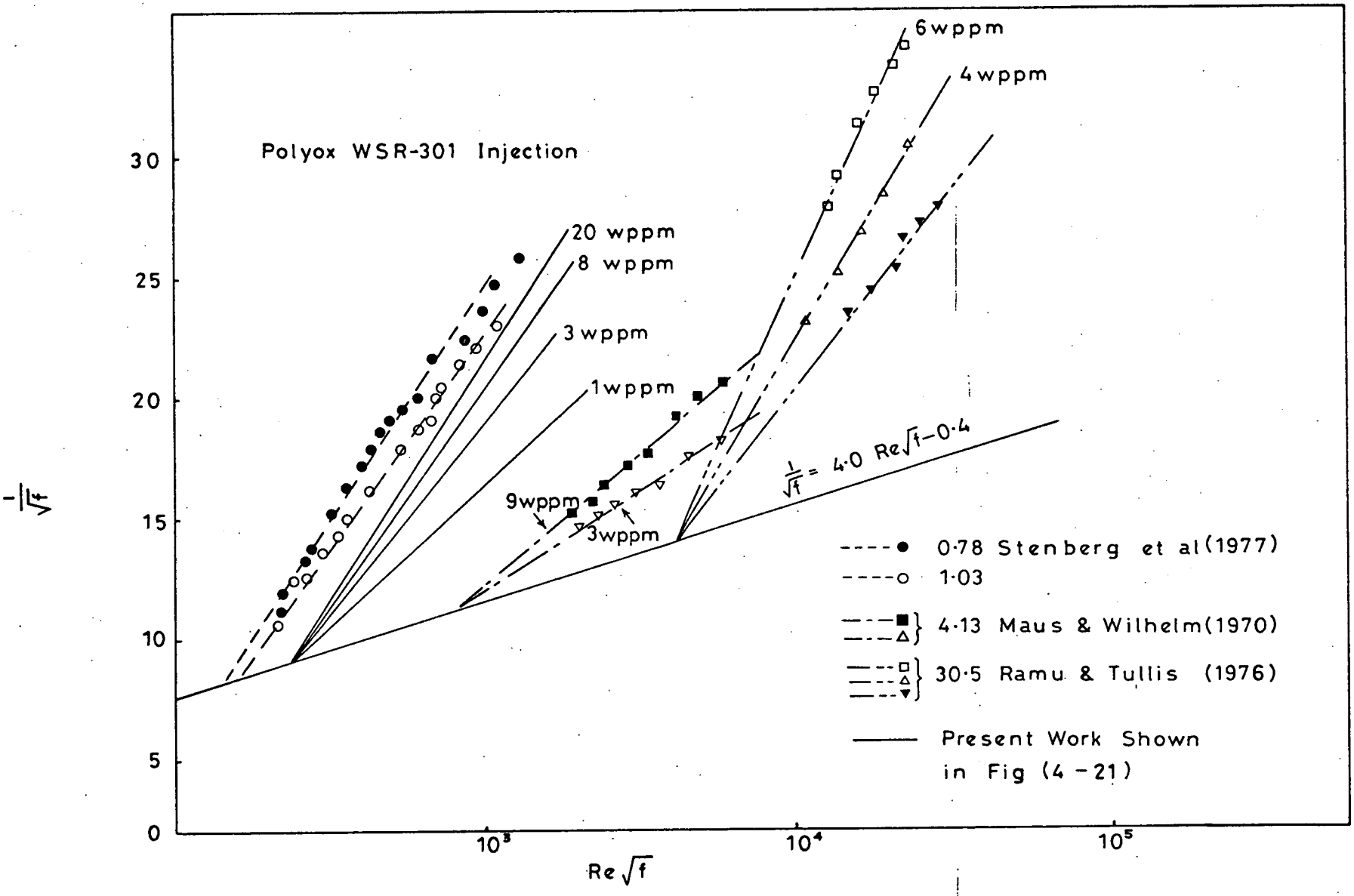
Polyox WSR-301 Injection
6wppm
4wppm
20 wppm
8 wppm
3 wppm
1wppm
9wppm
3wppm
$\frac{1}{\sqrt{f}} = 4.0\ Re\sqrt{f} - 0.4$
0·78 Stenberg et al(1977)
1·03
4·13 Maus & Wilhelm(1970)
30·5 Ramu & Tullis (1976)
Present Work Shown in Fig (4 – 21)
$-\frac{1}{\sqrt{f}}$
$Re\sqrt{f}$
0
5
10
15
20
25
30
10^3
10^4
10^5

FIG (4-26)

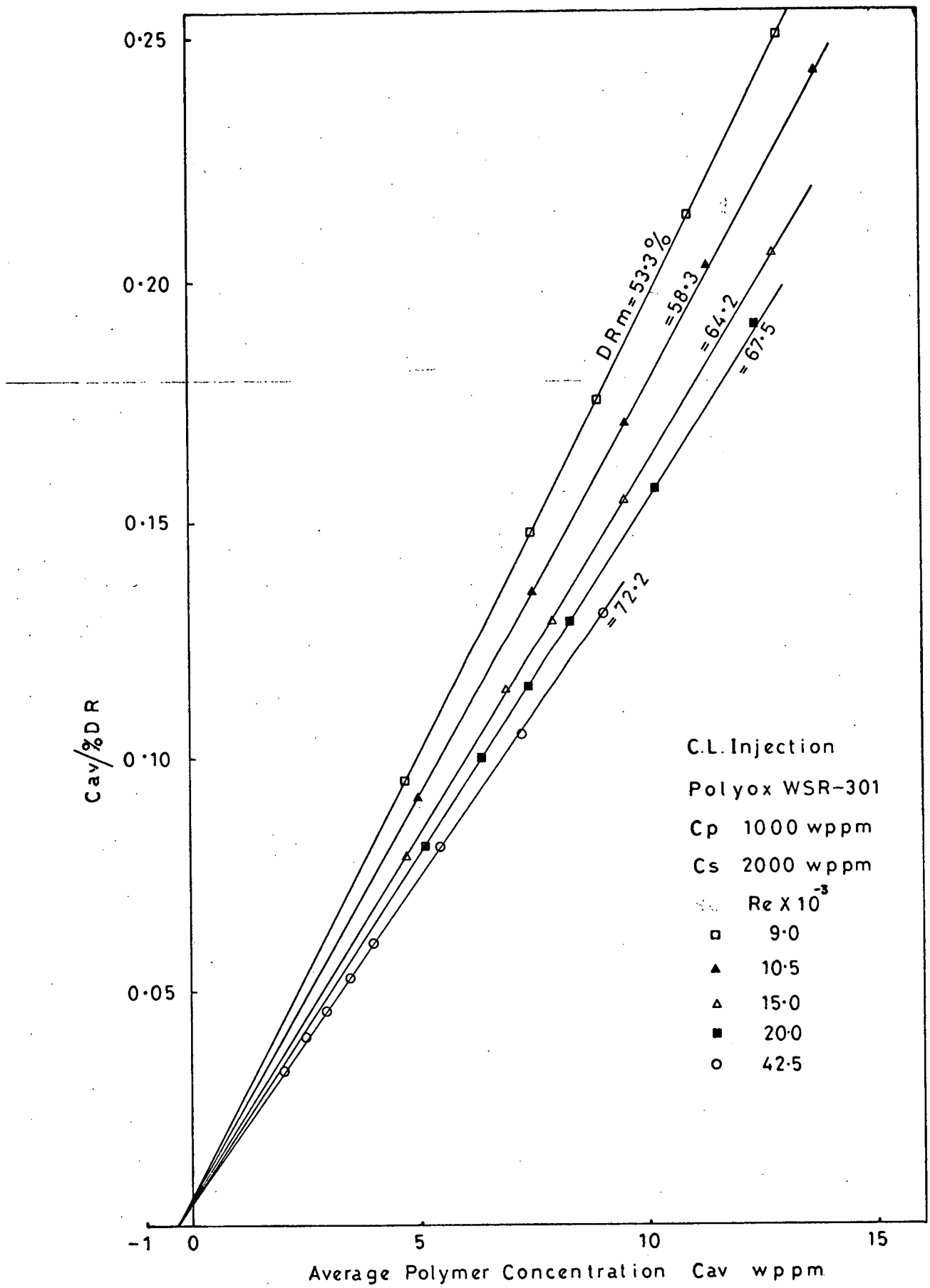
0·25
0·20
0·15
0·10
0·05
Cav/%DR
DRm=53·3%
=58·3
=64·2
=67·5
=72·2
C.L. Injection
Polyox WSR-301
Cp 1000 wppm
Cs 2000 wppm
Re X 10⁻³
9·0
10·5
15·0
20·0
42·5
-1
0
5
10
15
Average Polymer Concentration Cav wppm

FIG (4-27)

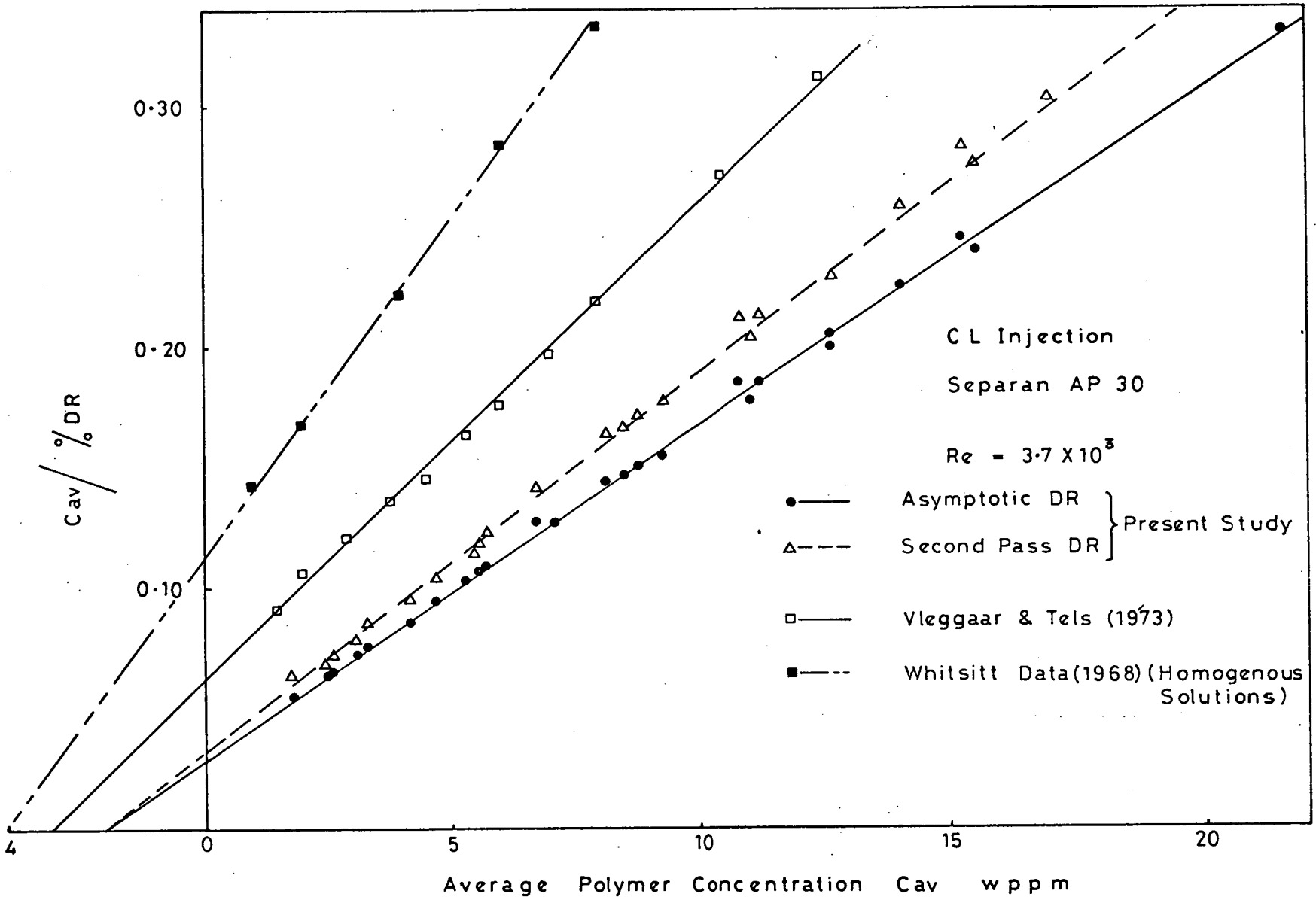
0·30
0·20
0·10
Cav / %DR
4
0
5
10
15
20
Average Polymer Concentration Cav w p p m
C L Injection
Separan AP 30
Re = 3·7 X 10³
Asymptotic DR
Second Pass DR
Present Study
Vleggaar & Tels (1973)
Whitsitt Data(1968)(Homogenous Solutions)

FIG (4 - 28)

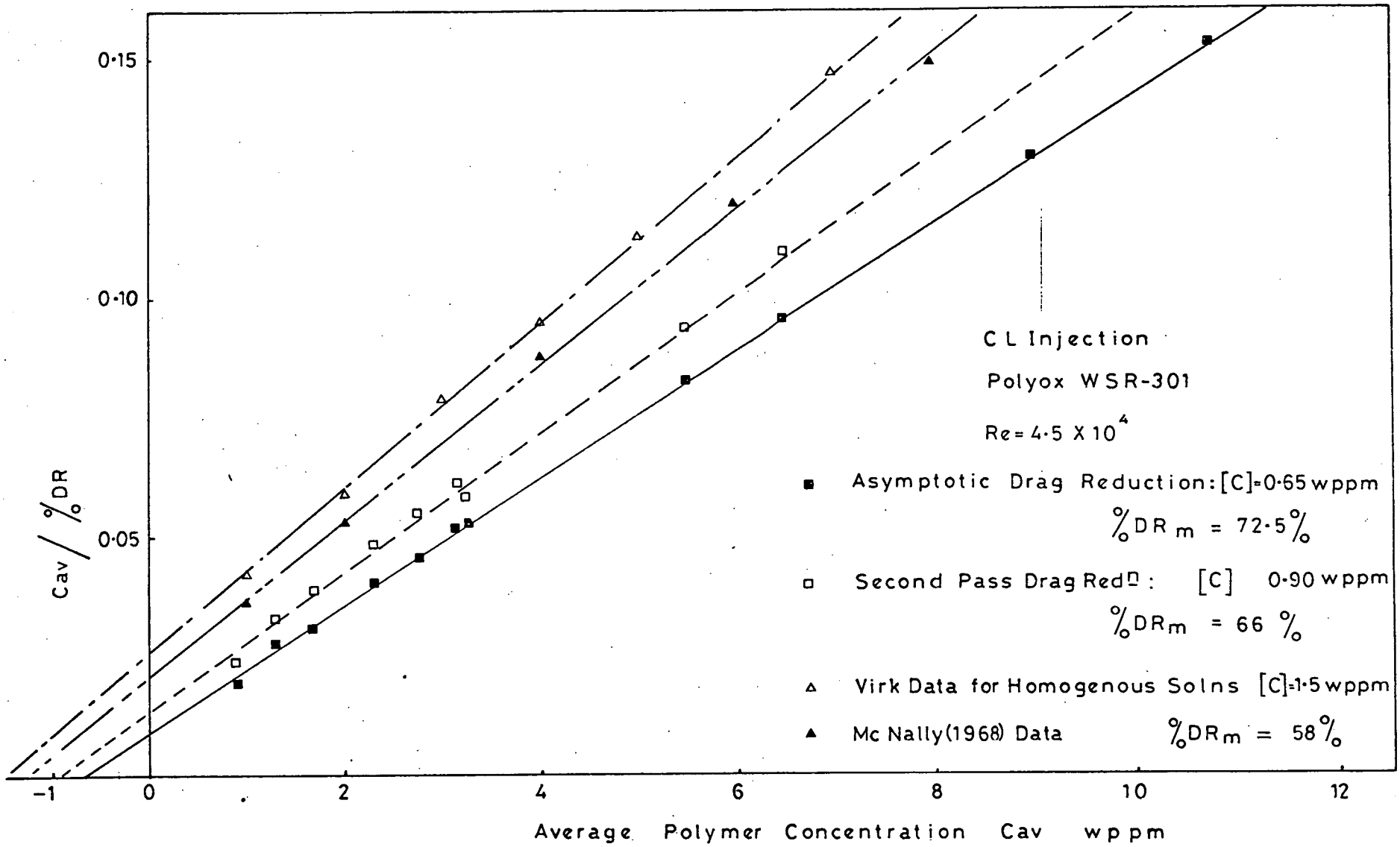
0·15
0·10
0·05
Cav / %DR
−1
0
2
4
6
8
10
12
Average Polymer Concentration Cav wppm
C L Injection
Polyox WSR-301
Re = 4·5 X 10^4
Asymptotic Drag Reduction: [C] = 0·65 wppm
%DR m = 72·5%
Second Pass Drag Red□ : [C] 0·90 wppm
%DRm = 66 %
Virk Data for Homogenous Solns [C] = 1·5 wppm
Mc Nally (1968) Data
%DRm = 58%

FIG (4 - 29)

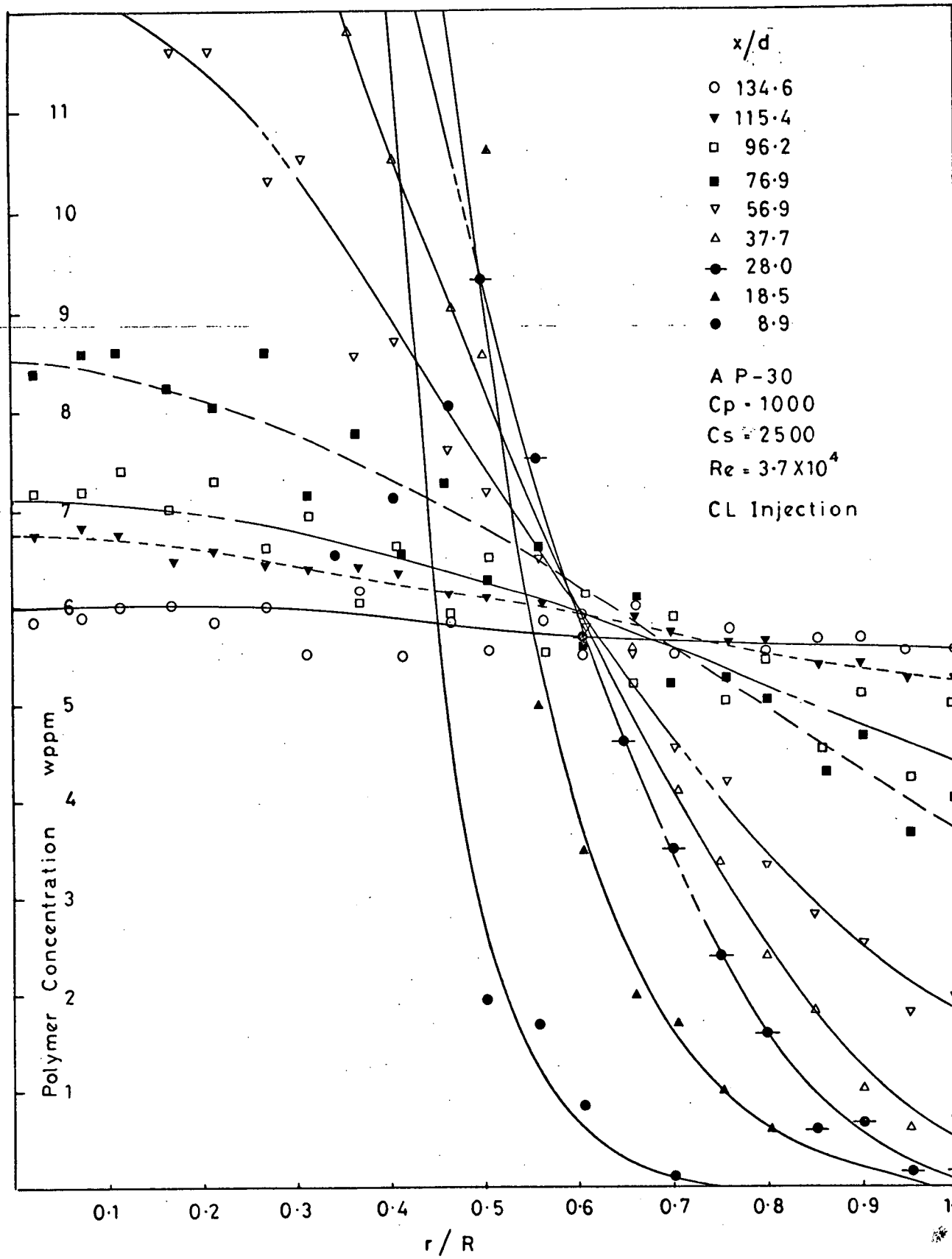
x/d
134·6
115·4
96·2
76·9
56·9
37·7
28·0
18·5
8·9
A P-30
Cp - 1000
Cs - 2500
Re = 3·7 X10⁴
CL Injection
Polymer Concentration wppm
r / R
0·1
0·2
0·3
0·4
0·5
0·6
0·7
0·8
0·9
1·0
1
2
3
4
5
6
7
8
9
10
11

FIG (4 - 30)

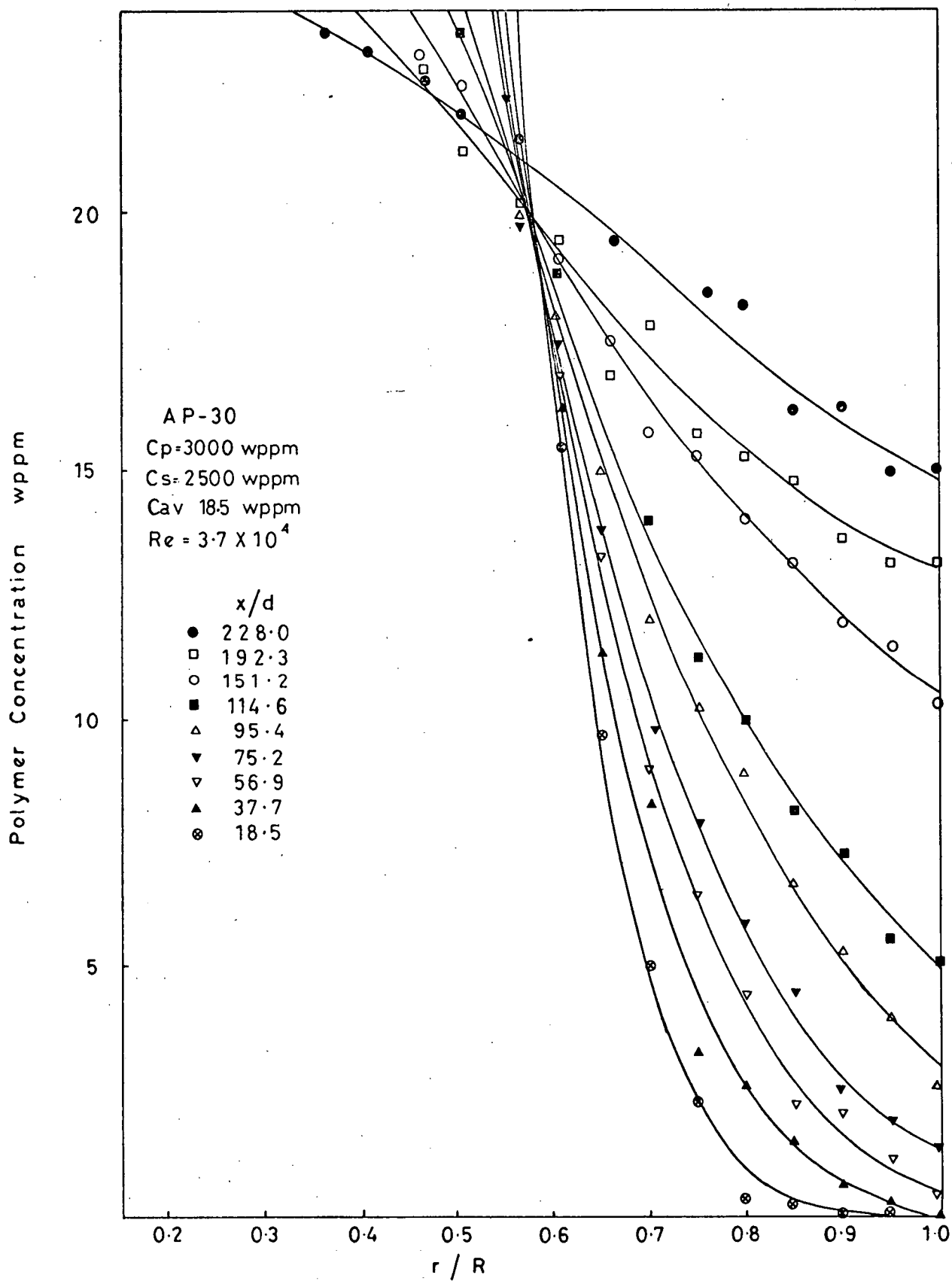
AP-30
Cp=3000 wppm
Cs=2500 wppm
Cav 18·5 wppm
Re = 3·7 X 10⁴
x/d
228·0
192·3
151·2
114·6
95·4
75·2
56·9
37·7
18·5
Polymer Concentration wppm
20
15
10
5
0·2
0·3
0·4
0·5
0·6
0·7
0·8
0·9
1·0
r / R

FIG (4 - 31)

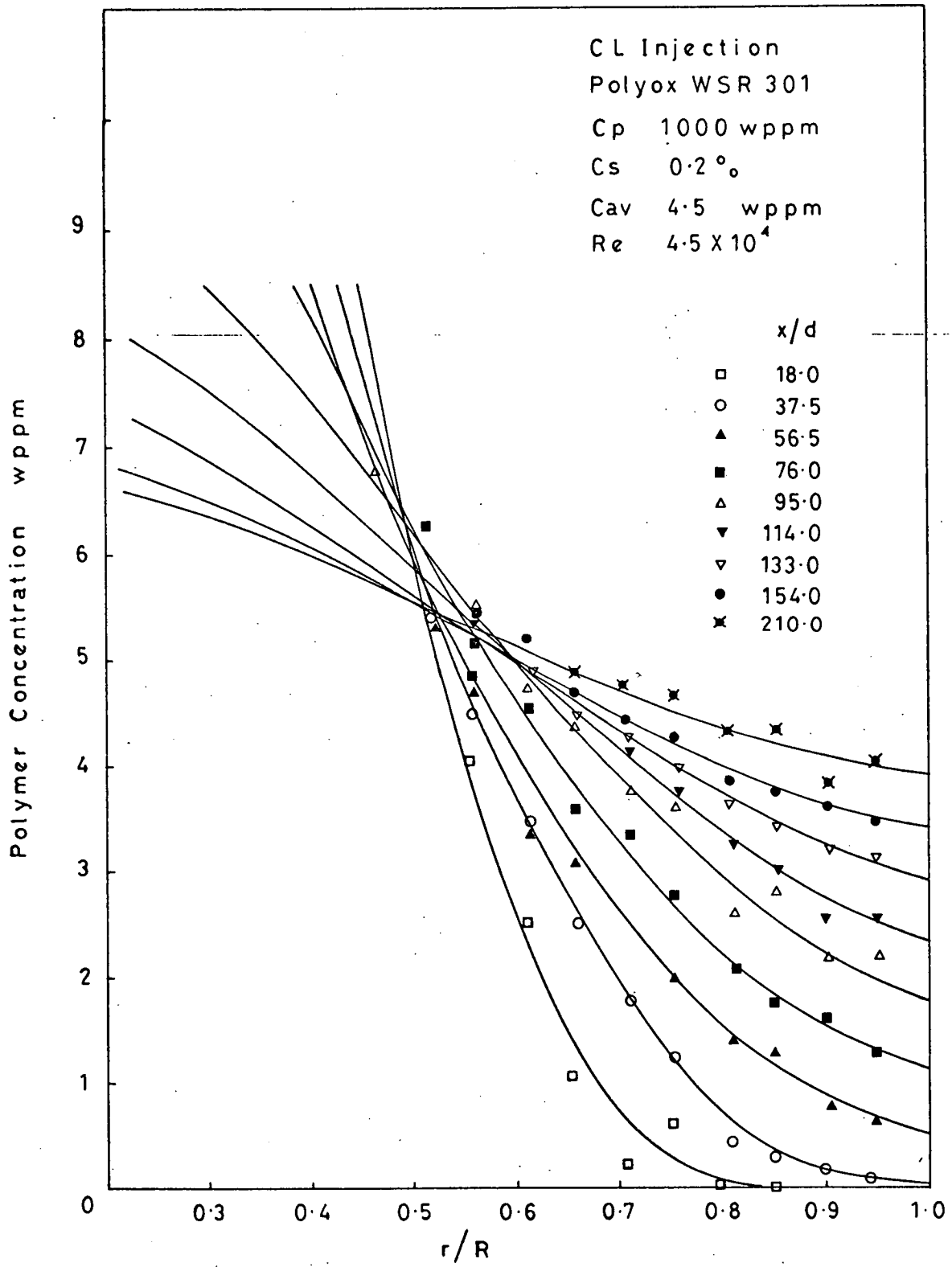
CL Injection
Polyox WSR 301
Cp 1000 wppm
Cs 0·2 %
Cav 4·5 wppm
Re 4·5 X 10⁴
x/d
18·0
37·5
56·5
76·0
95·0
114·0
133·0
154·0
210·0
Polymer Concentration wppm
r/R
0
1
2
3
4
5
6
7
8
9
0·3
0·4
0·5
0·6
0·7
0·8
0·9
1·0

FIG (4 – 32)

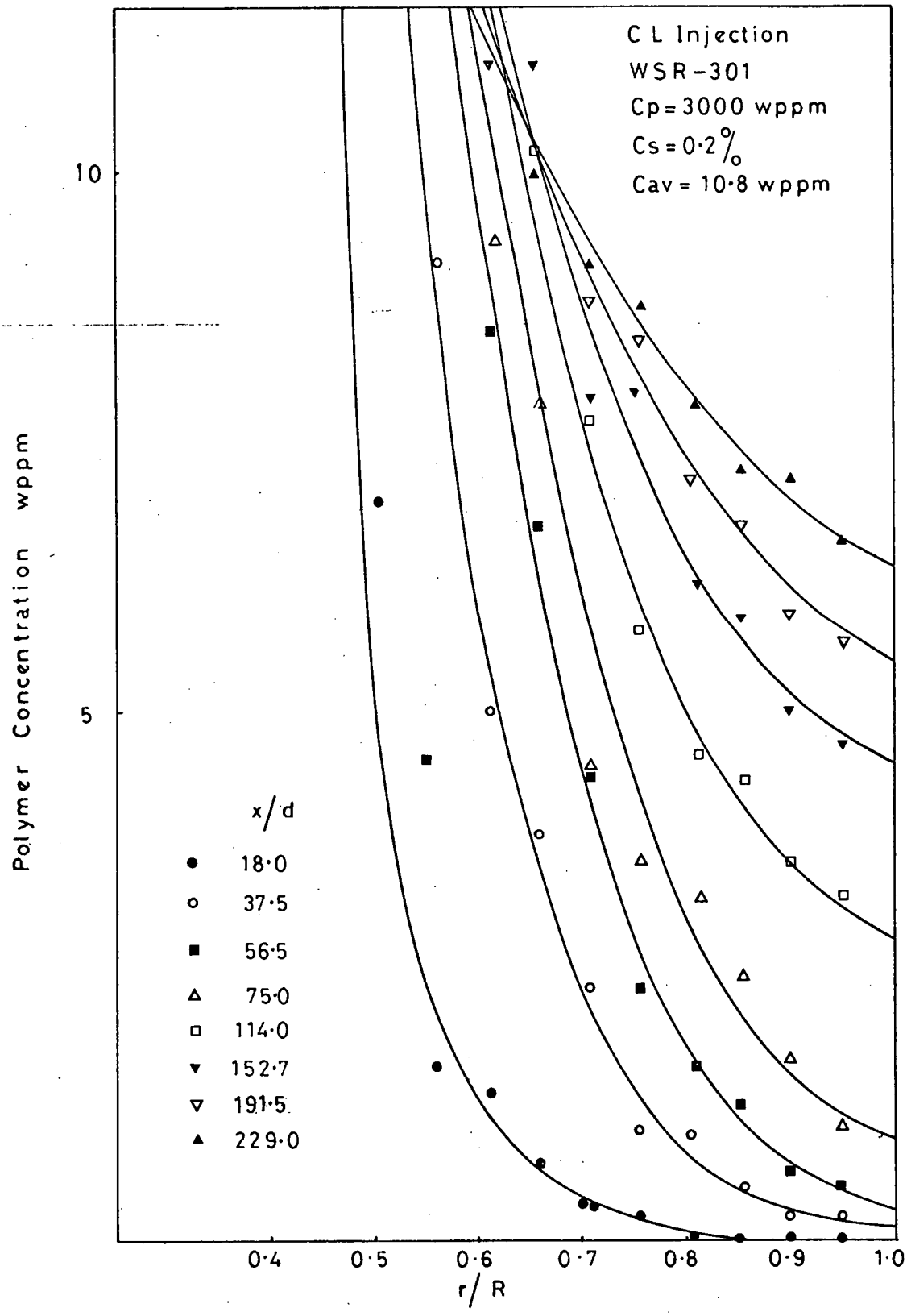
C L Injection
WSR-301
Cp = 3000 wppm
Cs = 0·2%
Cav = 10·8 wppm
Polymer Concentration wppm
10
5
x/d
18·0
37·5
56·5
75·0
114·0
152·7
191·5
229·0
0·4
0·5
0·6
0·7
0·8
0·9
1·0
r/R

FIG (4 - 33)

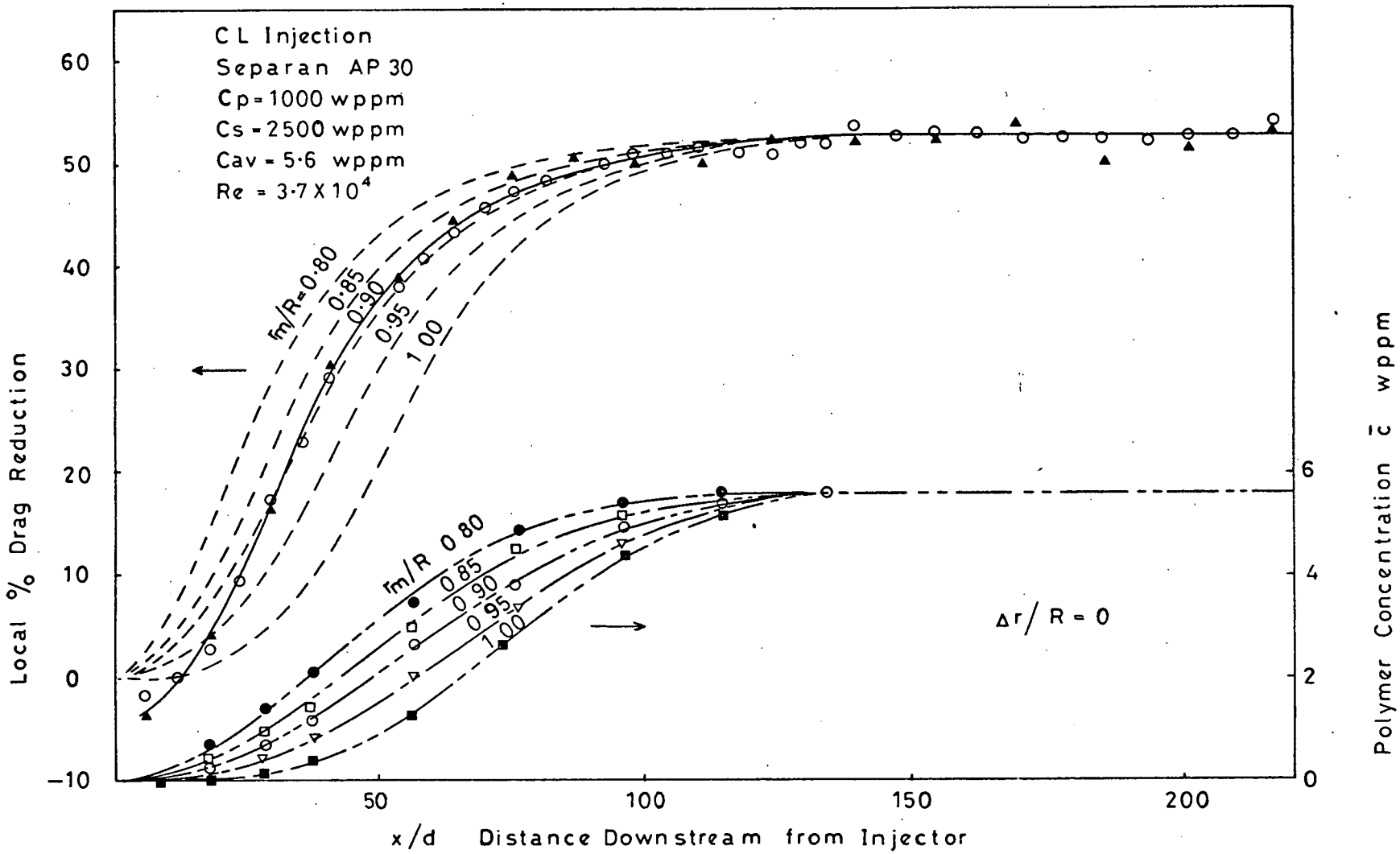
CL Injection
Separan AP 30
Cp = 1000 wppm
Cs = 2500 wppm
Cav = 5·6 wppm
Re = 3·7 X 10⁴
rm/R = 0·80
0·85
0·90
0·95
1·00
rm/R 0·80
0·85
0·90
0·95
1·00
Δr/R = 0
Local % Drag Reduction
Polymer Concentration c̄ wppm
x/d Distance Downstream from Injector
60
50
40
30
20
10
0
−10
6
4
2
0
50
100
150
200

FIG (4 — 34)

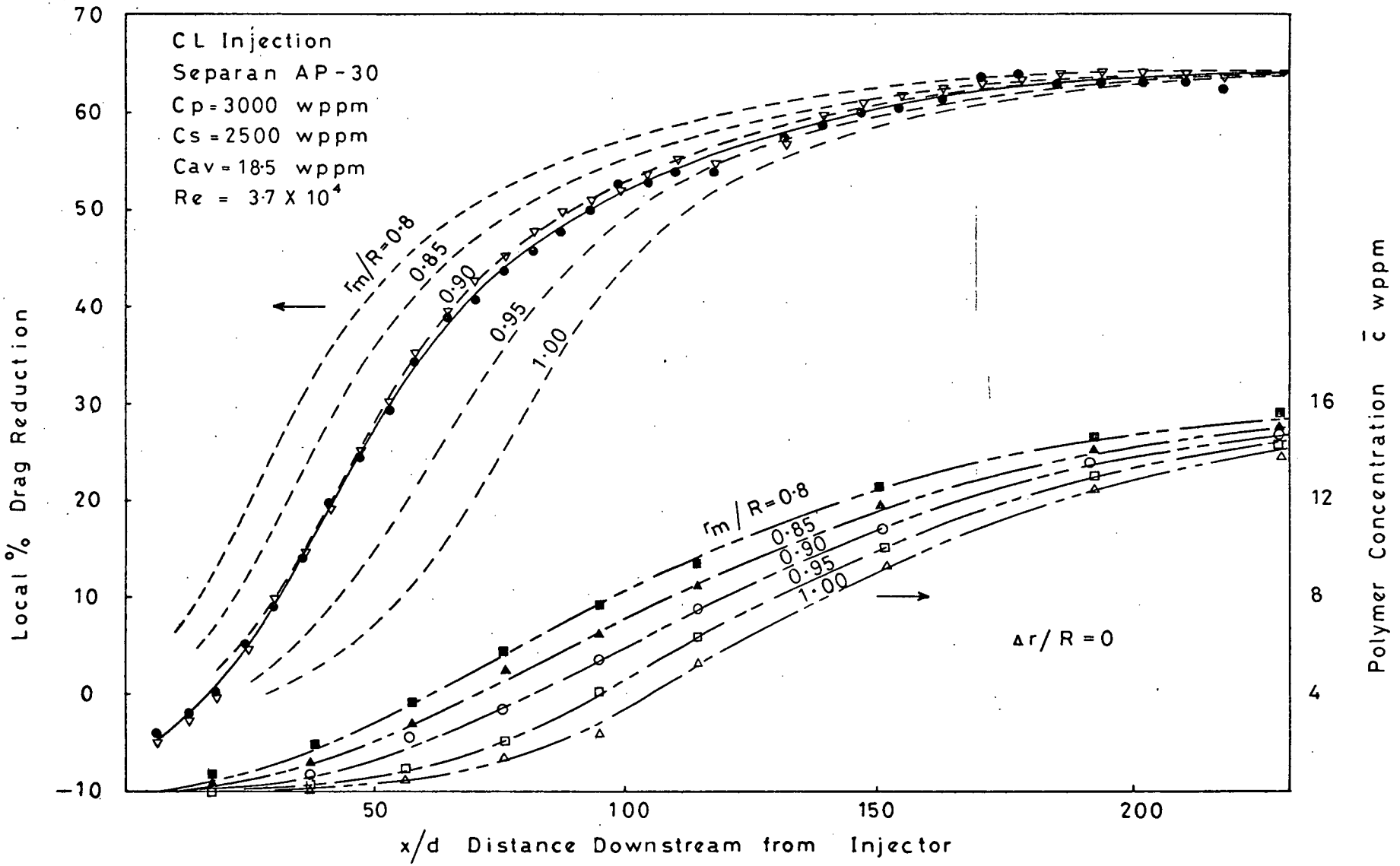
CL Injection
Separan AP-30
Cp = 3000 wppm
Cs = 2500 wppm
Cav = 18·5 wppm
Re = 3·7 X 10⁴
rm/R = 0·8
0·85
0·90
0·95
1·00
rm/R = 0·8
0·85
0·90
0·95
1·00
Δr/R = 0
Local % Drag Reduction
Polymer Concentration c̄ wppm
x/d Distance Downstream from Injector
70
60
50
40
30
20
10
0
−10
16
12
8
4
50
100
150
200

FIG (4 — 35)

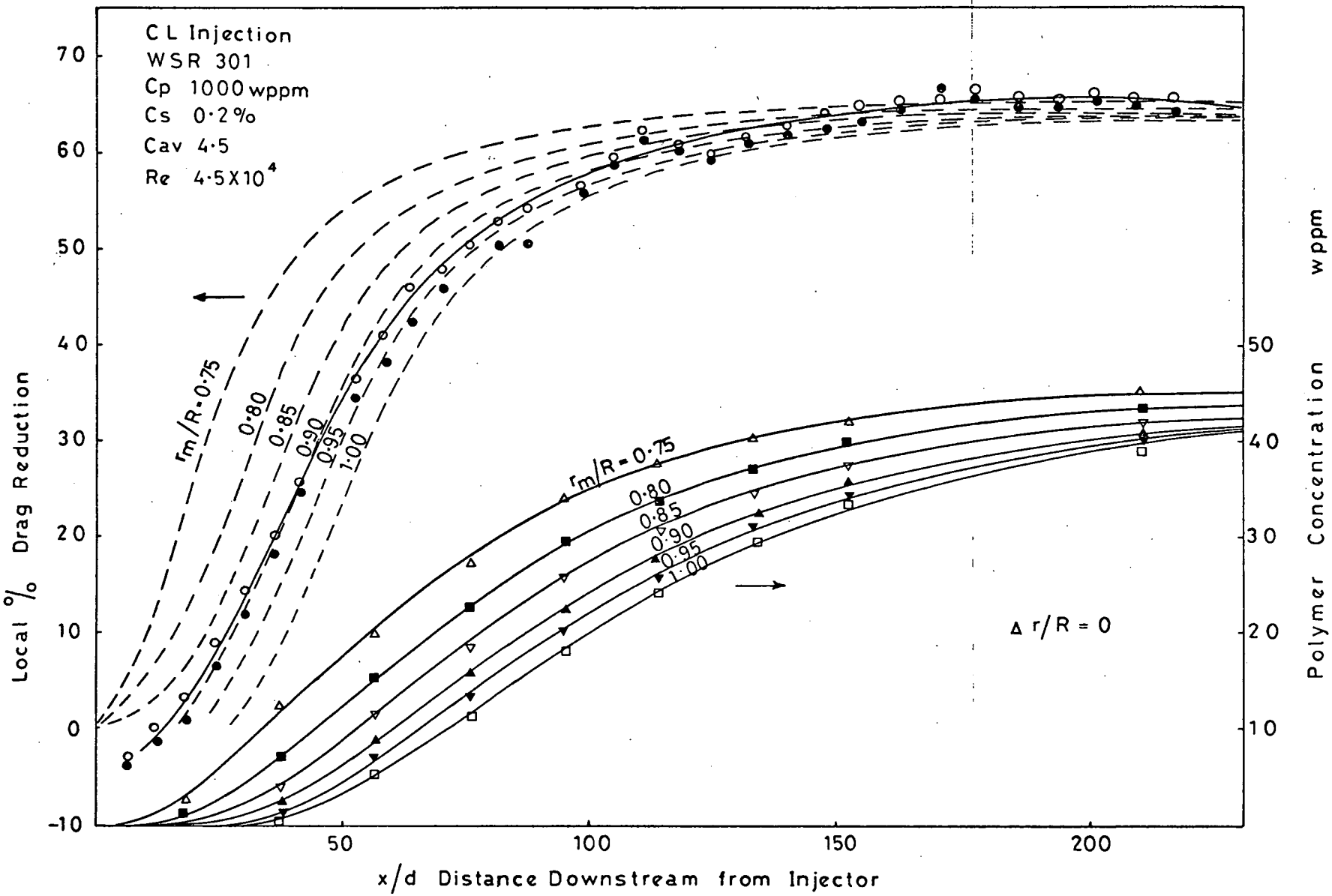
C L Injection
WSR 301
Cp 1000 wppm
Cs 0·2%
Cav 4·5
Re 4·5X10⁴
rm/R·0·75
0·80
0·85
0·90
0·95
1·00
rm/R = 0·75
0·80
0·85
0·90
0·95
1·00
Δ r/R = 0
Local % Drag Reduction
Polymer Concentration wppm
x/d Distance Downstream from Injector
70
60
50
40
30
20
10
0
-10
50
100
150
200
50
40
30
20
10

FIG (4 – 36)

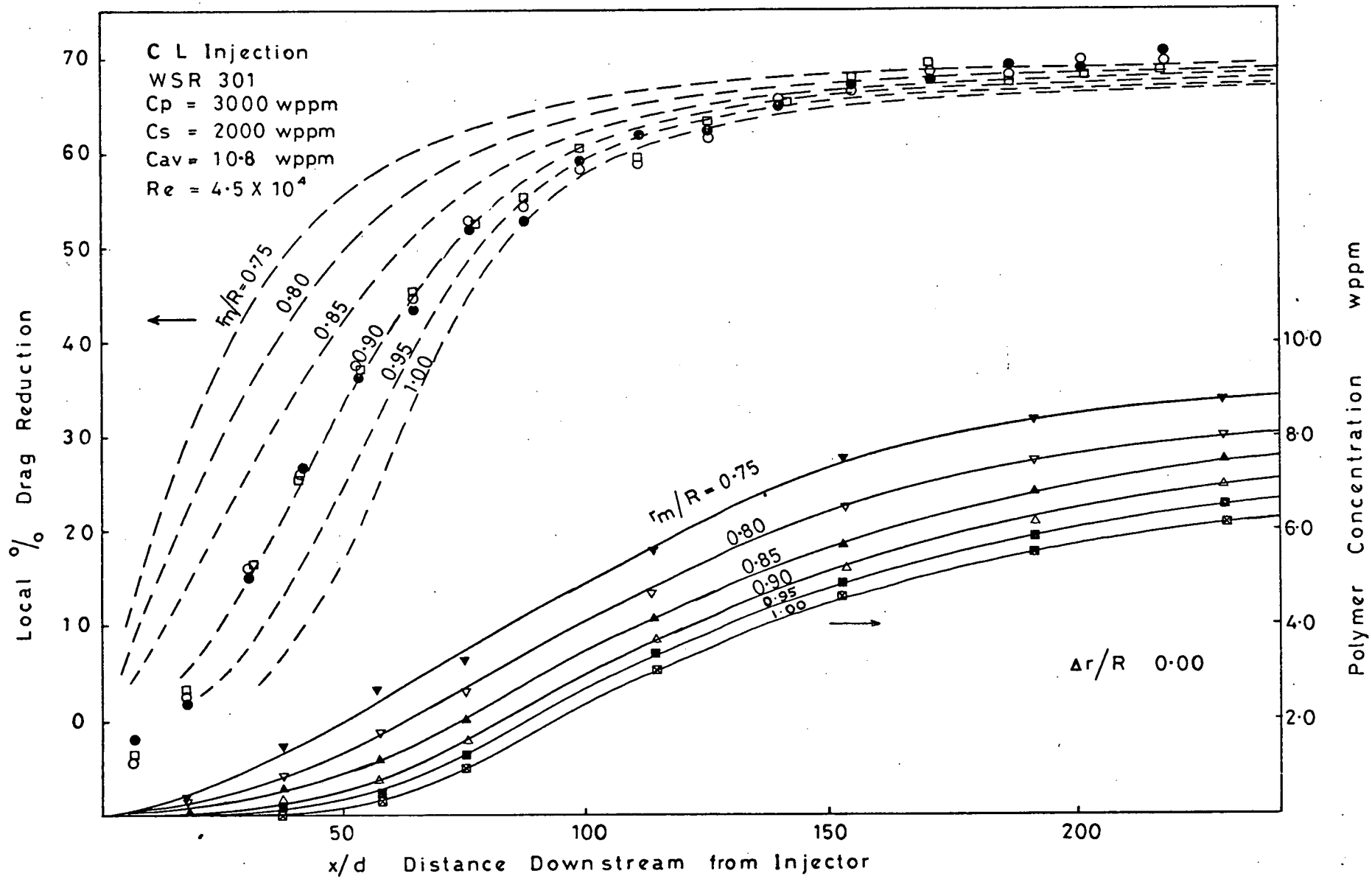
C L Injection
WSR 301
Cp = 3000 wppm
Cs = 2000 wppm
Cav = 10·8 wppm
Re = 4·5 X 10⁴
rm/R=0·75
0·80
0·85
0·90
0·95
1·00
Δr/R 0·00
Local % Drag Reduction
Polymer Concentration wppm
x/d Distance Downstream from Injector
0
10
20
30
40
50
60
70
2·0
4·0
6·0
8·0
10·0
50
100
150
200

FIG (4 - 37)

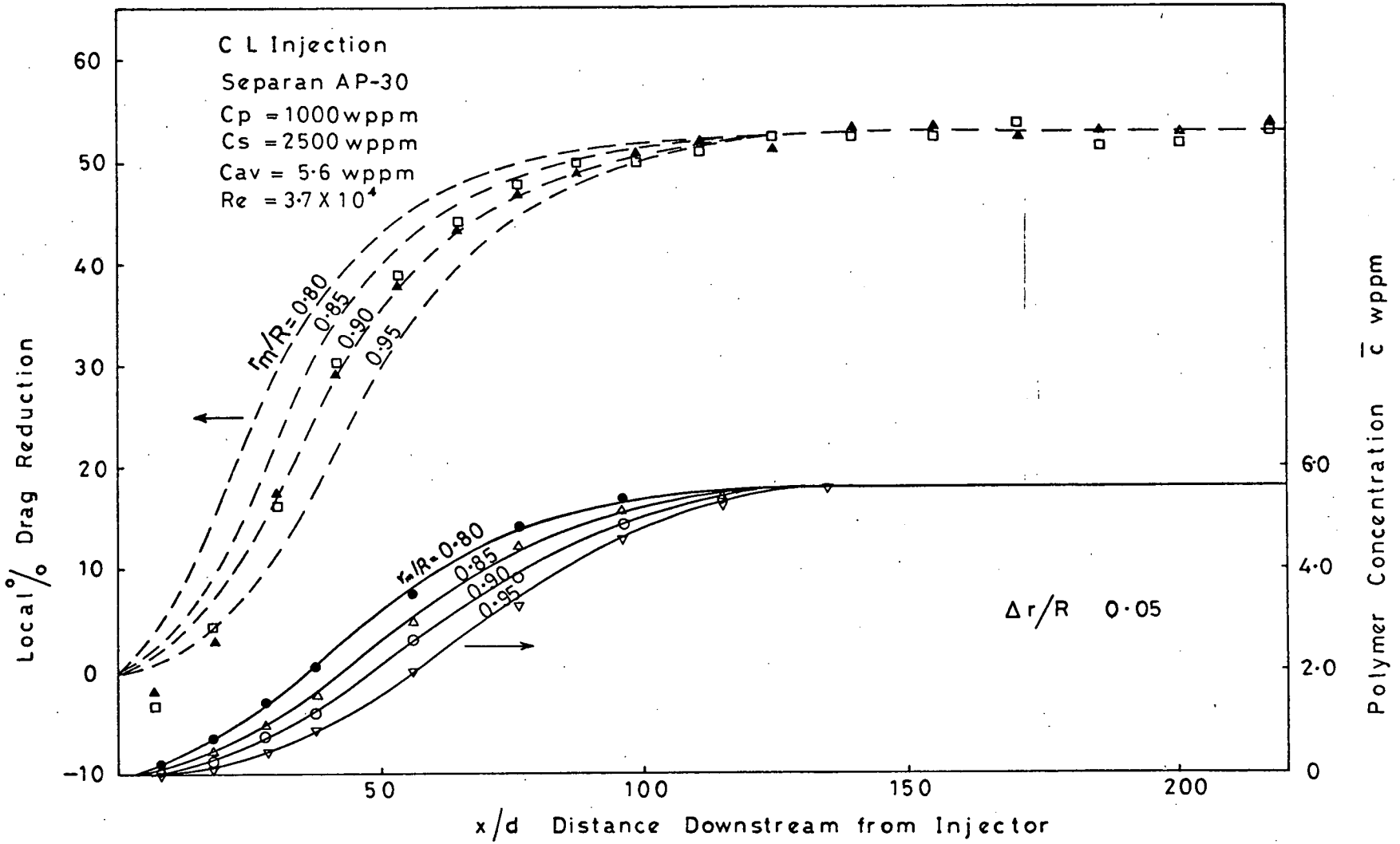
C L Injection
Separan AP-30
Cp = 1000 wppm
Cs = 2500 wppm
Cav = 5·6 wppm
Re = 3·7 X 10⁴
rm/R = 0·80
0·85
0·90
0·95
Δr/R 0·05
Local % Drag Reduction
Polymer Concentration c̄ wppm
x/d Distance Downstream from Injector
60
50
40
30
20
10
0
−10
6·0
4·0
2·0
0
50
100
150
200

FIG (4 - 38)

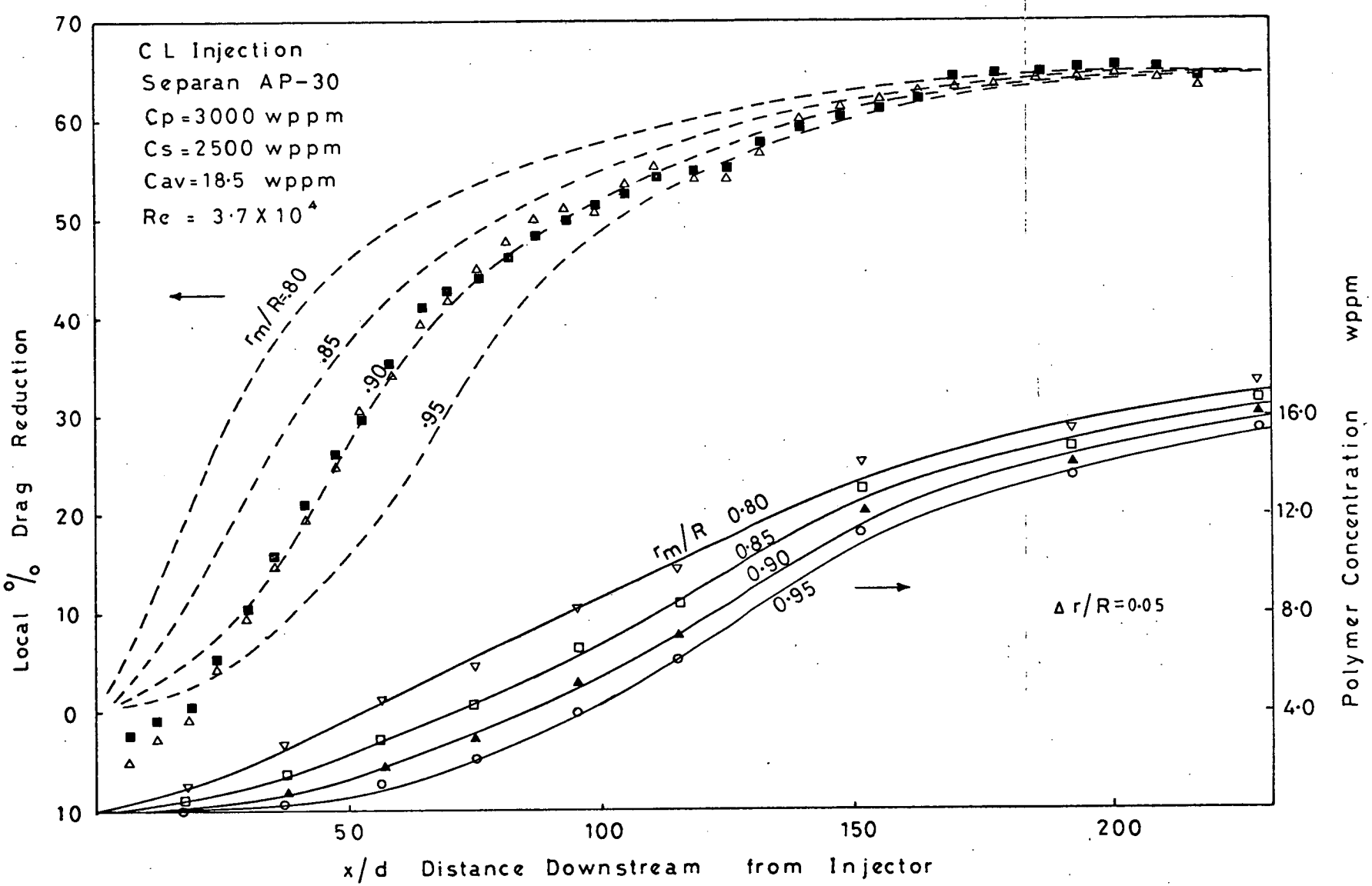
C L Injection
Separan AP-30
Cp = 3000 wppm
Cs = 2500 wppm
Cav = 18·5 wppm
Re = 3·7 X 10⁴
rm/R=80
·85
·90
·95
rm/R 0·80
0·85
0·90
0·95
Δ r/R = 0·05
Local % Drag Reduction
Polymer Concentration wppm
x/d Distance Downstream from Injector
70
60
50
40
30
20
10
0
10
16·0
12·0
8·0
4·0
50
100
150
200

FIG (4-39)

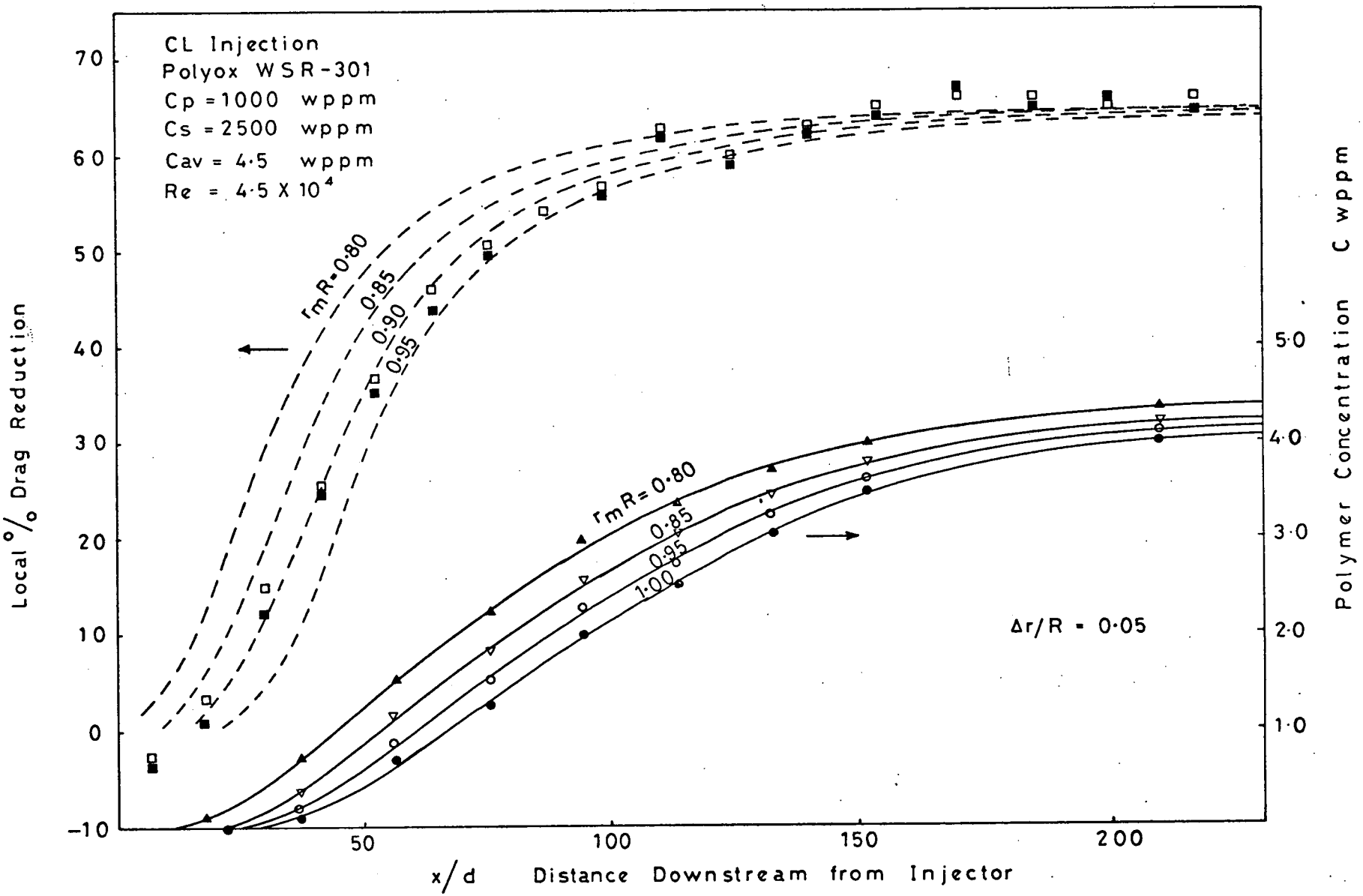
CL Injection
Polyox WSR-301
Cp = 1000 wppm
Cs = 2500 wppm
Cav = 4·5 wppm
Re = 4·5 X 10⁴
rmR=0·80
0·85
0·90
0·95
rmR=0·80
0·85
0·95
1·00
Δr/R = 0·05
Local % Drag Reduction
Polymer Concentration C wppm
x/d Distance Downstream from Injector
70
60
50
40
30
20
10
0
-10
5·0
4·0
3·0
2·0
1·0
50
100
150
200

FIG (4 – 40)

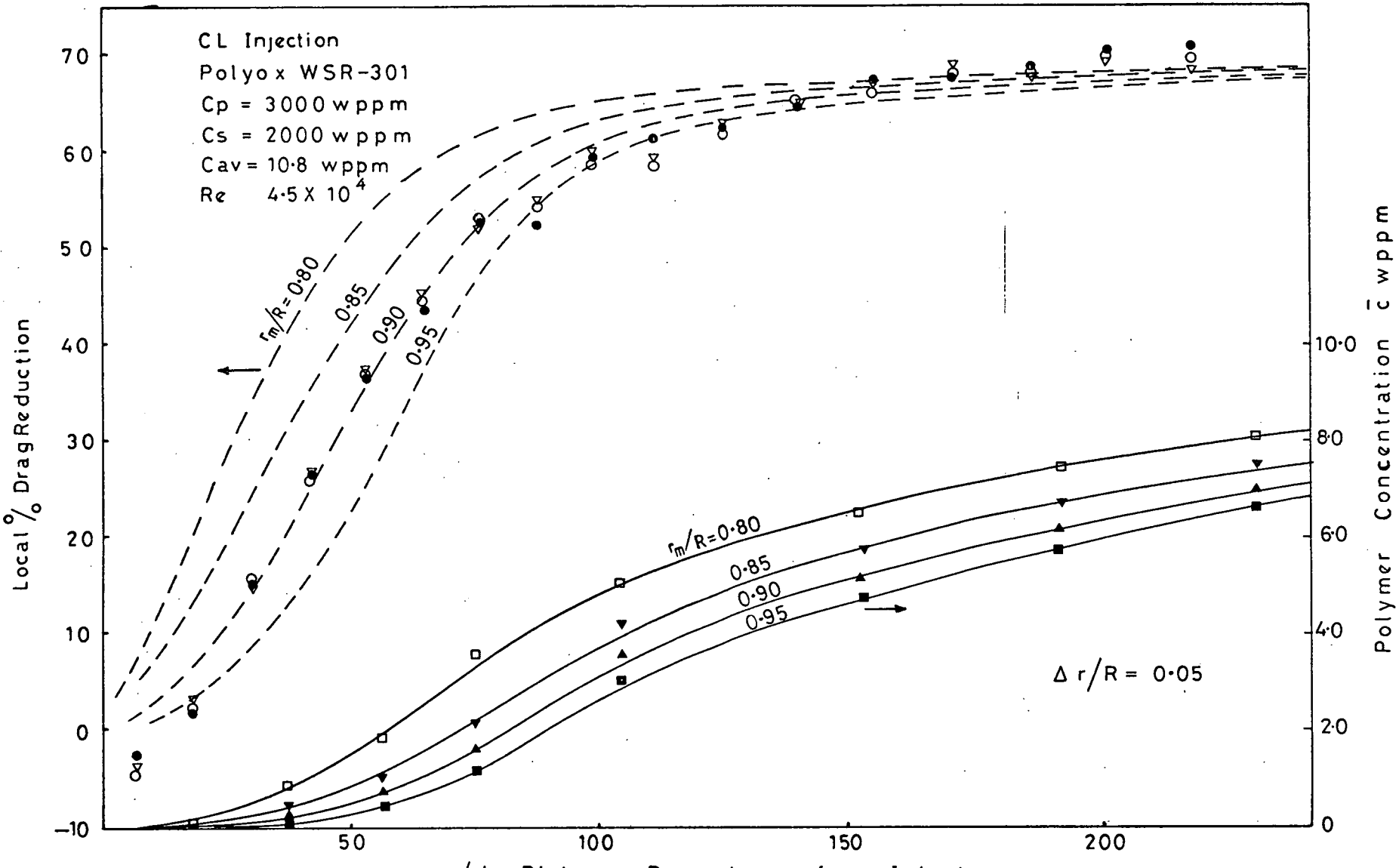
CL Injection
Polyox WSR-301
Cp = 3000 wppm
Cs = 2000 wppm
Cav = 10·8 wppm
Re 4·5 X 10⁴
rm/R = 0·80
0·85
0·90
0·95
Δ r/R = 0·05
Local % Drag Reduction
Polymer Concentration c̄ wppm
x/d Distance Downstream from Injector
70
60
50
40
30
20
10
0
−10
10·0
8·0
6·0
4·0
2·0
0
50
100
150
200

FIG (4 – 41)

	Polymer	Cp wppm
●	WSR 301	3000
○	WSR 301	1000
□	AP 30	1000
△	AP 30	3000

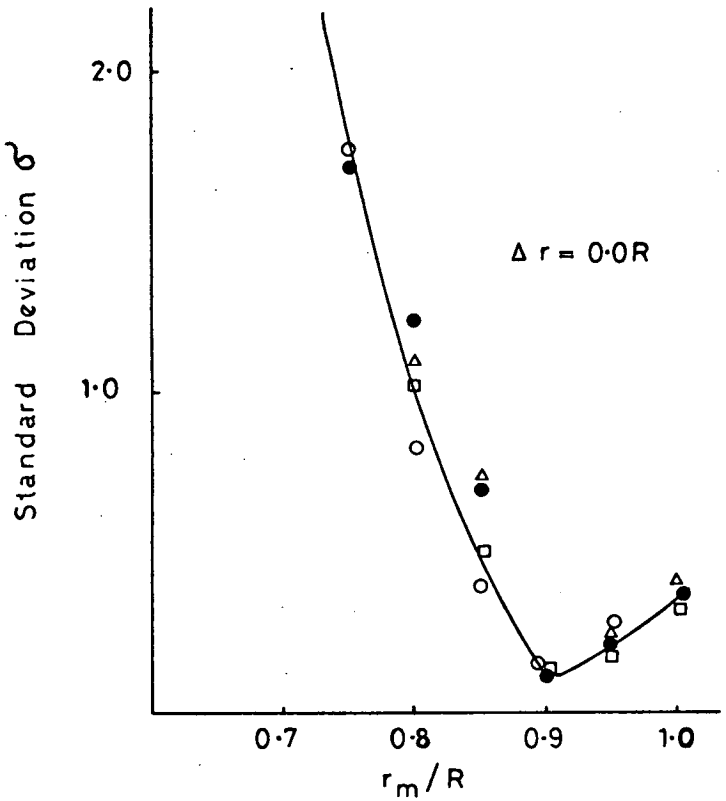

FIG (4 – 42)

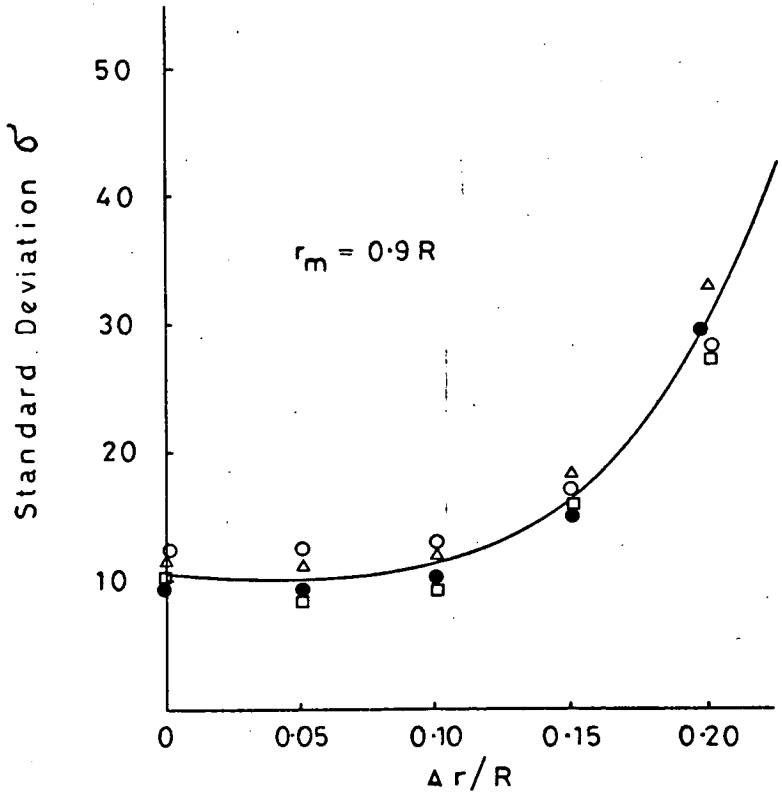

FIG (4 – 43)

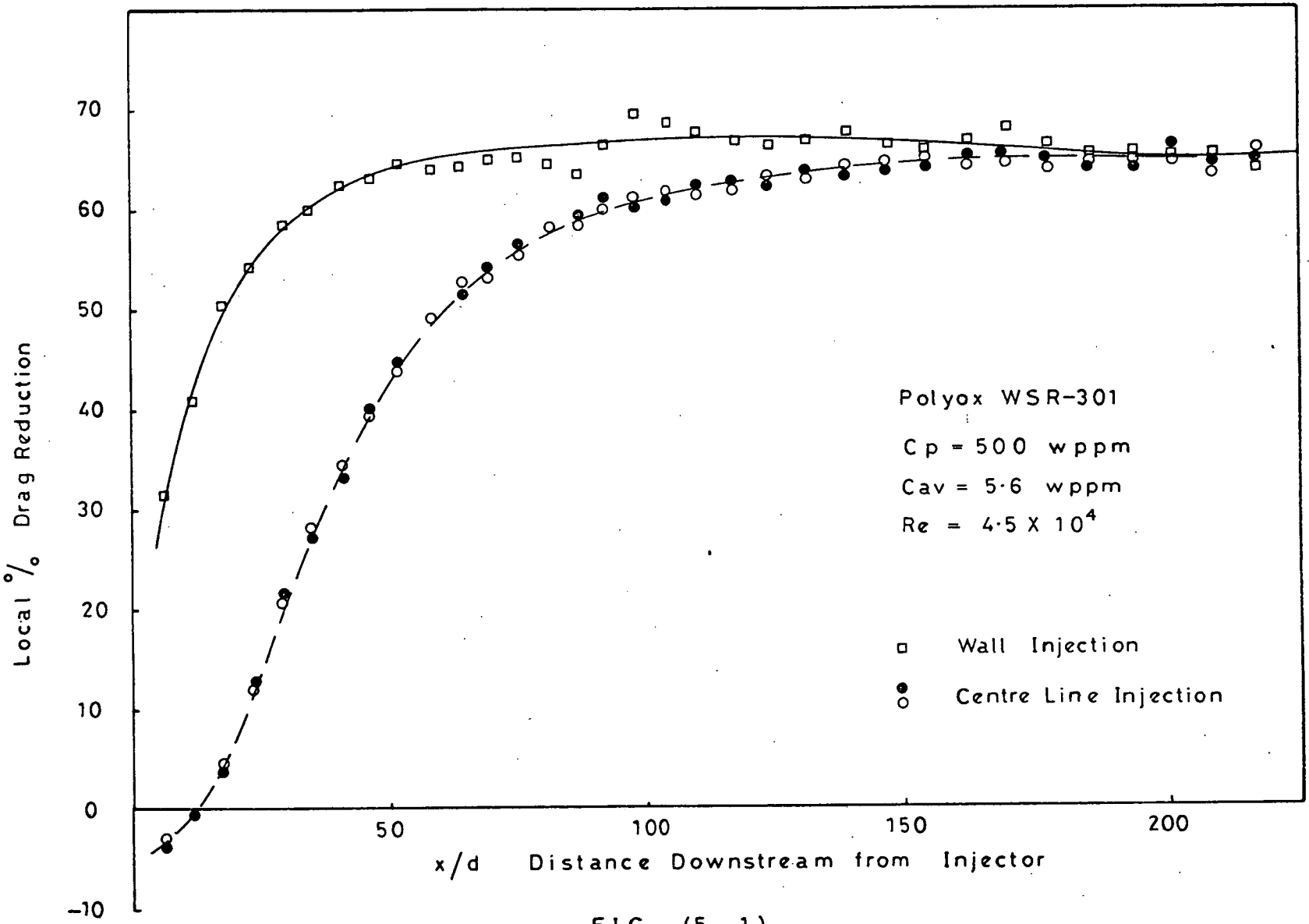
70
60
50
40
30
20
10
0
-10
Local % Drag Reduction
50
100
150
200
x/d Distance Downstream from Injector
Polyox WSR-301
Cp = 500 wppm
Cav = 5·6 wppm
Re = 4·5 X 10^4
Wall Injection
Centre Line Injection

FIG (5-1)

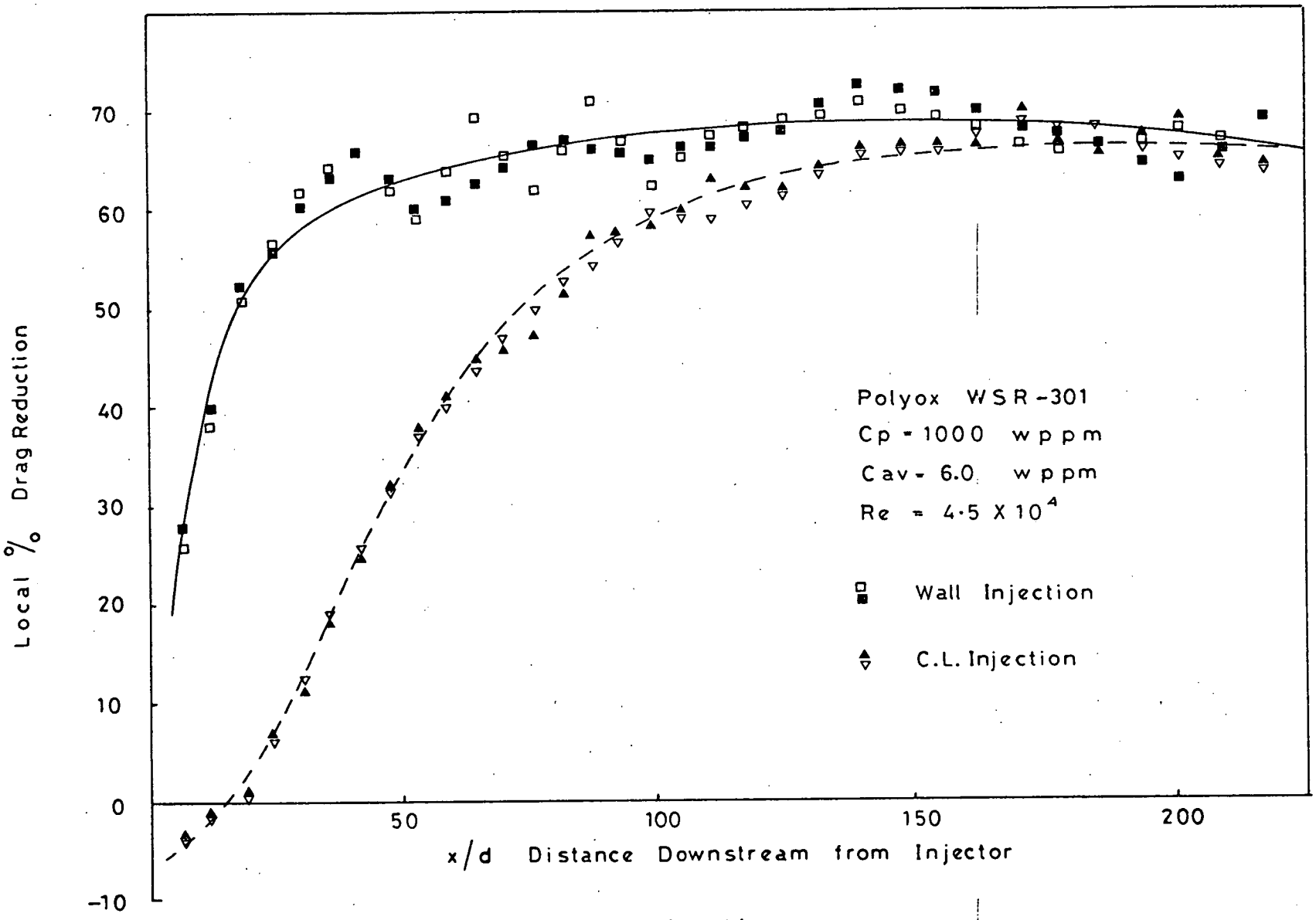
Local % Drag Reduction
70
60
50
40
30
20
10
0
-10
50
100
150
200
x/d Distance Downstream from Injector
Polyox WSR-301
Cp = 1000 wppm
Cav = 6.0 wppm
Re = 4·5 X 10⁴
Wall Injection
C.L. Injection

FIG (5-2)

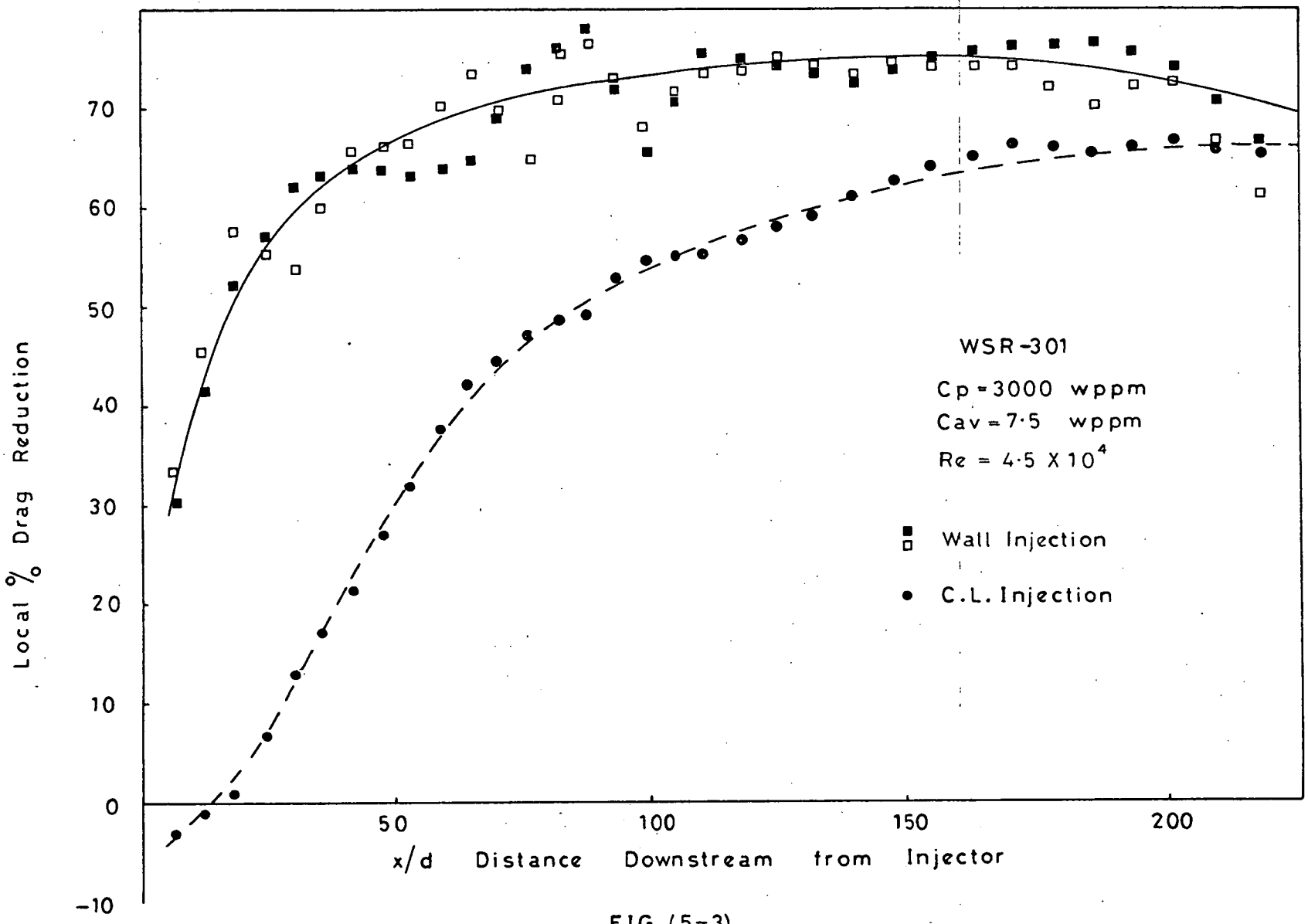
Local % Drag Reduction
70
60
50
40
30
20
10
0
-10
50
100
150
200
x/d Distance Downstream from Injector
WSR-301
Cp = 3000 wppm
Cav = 7·5 wppm
Re = 4·5 X 10^4
Wall Injection
C.L. Injection

FIG (5-3)

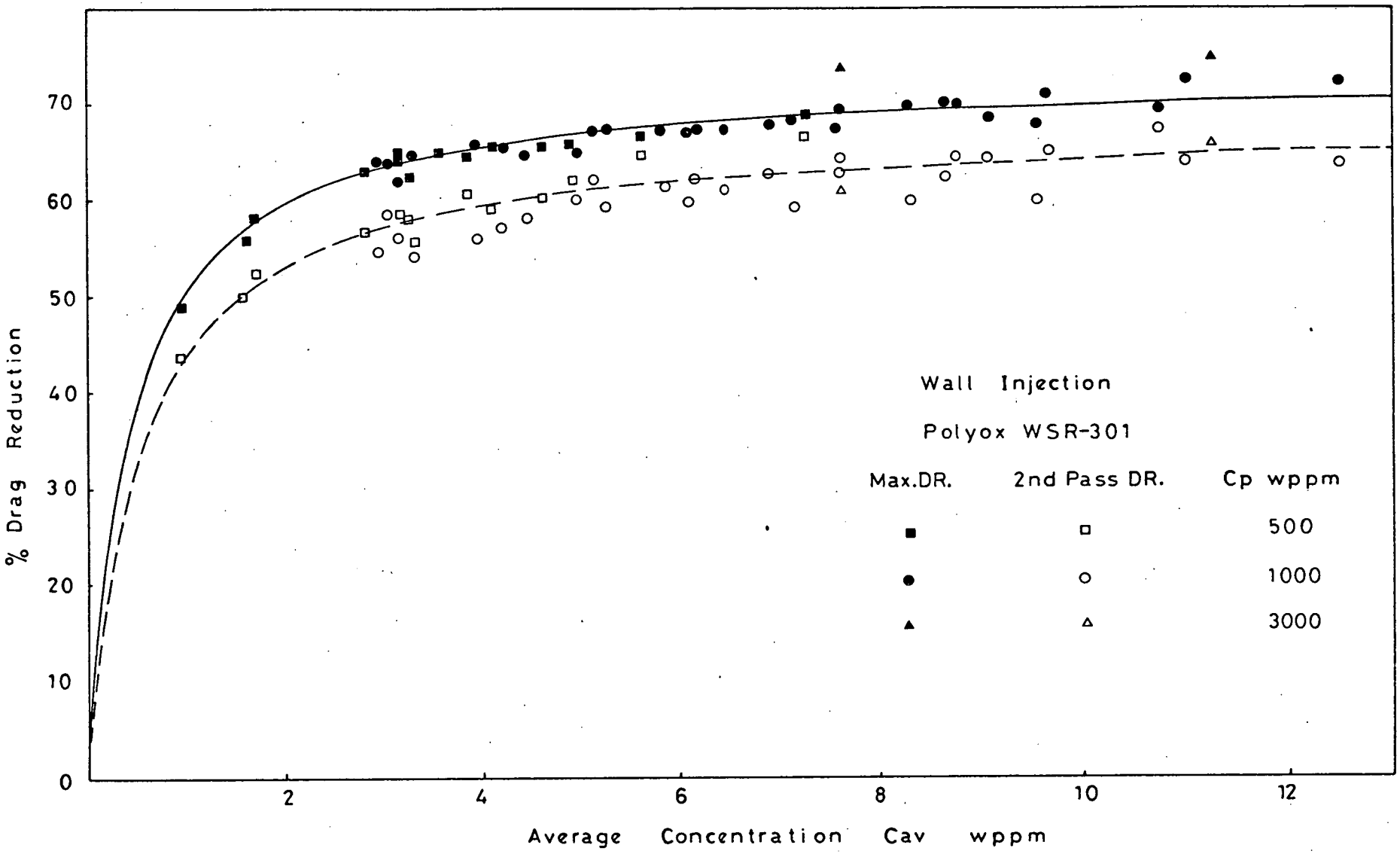
% Drag Reduction
0
10
20
30
40
50
60
70
2
4
6
8
10
12
Average Concentration Cav wppm
Wall Injection
Polyox WSR-301
Max.DR.
2nd Pass DR.
Cp wppm
500
1000
3000

FIG (5-4)

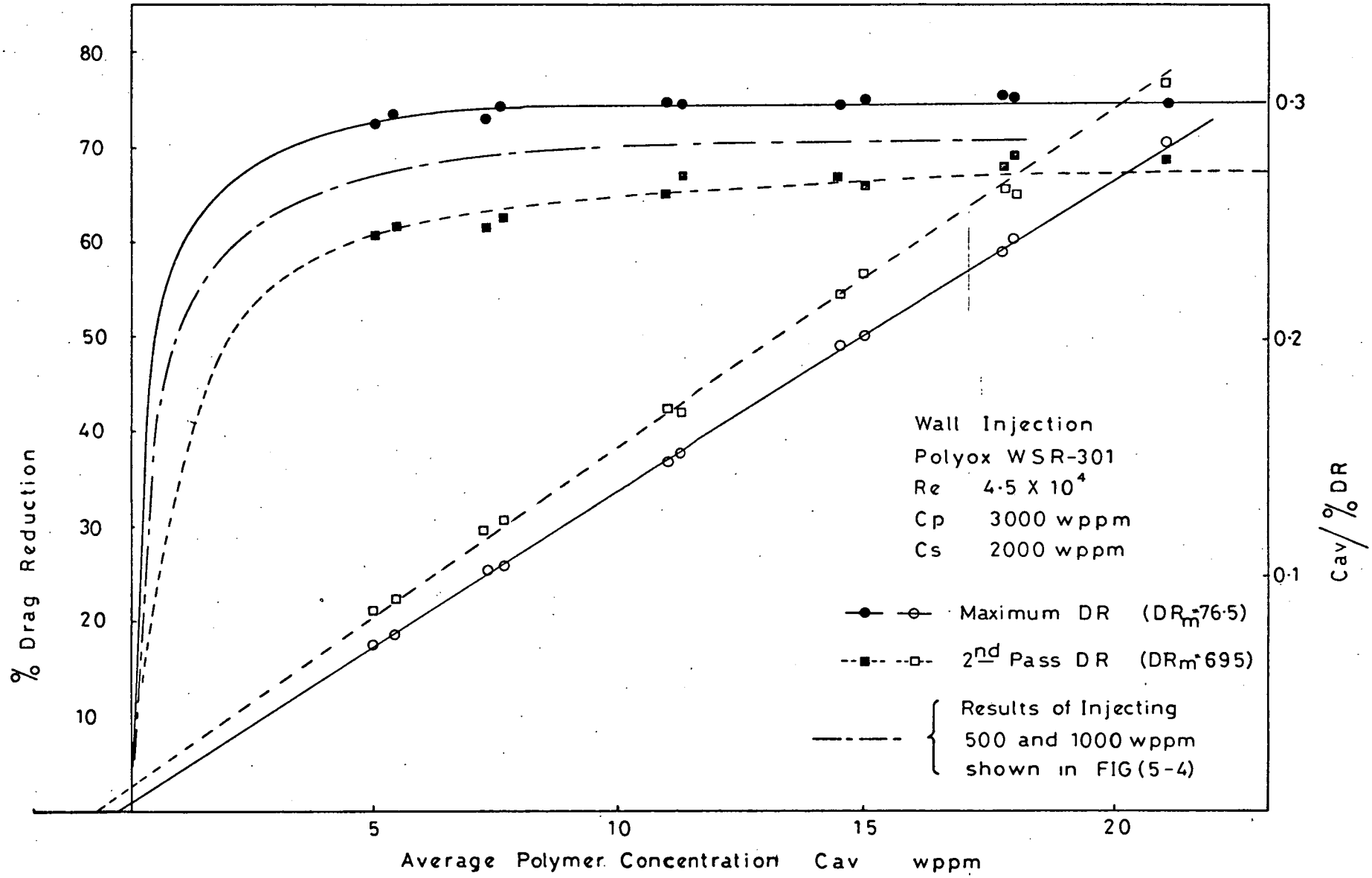
% Drag Reduction
80
70
60
50
40
30
20
10
5
10
15
20
Average Polymer Concentration Cav wppm
0·3
0·2
0·1
Cav/% DR
Wall Injection
Polyox WSR-301
Re 4·5 X 10⁴
Cp 3000 wppm
Cs 2000 wppm
Maximum DR (DRm=76·5)
2nd Pass DR (DRm=69·5)
Results of Injecting
500 and 1000 wppm
shown in FIG(5-4)

FIG (5-5)

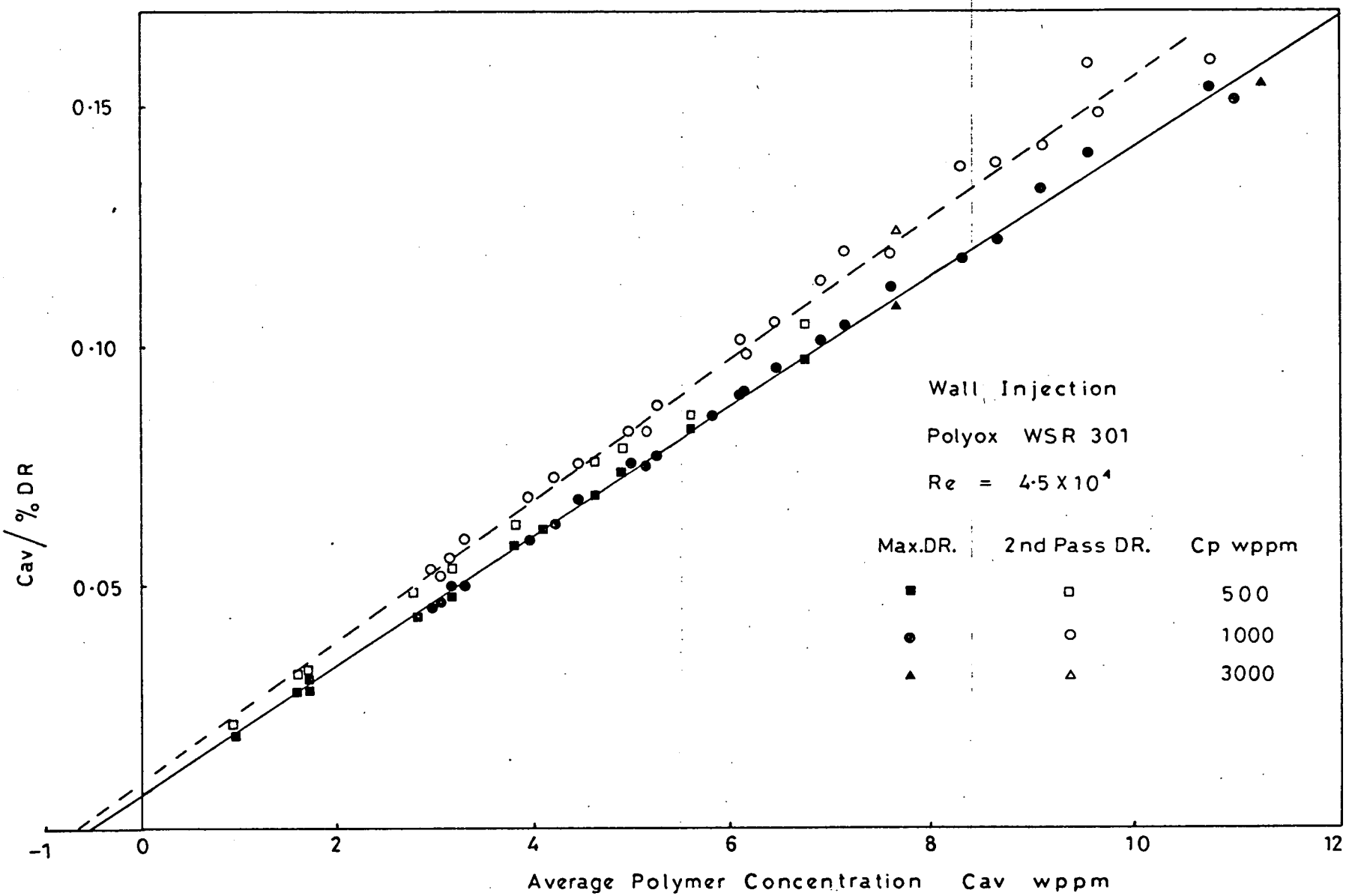
0·15
0·10
0·05
Cav / % DR
Wall Injection
Polyox WSR 301
Re = 4·5 X 10⁴
Max.DR.
2nd Pass DR.
Cp wppm
500
1000
3000
-1
0
2
4
6
8
10
12
Average Polymer Concentration Cav wppm

FIG (5−6)

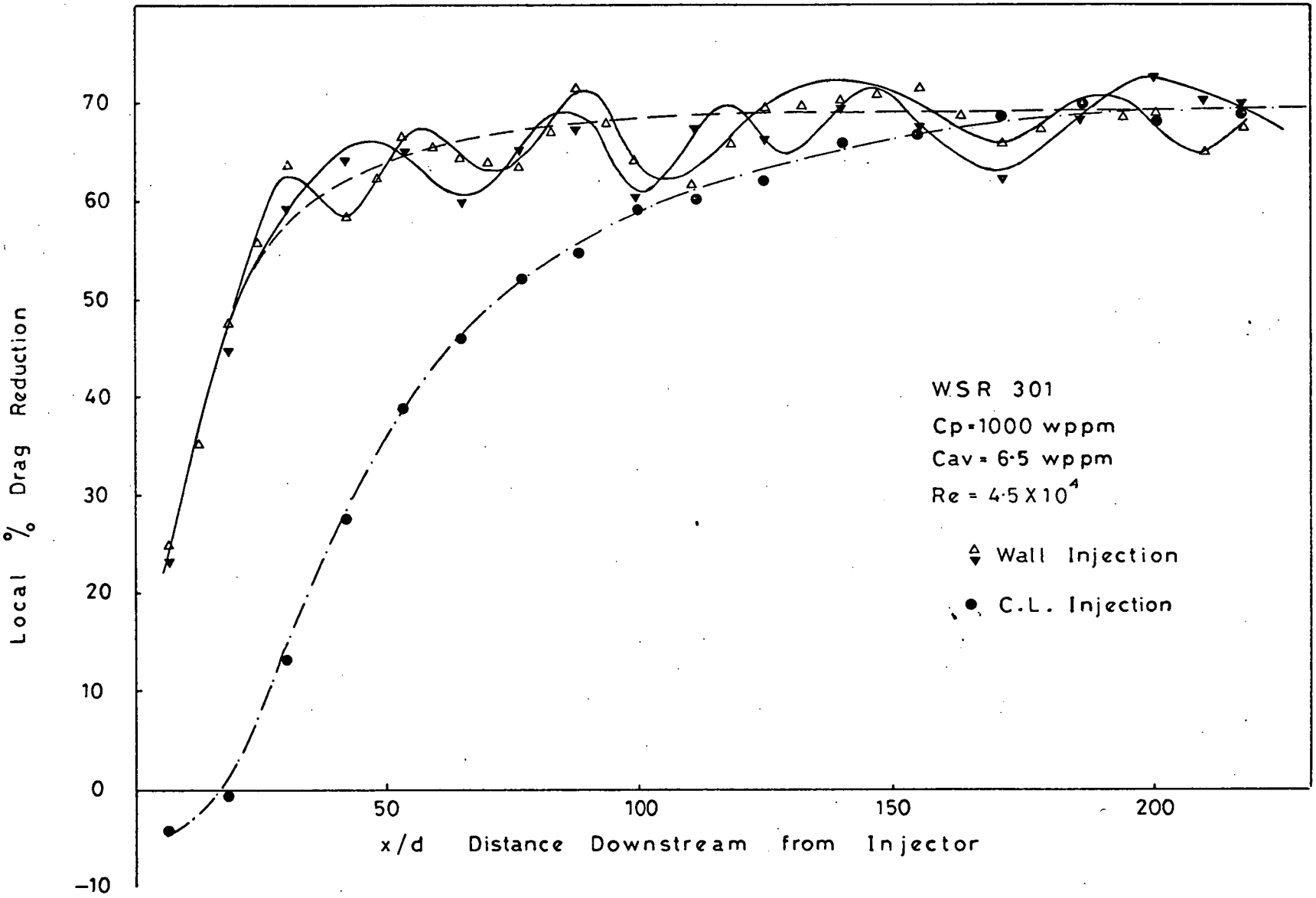
Local % Drag Reduction
70
60
50
40
30
20
10
0
-10
50
100
150
200
x/d Distance Downstream from Injector
WSR 301
Cp=1000 wppm
Cav = 6·5 wppm
Re = 4·5 X 10^4
Wall Injection
C.L. Injection

FIG (5-7)

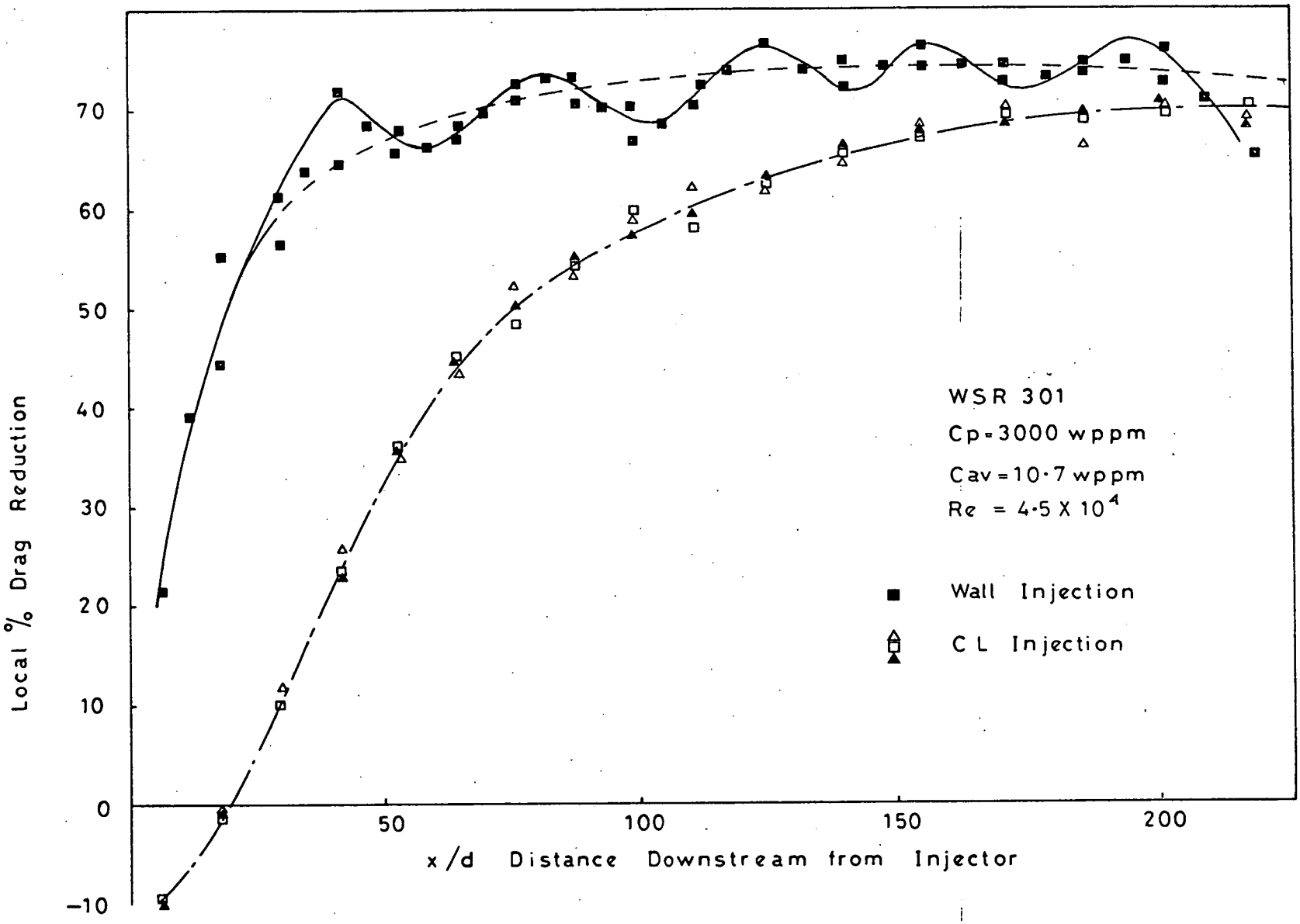
Local % Drag Reduction
70
60
50
40
30
20
10
0
−10
50
100
150
200
x/d Distance Downstream from Injector
WSR 301
Cp = 3000 wppm
Cav = 10·7 wppm
Re = 4·5 X 10⁴
Wall Injection
C L Injection

FIG (5-8)

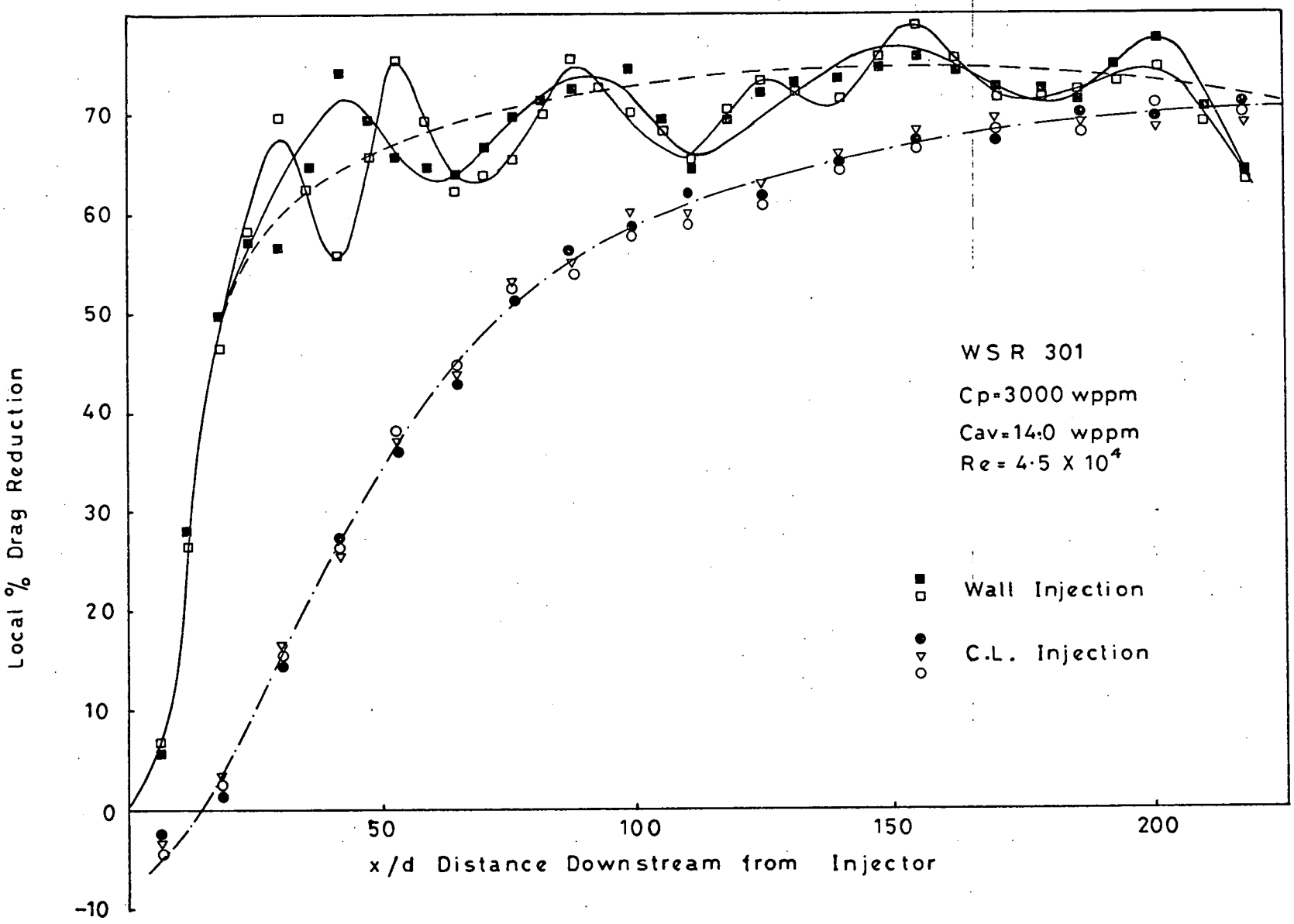
Local % Drag Reduction
70
60
50
40
30
20
10
0
-10
50
100
150
200
x/d Distance Downstream from Injector
WSR 301
Cp=3000 wppm
Cav=14.0 wppm
Re = 4·5 X 10⁴
Wall Injection
C.L. Injection

FIG (5-9)

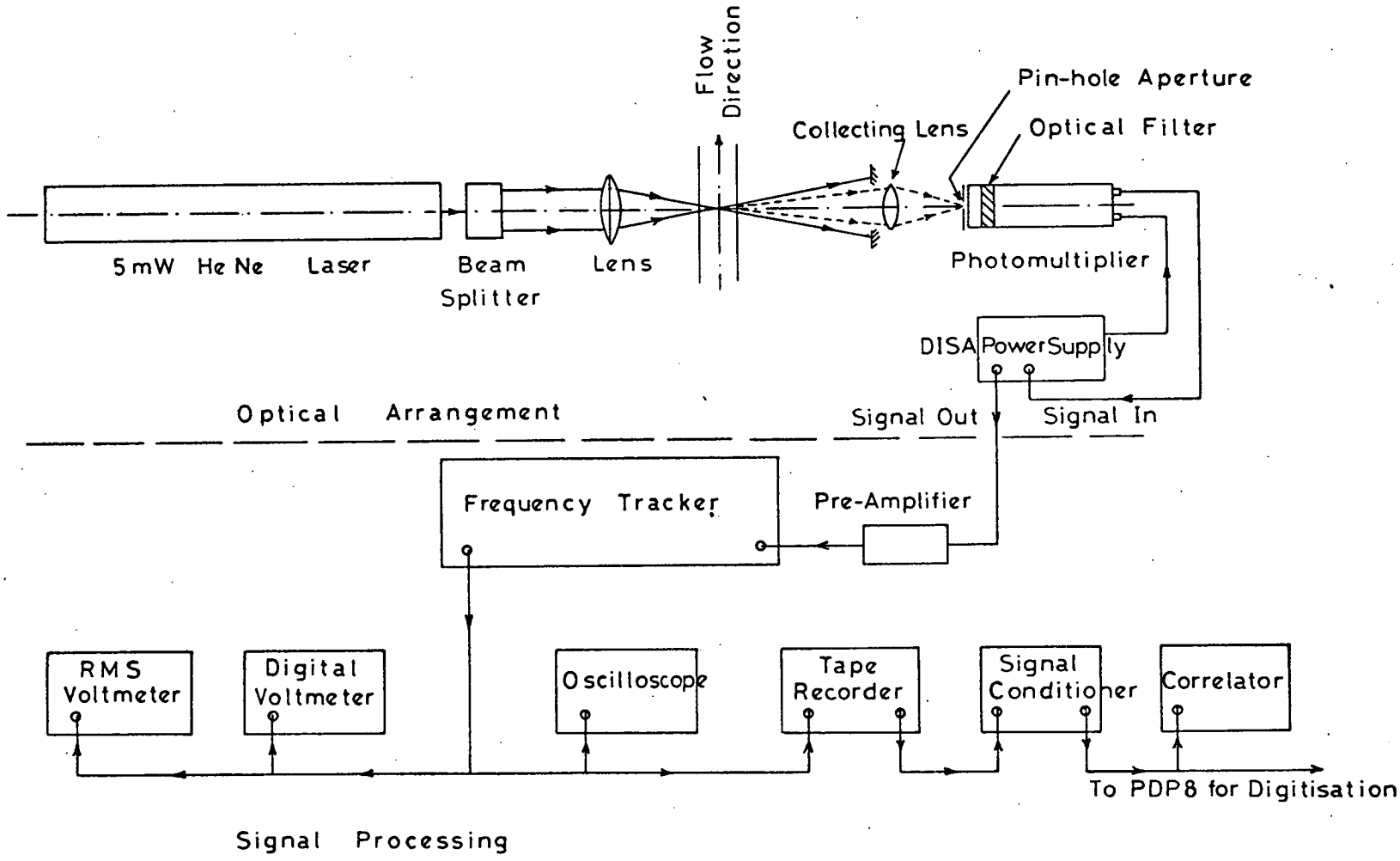
Flow Direction
Pin-hole Aperture
Collecting Lens
Optical Filter
5mW He Ne Laser
Beam Splitter
Lens
Photomultiplier
DISA Power Supply
Optical Arrangement
Signal Out
Signal In
Frequency Tracker
Pre-Amplifier
RMS Voltmeter
Digital Voltmeter
Oscilloscope
Tape Recorder
Signal Conditioner
Correlator
To PDP8 for Digitisation
Signal Processing

FIG (6-1)

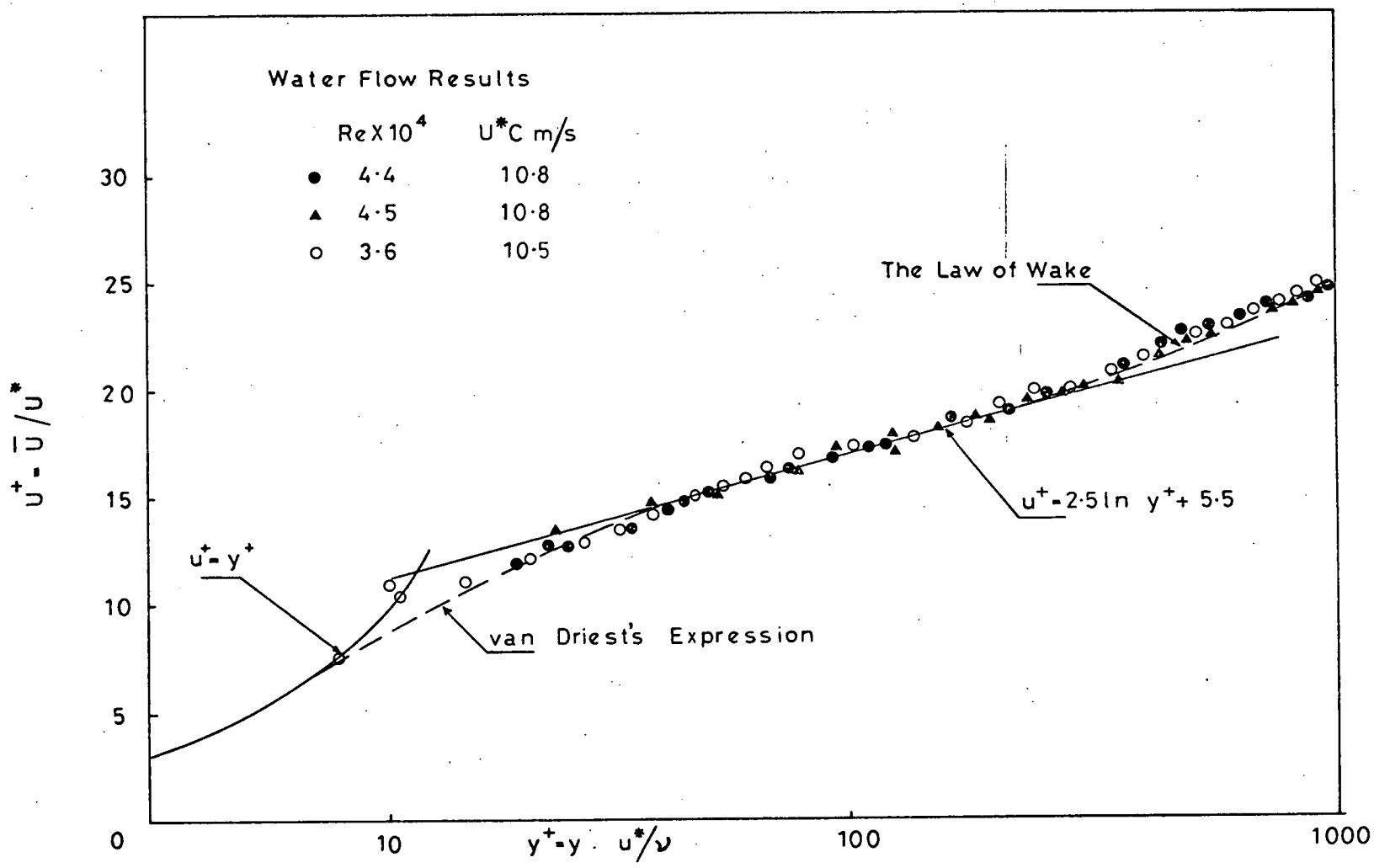
Water Flow Results
Re X 10^4
U*C m/s
4·4
10·8
4·5
10·8
3·6
10·5
The Law of Wake
u+ = 2·5 ln y+ + 5·5
u+ = y+
van Driest's Expression
u+ = ū/u*
y+ = y . u*/ν
0
5
10
15
20
25
30
10
100
1000

FIG (6-2)

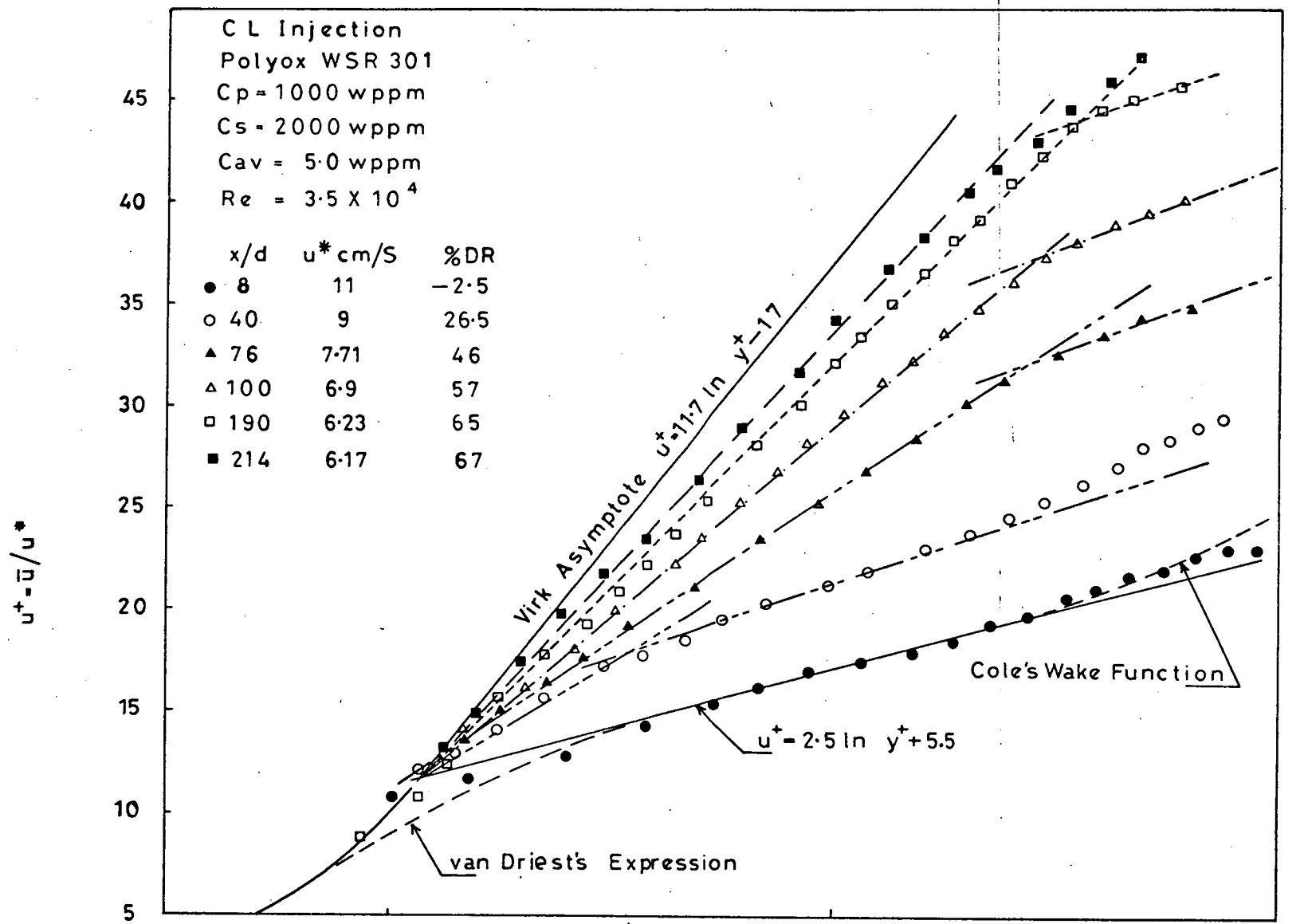
C L Injection
Polyox WSR 301
Cp = 1000 wppm
Cs = 2000 wppm
Cav = 5·0 wppm
Re = 3·5 X 10^4
x/d u* cm/S %DR
8 11 −2·5
40 9 26·5
76 7·71 46
100 6·9 57
190 6·23 65
214 6·17 67
Virk Asymptote u+=11·7 ln y+−17
Cole's Wake Function
u+= 2·5 ln y+ + 5.5
van Driest's Expression
u+ = ū/u*
y+ = y. u*/ν
45
40
35
30
25
20
15
10
5
10
100
1000

FIG (6-3)

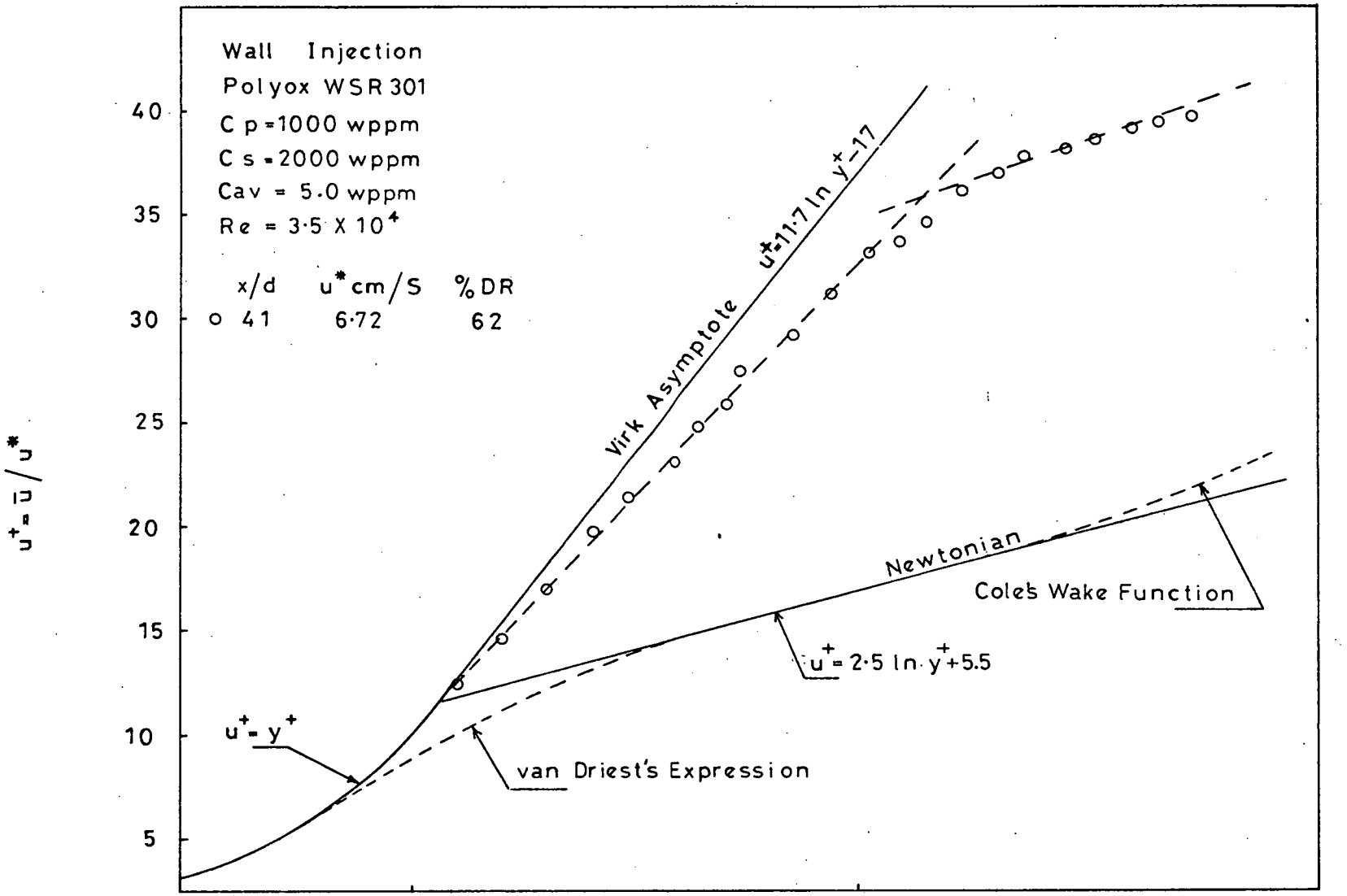
Wall Injection
Polyox WSR 301
C p =1000 wppm
C s =2000 wppm
Cav = 5.0 wppm
Re = 3·5 X 10⁴
x/d u* cm/S %DR
o 41 6·72 62
Virk Asymptote u⁺=11·7 ln y⁺-17
Newtonian
Coles Wake Function
u⁺= 2·5 ln y⁺+5.5
u⁺= y⁺
van Driest's Expression
u⁺= ū / u*
y⁺= y. u* /ν
40
35
30
25
20
15
10
5
10
100
1000

FIG(6-4)

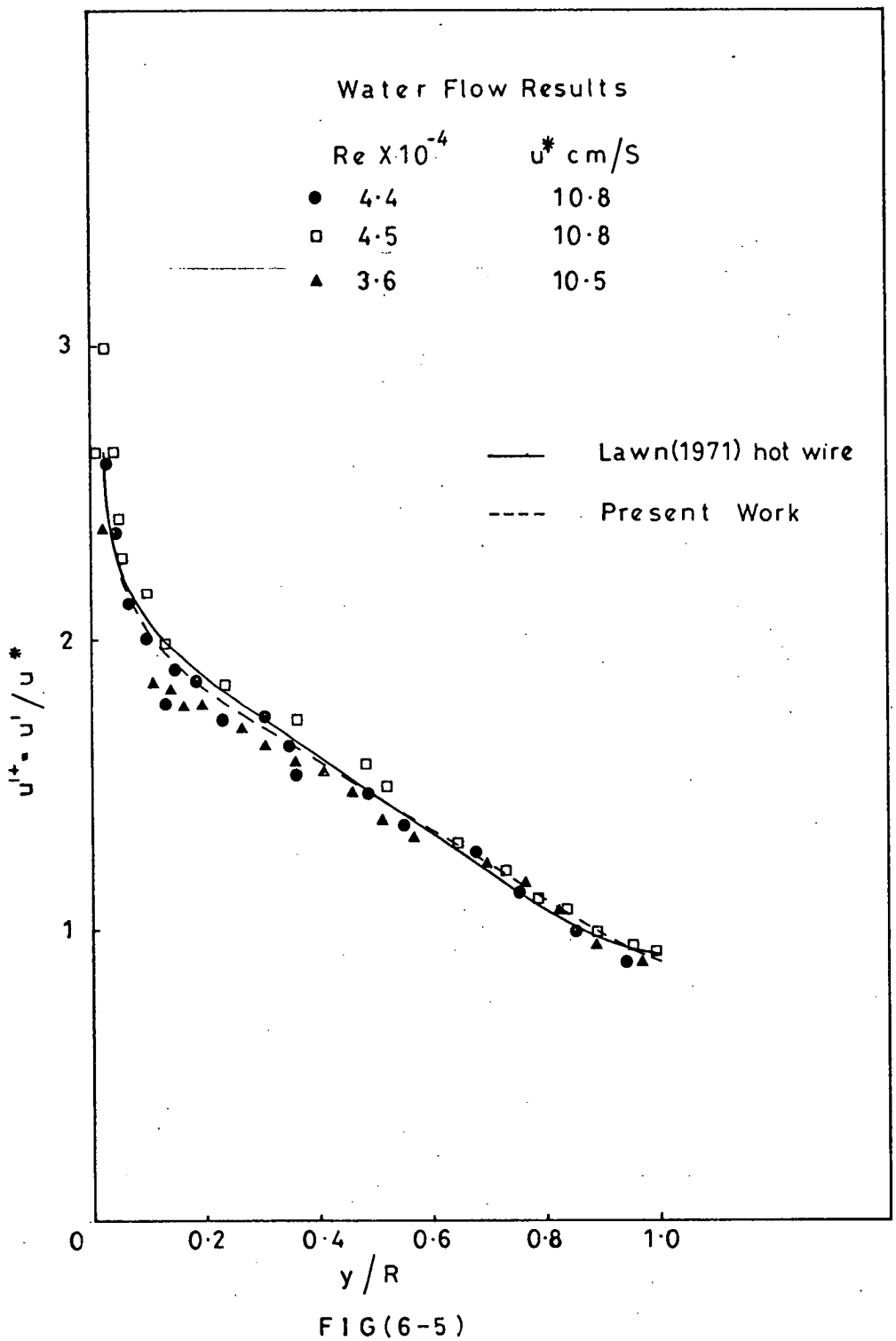
Water Flow Results
Re X 10^-4
u* cm/S
4·4
10·8
4·5
10·8
3·6
10·5
Lawn(1971) hot wire
Present Work
u'+ = u'/u*
y/R
0
0·2
0·4
0·6
0·8
1·0
1
2
3

FIG(6-5)

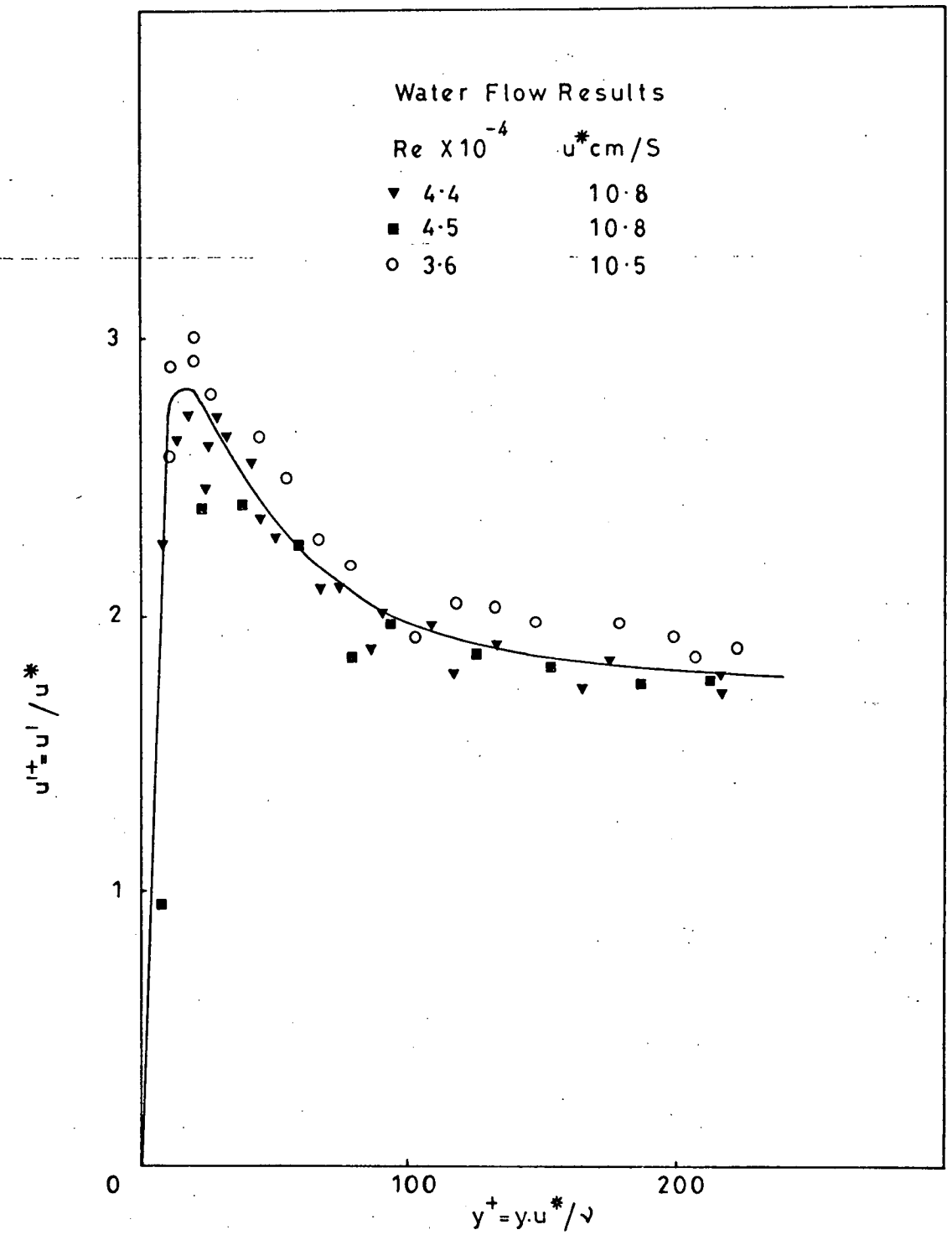
Water Flow Results
Re X10^-4
u*cm/S
4·4
10·8
4·5
10·8
3·6
10·5
3
2
1
0
100
200
u'+ = u'/u*
y+ = y.u*/ν

FIG (6 – 6)

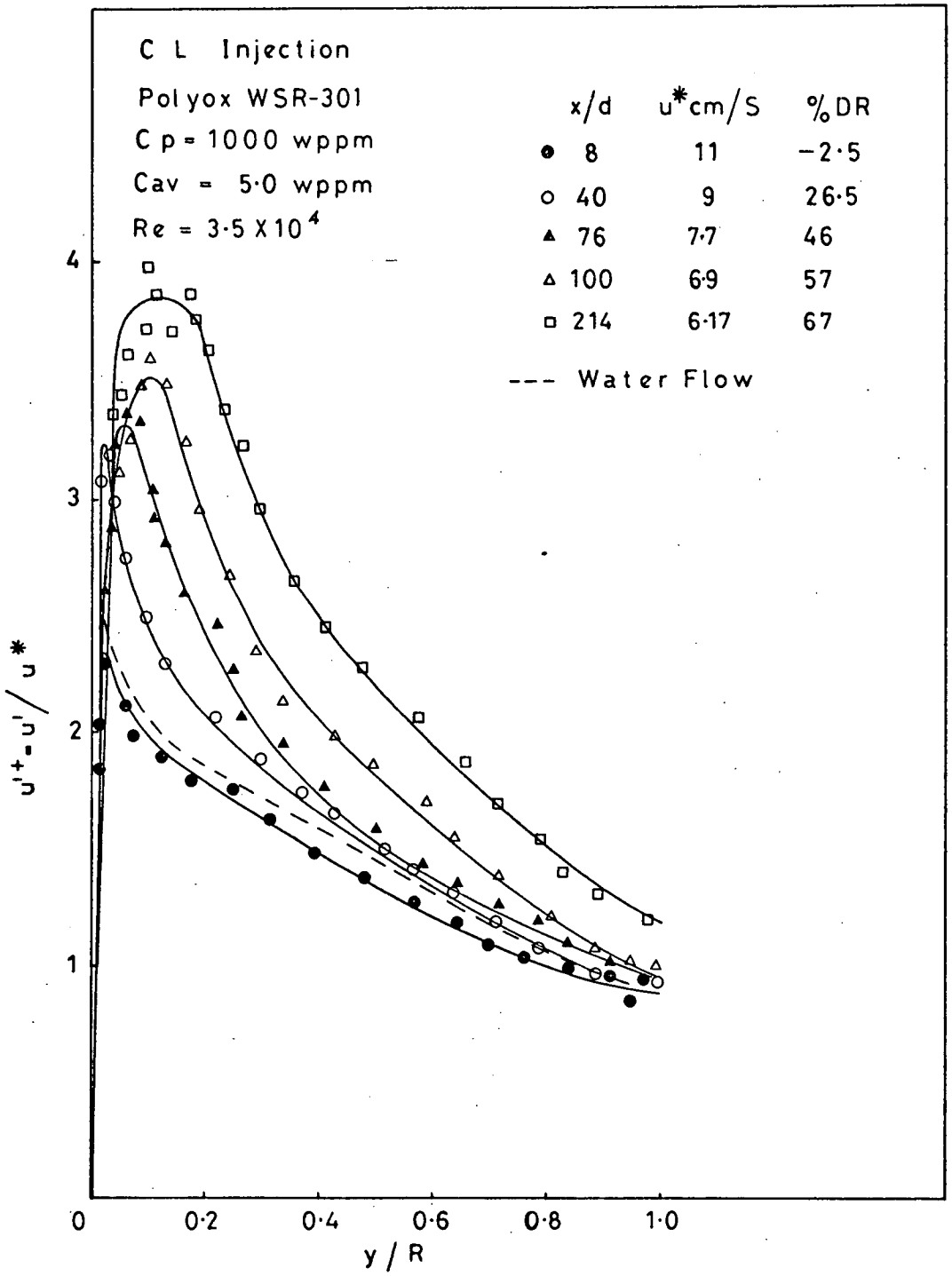
C L Injection
Polyox WSR-301
Cp = 1000 wppm
Cav = 5·0 wppm
Re = 3·5 X 10⁴
x/d u*cm/S %DR
8 11 −2·5
40 9 26·5
76 7·7 46
100 6·9 57
214 6·17 67
--- Water Flow
u'+ = u'/u*
y/R
0
0·2
0·4
0·6
0·8
1·0
1
2
3
4

FIG (6-7)

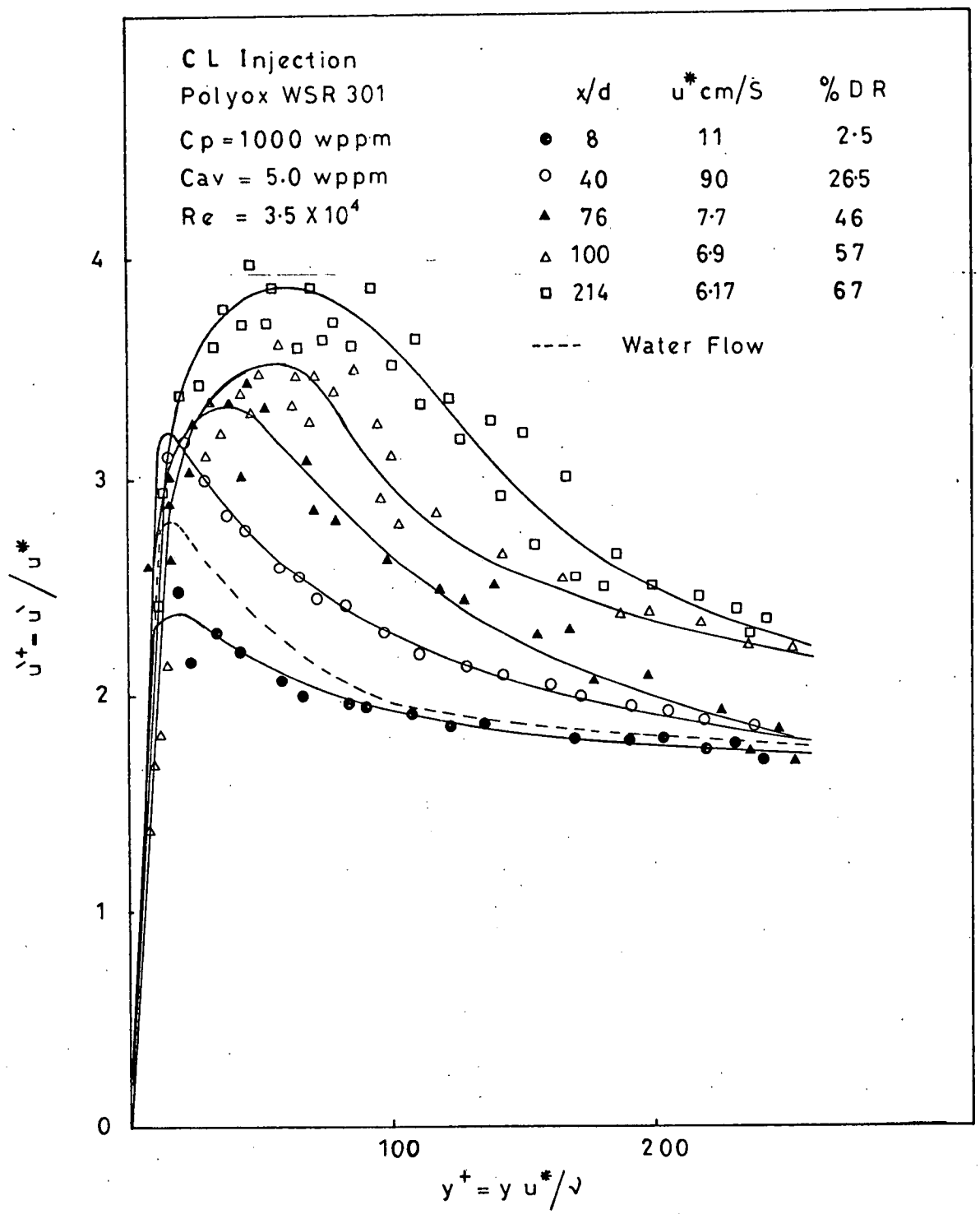
C L Injection
Polyox WSR 301
Cp = 1000 wppm
Cav = 5.0 wppm
Re = 3·5 X 10⁴
x/d
u* cm/S
% D R
8
11
2·5
40
90
26·5
76
7·7
46
100
6·9
57
214
6·17
67
Water Flow
4
3
2
1
0
100
200
y⁺ = y u*/ν

FIG (6-8)

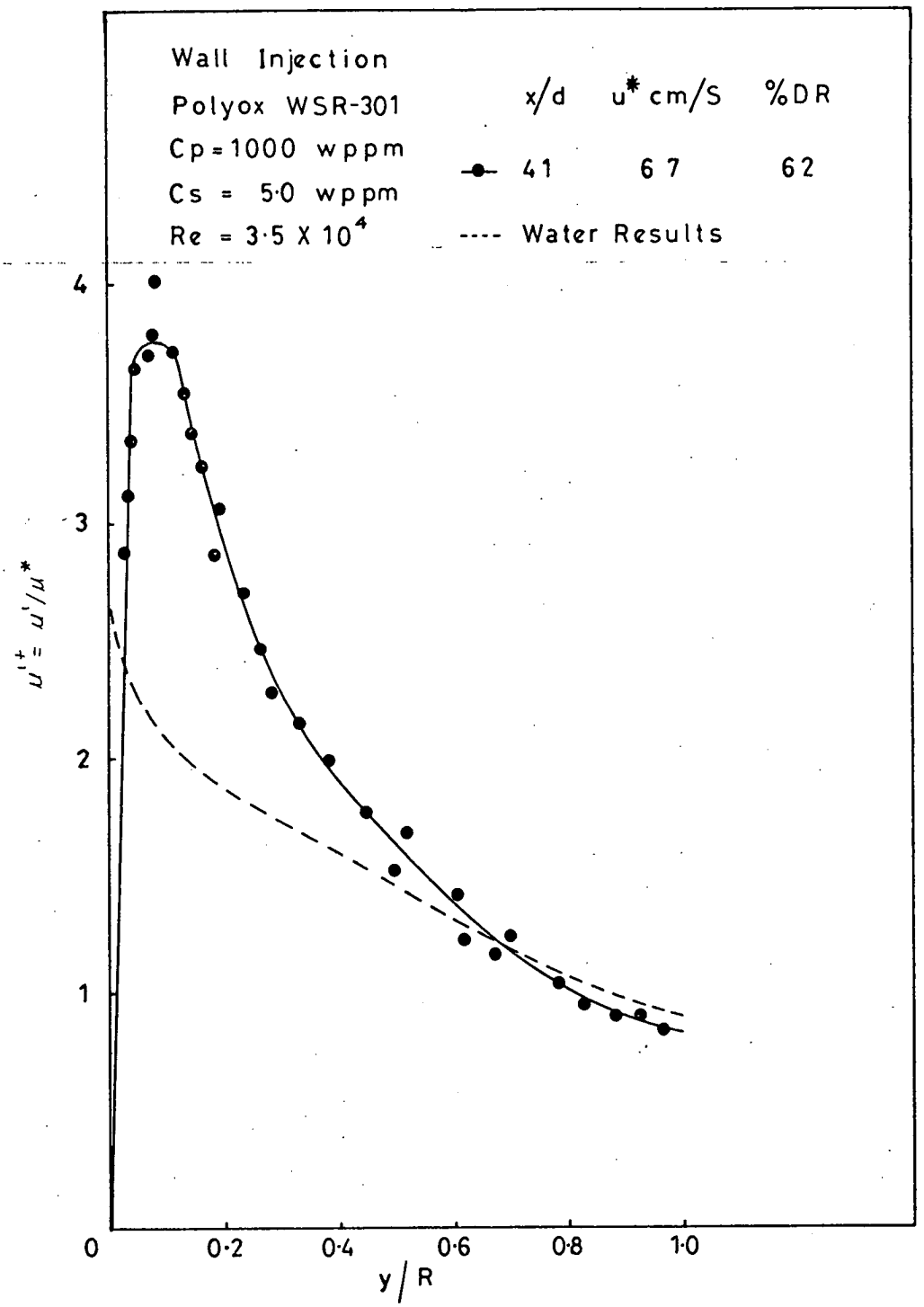
Wall Injection
Polyox WSR-301
Cp = 1000 wppm
Cs = 5·0 wppm
Re = 3·5 X 10⁴
x/d
u* cm/S
%DR
41
6 7
62
---- Water Results
4
3
2
1
0
0·2
0·4
0·6
0·8
1·0
y/R
u'+ = u'/u*

FIG (6-9)

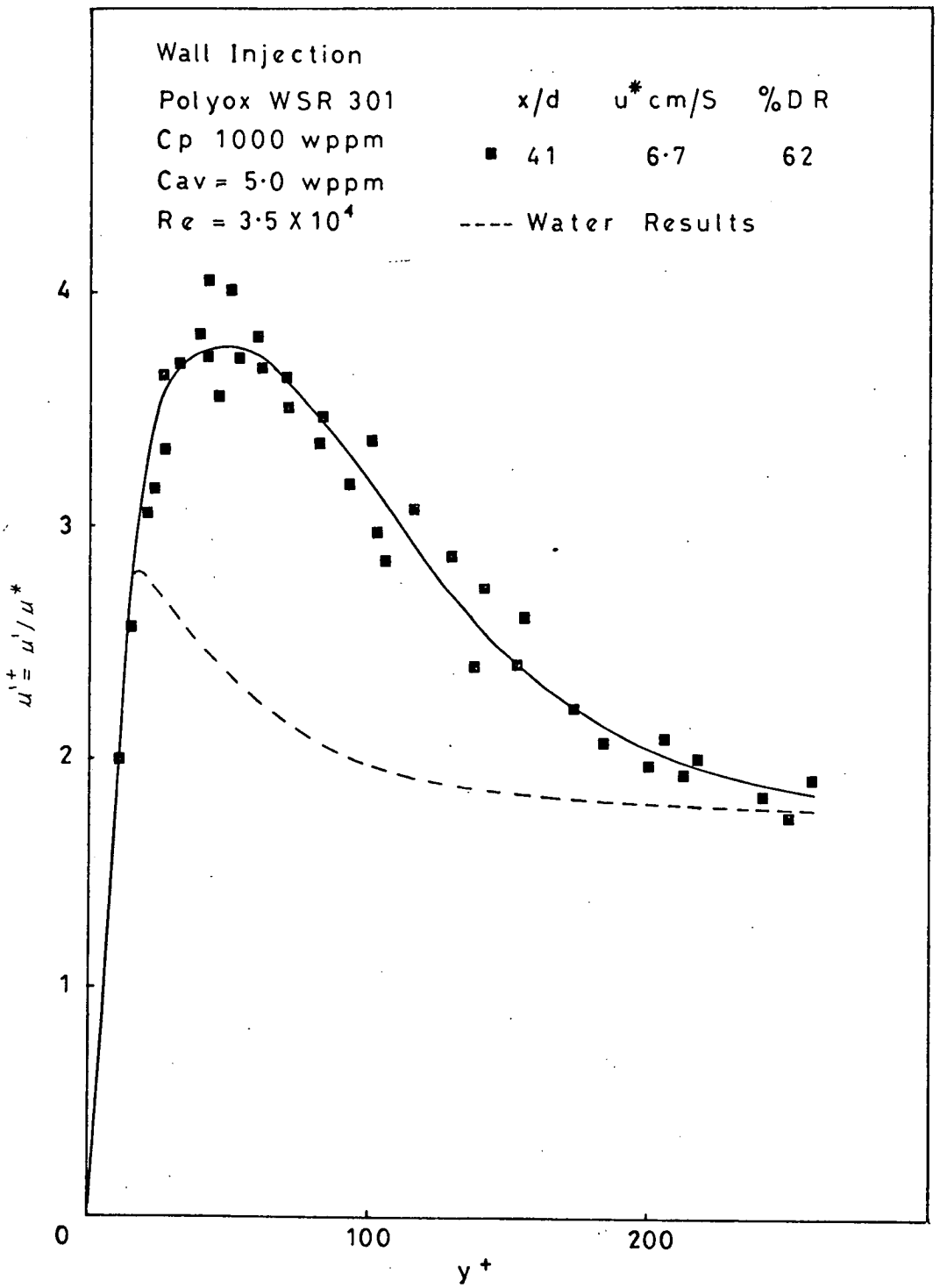
Wall Injection
Polyox WSR 301
Cp 1000 wppm
Cav = 5·0 wppm
Re = 3·5 X 10⁴
x/d
u* cm/S
%D R
41
6·7
62
---- Water Results
4
3
2
1
0
100
200
y +
u'+ = u'/u*

FIG (6 - 10)

FIG (6 – 11)

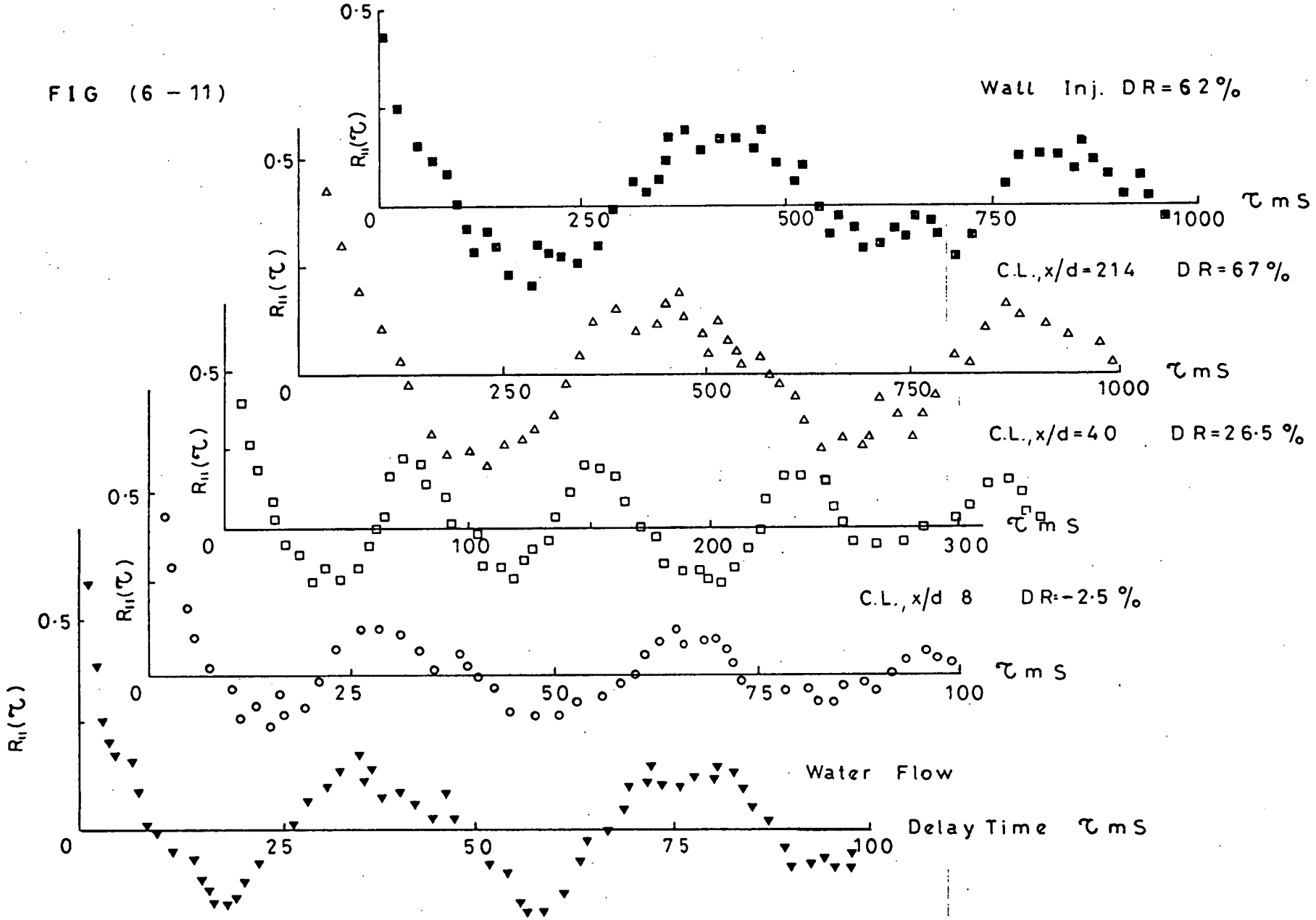
Wall Inj. DR = 62 %
C.L., x/d = 214 DR = 67 %
C.L., x/d = 40 DR = 26·5 %
C.L., x/d 8 DR = −2·5 %
Water Flow
$R_{11}(\tau)$
τ mS
Delay Time τ mS
0·5
0
250
500
750
1000
100
200
300
25
50
75
100

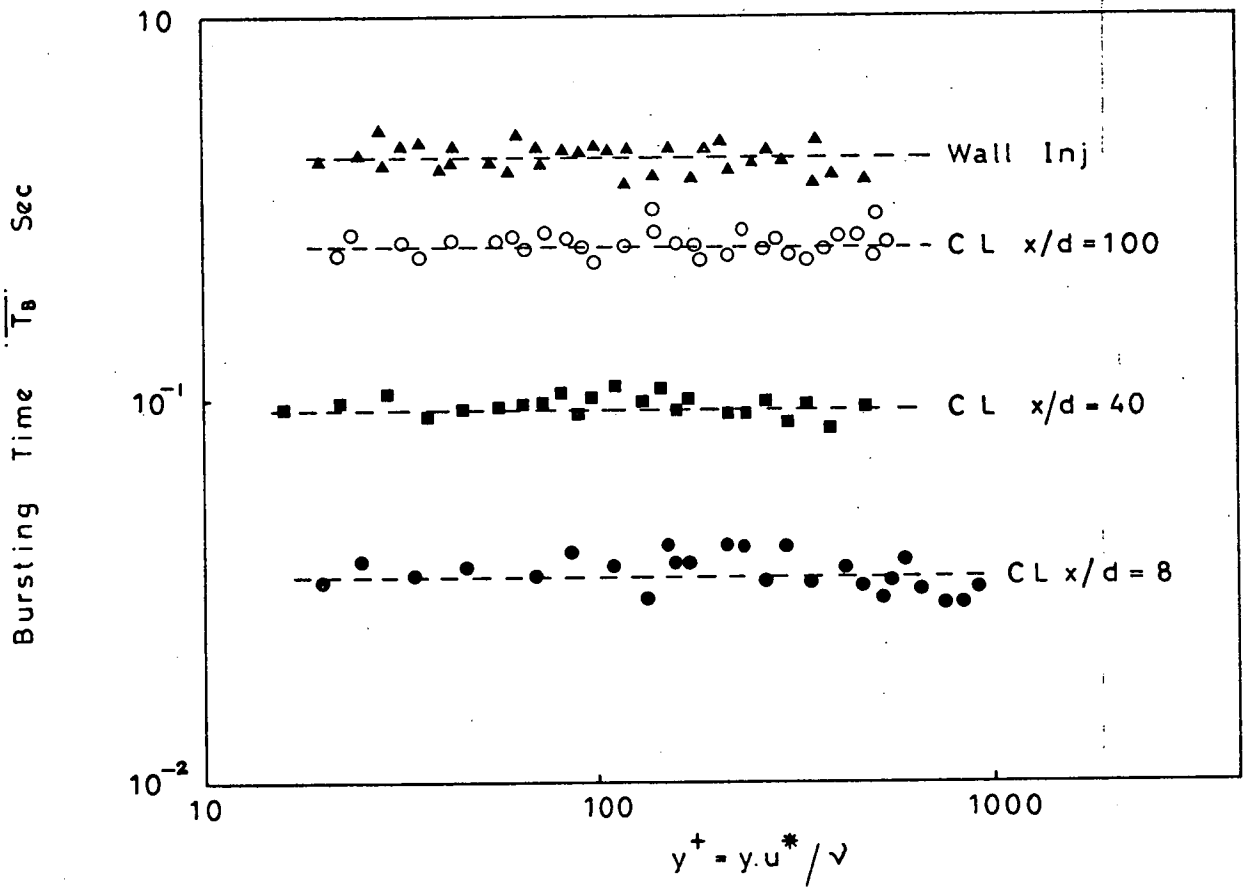
10
10^{-1}
10^{-2}
10
100
1000
Bursting Time $\overline{T_B}$ Sec
$y^+ = y.u^*/\nu$
Wall Inj
C L x/d = 100
C L x/d = 40
C L x/d = 8

FIG (6 -12)

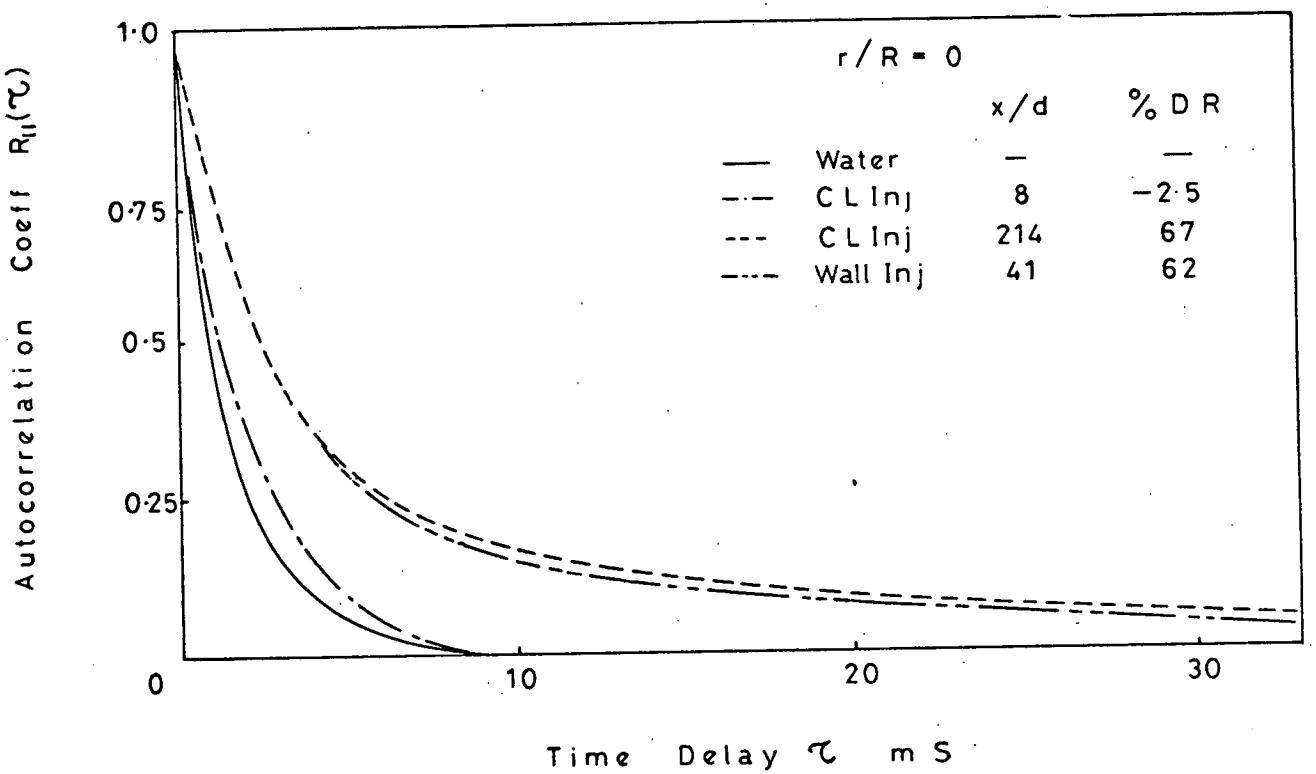
r/R = 0
x/d
% D R
Water — —
C L Inj 8 −2·5
C L Inj 214 67
Wall Inj 41 62
1·0
0·75
0·5
0·25
0
10
20
30
Autocorrelation Coeff $R_{11}(\tau)$
Time Delay τ m S

FIG (6 – 13)

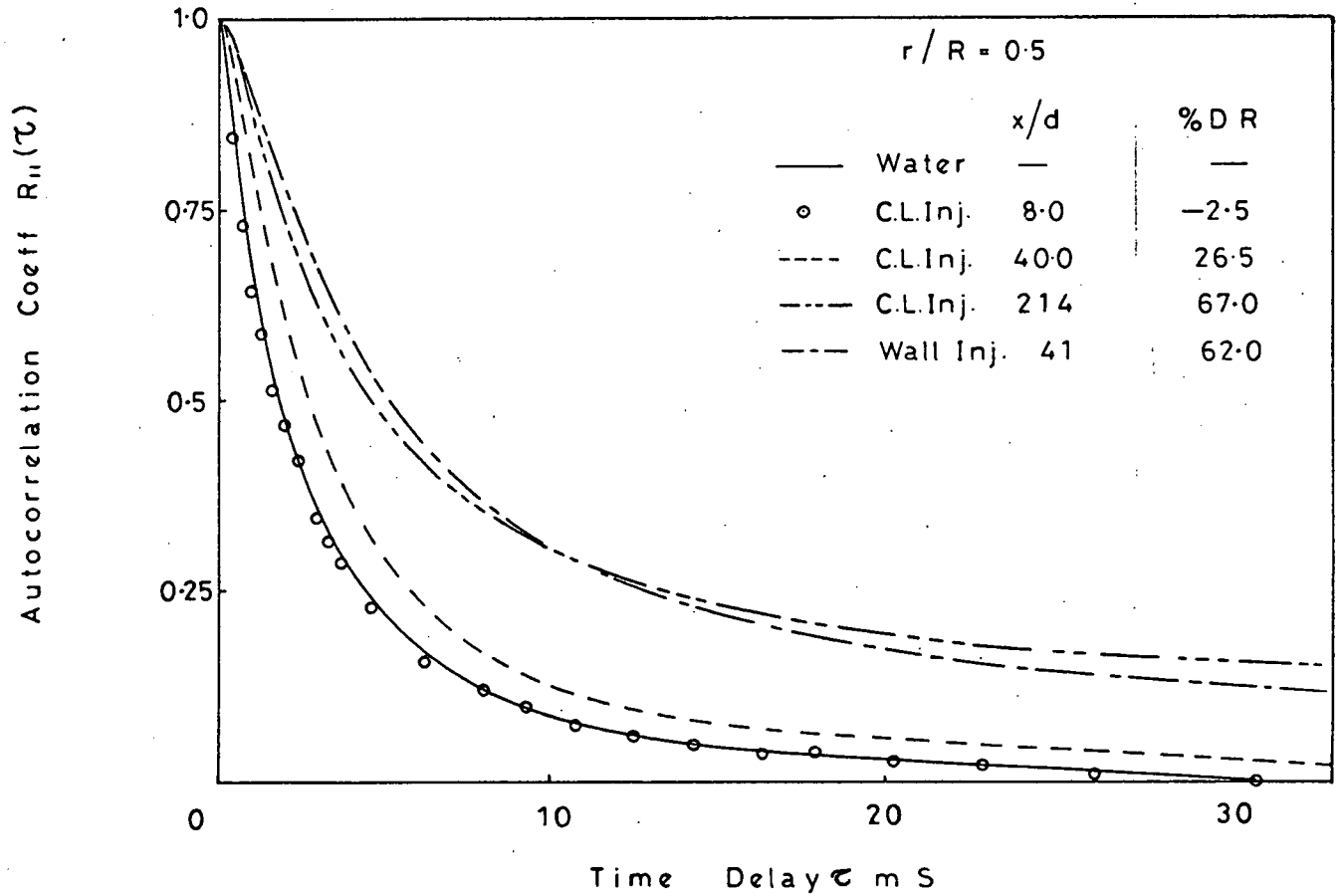
r / R = 0·5
x/d
%D R
Water — —
C.L.Inj. 8·0 −2·5
C.L.Inj. 40·0 26·5
C.L.Inj. 214 67·0
Wall Inj. 41 62·0
Autocorrelation Coeff $R_{11}(\tau)$
1·0
0·75
0·5
0·25
0
10
20
30
Time Delay τ m S

FIG (6 − 14)

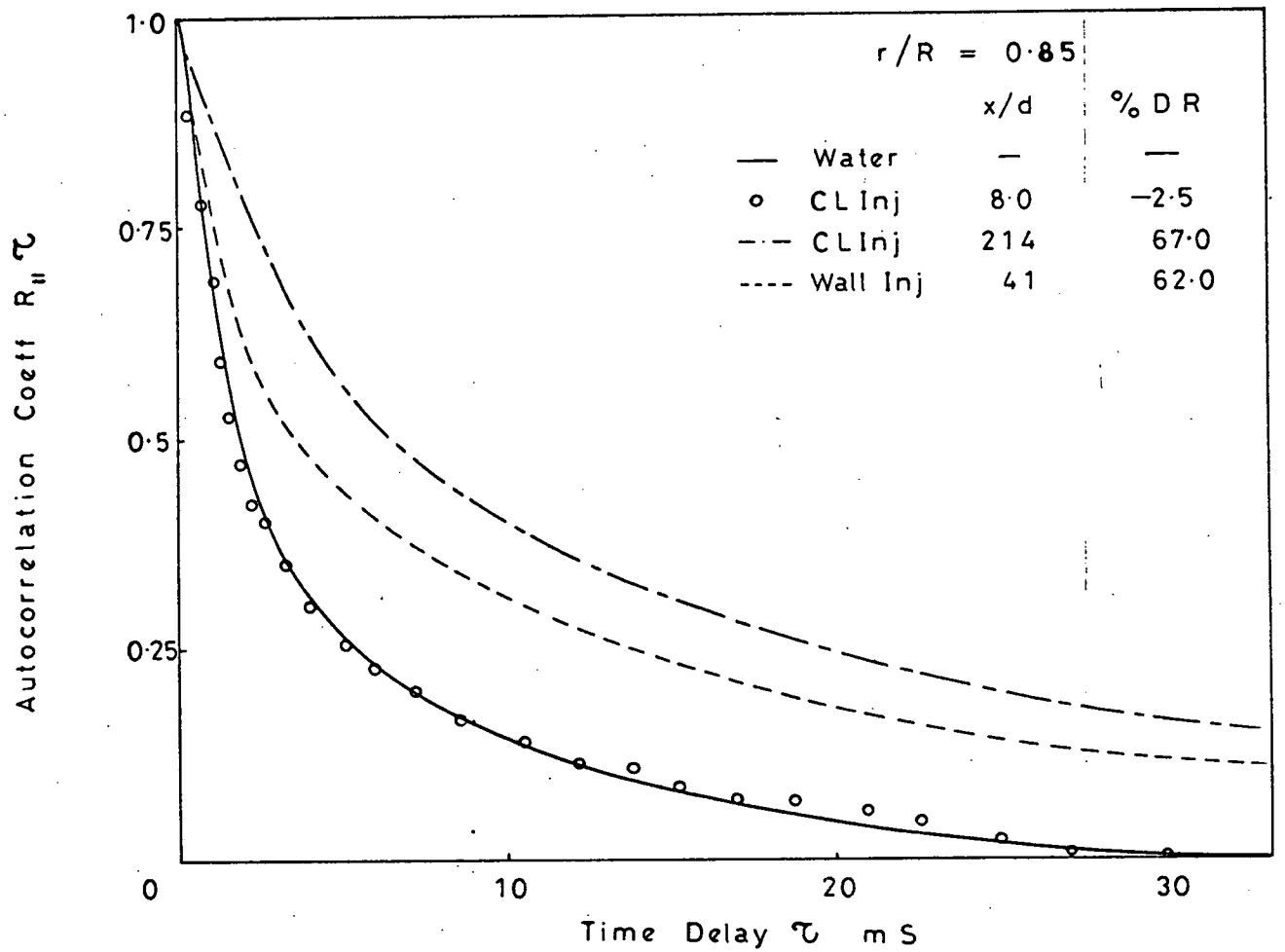
r/R = 0·85
x/d
% D R
Water — —
CL Inj 8·0 −2·5
CL Inj 214 67·0
Wall Inj 41 62·0
1·0
0·75
0·5
0·25
0
10
20
30
Autocorrelation Coeff R_{11} τ
Time Delay τ m S

FIG (6 - 15)

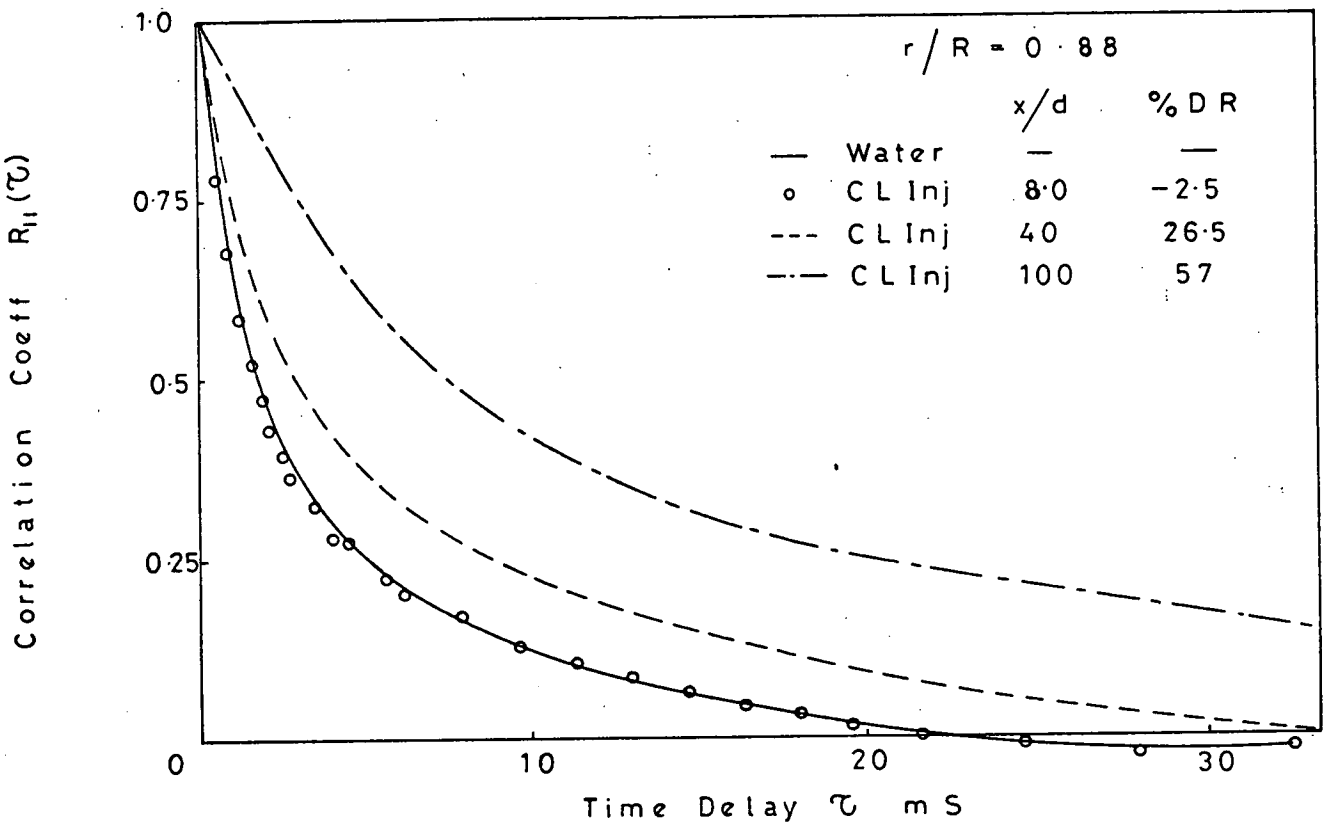
r / R = 0 · 88
x/d
% D R
Water — —
C L Inj 8·0 −2·5
C L Inj 40 26·5
C L Inj 100 57
1·0
0·75
0·5
0·25
0
10
20
30
Correlation Coeff $R_{11}(\tau)$
Time Delay τ m S

FIG (6 – 16)

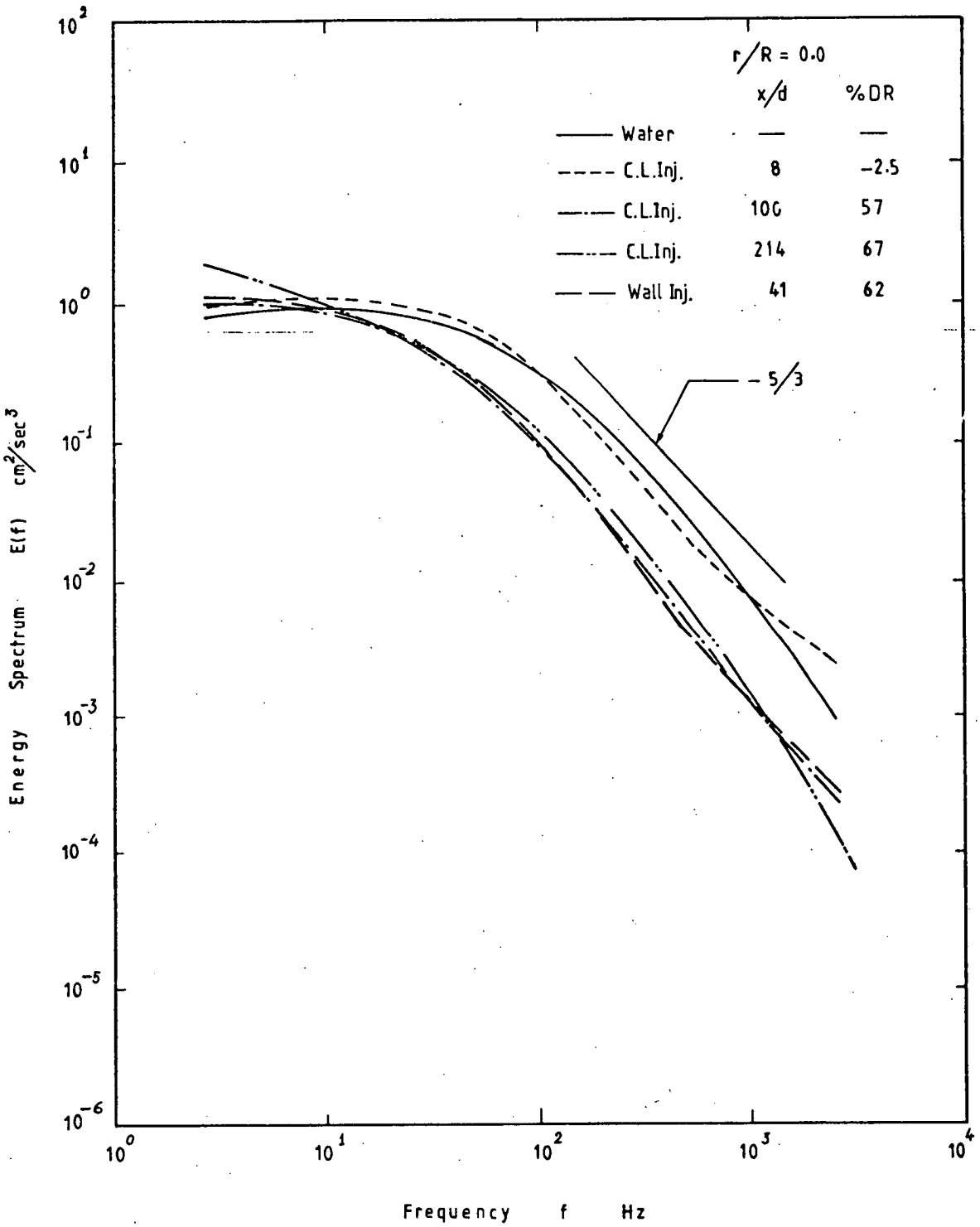
r/R = 0.0
x/d
%DR
Water
C.L.Inj. 8 -2.5
C.L.Inj. 100 57
C.L.Inj. 214 67
Wall Inj. 41 62
-5/3
Energy Spectrum E(f) cm²/sec³
Frequency f Hz

FIG (6-17)

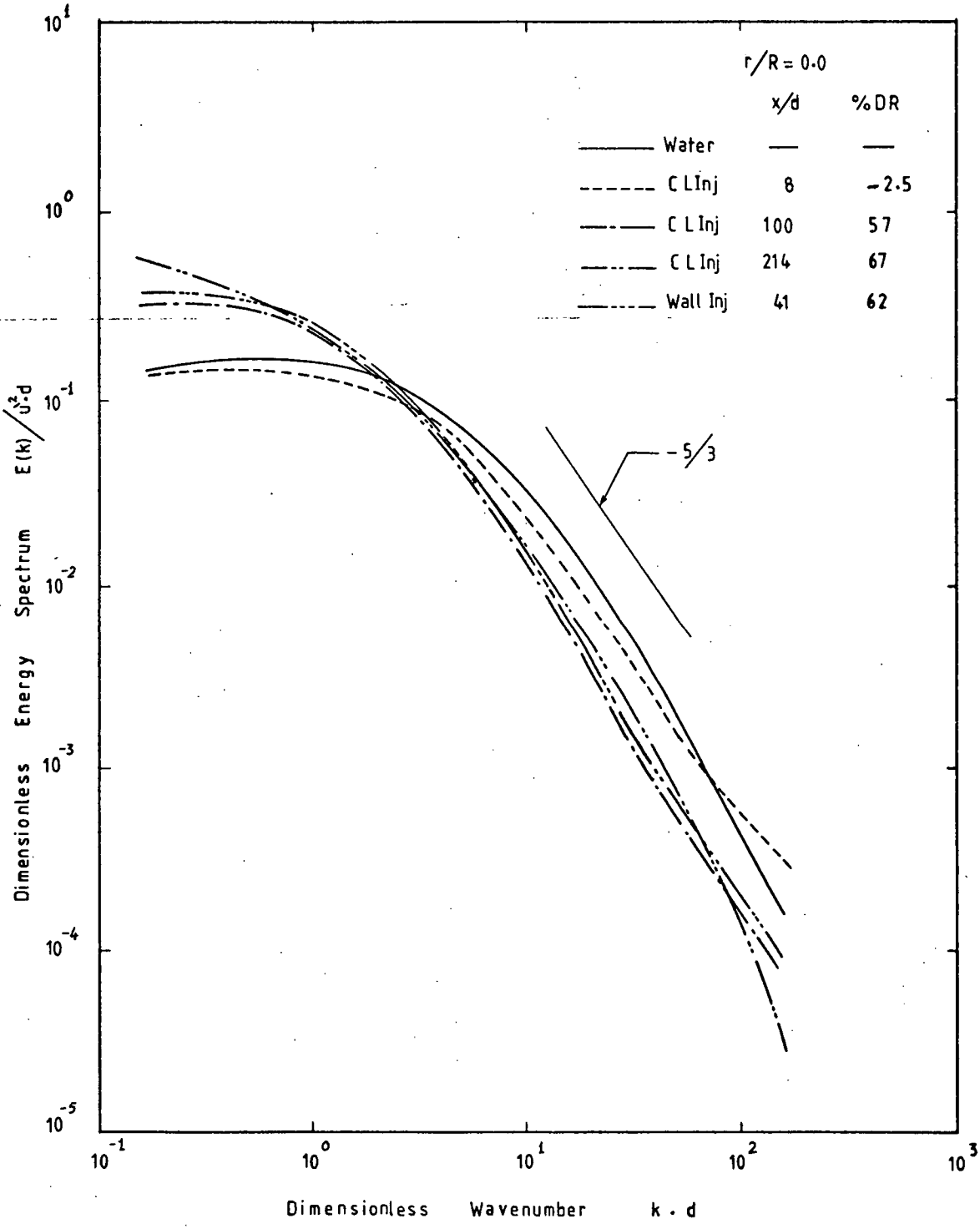
r/R = 0.0
x/d
%DR
Water
C L Inj 8 -2.5
C L Inj 100 57
C L Inj 214 67
Wall Inj 41 62
-5/3
Dimensionless Energy Spectrum E(k)/u².d
Dimensionless Wavenumber k . d
10¹
10⁰
10⁻¹
10⁻²
10⁻³
10⁻⁴
10⁻⁵
10⁻¹
10⁰
10¹
10²
10³

FIG (6-18)

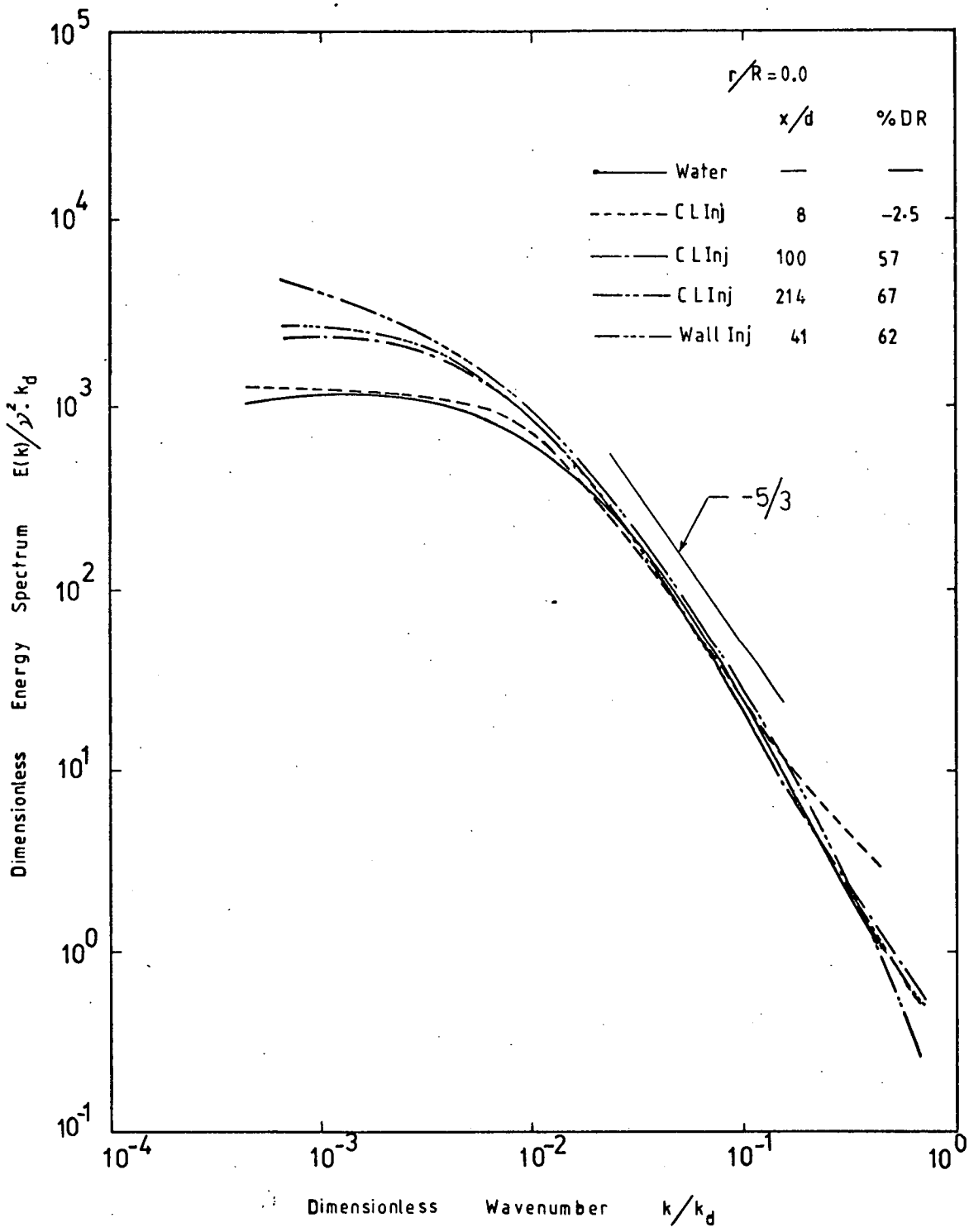
r/R = 0.0
x/d
%DR
Water
C L Inj 8 -2·5
C L Inj 100 57
C L Inj 214 67
Wall Inj 41 62
-5/3
Dimensionless Energy Spectrum E(k)/ν².k_d
Dimensionless Wavenumber k/k_d
10^5
10^4
10^3
10^2
10^1
10^0
10^-1
10^-4
10^-3
10^-2
10^-1
10^0

FIG (6-19)

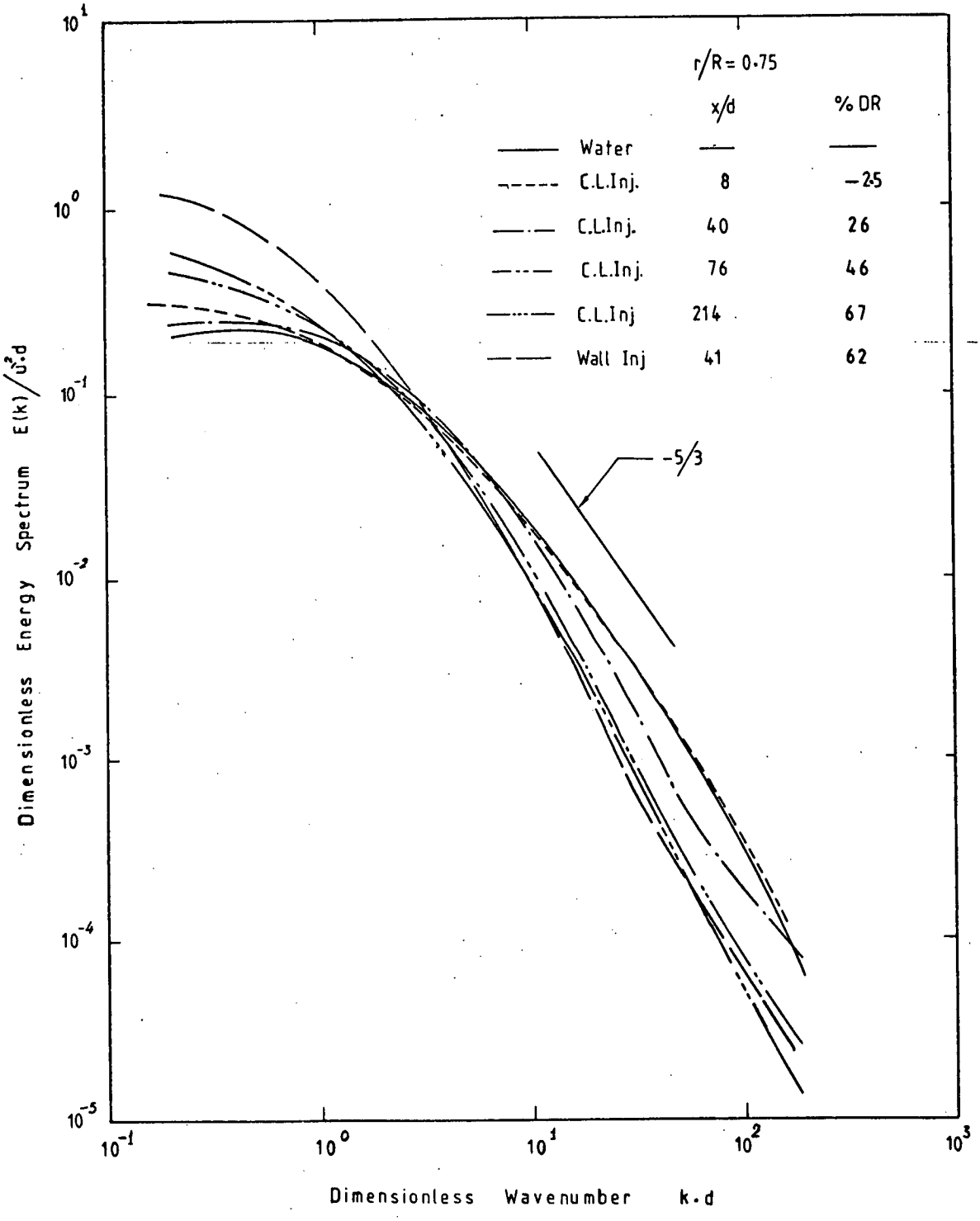
r/R = 0·75
x/d
% DR
Water
C.L.Inj. 8 −25
C.L.Inj. 40 26
C.L.Inj. 76 46
C.L.Inj 214 67
Wall Inj 41 62
-5/3
Dimensionless Energy Spectrum E(k)/u².d
Dimensionless Wavenumber k.d
10¹
10⁰
10⁻¹
10⁻²
10⁻³
10⁻⁴
10⁻⁵
10⁻¹
10⁰
10¹
10²
10³

FIG. (6-20)

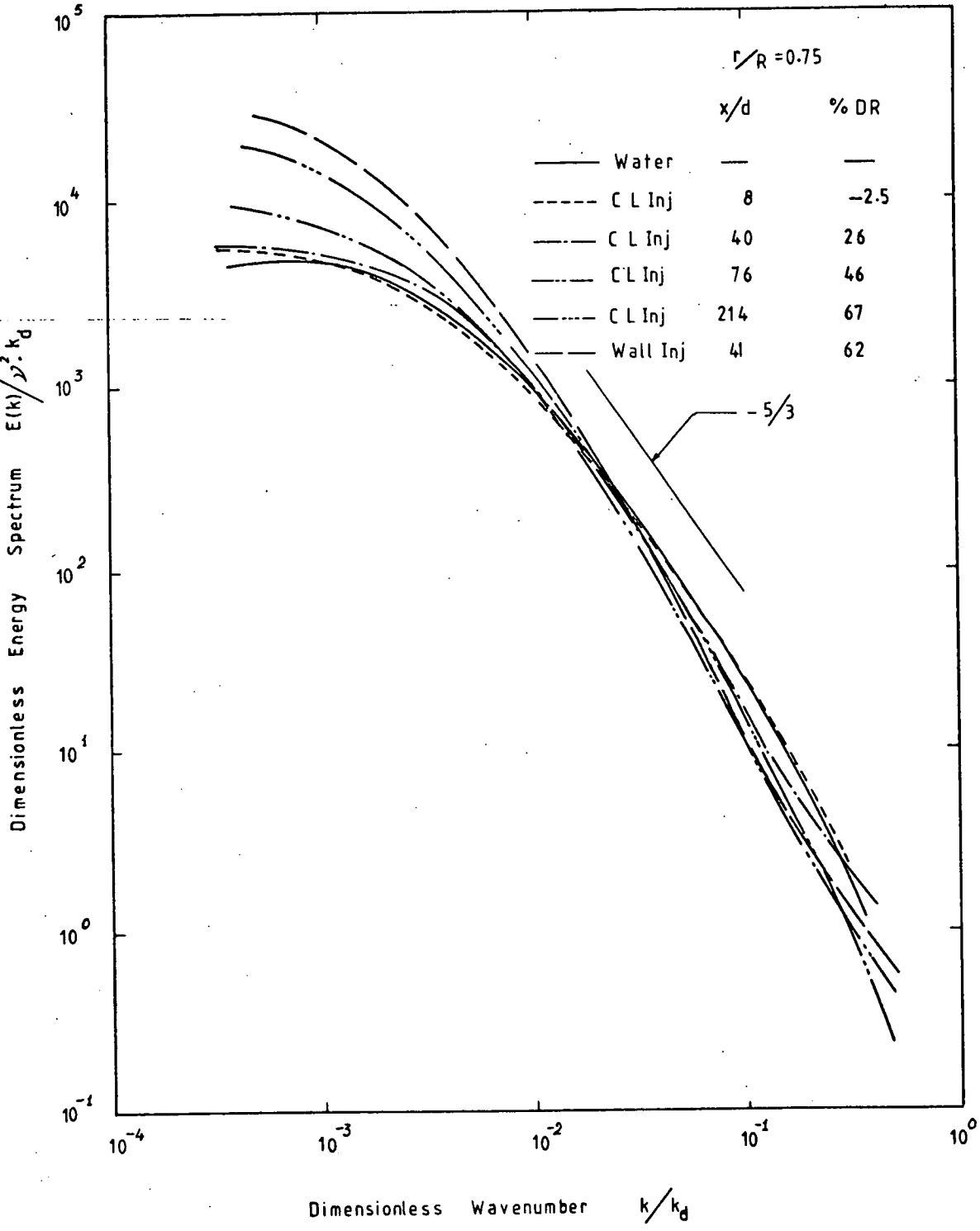
r/R =0.75
x/d
% DR
Water — —
C L Inj 8 −2.5
C L Inj 40 26
C L Inj 76 46
C L Inj 214 67
Wall Inj 41 62
−5/3
Dimensionless Energy Spectrum E(k)/ν²·k_d
Dimensionless Wavenumber k/k_d
10^5
10^4
10^3
10^2
10^1
10^0
10^-1
10^-4
10^-3
10^-2
10^-1
10^0

FIG (6-21)

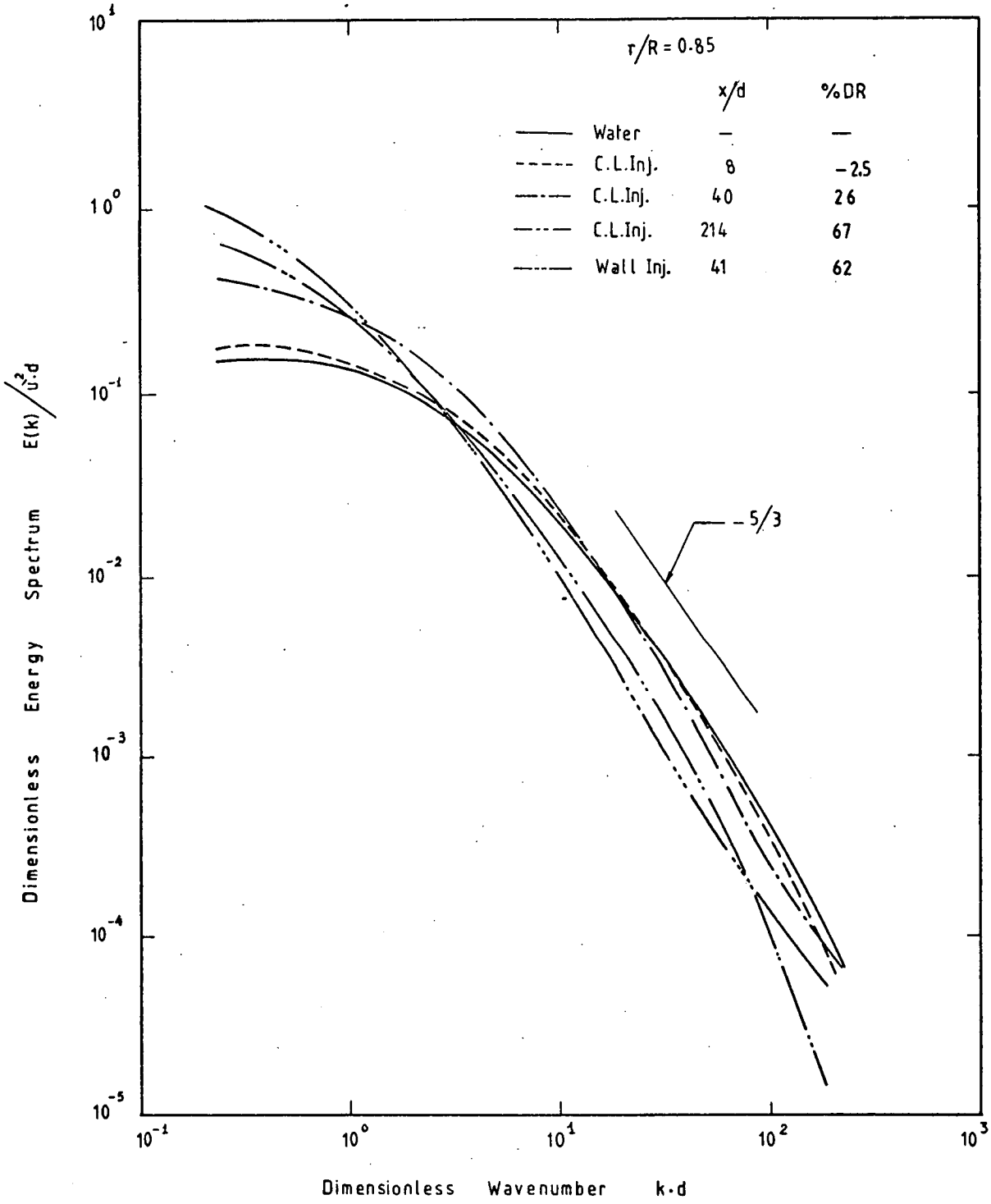
r/R = 0.85
x/d
%DR
Water
—
—
C.L.Inj.
8
-2.5
C.L.Inj.
40
26
C.L.Inj.
214
67
Wall Inj.
41
62
-5/3
Dimensionless Energy Spectrum E(k)/u².d
Dimensionless Wavenumber k·d
10¹
10⁰
10⁻¹
10⁻²
10⁻³
10⁻⁴
10⁻⁵
10⁻¹
10⁰
10¹
10²
10³

FIG (6-22)

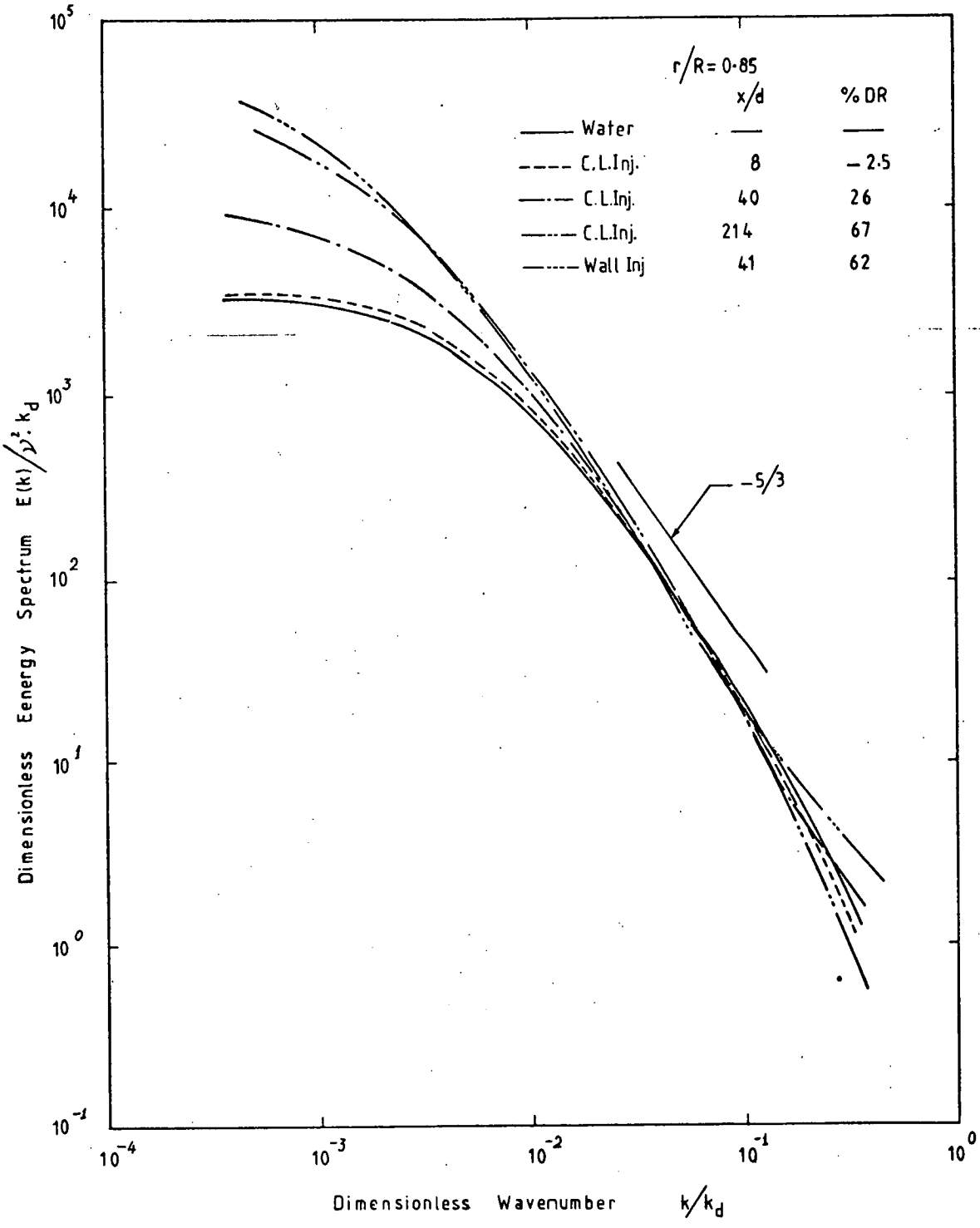
r/R = 0·85
x/d
% DR
Water
C.L.Inj. 8 −2·5
C.L.Inj. 40 26
C.L.Inj. 214 67
Wall Inj 41 62
−5/3
Dimensionless Eenergy Spectrum E(k)/ν²·k_d
Dimensionless Wavenumber k/k_d
10^5
10^4
10^3
10^2
10^1
10^0
10^-1
10^-4
10^-3
10^-2
10^-1
10^0

FIG (6 - 23)